STABILITY AND DYNAMIC BEHAVIOUR OF STEEL STRUCTURES WITH NON-LINEAR RESTRAINTS

AHMED EL-SAID A. BADR

B.Sc., M.Sc., Civil Eng. (Egypt)

A THESIS PRESENTED FOR THE DEGREE OF

DOCTOR OF PHILOSOPHY

IN THE DEPARTMENT OF

CIVIL ENGINEERING

UNIVERSITY OF STRATHLCYDE, GLASGOW

1986

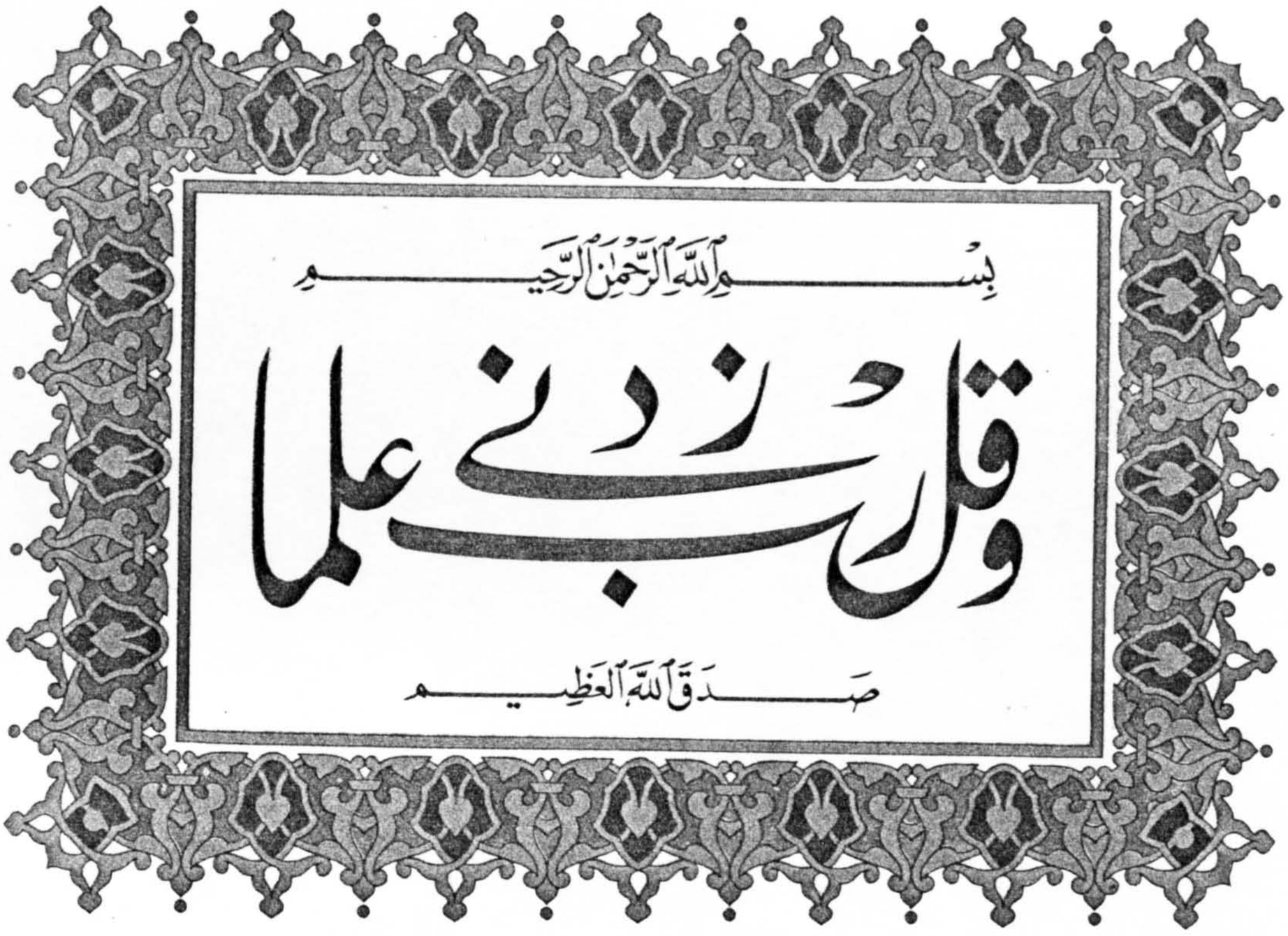

Dedicated to My Family

ACKNOWLEDGEMENTS

The study described in this thesis was carried out at the Department of Civil Engineering, University of Strathclyde, Glasgow.

The author is indebted to Dr. J. Marshall, B.Sc., Ph.D., A.R.C.S.T., C.Eng., M.I.C.E., M.I.Struct.E., for his supervision, advice, valuable guidance, numerous suggestions and stimulating discussions throughout this work and during the preparation of this thesis.

I would like to thank Professor I. MacLeod, Professor of Structural Engineering, University of Strathclyde, for his advice and encouragement during the preparation of this thesis.

The co-operation of the technical staff of the heavy structures laboratory is acknowledged. Special thanks are due to Messrs. J. Morrin, J. Harper, T. Towers and J. McLean, for their assistance in the construction and testing of the experimental models.

I would also like to thank Mr D. Evans of the Advisory at the University of Strathclyde's Computer Centre, and my colleagues of the structural section group for their useful contribution.

The author is deeply indebted to his Government and the University of El-Mansoura, Egypt, for providing the financial support to undertake this study.

Finally, the author records with deep appreciation the patience, understanding and endurance received from his direct and extended family. The marvellous support received from his wife "Eman", daughter "Lynda" and sons "Mohammad & Osama", during his stay in the U.K. is

gratefully acknowledged.

Thanks are due to Mrs MacKinnon for her neat and diligent typing of the thesis.

ABSTRACT

This study was undertaken to investigate the effects of imperfections in the initial geometry of bracing members on the stability of the structural frameworks. The general non-linear behaviour of frameworks, consisting of single columns, or multistorey frames stiffened by curved bracings, were studied under the effects of combined vertical and horizontal load systems. The study was divided into two main parts.

In part one, the study examined the structural frameworks in the following situations:

i) Influence of initial bowing on the behaviour of individual members subjected to axial or eccentric forces.

ii) General static behaviour of a single column restrained by curved member or members.

iii) General static behaviour and instability of multistorey frameworks with non-linear cross bracings.

It has been the goal of the thesis to reinforce the theory put forward to explain the particular type of instability encountered, therefore a critical state, or transient instability region, has been investigated.

The characteristics of individual curved members were determined using the theory of large deformations. The general behaviour and the stability of frameworks restrained by imperfect bracing systems were studied using tangent slope and influence coefficient techniques.

The results of this study have shown that the initial imperfections of bracings are very important and have major effects on the overall behaviour of the braced frame structures. The particular type of instability encountered, i.e. the critical state or the transient instability region, may be considerably influenced by the initial geometric imperfections of bracings and the relative magnitude of the ratio between vertical and horizontal applied loads on the frameworks. The critical loads have been presented in a series of curves and tables.

In part two of the study, the dynamic behaviour at the critical state, i.e. in the region of transient instability, has been investigated. Numerical methods for the dynamic analysis of structural frameworks have been discussed. A new procedure of numerical differentiation has been presented and its advantage over existing procedures has been shown. The method is convenient for use with a digital computer and can also be used for solving simple problems with a calculator.

In general the results of parameters studied were presented in a series of curves and tables to enable the stability and dynamic actions to be readily determined for a wide range of structural configurations.

Finally, a test programme was carried out to investigate experimentally the non-linear behaviour of frameworks restrained by these imperfect bracings. Three separate models were used in the experimental programme. The experimental results were used to verify the general accuracy of the theoretical methods of analyses. In general the theoretical results and the experimental ones were in very close agreement.

NOTATIONS

The principal symbols used in various chapters are listed below. Other subsidiary symbols are defined where they appear locally in the text.

A_o : Initial rise at mis-dpan of curved member

A_c : Cross sectional area of bracing member

b_s : Breadth of the bracing member

c : Length of the end connection of the bracing member

C_d : Damping coefficient

C_c : Critical damping coefficient

C_1, C_2, C_3, C_4 : Constants of integrations

C_{11} : Constant

D_p : Delay parameter

e : Eccentric length

E : Young's modulus

$E(p)$: Complete elliptic integral of the second kind

$E(p,\psi)$: Incomplete elliptic integral of the second kind

$f(\alpha)$: Mathematical function

F : Force in the bracing system

F_1 : Function of the restoring moment in the bracing system

F_2 : Function of the overturning action due to external loads

F_D : Damping force

F_I : Inertia force

F_c, F_t : Restoring force in compression and tension bracing respectively

$F(p,\psi)$: Incomplete elliptic integrals of the first kind

h : Height of a storey in a multistorey framework

H : Total height of the framework before deformation

H" : Vertical height of the framework after deformation

I : Second moment of inertia of bracing member

K_c, K_t : Axial stiffness of curved bracing in compression and in tension respectively

K : Axial stiffness of combined curved bracing system

K_o : Axial stiffness of initially straight member

K(p) : Complete elliptic integral of the first kind

L : Chord length of loaded member

L_o : Chord length of unloaded curved member

L_s : Total curved length of the member

m : Mass

M, M_o : Bending moments

M_A : Net restoring moment about the base of the equivalent column

n : Degree of the polynomial

N : Number of storeys of Multistorey framework

p : Modulus of elliptic integral

P : Vertical applied load

P_E : Euler buckling load

P_Q : Vertical load applied at the top of equivalent single column

P_{cr} : Elastic critical load defined at $\Delta=\infty$

P_{cr1} : Elastic critical load defined at the onset of transient instability region

$P_{o.w}$: Self weight of the column model

r : Radius of gyration.

R : Radius of curvature of initially curved member

R_i : Ratio between the applied vertical and horizontal loads

R_s : Elastic force in the combined bracing system

s : Slope of a straight line

t : Time

δt : Small time interval

u : Complementary solution for second order differential equation

v : Particular solution for second order differential equation

W : Hotizontal applied load

W_y : Applied load at the onset of plasticity

W_Q : Horizontal load applied at the top of equivalent single column

W_p : Applied load at fully plastic section

W_{cr} : Critical value of the horizontal load at the onset of transient instability region

$X_{d(t)}$: Dynamic displacement at instant of time "t"

$\dot{X}_{d(t)}$: Velocity at instant of time "t"

$\ddot{X}_{d(t)}$: Acceleration at instant of time "t"

δx : Small displacement interval

y_c : Central deflection of the curved member

Z : Span of the framework

Z_p : Plastic modulus of the bracing member

Z_y : Elastic modulus of the bracing member

α : Angle at the end of loaded curved member

α_o : Angle at the end of unloaded curved member

α_{oc} &. α_{ot} : Angles between the chord line of the compression and tension bracing and the vertical position of the framework

α_1 : Rotation angle of the equivalent column

α_{cc} , α_{tc} : Angles between the chord line of the deformed compression, tension bracing and the column respectively

$\theta, \gamma, \zeta, \psi, \varphi, \Omega$: Real angles

δ : Small displacement interval

δ_c & δ_t : Axial deformations in the compression & tenstion bracing in a framework respectively

Δ : Lateral displacement

Δ_1 : Critical displacement at the onset of transient instability

Δ_2 : Lateral displacement at the end of the transient instability region

Δ_y : Axial displacement at the onset of plasticity of bracing member

Δ_p : Axial displacement at fully plastic section for bracing member

ε : Strain

σ : Stress

σ_y : Yield stress

ω : Natural frequency

ω_D : Damping frequency

ζ_d : Damping ratio

CONTENTS

		Page No.
Acknowledgements		i
Abstract		iii
Notation		v
CHAPTER 1 :	INTRODUCTION	2
1.1	Preamble	2
1.2	Previous Work	2
1.3	Scope of Work	7
CHAPTER 2 :	THEORETICAL STATIC BEHAVIOUR OF BENT MEMBERS	12
2.1	Introduction	12
2.1.1	Fundamental Assumptions	12
2.2	Theoretical Analysis of Initially Curved Axially Loaded Strut	13
2.2.1	Basic Equations of Large Deformation Theory of Axially Loaded Strut	14
2.2.1.1	The Lateral Deflection of The Strut	21
2.2.1.2	Limits of Application of General Case of Loading($P \leqslant 1$)	22
2.2.1.3	Solution of Elliptic Integrals	27
2.2.2	Load-Displacement Relationship of Axially Loaded Strut	29
2.3	Theoretical Analysis of Initially Curved Eccentrically Loaded Strut	37
2.3.1	Basic Equations of Large Deformation Theory of Eccentrically Loaded Strut	38
2.3.2	Load Displacement Relationship of Eccentrically Loaded Strut	42
2.4	Theoretical Analysis of Initially Curved Axially Loaded Tie	43
2.4.1	Basic Equations of Large Deformation Theory of Axially Loaded Tie	43
2.4.2	Load Displacement Relationship of Axially Loaded Tie	47

		Page No
2.5	Theoretical Analysis of Initially Curved Eccentrically Loaded Tie	50
	2.5.1 Basic Equations of Large Deformation Theory of Eccentrically Loaded Tie	50
	2.5.2 Load Displacement Relationship of Eccentrically Loaded Tie	52
CHAPTER 3 :	ELASTIC STABILITY OF FRAMEWORKS WITH NON-LINEAR RESTRAINTS	64
3.1	Introduction	64
3.2	The Stability of A Column with Non-linear Lateral Restraints	65
	3.2.1 The Stability of a Column Restrained by a Spring with Non-linear Stiffness,K	65
	3.2.2 The Elastic Critical Loads of a Column with Non-linear Spring	67
	3.2.2.1 The Elastic Critical Load of a Column with a Non-Linear Spring Loaded by a Compressive Force	70
	3.2.2.2 The Elastic Critical Load of a Column with a Non-Linear Spring Loaded by a Tensile Force	71
	3.2.2.3 The Elastic Critical Loads for a Column Restrained by a Combined Bracing System	71
	3.2.2.3.1 Influence of the Ratio "R_i=P/W" on The Phenomenon of Transient Instability	77
	3.2.2.3.2 The Relationship Between The Applied Loads and The Displacement "Δ"	78
3.3	Numerical Solutions to Determine The Transient Instability Region and The Corresponding Critical Load P_{cr1}	79
	3.3.1 Tangent Slope Method	80
	3.3.2 Influence Coefficient Method	83
3.4	The Stability of Multistorey Frameworks Stiffened By Curved Diagonal Bracing	85
	3.4.1 The General Behaviour of A Multistorey Framework with Different Storey Height	93

		Page No
CHAPTER 4 :	EXPERIMENTAL INVESTIGATION UNDER STATIC LOADING	113
4.1	Introduction	113
4.2	Choice of Materials and Setting Out of the Models	113
4.3	Determination of Modulus of Elasticity "E" for the Bracing Members	115
4.4	First Series of Tests (Stiffness Tests)	116
4.4.1	Design and Construction of Model	117
4.4.2	Test Programme for Bracing Properties	118
4.4.3	Test Procedure and Evaluation of Test Results	118
4.4.3.1	Compressive Loading	118
4.4.3.2	Tensile Loading	119
4.4.3.3	Interaction Diagrams for Final Results	120
4.5	Second Series of Tests (Stability Tests)	120
4.5.1	Test Programme for Column Stability	121
4.5.2	Test Procedure and Evaluation of Test Results	122
4.6	Third Series of Tests (Framework Stability Tests)	122
4.6.1	Design and Construction of Model	123
4.6.2	Test Programme for Frame Stability	125
4.6.3	Experimental Procedure	126
CHAPTER 5 :	COMPARISON OF THEORETICAL AND EXPERIMENTAL STATIC RESULTS	136
5.1	Introduction	136
5.2	Comparison of Theoretical Results Obtained from The Theory of Large Deformation with Those From The Theory of Small Deformation (Swannell Formula)	136
5.3	Stiffness-Displacement Interaction Diagrams	138
5.3.1	Observations on Stiffness-Displacement Diagrams	139
5.4	Load-Displacement Interaction Diagrams Concerning the Behaviour of Individual Bracings	143
5.5	Interaction Diagrams Concerning The Stability of a Column Restrained by a Combined Curved Bracing System	145

		Page No
5.6	Interaction Diagrams Concerning the Stability of the Multistorey Framework Stiffened by Curved Diagonal Bracings	151
5.6.1	Comparison Between Theoretical and Experimental Results	152
5.6.1.1	Load-Displacement Interaction Diagrams Concerning the Stability of Frameworks	153
5.7	Effect of Initial Rise "A_o" of The Combined Bracing System on The Behaviour of the Framework	154
5.8	Comparison of Results Obtained by Tangent Slope and Influence Coefficient Methods	155
CHAPTER 6 :	DYNAMIC BEHAVIOUR OF FRAME STRUCTURE RESTRAINED BY NON-LINEAR RESTRAINTS	219
6.1	Introduction	219
6.2	Dynamic Equations for Idealized Frame Structure	220
6.2.1	Dynamic Equations for a Single Column Restrained by Curved Bracing System	220
6.2.2	Dynamic Equations for a Multistorey Framework Restrained by Diagonal Curved Bracing System	223
6.3	Numerical Methods for Dynamic Analysis	224
6.3.1	Constant Time Interval Method	224
6.3.2	Constant Displacement Interval Method	231
6.3.2.1	Incremental Equation of Equilibrium	232
6.3.2.2	Solution of Incremental Equation of Motion	234
6.3.2.3	Summary of the Constant Displacement Interval Method	241
CHAPTER 7 :	EXPERIMENTAL DYNAMIC BEHAVIOUR	246
7.1	Introduction	246
7.2	Design and Construction of Model	246
7.3	Test Programme	248
7.4	Instrumentation	248
7.4.1	Systematic Development of Experimental Work	248

		Page No
7.4.2	Measurement of the Dynamic Response of the Structure	248
7.4.2.1	Measurement of the Displacement by the Use of Potentiometer	249
7.4.3	Recording Instruments	251
7.4.3.1	Recording and Conversion of Data for Computer Analysis	251
7.5	Experimental Procedure	252
7.6	Evaluation of Test Results	254
CHAPTER 8 :	COMPARISON OF THEORETICAL AND EXPERIMENTAL DYNAMIC RESULTS	266
8.1	Introduction	266
8.2	Comparison of Theoretical Results Obtained by Constant Time Interval and Constant Displacement Interval Methods	266
8.3	Comparison of Experimental and Theoretical Results	267
8.3.1	Comparison of Dynamic Displacements	270
8.3.2	Comparison of Accelerations	271
8.4	Effect of Initial Rise "A_o" of the Bracings on the Dynamic Behaviour of the Framework	272
8.5	Discussion of the Results	273
8.5.1	Experimental Error Discussion	273
8.5.2	Theoretical Error Discussion	275
CHAPTER 9 :	CONCLUSIONS AND SUGGESTIONS FOR FUTURE WORK	284
9.1	Description of the Research	284
9.2	Characteristics of Individual Curved Bracings	285
9.3	General Behaviour of Braced Framework Stiffened by Curved Bracing System	286
9.3.1	Estimating the Efficiency of the Tangent Slope Method	287
9.3.2	Influence of Initial Rise "A_o" of the Combined Bracing System	287
9.4	Dynamic Behaviour of Braced Framework Stiffened by Curved Bracing System	288
9.4.1	Influence of Initial Rise "A_o" of the Bracing on the Dynamic Response	289
9.5	Suggestions for Future Work	290
REFERENCES		292

LIST OF TABLES

		Page No
Table (2.1)	: Comparison Between Theoretical Behaviour of Curved Struts	35
Table (2.2)	: Summary of Behaviour of Curved Tie	54
Table (4.1)	: Dimensions of Tested Bracing Members	128
Table (4.2)	: Properties and Young's Moduli of Tested Specimens	128
Table (4.3)	: Combinations of Bracings In Stability Test	129
Table (4.4)	: Combinations of Bracings In Frame Test	129
Table (5.1)	: Comparison Between Theoretical Results at The End of Partially Plastic Regions and Experimental Results	157
Table (5.2)	: The Theoretical And the Experimental Results of The Stability Test	158
Table (5.3)	: Theoretical And Experimental Results for the Stability of Two Storey Framework Model	159
Table (5.4)	: Comparison Between Tangent Slope and Influence Coefficient Results	160
Table (8.1)	: Comparison Between Constant Time Interval and Constant Displacement Interval Methods	267
Table (8.2)	: Summary of the Theoretical and Experimental Dynamic Results	276

PART ONE

STATIC INVESTIGATION

CHAPTER ONE
INTRODUCTION

1.1 Preamble

Problems of instability have engaged the attention of mathematicians and engineers for many years. Among the most important of these problems is that of the stanchion. Euler was the first to define a crippling load for a strut, and the Euler load is still a fundamental quantity in stanchion analysis. The classical analyses of the stability of structures are mostly based on the Euler concepts, which consist of the consideration that the structures have ideal geometrical and material properties, and that the buckling behaviour may be described by linear equations. Although the linearized theories have been proved to agree with the experimental results for structures having nearly idealized conditions, the actual behaviour appeared to be more involved than postulated by the theories. In fact, actual systems are always more or less imperfect in both geometry and material. In some cases, the effects of imperfections may not be pronounced, but in general they have substantial effects on the buckling behaviour.

1.2 Previous Work

Much of the literature on the subject of frame stability has emphasized the need to evaluate the effect of horizontal joint displacements, commonly called the P-delta effect, and the influence of axial force on stability. Undue emphasis on either one or both of these factors could result in a restricted approach to the frame stability problem. Actually, there are other factors that also

influence the stability limit of structural frameworks. Johnston[42] has listed many of these influences but Charles and Jorame [19] classified all these into three groups, i.e. geometry, material and loading.

Geometrical Effects : These consist of:

1. The influence of axial force on member bending stiffness.
2. The effect of horizontal joint displacements, commonly called the P-delta effect.
3. Changes in member chord length resulting from axial strain and bowing.
4. Accidental initial geometric imperfections of member (e.g. camber, twist,etc.)
5. Dimensional variations in the framework due to erection tolerances.
6. Shearing deformations.
7. Local buckling or other local distortions.
8. Out of plane movement of frames.

Material Effects : These consist of:

1. Non-linear stress-strain relationship.
2. Residual stresses present in members prior to loading as a result of manufacturing and fabricating processes.
3. Spread of inelastic zone in members as member forces increase.

Loading Effects : These consist of:

1. Non-proportional loading.
2. Variable repeated loading.

All the above listed factors influence the stiffness of the frame and the first two are the most important. There are situations where one or several of the others could significantly reduce the frame stiffness and thereby reduce the factor of safety with respect to stability.

General instability of multistorey building frames have been discussed from various standpoints by many authors. Bleich [6] shows the analysis for an approximate critical load for buckling in a sway mode for unbraced, uniform multistorey, frames under constant load. The elastic critical loads of multistorey rigidly-jointed sway frame and the frame design were studied by Horne [35], Merchant [59] and Salem [80]. Also an experimental study was carried out by Low [51].

Buckling of braced frames was considered by Goldberg [29] who presented simple formulas for upper and lower bounds on the stiffness of the bracing required to prevent buckling in the sway mode.

However, a problem of increasing concern in the field of elastic stability is the buckling behaviour of structural systems that have small imperfections in the initial geometry of the structure. Such imperfection may have a drastic effect on the critical load. For instance, the critical load of an axially loaded column may be

reduced to one third of the classical buckling load due to the presence of small imperfections in the column. It has been found by Roorda [73] that the critical load of certain types of frame structures as well as arches may be affected by the presence of imperfections.

Many authors have examined particular structures to find out the effect of imperfections on the buckling behaviour, for instance Cox [20] who treated a model structure of a simple supported strut with a non-linear support in the middle, and Swannell [77] who studied the elastic buckling of columns constrained by an initially curved side rail at the middle. The latter considered the axial stiffness of elastic, curved, side rails, using small deflection theory, in which the side rail effect is simulated by an elastic spring. He described the use of this equivalent spring stiffness in an attempt to provide a unified description on the constraint given to a main column member by the provision of side rails at mid-height. The classical analysis of the problem is available in standard texts [35,55,66,85].

A type of buckling which sometimes occurs is when curved elastic elements are so loaded that the loads tend to reduce the curvature. In this case, the buckling consists of a sudden change of curvature or the structure snaps through to a new equilibrium position. This type of buckling has been discussed by a number of authors. The significance of the problem, in so far as it illustrates certain important features in more complicated buckling problems of structures, was pointed out by Fung [22], Fraser [23], Timoshenko [84, 85] and Hoff [109].

In this research the problem is studied not only from the usual static treatment but also from the dynamic point of view. A familiar example, which illustrates the essential feature of the phenomenon of snap through, or transient instability, is the framework restrained by an initially curved bracing system. It is this example that will be treated here.

The general procedures for the solution of problems in structural dynamics are available in standard dynamic texts (95, 104, 111,112,121).

Probably the most powerful technique for dynamic non-linear analysis is the step by step integration procedure using a constant time interval.

In this thesis the numerical methods for the dynamic analysis of structural frameworks have been discussed. A new procedure of numerical differentiation has been presented and its advantage over existing procedures has been shown. The method is convenient for use with a digital computer and can also be used for solving simple problems with a calculator. Consideration is given to various types of damping. The method is capable of application to structures of any degree of complication, with any relationship between force and displacement. Any type of dynamic loading, such as that due to shock or impact, vibration, etc., can be considered.

The method has been used for the computation of the dynamic response of the non-linear behaviour of frameworks restrained by curved bracing systems. The basic technique of analysis is a general

step-by-step method of differentiation of the equations of motion, using a constant displacement interval.

1.3 Scope of Work

The work described in this thesis is concerned with the general investigation of buckling and vibration problems, and to show how initial geometric imperfections affect the buckling behaviour of structural systems. Simple models are included to illustrate the theory of buckling stability for such systems.

The behaviour of braced frames, when the bracing system has an initial bow are studied. This type of imperfection commonly exists in buckling frames and once the bracing members are not perfectly straight, then their behaviour is no longer linear. Analysis shows that the behaviour of frame instability is very much dependent on the initial bowing of the non-linear restraints.

In this thesis three simple models have been set up to study the behaviour of such structures. The first consists of a single column and a bracing member or members. The second consists of a two storey framework with curved diagonal bracing system. The third consists of two frameworks, each frame of which is identifical to the second model which is restrained by curved diagonal bracings. It is intended to represent the initial condition of the framework restrained by initially curved bracings, and then cause failure under controlled conditions observing the phenomenon of "snap through" or "transient instability" between the points when the compression bracing buckles and the tension bracing re-establishes stability.

The work described in this research consists of two main parts, the first deals with the static investigations of the problem, while the second part deals with the dynamic investigation in the region of transient instability. The static investigations are described in Chapters 2,3,4 and 5. The dynamic investigations are presented in Chapters 6,7 and 8.

In Chapter two, the theoretical behaviour and the axial stiffnesses of bent bracing members subjected to compressive or tensile forces are investigated. The general procedure of the large deformation theory is described by using the Bernoulli-Euler equation. The influence of two imperfect parameters on the individual members, i.e. initial bowing and eccentric loading, are investigated. Axially and eccentrically loaded curved members are considered.

In Chapter three, the elastic stability and the theoretical behaviour of frameworks with non-linear restraints are investigated.

The elastic critical load for a column restrained by an equivalent non-linear spring, for curved member or members, is determined. The fundamentals in the theory for simple structures restrained by non-linear restraints are derived. The general procedures of determining the elastic critical loads for multistorey frameworks, restrained by curved bracing systems, are described. The general behaviour of this type of structure can be summarized in three regions such that:

i) The structure is stable and represented by the first stable equilibrium region.

ii) The equilibrium of the structure is unstable and represented by the transient instability region.

iii) The structure is stable again, and represented by the second stable equilibrium region.

The conditions of each region are adopted.

Two numerical methods are developed to determine the limits of the transient instability region and the corresponding applied critical loads. Influence coefficient method and tangent slope technique are employed in the investigation.

Experimental investigations, under static loading carried out to support the theoretical investigations, are described in Chapter four. Three separate groups of tests have been performed on a small scale for a single column with non-linear restraint or restraints, and also for a two-storey framework model with non-linear cross bracings.

In Chapter five, the theoretical techniques are applied to the analyses of initially curved members, column model, and two storey framework model restrained by non-linear restraints. The convergence characteristics, accuracy,and computing efficiency of the techniques are evaluated by comparing the results obtained by experiment with the theoretical results available by others and those obtained by the methods described. Curves are presented to explain the general behaviour of these types of structures.

In part two of this research, the problem of frame structures restrained by non-linear bracing systems is approached from the dynamic point of view, in contrast to the usual static treatment. The buckling of this type of frame structure occurs when the curved bracing elements are so loaded that the loads tend to reduce the curvatures of the tension bracings while increasing the curvatures of

the compression bracings. In this case the structure snaps through to a new equilibrium position, and a dynamic effect is very important on the overall behaviour of the structure. The dynamic behaviour allows the structure to sway freely through the region of transient instability. The structure may or may not, return to its original configuration.

The dynamic behaviour of this type of structure, in the transient instability region,is investigated in Chapter six. Two methods are employed to evaluate the dynamic response. Constant time interval and constant displacement interval techniques are employed in the investigation.

In Chapter seven, the results of an experimental dynamic investigation carried out to support the theoretical investigations of frame structures restrained by curved diagonal bracing system have been presented. Accelerations and displacements at the top of the framework are obtained in the tests using a small scale two storey frame model. The dynamic response has been recorded onto 4 channel tape recorder. An Apple II_e micro computer has been used to digitise the records.

In Chapter eight, the influence of various combinations of bracing sets on the dynamic behaviour of a framework,is investigated by applying the theoretical techniques to the two storey framework model. The convergence of dynamic characteristics, accuracy, and computing efficiency of the technique are evaluated by comparing the results obtained from the theoretical analysis with those from experimental results. Curves and tables are presented

to explain the general dynamic behaviour of such types of structures.

The closing chapter summarizes the main conclusions reached in this thesis and indicates possible areas for future investigations.

CHAPTER TWO

THEORETICAL STATIC BEHAVIOUR OF BENT MEMBERS

2.1 Introduction

This chapter is divided into two parts, the first deals with methods for the calculation of displacements and axial stiffnesses of elastic curved struts, subjected to axial forces, using a theory for large deformations. The second part explains how the large deformation theory can be applied to ties loaded by axial tensile forces. Methods are described also for the calculation of the axial stiffnesses and the displacements of these ties.

The basic equations are derived in both parts by using Bernoulli-Euler equation, which states that the change of curvature of a rod is proportional to the bending moment producing it.

2.1.1 Fundamental Assumptions

The fundamental assumptions made in the development of the theory of the initially curved members are as follows:

1. The material of the member is linearly elastic.
2. The member is of uniform cross-section.
3. The initial curvature is circular.
4. The member is unstressed when it is not loaded.
5. Each end of the member is connected to a frictionless pin which ensures that the bending moment at each end is zero.
6. The member is assumed to be inextensible, hence its length is the same before and after loading.

2.2 Theoretical Analysis of Initially Curved Axially Loaded Strut

Compression members are key elements of almost all structures. The study of their behaviour is essential for the understanding of the behaviour of structures, such as columns, beams or components of frames. Compressed members may be defined as members carrying a compressive load, and whose length is considerably greater than the cross-sectional dimensions. Such a member may carry other loading, and may have end conditions and moments of any type. This section is concerned only with members carrying a compressive load.

Generally in practice a strut will not be exactly straight, and the line of thrust will not pass exactly through the centroids of its terminal cross-sections. On both accounts it will be subjected to bending action, and lateral deflection will occur from the first application of load.

To study the behaviour of an initially curved strut under axial loads at both ends, consider an initially curved (circular) strut shown in Figure (2.1). The strut is hinged at one end (a) and supported on a frictionless roller at the other end (b). The strut is initially curved to form an arc of a circle of radius (R), and rise (A_o) at the mid-span. Also the strut is subjected to end loading with the line of action along the line of the supports.

Before starting the basic equations of large deformation theory it is important to define the axial stiffness which is denoted by K. This is defined as the load, applied along the chord-line of the member, which will produce a total shortening of the chord line equal to unity.

i.e. $W = K.\Delta$ (2.1)

where,

W is the axial load applied along the chord line of the member,

K is the axial stiffness of the member

Δ is the shortening of the chord-line of the member.

2.2.1 Basic Equations of Large Deformation Theory of Axially Loaded Strut

The co-ordinate axes are shown in the Figure (2.1a). The distance s is measured along the curved length of the strut from the origin a. Curvature can be expressed in terms of the slope of the member at any point as $d\theta/ds$. Since the bending moment in the strut is equal to the flexural rigidity times the curvature, the differential equation expressing the bending moment is:

$$-EI\left(\frac{d\theta}{ds} - \frac{d\theta_o}{ds}\right) = M \qquad (2.2)$$

where,

EI is the flexural rigidity, s denotes the distance of the section considered from the origin (a) measured along the central-line of the loaded strut, θ is the inclination of the centre-line of the deflected form to the line of thrust, at the section considered, θ_o is the inclination of the centre-line of the initially curved strut to the line of thrust at the section considered, and M is the bending moment at this section.

From Fig. (2.1a), the bending moment M at section s_1-s_1 is:

$$M = + wy \qquad (2.3)$$

Thus, equation (2.2) becomes:

$$-EI\left(\frac{d\theta}{ds} - \frac{d\theta_o}{ds}\right) = W.y \qquad (2.4)$$

Differentiating equation (2.4) with respect to s and using the relation; $\frac{dy}{ds} = \sin(\theta)$, as shown in Fig. (2.1b), the following equation is obtained:

$$\left(\frac{d^2\theta}{ds^2} - \frac{d^2\theta_o}{ds^2}\right) = -\frac{W}{EI}.\ \sin(\theta) \qquad (2.5)$$

Equation (2.5) can be rearranged by noting that $\frac{d^2\theta_o}{ds^2} = 0$ for a circle and substituting $\mu^2 = \frac{W}{EI}$ to give:

$$\frac{d^2\theta}{ds^2} = -\mu^2\sin(\theta) \qquad (2.6)$$

Multiplying both sides of equation (2.6) by $2d\theta = 2(d\theta/ds)\,ds$ and integrating, yields

$$2\int \frac{d^2\theta}{ds^2} \cdot \frac{d\theta}{ds} \cdot ds = -2\mu^2 \int \sin(\theta).\ d\theta \qquad (2.7)$$

Which can then be expressed in the form:

$$2\int \left[\frac{d}{ds}\left(\frac{d\theta}{ds}\right)\right].\left(\frac{d\theta}{ds}\right).ds = -2\mu^2 \int \sin(\theta)\ .\ d\theta$$

or

$$\int \left[\frac{d}{ds}\left(\frac{d\theta}{ds}\right)^2\right] .\ ds = -2\mu^2 \int \sin(\theta).\ d\theta \qquad (2.8)$$

Evaluation of the integrals, gives

$$\left(\frac{d\theta}{ds}\right)^2 = 2\mu^2\cos(\theta) + C_1 \qquad (2.9)$$

where,

C_1 is a constant of integration which is determined from the boundary condition, which states that;

At : x=0 (i.e. at the hinged end 'a')

$$\frac{d\theta}{ds} = -\frac{1}{R} \quad \text{and} \quad \theta = \alpha \tag{2.10}$$

where,

R is the radius of curvature of the initially curved member and

α is the angle at the ends of the loaded form.

Since the bending moment at 'a' is zero, hence the curvature remains the original curvature $\frac{1}{R}$ of the unloaded form. Therefore substituting of Eq. (2.10) in Eq. (2.9) gives:

$$C_1 = \frac{1}{R^2} - 2\mu^2\cos(\alpha) \tag{2.11}$$

Therefore equation (2.9) becomes:

$$(\frac{d\theta}{ds})^2 = 2\mu^2\,[\cos(\theta) - (\cos(\alpha) - \frac{1}{2\mu^2R^2})\,] \tag{2.12}$$

using the substitution;

$$\cos(\gamma) = \cos(\alpha) - \frac{1}{2\mu^2R^2} \tag{2.13}$$

where, γ is a real angle, transforms the equation (2.12) into:

$$(\frac{d\theta}{ds})^2 = 2\mu^2\,[\cos(\theta) - \cos(\gamma)]$$

Taking the square root on both sides, yields:

$$\frac{d\theta}{ds} = \pm \mu\sqrt{2} \cdot \sqrt{\cos(\theta) - \cos(\gamma)} \qquad (2.14)$$

The sign of the right-hand side of this equation depends on the sign of $\frac{d\theta}{dS}$. Assuming that the strut buckles as shown in Fig. (2.1a), so that θ decreases while S increases according to the axes shown in the figure, then the curvature $\frac{d\theta}{ds}$ is always negative and the positive sign will be dropped from the right hand side of Eq. (2.14). The equation can be rearranged to give:

$$ds = -\frac{d\theta}{\mu\sqrt{2}\sqrt{\cos(\theta)-\cos(\gamma)}} \qquad (2.15)$$

The total length of the strut (L_s), which equals two times the length of the arc in the first half, can be written as a function of the angle α by integrating Eq. (2.15). This length is given by the following:

$$L_s = 2\int_0^{L_s/2} ds = -\frac{\sqrt{2}}{\mu}\int_{\alpha}^{0} \frac{d\theta}{\sqrt{\cos(\theta)-\cos(\gamma)}}$$

or

$$L_s = \frac{\sqrt{2}}{\mu}\int_0^{\alpha} \frac{d\theta}{\sqrt{\cos(\theta)-\cos(\gamma)}} \qquad (2.16)$$

The integral on the right-hand side of Eq. (2.16) cannot be evaluated in closed form in terms of an elementary function. However this integral represents a new non-elementary function of α and γ, called an elliptic integral[7,81] of the first kind, which can be written in a standard form. This form may be obtained by means of suitable changes in the variables of integration.

For this purpose, use the identities

$$\cos(\theta) = 1 - 2\sin^2\left(\frac{\theta}{2}\right),$$

$$\cos(\gamma) = 1 - 2\sin^2\left(\frac{\gamma}{2}\right),$$

and substitute

$$\sqrt{\cos\theta - \cos\gamma} = \sqrt{2\left(\sin^2\frac{\gamma}{2} - \sin^2\frac{\theta}{2}\right)}$$

$$= \sqrt{2}\sin\frac{\gamma}{2}\sqrt{1 - \frac{\sin^2\frac{\theta}{2}}{\sin^2\frac{\gamma}{2}}} \qquad (2.17)$$

Since,in Eq. (2.16) the limit of integration is from 0 to α therefore the variable θ will satisfy the condition $0 < \theta < \alpha$ and, by assumption according to Eq. (2.13), $0 < \alpha < \gamma$

i.e. $\sin\frac{\theta}{2} < \sin\frac{\gamma}{2}$ or $0 < \sin\frac{\theta}{2} / \sin\frac{\gamma}{2} < 1$

The ratio $\sin\frac{\theta}{2} / \sin\frac{\gamma}{2}$ being a positive number not greater than unity, may be considered the sine of an angle φ.

$$\sin\varphi = \frac{\sin\frac{\theta}{2}}{\sin\frac{\gamma}{2}} = \frac{\sin\frac{\theta}{2}}{p} \qquad (2.18)$$

where, $p = \sin\frac{\gamma}{2}$ (2.19)

Substituting Eqs. (2.18) and (2.19) in Eq. (2.17),hence Eq. (2.17) becomes in terms of φ , such as:

$$\sqrt{\cos\theta - \cos\gamma} = \sqrt{2}\sin\frac{\gamma}{2}\sqrt{1 - \frac{\sin^2\frac{\theta}{2}}{\sin^2\frac{\gamma}{2}}} = \sqrt{2}\,p\sqrt{1-\sin^2\varphi}$$

$$= \sqrt{2}\,p\cos\varphi \qquad (2.20)$$

To obtain the differential of θ in terms of the new variable of integration φ , multiply Eq. (2.18) by p and differentiate both sides:

$$\frac{1}{2}\cos\frac{\theta}{2}\,.\,d\theta \;=\; p.\cos\varphi\;\; d\varphi \quad ,$$

from which,

$$d\theta \;=\; \frac{2p\,\cos\varphi d\varphi}{\cos\frac{\theta}{2}} \;=\; \frac{2p\,\cos\varphi d\varphi}{\sqrt{1-p^2\sin^2\varphi}} \qquad (2.21)$$

Noting finally that, according to Eq. (2.18):

$$\varphi \;=\; 0 \text{ at } \;\theta = 0\;,\;\; \varphi = \sin^{-1}\left(\frac{\sin\frac{\alpha}{2}}{\sin\frac{\gamma}{2}}\right) \equiv \psi \;\text{ at } \theta = \alpha \qquad (2.22)$$

i.e. $$\sin\psi \;=\; \frac{\sin\frac{\alpha}{2}}{\sin\frac{\gamma}{2}}$$

or

$$\sin^2\psi \;=\; \frac{1-\cos\alpha}{2\sin^2\frac{\gamma}{2}} \qquad (2.23)$$

By substituting Eqs. (2.13) and (2.19) into Eq. (2.23), the angle ψ can be written as follows:

$$\sin^2\psi = \frac{2p^2 - \frac{1}{2\mu^2R^2}}{2p^2} = 1 - \frac{1}{4p^2\mu^2R^2}$$

and therefore $$\cos^2\psi \;=\; \left(\frac{1}{2p\mu R}\right)^2$$

or

$$\psi \;=\; \cos^{-1}\left(\frac{1}{2p\mu R}\right) \qquad (2.24)$$

By substituting Eqs. (2.20), (2.21) and (2.22) into Eq. (2.16), the curved length L_s can be expressed as:

$$L_s = \frac{2}{\mu} \int_0^{\psi} \frac{d\varphi}{\sqrt{1-p^2\sin^2\varphi}} \tag{2.25}$$

The integral on the right-hand side of Eq. (2.25) is a function of the upper limit of integration ψ and the parameter p, and is called the incomplete elliptic integral of the first kind [81] which it can be written in the form $F(p,\psi)$.

The length L_s of the strut (2.25) is thus written as:

$$L_s = \frac{2}{\mu} F(p,\psi) = \frac{2}{\mu} \int_0^{\psi} \frac{d\varphi}{\sqrt{1-p^2\sin^2\varphi}} \qquad (p < 1) \tag{2.26}$$

The upper limit "ψ" of this integral is called the amplitude of "F" and p is called its modulus.

As the variable θ of the integral of Eq. (2.16) varies between zero and its maximum value α, the variable φ of the integrals of Eqs. (2.25) and (2.26) varies between zero and ψ , where ψ depends on the value of μ (i.e. the applied load W) and the radius of curvature "R," as seen from Eq. (2.24).

When the initial rise "A_o" of the strut is very small and approaches zero, the radius of curvature "R" will approach infinity and therefore the angle ψ in Eq. (2.24) will tend to $\pi/2$, hence Eq. (2.26) will change to the following:

$$L_s = \frac{2}{\mu} \int_0^{\pi/2} \frac{d\varphi}{\sqrt{1-p^2\sin^2\varphi}} \tag{2.27}$$

The integral appearing in this equation is known as a complete elliptic integral of the first kind, this integral is a function of the parameter p only and it is usually symbolized by K(p) [7,81].

The solution of the flat strut problem may now be written in terms of the elliptic integrals as,

$$L_s = \frac{2}{\mu} \int_0^{\pi/2} \frac{d\varphi}{\sqrt{1-p^2\sin^2\varphi}} = \frac{2}{\mu} K(p) \qquad (2.28)$$

Now, when the deflection of the strut is very small, the angle α and the modulus p will also be small and the term $p^2\sin^2\varphi$ in Eq. (2.28) can be neglected in comparison with unity, then the following is obtained,

$$L_s = \frac{2}{\mu} \int_0^{\pi/2} d\varphi = \frac{\pi}{\mu} = \pi\sqrt{\frac{EI}{W}} \quad (\text{since } \mu^2 = \frac{W}{EI}) \qquad (2.29)$$

and
$$W = P_E = \frac{\pi^2 EI}{L_s^2} \qquad (2.30)$$

The value of the applied load "P_E" in Eq. (2.30) is called the Euler buckling load [2,85], and represents the value of W at which the flat strut starts buckling.

2.2.1.1 The Lateral Deflection of the Strut

In order to calculate the lateral deflection of the strut, it can be seen from Fig. (2.1.b) that:

$$dy = \sin\theta \, .ds \qquad (2.31)$$

By substituting Eq. (2.15) in Eq. (2.31), yields,

$$dy = - \frac{\sin\theta \, d\theta}{\mu\sqrt{2}\sqrt{\cos\theta - \cos\gamma}} \qquad (2.32)$$

The deflection at any point can be obtained by integration of this expression. Then the central deflection is given by:

$$y_c = \frac{1}{\sqrt{2}\mu} \int_0^{\alpha} \frac{\sin\theta \, d\theta}{\sqrt{\cos\theta - \cos\gamma}} \qquad (2.33)$$

From Eqs. (2.18) and (2.19) it is known that:

$$\sin\frac{\theta}{2} = p \sin\varphi \qquad (2.34)$$

therefore $\cos\frac{\theta}{2} = \sqrt{1-p^2\sin^2\varphi}$

Using the relationship $\sin\theta = 2\sin\frac{\theta}{2}\cos\frac{\theta}{2}$, the value $\sin\theta$ can be written as follows:

$$\sin\theta = 2p\sin\varphi \sqrt{1-p^2\sin^2\varphi} \qquad (2.35)$$

Substituting Eqs. (2.20), (2.21), (2.22) and (2.35) into Eq. (2.33) and changing the limits of integration to φ ($\varphi=\psi$ when $\theta=\alpha$), the central deflection"y_c"is represented by the expression :

$$y_c = \frac{1}{2\mu} \int_0^{\psi} 4p \sin\varphi . \, d\varphi = \frac{2p}{\mu}(1-\cos\psi) \qquad (2.36)$$

Once the end angle"α"is known, Eqs. (2.13), (2.19), (2.24) and (2.36) can be used to determine the vertical deflection"y_c", at the mid-span of the strut, measured from the chord line 'ab'.

2.2.1.2 Limits of Application of General Case of Loading ($p \leqslant 1$)

A close inspection of Eq. (2.13) reveals that:

$$\cos\alpha = \cos\gamma + \frac{1}{2\mu^2R^2} \qquad (2.37)$$

fails for small values of W (or μ) since $-1 \leqslant \cos\alpha \leqslant 1$ for real α. Therefore it becomes necessary to establish the range of application of the equations derived in sections (2.2.1) and (2.2.1.1)

Explanation of the failure of Eq. (2.37) will more readily be understood if the analysis of the curved strut begins from the basic horizontal strut. Consider a straight horizontal strut subjected to a load W at its ends and moments $M_o = \frac{EI}{R}$ acting at the same points, Fig. (2.2.a). The action of the moments M_o will bend the strut into a circular arc of radius R, while the load W is still acting on the ends, Fig. (2.2.b). This strut is, therefore, the circular strut of the original problem. Consider the left half of the strut, where the central point c is held in its position and the end"a"becomes free, Fig. (2.2.c). The moment M_o and the load W will now be replaced by a force W acting on a rigid lever of length $e = \frac{M_o}{W}$, Fig. (2.2.c), and so far as the shape"ca"is concerned, it does not matter whether the load acts on the bar"cad"or through the lever e. It is known that:

$$e = \frac{EI}{R.W} = \frac{1}{\mu^2 R} \qquad (2.38)$$

$$p = \sin\left(\frac{\gamma}{2}\right) \quad , \quad \text{and} \quad \sin\left(\frac{\alpha}{2}\right) = p \sin\psi$$

where, the expression $\sin(\frac{\alpha}{2}) = p \sin\psi$ is satisfied for all points along the strut 'cad' , Fig. (2.2.c).

Also it is seen from Fig. (2.2.c) that:

$$e = h \cos\psi \qquad (2.39)$$

where, h represents the maximum vertical deflection of the strut, when $\psi \to \frac{\pi}{2}$. This max deflection (h) can be determined from equation (2.36) when $\psi = \frac{\pi}{2}$, and is equal to :

$$h = \frac{2p}{\mu} \tag{2.40}$$

By substituting of Eqs. (2.38) and (2.40) into Eq. (2.39) the value of ψ can be obtained:

$$\psi = \cos^{-1}\left(\frac{1}{2p\mu R}\right)$$

which is identical with equation (2.24).

Also, $\cos\gamma = 1-2\sin^2(\frac{\gamma}{2}) = 1 - 2p^2$

and

$$\cos\alpha = 1-2\sin^2(\tfrac{\alpha}{2}) = 1 - 2p^2\sin^2\psi$$

$$= 1-2p^2 + \frac{1}{2\mu^2R^2} = \cos\gamma + \frac{1}{2\mu^2R^2}$$

(this equation is obtained from $\sin^2\psi = 1 - \frac{1}{4p^2\mu^2R^2}$)

This shows that the auxiliary angle γ in equation (2.13) is actually the end slope of the imaginary extension of the basic strut. And this angle should satisfy the following condition.

$$\gamma \leqslant \pi \quad \text{, to give} \quad p \leqslant 1 \tag{2.41}$$

Now, as seen clearly from Fig. (2.2.c) and Eq. (2.38), decreasing W means increasing the rigid lever e, since the moment M_o depends on EI and R only, and these are given. On the other hand, e cannot grow indefinitely, as at some value of e the line of action of W will bypass

the imaginary extension of the strut, Fig. (2.2.d). Also note that e will increase with γ , but $\gamma \leqslant \pi$, hence $p_{max} = 1$. With p=1 equation (2.26) reduces to:

$$\frac{\mu L_s}{2} = \int_0^{\psi} \sec\varphi \, d\varphi = \text{Ln} \tan(\frac{\pi}{4} + \frac{\psi}{2}) \qquad (2.42)$$

Since $\psi = \cos^{-1}(\frac{1}{2\mu R})$, equation (2.42) can be solved for $\mu = \mu_o$ and hence for $W = W_o$. W_o marks the lower limit of the applicability of the equations corresponding to the general case of loading and derived in the sections (2.2.1) and (2.2.1.1.).

To study the behaviour of the strut when $W < W_o$, i.e. when $p > 1$, consider the following assumption:

$$p_o = \frac{1}{p} \leqslant 1 \qquad (2.43)$$

According to this assumption the end angle α can be written in terms of the new parameter p_o by replacing the expression $\cos\gamma$, $(\cos\gamma = 1-2p^2)$ in equation (2.13) by $(1-\frac{2}{p_o^2})$. Then the end angle α is given by:

$$\sin(\frac{\alpha}{2}) = [(\frac{1}{p_o})^2 - (\frac{1}{2\mu R})^2]^{\frac{1}{2}} \qquad (2.44)$$

This equation will not fail for small values of W because p_o decreases with W at such a rate the expression under the square root remains positive. No matter how small W is chosen, there is always a positive p_o for which

$$2R\sqrt{W/EI} > p_o \qquad (2.45)$$

The curved length of the strut L_s can be written in terms of p_o by transforming the terms ψ, φ and p relatively to p_o, as follows:

Eq. (2.18) can be written in the form:

$$p\sin\varphi = \sin\varphi_1 \tag{2.46}$$

or

$$\sin\varphi = p_o\sin\varphi_1 \tag{2.47}$$

Then, the differential of φ can be obtained in terms of the new variable φ_1 by differentiating both sides of equation (2.47), hence

$$d\varphi = \frac{p_o\cos\varphi_1\, d\varphi_1}{\sqrt{1-p_o^2\sin^2\varphi_1}} \tag{2.48}$$

According to Eqs (2.43) and (2.47) noting that:

$$\sqrt{1-p^2\sin^2\varphi} = \cos\varphi_1 \tag{2.49}$$

Also according to Eqs (2.34) and (2.47) noting finally that:

$$\varphi_1 = 0 \quad \text{at } \varphi = 0$$

$$\varphi_1 = \frac{\alpha}{2} \quad \text{at } \varphi = \psi \text{ or } \theta = \alpha \tag{2.50}$$

Finally substution of Eqs. (2.48), (2.49) and (2.50) in Eq. (2.26) gives:

$$L_s = \frac{2p_o}{\mu}\int_o^{\frac{\alpha}{2}} \frac{d\varphi_1}{\sqrt{1-p_o^2\sin^2\varphi_1}} = \frac{2p_o}{\mu}\, F(p_o, \tfrac{\alpha}{2}) \tag{2.51}$$

where $p_o < 1$ and $F(p_o, \frac{\alpha}{2})$ represent the elliptic integral of the first kind with modulus p_o and amplitude $\frac{\alpha}{2}$.

2.2.1.3 Solution of Elliptic Integrals

The value of $F(\varphi, \psi)$ or $F(\varphi_o, \frac{\alpha}{2})$ stands for the elliptic integral of the first kind with modulus p or p_o and amplitude ψ or $\frac{\alpha}{2}$ respectively. These integrals contain the unknown p or p_o only. It is seen clearly from Eqs. (2.13) and (2.19) or (2.43) that the modulus p or p_o depends only on the end angle α. Therefore the elliptic integral $F(\varphi, \psi)$ or $F(\varphi_o, \frac{\alpha}{2})$, for given values of the applied load W and rise A_o (i.e. μ and R are given), may be obtained, step by step, by giving to α arbitrary values, deriving the corresponding values of p or p_o and ψ or $\frac{\alpha}{2}$ from equations (2.13), (2.19) or (2.43) and (2.24) respectively, and evaluating the corresponding value of $F(\varphi, \psi)$ or $F(\varphi_o, \frac{\alpha}{2})$ using tables of elliptic integrals [71]. However, $F(\varphi, \psi)$ or $F(\varphi_o, \frac{\alpha}{2})$ can be evaluated more accurately by using the computer library routine "S21BBF" [67]. This routine returns a value of the symmetrisied elliptic integral of the first kind, via the routine name. The accurate value of α and, hence, the exact numerical evaluation of the first elliptic integral $F(\varphi, \psi)$ or $F(\varphi_o, \frac{\alpha}{2})$ can be determined from the equation (2.26) or (2.51), where the relations between these functions and α can be obtained explicitly for a given value of L_s. These explicit functions can be solved by using iterative methods [9]. These methods are suitable for use in cases where the solution is to be carried out by a computer. Several methods of successive approximation may be used to determine the value of the roots of an equation to a specified degree of accuracy, and one of these methods is used to solve this problem, namely linear interpolation. The method attempts to obtain an approximation to a simple continuous zero of the function $f(\alpha)$. In a given initial

interval (α_{min}, α_{max}), such that $f(\alpha_{min}) \times f(\alpha_{max}) \leqslant 0$. Hence, an approximate value of the root "α" is estimated, called the first approximation, and then a more accurate result is determined by the repitition of the same procedure. The more accurately the first approximation is obtained, the less the number of repetitive cycles, called iterations, need be obtained for a given degree of accuracy. The first approximation can be estimated by a method involving functional notation as shown below.

The approximate value of "α" at the point where the curve of $f(\alpha) = 0$ crosses the x-axis is used as the first approximation. This occurs when the value of $F(\alpha)$ changes from positive to negative or from negative to positive.

Consider the equation $f(\alpha) = L_s - \frac{2}{\mu} F(p,\psi) = 0$ (from Eq. (2.26)) and when $\alpha = \alpha_o$, $f(\alpha_o)$ is positive value,

when $\alpha = \alpha_1$, $f(\alpha_1)$ is positive value,

when $\alpha = \alpha_2$, $f(\alpha_2)$ is negative value.

Since the sign of $f(\alpha)$ changes from a positive value at $f(\alpha_1) = f(\alpha_{min})$ to a negative value at $f(\alpha_2) = f(\alpha_{max})$, then the first approximation is between $\alpha_1 = \alpha_{min}$ and $\alpha_2 = \alpha_{max}$. If a straight line is drawn between co-ordinates (α_{min}, $f(\alpha_{min})$) and (α_{max}, $f(\alpha_{max})$), it will cut the x-axis at $\alpha_3 = \alpha_{app}$ where

$$\alpha_{app} = \alpha_{max} - \frac{f(\alpha_{max}) \times (\alpha_{min} - \alpha_{max})}{f(\alpha_{min}) - f(\alpha_{max})} \qquad (2.52)$$

so, a first approximation of α is taken as α_3.

A more accurate value of the root (α) can be determined by estimating the value of $f(\alpha)$ when $\alpha = \alpha_3$ and the product of $f(\alpha_{min}) \times f(\alpha_3)$ and $f(\alpha_{max}) \times f(\alpha_3)$ can be calculated. Then assume one of these products is less than or equal to zero, such that $f(\alpha_{min}) \times f(\alpha_3) < 0$, and the other product is greater than zero. In this case the value of $f(\alpha_{max})$ will be replaced by the value of $f(\alpha_3)$, then the second approximation is between $\alpha_1 = \alpha_{min}$ and $\alpha_3 = \alpha_{max}$. If again a straight line is drawn between the new minimum and maximum co-ordinates "α_{min}, $f(\alpha_{min})$ and (α_{max}, $f(\alpha_{max})$" it will cut the x-axis at a new approximate value, $\alpha_{app} = \alpha_4$, where α_4 can be determined from equation (2.52). Therefore a second approximation of α is taken as α_4. A better approximation of the root (α) can be obtained by repeating the procedure for $\alpha = \alpha_5, \alpha_6, \ldots$ until the root does not change on two conseucutive iterations when expressed to the stipulated degree of accuracy.

Finally a gradual increase of the applied load"W"will be followed by a new value of the end angle"α", and hence, new values for the modulus p or p_o and amplitude ψ or $\frac{\alpha}{2}$. However these values can be found readily for any value of"W".

2.2.2 Load Displacement Relationship of Axially Loaded Strut

A problem of more practical interest is to relate the applied load (W) with its corresponding relative displacement of the loaded ends. This displacement will be given by "Δ" (Fig. 2.1.b), which consists of two parts. The first part is the shortening due to bowing, "Δ_B" and that can be represented by the following equation,

$$\Delta_B = L_o - L \tag{2.53}$$

where, L_o is the chord length of the unloaded strut;,

L is the chord length of the deflected shape.

The second part is the axial shortening of the strut due to direct stress and this is equal to $\frac{W}{EA_c} \times L_s$ or $\frac{Wr^2}{EI} \cdot L_s$

where, A_c is the cross sectional area of the strut

E is the Young's modulus

and $r = (\frac{I}{A})^{\frac{1}{2}}$ is the radius of gyration.

This component represents a very small value, if it is compared to the shortening due to bowing and therefore it can be neglected. This assumption is justified for large deflections of columns, by Chen [14].

It is now only necessary to compute the shortening of the chord line $\Delta = \Delta_B$ and this can be calculated from Eq. (2.53).

The chord length L_o is usually known, but the length "L" (Fig. 2.1.a) measured along the line of thrust is given by the equation:

$$L = 2 \int_0^{L/2} dx \tag{2.54}$$

And from Fig. (2.1.b) it is noted that:

$$dx = ds \cdot \cos\theta \tag{2.55}$$

Substituting Eqs. (2.15) and (2.55) in Eq. (2.54), and changing the limits of integration to α ($\theta=\alpha$ at $x=0$ and $\theta=0$ at $x=\frac{L}{2}$), then the chord length L can be written in the form:

$$L = \frac{\sqrt{2}}{\mu} \int_{o}^{\alpha} \frac{\cos\theta \cdot d\theta}{\sqrt{\cos\theta - \cos\gamma}} \qquad (2.56)$$

The integral on the right-hand side of this equation can be written in the standard elliptic integral forms. These forms may be obtained, by making use of Eqs. (2.20), (2.21), (2.22) and (2.24) and noting that

$$\cos(\theta) = 1-2\sin^2\left(\frac{\theta}{2}\right) = 1 - 2p^2\sin^2\varphi \qquad (2.57)$$

Then, the equation of the chord length of the loaded strut is given by

$$L = \frac{2}{\mu} \int_{o}^{\psi} \frac{(1-p^2\sin^2\varphi).d\varphi}{\sqrt{1-p^2\sin^2(\varphi)}}$$

or

$$L = \frac{2}{\mu} \int_{o}^{\psi} \frac{d\varphi}{\sqrt{1-p^2\sin^2(\varphi)}} - \frac{4p^2}{\mu} \int_{o}^{\psi} \frac{\sin^2(\varphi) .d\varphi}{\sqrt{1-p^2\sin^2(\varphi)}} \qquad (2.58)$$

The first integral in Eq. (2.58) can be written in the standard form of the first kind of elliptic integral $"F(p,\psi)$ as mentioned before. The second integral in Eq. (2.58) is equal to:

$$\int_{o}^{\psi} \frac{\sin^2(\varphi).\, d\varphi}{\sqrt{1-p^2\sin^2(\varphi)}} = \frac{1}{p^2} \{ \int_{o}^{\psi} \frac{d\varphi}{\sqrt{1-p^2\sin^2(\varphi)}} - \int_{o}^{\psi} \sqrt{1-p^2\sin^2(\varphi)}.d\varphi \}$$

.....(2.59)

The first integral on the right-hand side of Eq. (2.59) is again $F(p,\psi)$, while the second is another non-elementary function of p and ψ, usually indicated by $E(p,\psi)$ and called the incomplete elliptic integral of the second kind [7,8.1]. The numerical value of $E(p,\psi)$ can

be evaluated accurately by using the "NAG" library routine "S21BCF"[67] and following the procedure explained in the previous article (2.2.1.3).

Therefore, the chord length "L" of the loaded strut can be written in terms of the elliptic integrals, such as :

$$L = \frac{2}{\mu}\,[2E(p,\psi) - F(p,\psi)] \qquad (2.60)$$

Also this length "L" can be written in terms of the arc length of the strut by using Eq. (2.26) such as:

$$L = \frac{4}{\mu}\,E(p,\psi) - L_s \qquad (2.61)$$

where, the modulus p is restricted by the condition:

$$0 \leqslant p \leqslant 1$$

To determine the chord length of the loaded strut "L" when $p > 1$, consider the assumptions mentioned in Eqs. (2.43) and (2.47) and note that $F(p, \psi)$ in Eq. (2.26) is changed to $p_o F(p_o, \alpha/2)$ in Eq. (2.51), according to these assumptions, (since $\frac{\alpha}{2} = \sin^{-1}(p\sin\psi)$).

Similarly, for $p > 1$, the elliptic form of the second kind $E(p,\psi)$ will change to a new form by using Eqs. (2.43), (2.47), (2.48), (2.49) and (2.50) as follows:

$$E(p,\psi) = \int_0^{\psi} \sqrt{1-p^2\sin^2\varphi}\; d\varphi \quad \text{will change to}$$

$$\int_0^{\frac{\alpha}{2}} \frac{p_o\cos^2\varphi_1 d\varphi_1}{\sqrt{1-p_o^2\sin^2\varphi_1}} = p_o \int_0^{\frac{\alpha}{2}} \frac{d\varphi_1}{\sqrt{1-p_o^2\sin^2\varphi_1}} - p_o \int_0^{\frac{\alpha}{2}} \frac{\sin^2\varphi_1\, d\varphi_1}{\sqrt{1-p_o^2\sin^2\varphi_1}}$$

.....(2.62)

The first integral in the right-hand side of this equation is equal to $F(\varphi_o, \frac{\alpha}{2})$, while the second integral can be written in the form $\{F(\varphi_o, \frac{\alpha}{2}) - E(\varphi_o, \frac{\alpha}{2})\} / p_o^2$.

Therefore, for $p > 1$, $E(p, \psi)$ becomes:

$$E(p,\psi) = \frac{1}{p_o} E(\varphi_o, \frac{\alpha}{2}) - (\frac{1}{p_o} - p_o) F(\varphi_o, \frac{\alpha}{2}) \qquad (2.63)$$

Now, the chord length of the loaded strut can be obtained in the case of $p > 1$, by substituting Eq. (2.63) in Eq. (2.61), so that:

$$L = \frac{4}{\mu} \{ \frac{1}{p_o} E(\varphi_o, \frac{\alpha}{2}) - (\frac{1}{p_o} - p_o) F(\varphi_o, \frac{\alpha}{2}) \} - L_s \qquad (2.64)$$

Finally, Eqs. (2.61) or (2.64) with Eq. (2.53) can be used to determine the shortening of the chord line "Δ", due to the applied force "W".

Also it is seen from expression (2.1) that, once the axial shortening "Δ" is known, the actual axial stiffness "K_c" may be easily determined using the expression:

$$K_c = \frac{W}{\Delta} \qquad (2.65)$$

The behaviour of the strut may now be summarized by referring to Figs. (2.3) and (2.4).

Fig. (2.3) shows the load-displacement relationship plotted in non-dimensional form. The horizontal axis represents the axial displacement "Δ" or the relative approach of the two ends of the strut, divided by

L_o (the chord length of the strut). The vertical axis represents the axial load "W" divided by a constant P_E(in which the quantity π^2EI/L_s^2 has been denoted by P_E , Eq. (2.30)). The limiting value of Δ/L_o is reached when the strut has been pulled completely inside-out to form a straight tension member. It is seen clearly that the applied load "W" must increase as the axial displacement increases and the relationship between the applied load and the displacement will follow the curve (i). In this curve, at small loads a non-linear relationship between W and Δ is indicated, and the axial displacement "Δ" will occur from the first application of the load, but, as the load rises the displacement increases more and more rapidly. In the region of the load "$W/P_E \doteq 1$" the displacement is very sensitive to small changes in "W". At higher loads, the curve approaches curve (iii), which is for a strut that is initially straight. The broken curve (ii) indicates the effect of smaller initial rise than it had taken in curve (i), evidently, as the rise "A_o" approaches zero, the curve (ii) merges completely with the curve OAE. Curves (i) and (ii) represent positions of stable equilibrium of an initially curved strut with different initial rise "A_o".

All of these remarks are valid only if the strut remains perfectly elastic.

The axial stiffness "K_c" of the curved struts are illustrated in Fig. (2.4), again in terms of the non-dimensional axial displacement ratio "Δ/L_o". The horizontal axis represents the axial displacement, "Δ" divided by L_o. The vertical axis represents the axial stiffness K_c. It is seen clearly that at the beginning, the stiffness decreases very

rapidly as the variation in the ratio "Δ/L_o" is very small, and this means that the stiffness "K_c" is very sensitive to small changes in Δ. As the displacement "Δ" increases more and more, the variation in the stiffness is very small until the strut starts to retake its stiffness and becomes much stiffer when the strut has been pulled completely inside-out to form a straight tensile member.

Curve (ii) in this figure represents the variation in axial stiffness of initially curved strut with smaller rise"A_o" than it had taken in curve (i). Evidently, as the rise"A_o" approaches zero, the axial stiffness "K_c" at the beginning approaches to the value of the axial stiffness of the flat strut $K_o = \frac{EA}{L_o}$ as given in Table 2.1.

In Table (2.1) values are given of the ratios Δ/L_o and K_c/K_o and the angle α for various values of the ratio W/P_E. All of these values are given for three different curved struts, having the same chord length "L_o=520" and different initial rise"A_o". The initial rises 0.0, 0.05, 35 mm are chosen for comparison.

Table (2.1) : Comparison Between Theoretical Behaviour of Curved Struts

W/PE	Initial rise A_o (mm)	Δ/L_o	K_c/K_o	End angle α (degree)
0.001	0.0	0.0000000	1.0000000	0.000
	0.05	0.0000000	0.9905596	0.022
	35	0.0000241	0.0001815	15.346
0.25	0.0	0.0000011	1.0000000	0.000
	0.05	0.0000011	0.9831576	0.028
	35	0.0093569	0.0001170	19.589

Table (2.1) Cont'd

W/PE	Initial rise A_o (mm)	Δ/L_o	K_c/K_o	end angle α (degree)
0.5	0.0	0.0000022	1.0000000	0.000
	0.05	0.0000023	0.9678166	0.044
	35	0.0350482	0.0000625	30.388
0.75	0.0	0.0000033	1.0000000	0.000
	0.05	0.0000036	0.9258050	0.076
	35	0.1272003	0.0000312	46.215
1.00	0.0	0.0000044	1.0000000	0.000
	0.05	0.0045987	0.0009524	7.775
	35	0.3556754	0.0000123	75.187
1.05	0.0	0.0946690	0.0000486	35.613
	0.05	0.0956002	0.0000481	35.796
	35	0.4072779	0.0000113	80.588
1.5	0.0	0.6364183	0.0000103	98.671
	0.05	0.6366181	0.0000103	98.695
	35	0.7761843	0.0000085	114.950
2.0	0.0	0.9291469	0.0000094	124.553
	0.05	0.9292476	0.0000094	124.567
	35	1.0106373	0.0000087	135.367
3.0	0.0	1.2041366	0.0000109	148.433
	0.05	1.2041787	0.0000109	148.442
	35	1.2459588	0.0000105	155.717

Table(2.1) Cont'd

W/PE	Initial rise A_o (mm)	Δ/L_o	K_c/K_o	end angle α (degree)
4.0	0.0	1.3373489	0.0000131	159.754
	0.05	1.3373715	0.0000131	159.761
	35	1.3652077	0.0000128	165.592
6.0	0.0	1.4738235	0.0000178	170.160
	0.05	1.4738322	0.0000178	170.165
	35	1.4917701	0.0000176	174.598

N.B. $K_o = \frac{EA}{L_o}$ (for flat member)

2.3 Theoretical Analysis of Initially Curved Eccentrically Loaded Strut

In practice a bar may have imperfections of form such as initial crookedness, or imperfections of loading such as the fact that the loads may be applied at the ends with some eccentricity from the centre of the bar. All these imperfections have their effect on the behaviour of the bar. The effect of initial curvature has already been studied in article (2.2). The analysis of the combined effects of initial curvature and eccentric loading will now be undertaken. The question arises now as to how and to what extent a given eccentricity of the load will affect the previous results.

Figure (2.5) shows a uniform elastic initially curved strut. The pins are offset from the centre-line of the strut in such a way that the end-load "W" is applied through a rigid lever arm, of length c,

which is tangential to the ends of the curved strut, as shown in Fig. (2.5.a). This means that the load is applied with an eccentricity $e = c \sin(\alpha)$, where α is the angle at the ends of the loaded strut.

2.3.1 Basic Equations of Large Deformation Theory of Eccentrically Loaded Strut

The solution of this strut depends upon the two equal and opposite loads, which are applied at the ends of the rigid lever arms, being replaced by two equal and opposite loads in addition to two equal and opposite couples, all applied at the ends of the curved strut, as shown in Fig. (2.5.b). The values of bending moments produced at the ends of the curved part of the strut under the action of the loads are,

$$M_o = +W.\, c \sin(\alpha) \tag{2.66}$$

If the transverse displacement y is measured from the chord length at the ends of the curved part of the strut, Fig. (2.5.b), then the bending moment at any section s_1-s_1 is:

$$M = M_o + W.y \tag{2.67}$$

The relationship between the curvature and the bending moment at the considered section s_1-s_1 may be expressed by the following non-linear differential equation as:

$$-EI \left(\frac{d\theta}{ds} - \frac{d\theta_o}{ds}\right) = M = (M_o + W.y)$$

or

$$\frac{d\theta}{ds} - \frac{d\theta_o}{ds} = -\frac{W}{EI} (c \sin\alpha + y) \tag{2.68}$$

Differentiating equation (2.68) with respect to s, and substituting $\sin\theta$ for dy/ds, leads to:

$$\frac{d^2\theta}{ds^2} - \frac{d^2\theta_o}{ds^2} = -\frac{W}{EI}\sin(\theta) \qquad (2.69)$$

This is identical to Eq. (2.5). Following the same procedure as in Art. (2.2.1), the solution of Eq. (2.69) is:

$$(\frac{d\theta}{ds})^2 = 2\mu^2\cos(\theta) + C_2 \qquad (2.70)$$

where, C_2 is a constant of integration.

Thus, the problem is concerned only with a change in the boundary conditions. These new conditions are:

(i) at the end of the loaded curved part of the strut,E',

$$-\frac{d\theta}{ds} = \frac{M}{EI}$$

or

$$\frac{d\theta}{ds} = -\frac{1}{EI}(\frac{EI}{R} + M_o)$$

or

$$\frac{d\theta}{ds} = -\frac{1}{R} - \mu^2 c \sin(\alpha) \quad \text{and} \quad \theta=\alpha \qquad (2.71)$$

substitute m for c $\sin(\alpha)$

Therefore,the constant of integration C_2 in Eq. (2.70) is:

$$C_2 = (-\frac{1}{R} - \mu^2 m)^2 - 2\mu^2\cos(\alpha) \qquad (2.72)$$

Substituting Eq. (2.72) in Eq. (2.70) thus:

$$(\frac{d\theta}{ds})^2 = 2\mu^2 \cos(\theta) + (\frac{1}{R^2} + \frac{2\mu^2 m}{R} + \mu^4 m^2) - 2\mu^2 \cos(\alpha)$$

i.e. $$(\frac{d\theta}{ds})^2 = 2\mu^2[\cos(\theta) - \{ \cos(\alpha) - \frac{(1+\mu^2 Rm)^2}{2\mu^2 R^2} \}] \qquad (2.73)$$

Equation (2.73) can be simplified after using the following expression:

$$\cos(\Omega) = \cos(\alpha) - \frac{(1+\mu^2 Rm)^2}{2\mu^2 R^2} \qquad (2.74)$$

then the form of equation (3.73) becomes:

$$\frac{d\theta}{ds} = \pm \mu\sqrt{2} \{ \cos(\theta) - \cos(\Omega) \}^{\frac{1}{2}}. \qquad (2.75)$$

Equation (2.75) is identical to the previous equation (2.14), only the difference being that the auxiliary angle γ is replaced by the angle Ω , where Ω is defined in equation (2.74). Therefore,a similar analysis to that explained in article (2.2.1) will be considered for solving Eq. (2.75), and the arc length of the curved part of eccentrically loaded strut "L_s" can be expressed in terms of the elliptic function as follows:

$$L_s = \frac{2}{\mu} \int_0^{\psi_1} \frac{d\varphi_e}{\sqrt{1-p_e \sin^2(\varphi_e)}} = \frac{2}{\mu} F(p_e, \psi_1) \qquad (2.76)$$

where,

$$p_e = \sin(\frac{\Omega}{2}) \qquad (2.77)$$

is the new modulus corresponding to the angle at the ends of the loaded strut "α".

$$\text{Also, } p_e \sin(\varphi_e) = \sin(\frac{\Theta}{2}) = \sin(\frac{\Omega}{2}) \cdot \sin(\varphi_e) \qquad (2.78)$$

and

$$\psi_1 = \cos^{-1}\left(\frac{1+\mu^2 Rm}{2p_e \mu R}\right) \qquad (2.79)$$

is the value of the new amplitude in the elliptic integral of the first kind $F(p_e, \psi_1)$.

The application of equations (2.76) to (2.79) is restricted by the following condition:

$$0 \leqslant p_e \leqslant 1 \qquad (2.80)$$

In the case of $p_e > 1$, as in section (2.2.1.2), consider the following assumption:

$$p_{oe} = \frac{1}{p_e} < 1 \qquad (2.81)$$

and by replacing the expression $\cos(\Omega) = 1-2p_e^2$ by $1 - \frac{2}{p_{oe}^2}$, then the end angle α is given by:

$$\sin(\frac{\alpha}{2}) = \left[(\frac{1}{p_{oe}})^2 - (\frac{1+\mu^2 Rm}{2\mu R})^2 \right]^{\frac{1}{2}} \qquad (2.82)$$

Therefore the arc length of the curved part of eccentrically loaded strut, according to this case, can be written as:

$$L_s = \frac{2p_{oe}}{\mu} \int_0^{\frac{\alpha}{2}} \frac{d\varphi_{e1}}{\sqrt{1 - p_{oe}^2 \sin^2(\varphi_{e1})}} = \frac{2p_{oe}}{\mu} F(p_{oe}, \frac{\alpha}{2}) \qquad (2.83)$$

where $p_{oe} < 1$,

$$p_{oe} \sin(\varphi_{e1}) = \sin(\varphi_e) \qquad (2.84)$$

and the upper limit of integration $\frac{\alpha}{2}$ is given in Eq. (2.82). Also, $F(p_{oe}, \frac{\alpha}{2})$ represents the incomplete elliptic integral of the first kind with modulus p_{oe} and amplitude $\frac{\alpha}{2}$.

Finally, for given values of c, L_s, W and the initial rise"A_o", the values of the end angle α , the modulus p_o or p_{oe} and the amplitude ψ_1 or $\frac{\alpha}{2}$ can be obtained, by following the same procedure explained before in section (2.2.1.3) .

2.3.2 Load Displacement Relationship of Eccentrically Loaded Strut

The relationship between the applied load"W"with its corresponding displacement "Δ", for eccentrically loaded strut can be considered as in Eq. (2.65). The length L_o in this case is usually known, but the co-ordinate distance L, Fig. (2.5.a),measured along the line of thrust is given by the equation:

$$L = 2c\cos(\alpha) + 2\int_{o}^{\frac{L'}{2}} dx \qquad (2.85)$$

where L' is the chord length of the curved part of the loaded strut (Fig. 2.5.b)).

Thus, the co-ordinate distance,L , can be determined by solving equation (2.85) for ds (n.b. dx = ds cos (θ)).

As in section (2.2.2) the solution is:

$$L = 2\,c\cos(\alpha) + \frac{4}{\mu}E(p_e, \psi_1) - L_s \qquad (2.86)$$

where p_e is restricted by the condition in Eq. (2.80).

In the case of $p_e > 1$ the length L can be written as:

$$L = 2c.\cos(\alpha) + \frac{4}{\mu}\left[\frac{1}{p_{oe}} E(p_{oe}, \frac{\alpha}{2}) - (\frac{1}{p_{oe}} - p_{oe})F(p_{oe}, \frac{\alpha}{2})\right] - L_s$$

.....(2.87)

Finally, Eqs. (2.86) or (2.87) with Eq. (2.53) can be used to determine the relative travel of the loaded ends of the strut "Δ" . Also the stiffness of the eccentrically loaded strut can be obtained from Eq. (2.65).

2.4 Theoretical Analysis of Initially Curved Axially Loaded Tie

Similar analysis explained in Art. (2.2) will be considered for the case of axially loaded tie.

2.4.1 Basic Equations of Large Deformation Theory of Axially Loaded Tie

The tie geometry and loading are shown in Fig. (2.6) . The equilibrium equation for large deformations is based on the deformed configuration shown in Fig. (2.6), so that the Euller-Bernoulli equation for bending due to tensile loading is expressed as:

$$\left(\frac{d\theta}{ds} - \frac{d\theta_o}{ds}\right) = \frac{1}{EI}(W.y) \qquad (2.88)$$

The solution of this equation can be obtained by differentiating it with respect to s, and substituting sin(θ) by dy/ds, such as:

$$\frac{d^2\theta}{ds^2} - \frac{d^2\theta_o}{ds^2} = \frac{W}{EI}\sin(\theta) \qquad (2.89)$$

As in sec. (2.2), the solution is

$$\left(\frac{d\theta}{ds}\right)^2 = -2\mu^2\cos(\theta) + C_3 \qquad (2.90)$$

where, the constant of integration, C_3, may be determined from the boundary conditions which state that:

At the hinged end 'a' (Fig.(2.6.a))

$$\frac{d\theta}{ds} = -\frac{1}{R} \quad \text{and} \quad \theta = \alpha \tag{2.91}$$

These conditions are satisfied to determine the constant of integration, C_3, in Eq. (2.90), therefore:

$$C_3 = \frac{1}{R^2} + 2\mu^2 \cos(\alpha) \tag{2.92}$$

Substituting Eq. (2.92), in Eq. (2.90), hence:

$$(\frac{d\theta}{ds})^2 = 2\mu^2 \left[\{ \cos(\alpha) + \frac{1}{2\mu^2 R^2} \} - \cos(\theta) \right] \tag{2.93}$$

using the expression

$$\cos(\beta) = \cos(\alpha) + \frac{1}{2\mu^2 R^2} \tag{2.94}$$

then the form of Eq. (2.93) becomes:

$$\frac{d\theta}{ds} = \pm \mu\sqrt{2} \cdot \sqrt{\cos(\beta) - \cos(\theta)} \tag{2.95}$$

Since $\frac{d\theta}{ds}$ is negative the positive sign will be dropped from this equation and it can be written in the form:

$$ds = \frac{-\, d\theta}{\mu\sqrt{2}\sqrt{\cos(\beta)-\cos(\theta)}} \tag{2.96}$$

The total curved length of the tie "L_s" can be determined by integrating Eq. (2.96) from zero to $L_s/2$ on the left hand and between the corresponding limits $\theta = \alpha$ and $\theta = 0$ on the right hand, such as:

$$L_s = 2 \int_0^{L_s/2} ds = -\frac{\sqrt{2}}{\mu} \int_\alpha^0 \frac{d\theta}{\sqrt{\cos(\beta)-\cos(\theta)}} \qquad (2.97)$$

The integral in Eq. (2.97) can be simplified to the standard elliptic forms by using the identities:

$$\cos(\beta) = 2\cos^2(\frac{\beta}{2}) - 1$$
$$\cos(\theta) = 2\cos^2(\frac{\theta}{2}) - 1 \qquad (2.98)$$

and following a procedure analogous to that for the case of compressive loading, and employing a new variable φ_t, such that:

$$\cos(\frac{\beta}{2}) = p_t \qquad (2.99)$$

and

$$\cos(\frac{\theta}{2}) = \sin(\varphi_t) \qquad (2.100)$$

(n.b. the cosine forms of the half angles β and θ are used in this case instead of the sine forms as in case of the strut (sec. 2.2), because the forms of cosine are suitable to change the integral in Eq. (2.97) to its standard elliptic form).

After obtaining the differential of θ in terms of the new variable "φ_t", the substitutions in Eq. (2.99) and (2.100) change Eq. (2.97) into:

$$L_s = \frac{2}{\mu} \int_{\varphi_E}^{\varphi_c} \frac{d\varphi_t}{p_t\sqrt{1-\frac{1}{p_t}^2 \sin^2(\varphi_t)}}$$

Using the substitution $p_{ot} = \frac{1}{p_t}$ (2.101)

the length L_s can be written as:

$$L_s = \frac{2p_{ot}}{\mu} \int_{\varphi_E}^{\varphi_c} \frac{d\varphi_t}{\sqrt{1-p_{ot}^2 \sin^2(\varphi_t)}} \quad (2.102)$$

The limits of integration "φ_E and φ_c" in this equation have to be found before the unknown modulus "p_{ot}" can be evaluated. It is seen from Eq. (2.100) that:

i) when $\theta = 0$, $\varphi_t = \varphi_c$

$$\text{where} \quad \varphi_c = \sin^{-1}[\cos(0)] = \sin^{-1}(1) = \frac{\pi}{2} \quad (2.103)$$

ii) when $\theta = \alpha$, $\varphi_t = \varphi_E$

$$\text{where} \quad \varphi_E = \sin^{-1}[\cos(\tfrac{\alpha}{2})] \quad (2.104)$$

the value $\cos(\frac{\alpha}{2})$ can be determined from Eqs. (2.94), (2.99) and (2.101) after using the identities in Eq. (2.98), such as:

$$\cos(\tfrac{\alpha}{2}) = [(\frac{1}{p_{ot}})^2 - (\frac{1}{2\mu R})^2]^{\frac{1}{2}} \quad (2.105)$$

Substituting Eqs. (2.103) and (2.104) into Eq. (2.102) then:

$$L_s = \frac{2p_{ot}}{\mu} \int_{\varphi_E}^{\pi/2} \frac{d\varphi_t}{\sqrt{1-p_{ot}^2 \sin^2(\varphi_t)}} \quad (2.106)$$

or,

$$L_s = \frac{2p_{ot}}{\mu} \{ K(p_{ot}) - F(p_{ot}, \varphi_E) \} \qquad (2.107)$$

where, $K(p_{ot})$ and $F(p_{ot},\varphi_E)$ are respectively, the complete and incomplete elliptic integrals of the first kind, [7,81].

A close inspection of Eq. (2.107) reveals at once, that

i) if $\mu = 0$, then $p_{ot} = 0$

ii) if $\mu = \infty$, then $\mu L_s = \infty$, therefore the value of $K(p_{ot}) - F(p_{ot},\varphi_E)$ must equal infinity and this will occur at $p_{ot} = 1$. (from tables of elliptic functions[71] the value $K(1)=\infty$).

It follows that Eq. (2.107) covers the whole range of the tensile forces acting on the tie.

The unknown modulus p_{ot} in Eq. (2.107) can be evaluated for given values of L_s and μ , using the procedure explained before in section (2.2.1.3).

2.4.2 Load Displacement Relationship of Axially Loaded Tie

The relative travel of the loaded ends of the tie, or the extension in the chord length due to the tensile loading can be calculated as before as:

$$\Delta_T = L - L_o \qquad (2.108)$$

where, Δ_T is the extension in the chord length due to tensile loading.

As before the original chord length, L_o, is known.

Again, to develop an expression for the projection of the deformed tie on the x axis, the following equation is used.

$$L = 2 \int_{\alpha}^{0} dx \qquad (2.109)$$

and it is seen from Fig. (2.6.b) that:

$$dx = ds.\ \cos(\theta) \qquad (2.110)$$

Substituting Eq. (2.96), (2.98) and (2.110) into Eq. (2.109), then the resulting equation is:

$$L = \frac{1}{\mu} \int_{\alpha}^{0} \frac{-2\{\cos^2(\frac{\theta}{2})-1\}d\theta}{\sqrt{\cos^2(\frac{\beta}{2})-\cos^2(\frac{\theta}{2})}} \qquad (2.111)$$

By using the substitutions of Eq. (2.99), (2.100), (2.101), (2.103) and (2.104) into Eq. (2.111), to determine the chord length, L , in terms of the variable φ_t, changing the limits of integration accordingly, and noting that:

$$d\theta = -2\ d\varphi \quad \text{(from the differentiation of Eq. (2.100)} \qquad .....(2.112)$$

then,

$$L = \frac{2p_{ot}}{\mu} \{ 2 \int_{\varphi_E}^{\pi/2} \frac{\sin^2(\varphi_t)d\varphi_t}{\sqrt{1-p_{ot}{}^2\sin^2(\varphi_t)}} - \int_{\varphi_E}^{\pi/2} \frac{d\varphi_t}{\sqrt{1-p_{ot}{}^2\sin^2(\varphi_t)}} \}$$

.....(2.113)

The first integral in this equation can be written in its general forms of elliptic integrals, such as:

$$\int_{\varphi_E}^{\pi/2} \frac{\sin^2(\varphi_t)\, d\varphi_t}{\sqrt{1-p_{ot}^2\sin^2(\varphi_t)}} = \frac{1}{p_{ot}^2} \int_{\varphi_E}^{\pi/2} \frac{\{1-(1-p_{ot}^2\sin^2(\varphi_t)\}\, d\varphi_t}{\sqrt{1-p_{ot}^2\sin^2(\varphi_t)}}$$

$$= \frac{1}{p_{ot}^2} \{ \int_{\varphi_E}^{\pi/2} \frac{d\varphi_t}{\sqrt{1-p_{ot}^2\sin^2(\varphi_t)}} - \int_{\varphi_E}^{\pi/2} \sqrt{1-p_{ot}^2\sin^2(\varphi_t)}\, d\varphi_t \}$$

$$= \frac{1}{p_{ot}^2} \{ K(p_{ot}) - F(p_{ot},\varphi_E) - E(p_{ot}) + E(p_{ot},\varphi_E) \} \quad (2.114)$$

where,

$K(p_{ot})$ and $F(p_{ot},\varphi_E)$ are, respectively, the complete and incomplete elliptic integrals of the first kind,[7,81] while $E(p_{ot})$ and $E(p_{ot},\varphi_E)$ are, respectively, the complete and incomplete elliptic integrals of the second kind, [7,81].

The second integral in Eq. (2.113) can be written in the standard forms of the first kind of elliptic integrals $K(p_{ot}) - F(p_{ot},\varphi_E)$ as mentioned before.

Now, the chord length "L" of the deformed tie can be written relative to the curved length "L_s" of the tie, by using Eq. (2.107) and Eq. (2.113) in its elliptic form, as follows:

$$L = \frac{4}{p_{ot}\mu} \{K(p_{ot}) - E(p_{ot}) - F(p_{ot},\varphi_E) + E(p_{ot},\varphi_E)\} - L_s \quad \text{.....(2.115)}$$

Finally the extension in the chord length "Δ_T" can be determined by substituting Eq. (2.115) into Eq. (2.108) and consequently the axial stiffness "K_t" in tension, may be easily determined using the expression:

$$K_t = \frac{W}{\Delta_T} \tag{2.116}$$

2.5 Theoretical Analysis of Initially Curved Eccentrically Loaded Tie

In this article, the initially curved tie will be examined for the effect of eccentric tensile loading, as shown in Fig. (2.7). A similar analysis to that in Arts. (2.3) and (2.4) will be used.

2.5.1 Basic Equations of large Deformation Theory of Eccentrically Loaded Tie

The basic differential equation of an eccentrically loaded tie is similar to equation (2.68), in Art. (2.3.1) for a case of eccentrically loaded strut, but there is a difference in the sign of the external bending moment, M, so that the governing differential equation becomes:

$$\frac{d\theta}{ds} - \frac{d\theta_o}{ds} = \frac{M}{EI} = \frac{W}{EI}\ (c.\sin(\alpha) + y) \tag{2.117}$$

Differentiating this equation with respect to s, and substituting μ^2 for $\frac{W}{EI}$ and $\sin(\theta)$ for $\frac{dy}{ds}$, therefore:

$$\frac{d^2\theta}{ds^2} = \mu^2 . \sin\theta \tag{2.118}$$

As in section (2.2.1), the solution of this equation is:

$$(\frac{d\theta}{ds})^2 = -2\mu^2 \cos(\theta) + C_4 \tag{2.119}$$

The constant of integration C_4, is determined from the boundary conditions at the end of the curved part of the loaded tie (E'), which state that:

$$\frac{d\theta}{ds} = -\frac{1}{R} + \mu^2.m \quad \text{and} \quad \theta = \alpha \tag{2.120}$$

where $m = c.\sin(\alpha)$.

From these conditions, the constant of integration C_4 is:

$$C_4 = (\frac{1}{R} - \mu^2 m)^2 + 2\mu^2\cos(\alpha) \tag{2.121}$$

Again, substituting Eq. (2.121) in Eq. (2.119), hence:

$$(\frac{d\theta}{ds})^2 = 2\mu^2 \{ [\cos(\alpha) + \frac{(1-\mu^2 Rm)^2}{2\mu^2 R^2}] - \cos(\theta)\} \tag{2.122}$$

By using the expression:

$$\cos(\zeta) = \cos(\alpha) + \frac{(1-\mu^2 Rm)^2}{2\mu^2 R^2} \tag{2.123}$$

Eq. (2.122) can be simplified to the form:

$$\frac{d\theta}{ds} = \pm \mu\sqrt{2} . \sqrt{\cos(\zeta) - \cos(\theta)} \tag{2.124}$$

Since $\frac{d\theta}{ds}$ is negative, Eq. (2.124) can be written in the form:

$$ds = \frac{-\, d\theta}{\mu\sqrt{2}\,\sqrt{\cos(\zeta)-\cos(\theta)}} \tag{2.125}$$

This equation is identical to the previous equation (2.96) the only difference being the angle β is changed to the angle ζ, where ζ is given in Eq. (2.123). Therefore , as in section (2.4.1) the following is obtained:

$$L_s = \frac{2p_{et}}{\mu} \int_{\varphi_{Ee}}^{\pi/2} \frac{d\varphi_{et}}{\sqrt{1-p_{et}^2 \sin^2(\varphi_{et})}}$$

$$= \frac{2p_{et}}{\mu} \{ K(p_{et}) - F(p_{et},\varphi_{Ee}) \} \qquad (2.126)$$

where,

$$(\frac{1}{p_{et}})^2 = \cos^2(\frac{\alpha}{2}) + (\frac{1-\mu^2 Rm}{2\mu R})^2 \quad , \qquad (2.127)$$

$$\cos(\frac{\theta}{2}) = \sin(\varphi_{et}) \quad , \qquad (2.128)$$

$$\varphi_{Ee} = \sin^{-1}(\cos(\frac{\alpha}{2})) \quad , \qquad (2.129)$$

$$\cos(\frac{\alpha}{2}) = \{ (\frac{1}{p_{et}})^2 - (\frac{1-\mu^2 Rm}{2\mu R})^2 \}^{\frac{1}{2}} \qquad (2.130)$$

and L_s represents the length of the curved part of the tie. (n.b. when the length of the rigid lever arm, c, is equal to zero, then the value m will vanish, thus the term $\mu^2 Rm$ in Eqs. (2.122) and (2.123) will be equal to zero, therefore, all of equations (2.125) to (2.129) will be exactly the same as in the case of the axially loaded tie.)

2.5.2 Load Displacement Relationship of Eccentrically Loaded Tie

The same procedure for the case of axially loaded tie, Art. (2.4.2) is considered in this case.

Therefore the expression of the projection of the deformed tie on x-axis. is gives by the equation:

$$L = \frac{4}{p_{et}{}^{\mu}} \{ K(p_{et}) - E(p_{et}) - F(p_{et},\varphi_{Ee}) + E(p_{et},\varphi_{Ee}) \}$$

$$- L_s + 2c \cos(\alpha) \qquad (2.131)$$

And, consequently, the value of the horizontal displacement"Δ_T" and the axial stiffness"K_t"for the eccentrically loaded tie,can be easily determined by using Eqs. (2.108) and (2.116) respectively.

The behaviour of the tie may now be summarised by referring to Figs. (2.8) and (2.9).

In Fig. (2.8) the quantity (L_s-L_o) has been denoted by Δ_{max} and a non-dimensional parameter Δ/Δ_{max} has been plotted against the applied horizontal load "W". It is seen that the axial displacement increases as the load increases until the ratio Δ/Δ_{max} reaches to its limiting value $\frac{\Delta}{L_s-L_o} = 1$, which occurs when the deformed tie has been pulled completely to form a straight tension member.

In Fig. (2.9) the axial stiffness "K_t" of the curved tie is illustrated , again in terms of the non-dimensional axial displacement ratio Δ/Δ_{max} . The horizontal axis represents the ratio Δ/Δ_{max} . The vertical axis represents the axial stiffness"K_t"of the curved tie. It is seen, from the figure, that the stiffness of the tie increases as the axial displacement increases until the ratio Δ/Δ_{max} reaches the limiting value $\Delta/(L_s-L_o) = 1.0$, then the stiffness of the tie tends to the value of the axial stiffness of the flat tie $K_o = \frac{EA}{L_o}$ as shown.

In Table (2.2) are given values of the ratio Δ/Δ_{max}, K_t/K_o and the angle α , for a loaded curved tie with an initial rise A_o = 5 mm. All of these values are calculated for various values of the applied load W. It is seen from the table that, when the applied load W is increased the ratios Δ/Δ_{max} and K_t/K_o are increased as the end angle α is decreased. When the end angle α approaches to zero, the ratio Δ/Δ_{max} and K_t/K_o approach the terminal values of unity.

Table(2.2) : Summary of Behaviour of Curved Tie

Applied load (W)^N	$\Delta/(L_s-L_o)$	K_t/K_o	end angle α (degree)
0.846	0.0920282	0.0096552	2.117
3.384	0.3020007	0.0117688	1.901
5.921	0.4460567	0.0139441	1.731
10.151	0.6024679	0.0176982	1.519
15.227	0.7151148	0.0223655	1.336
20.302	0.7851046	0.0271622	1.201
25.378	0.8316026	0.0320543	1.097
42.296	0.9104155	0.0487991	0.875
84.592	0.9661408	0.0919689	0.627
253.777	0.9935932	0.2682836	0.362
422.961	0.9975113	0.4453830	0.280
507.554	0.9978224	0.5293066	0.256
676.738	0.9991290	0.7270311	0.222
845.923	0.9991290	0.9087888	0.00

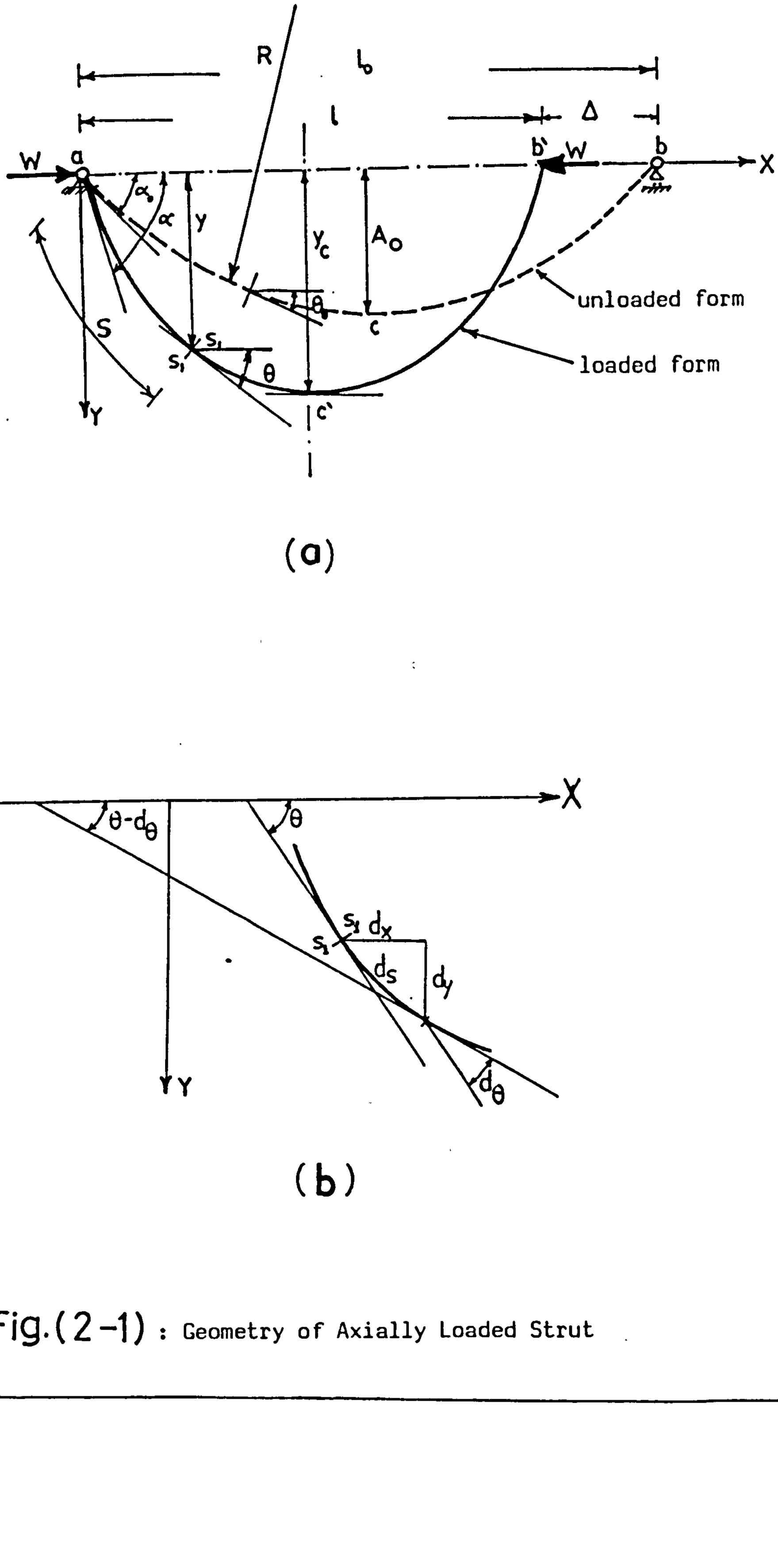

Fig.(2-1) : Geometry of Axially Loaded Strut

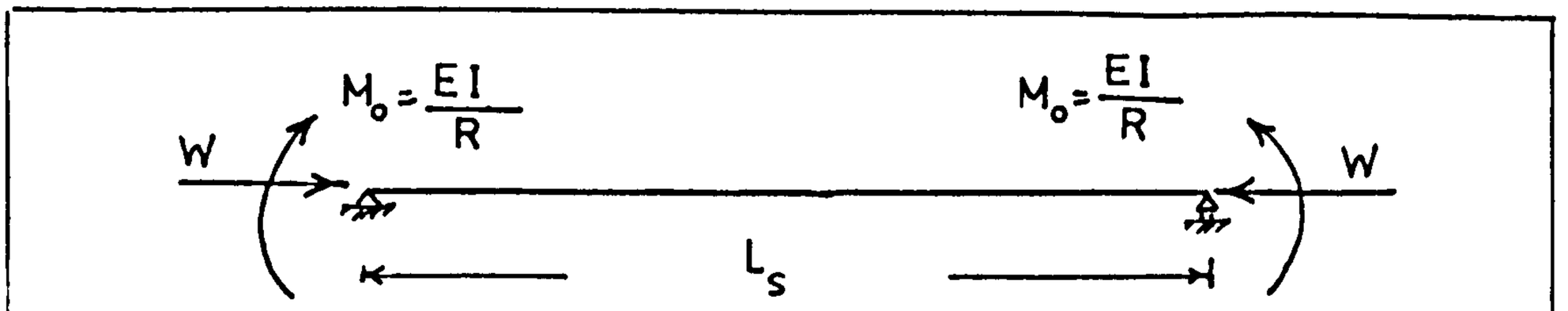
$M_o = \frac{EI}{R}$
$M_o = \frac{EI}{R}$
W
W
L_s

(a)

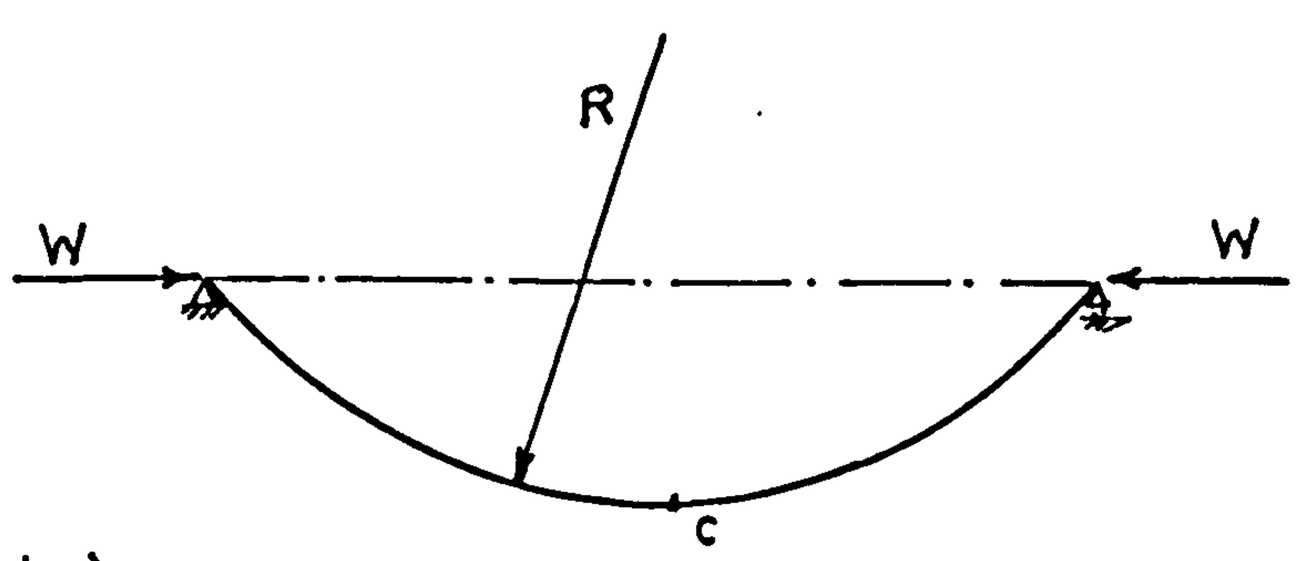
R
W
W
c

(b)

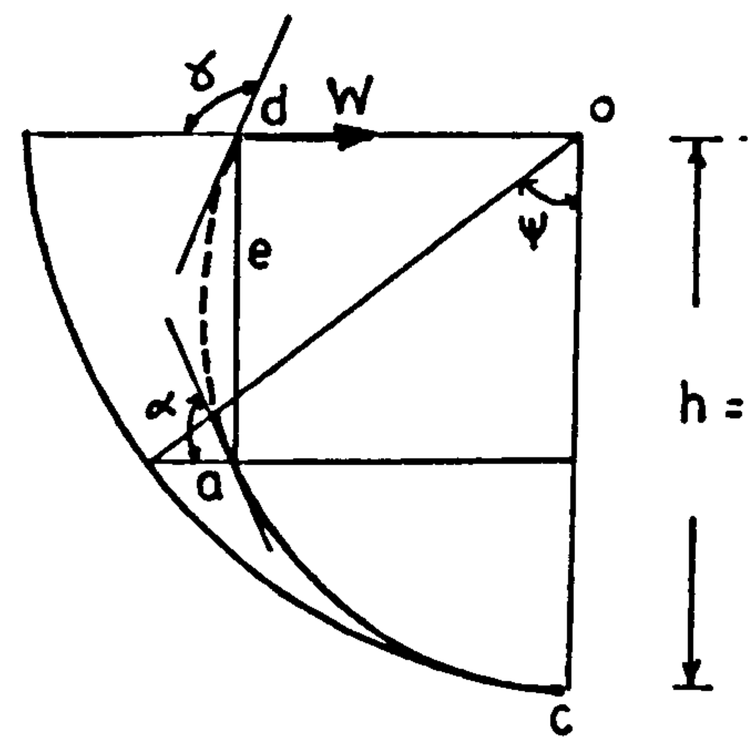
γ
d
W
o
e
ψ
α
a
c
$h = \frac{2P}{\mu}$

(C)

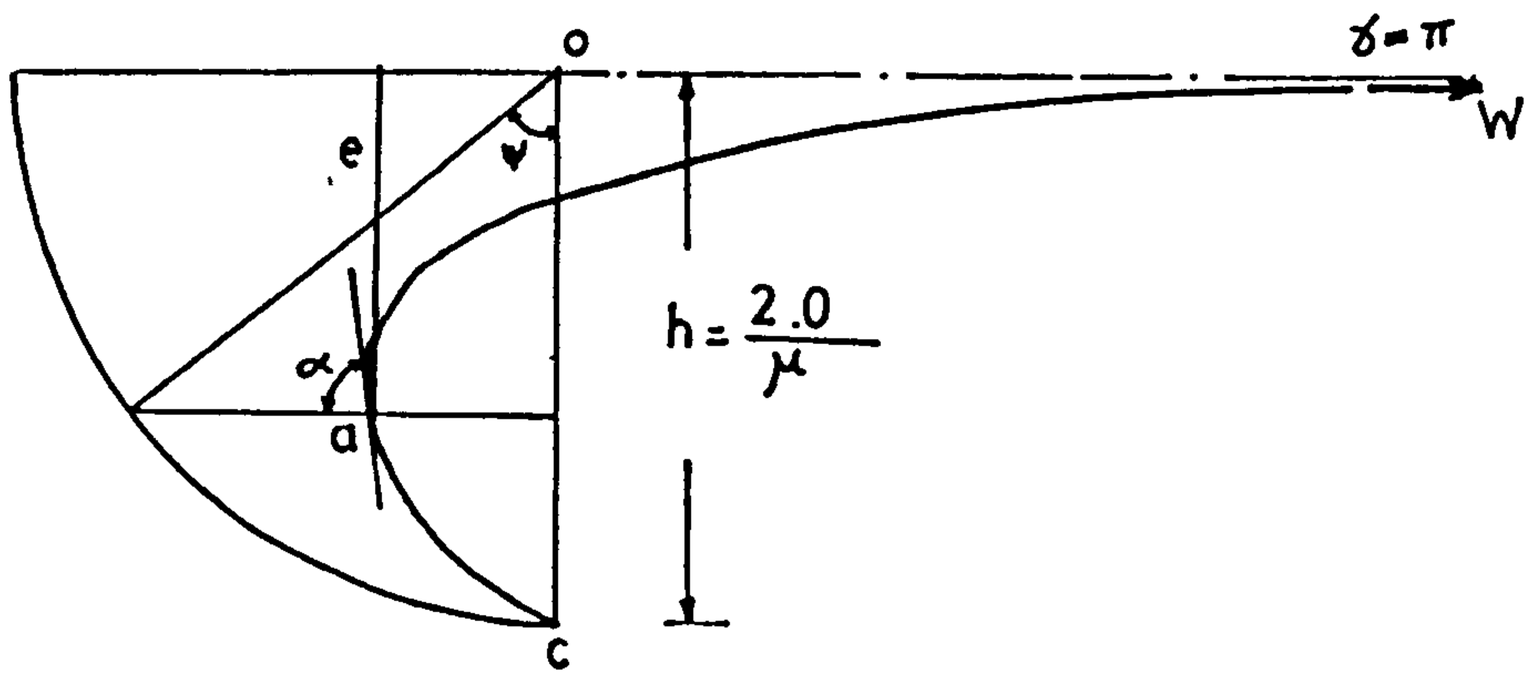
o
γ = π
W
e
ψ
α
a
c
$h = \frac{2.0}{\mu}$

(d)

Fig.(2-2)

NON-DIMENSIONAL
LOAD-DISP. RELATIONSHIP
FOR CURVED STRUT

THEORY OF LARGE DEFORMATION
(AXIAL LOADING)

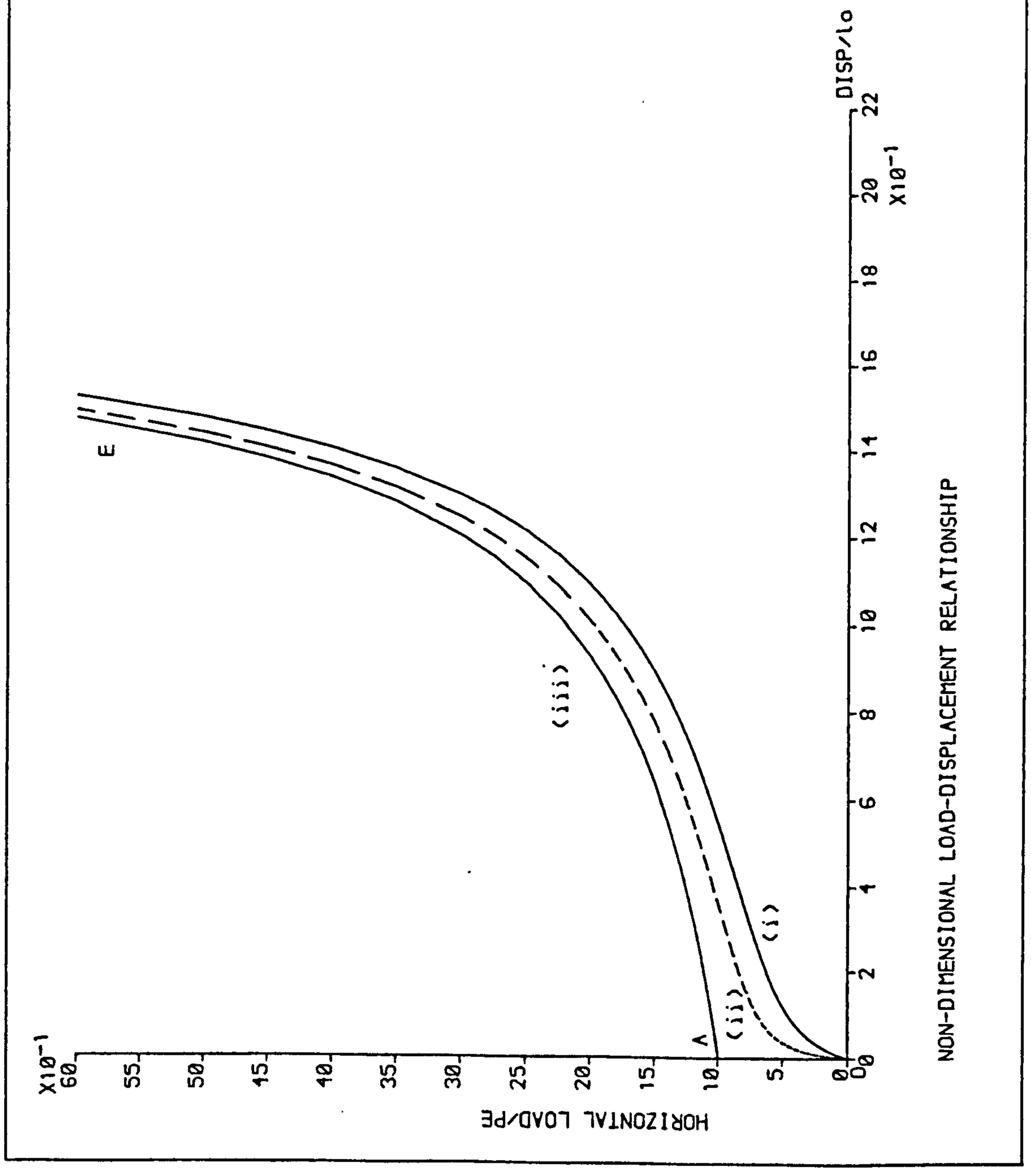

FIG.(2.3)

AXIAL STIFFNESSES OF CURVED STRUTS

THEORY OF LARGE DEFORMATION

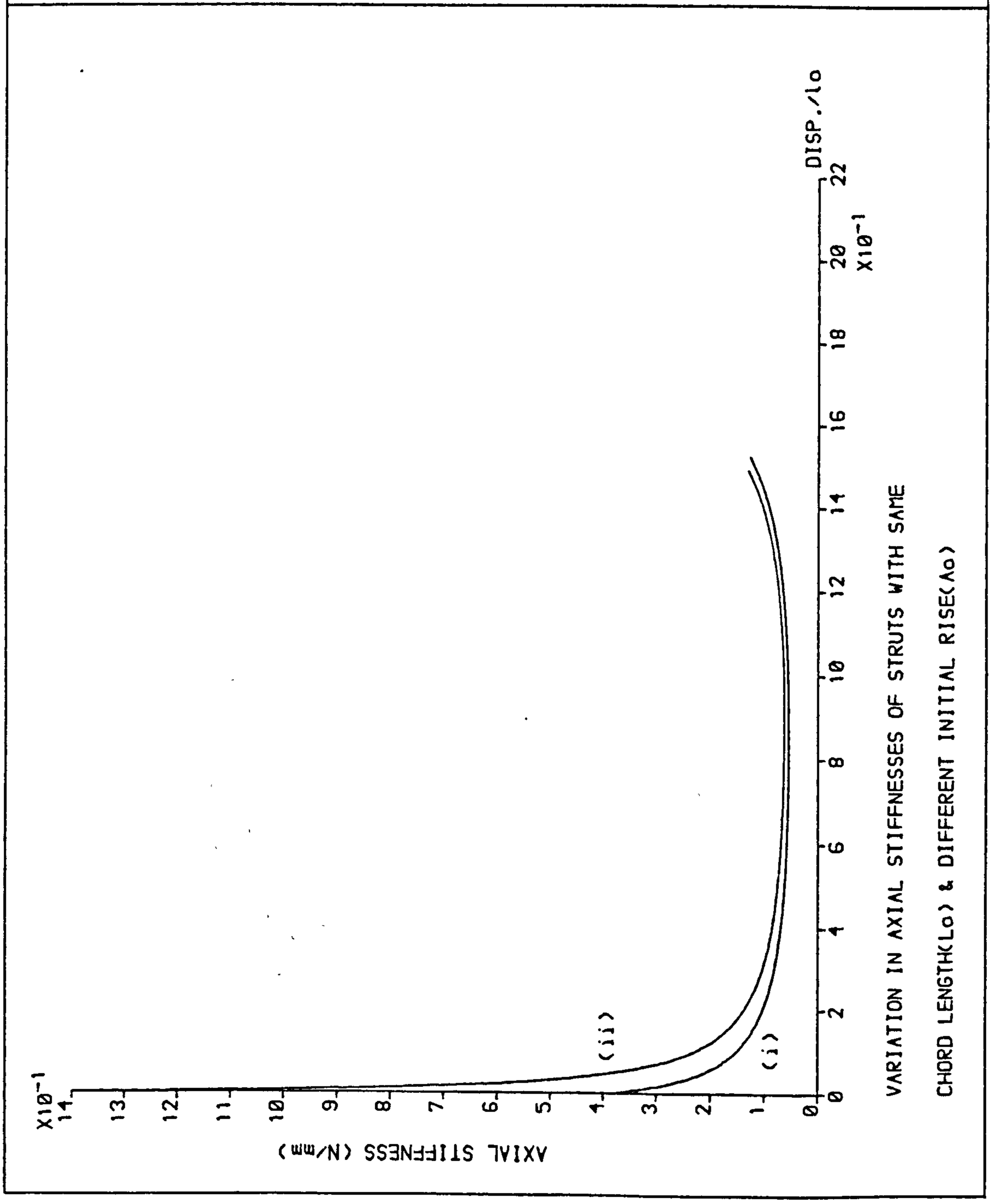

FIG.(2.4)

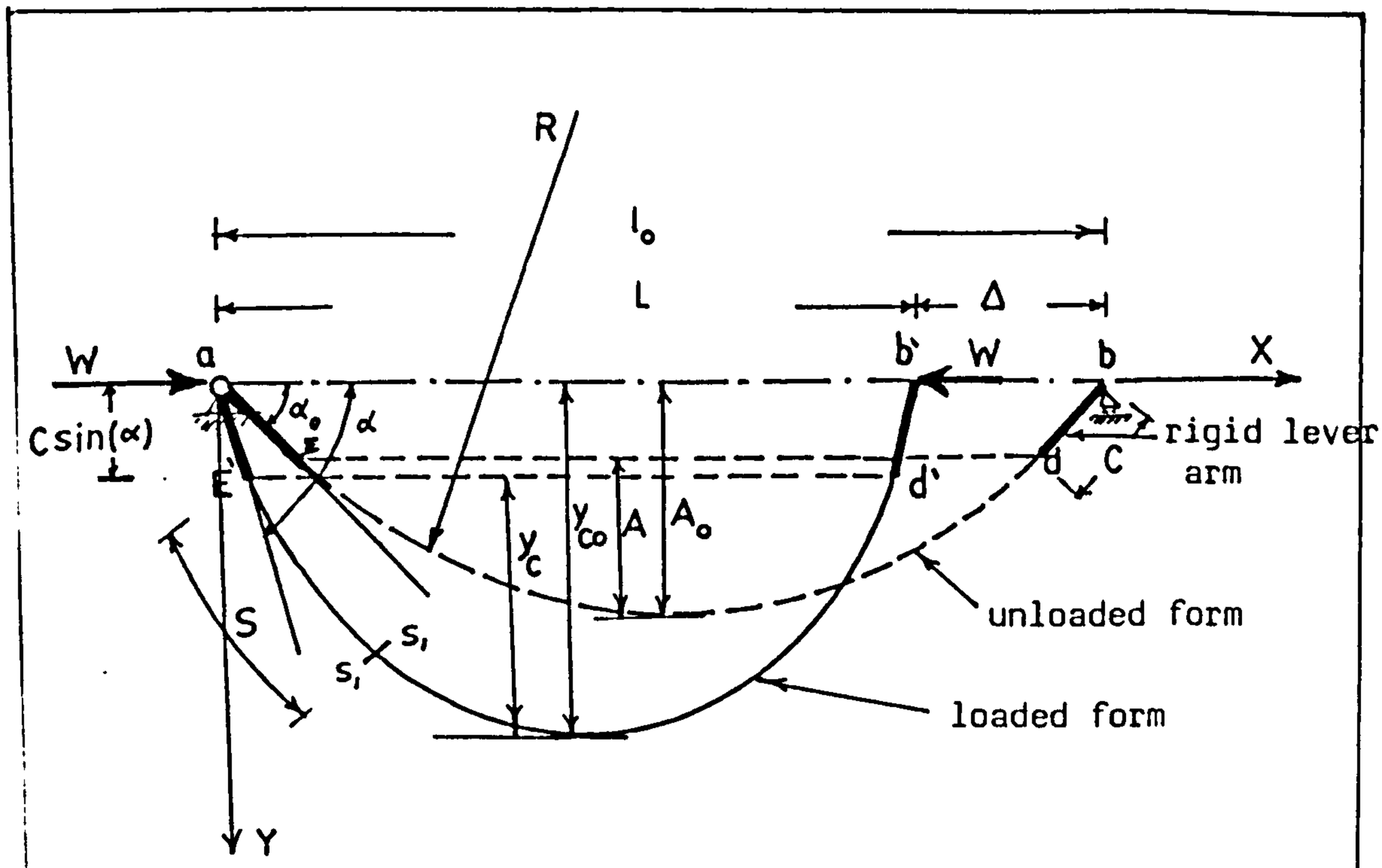

(a) Initially curved strut under eccentric loading

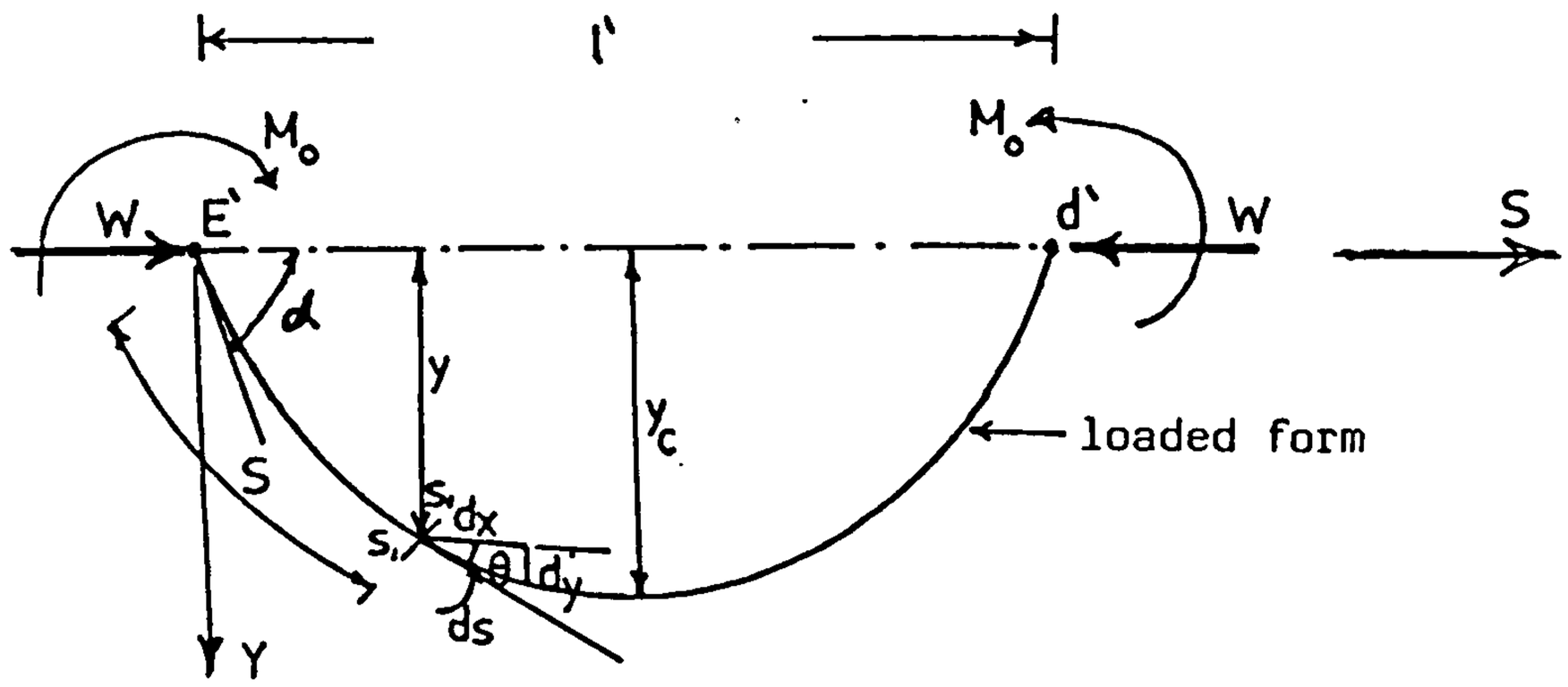

(b) Curved part of strut after deformation

Fig.(2-5) : Geometry of Eccentrically Loaded Strut

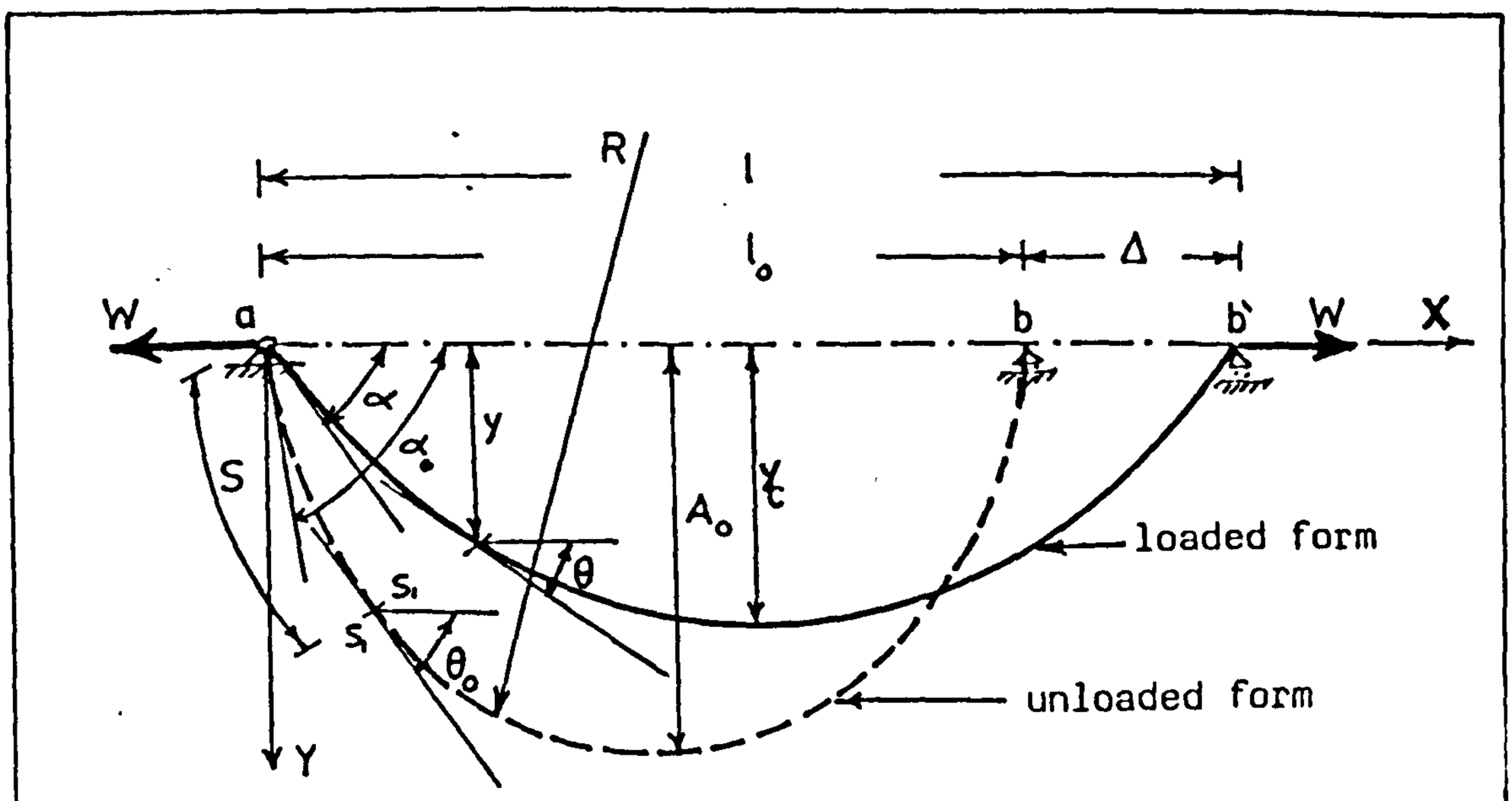

(a)

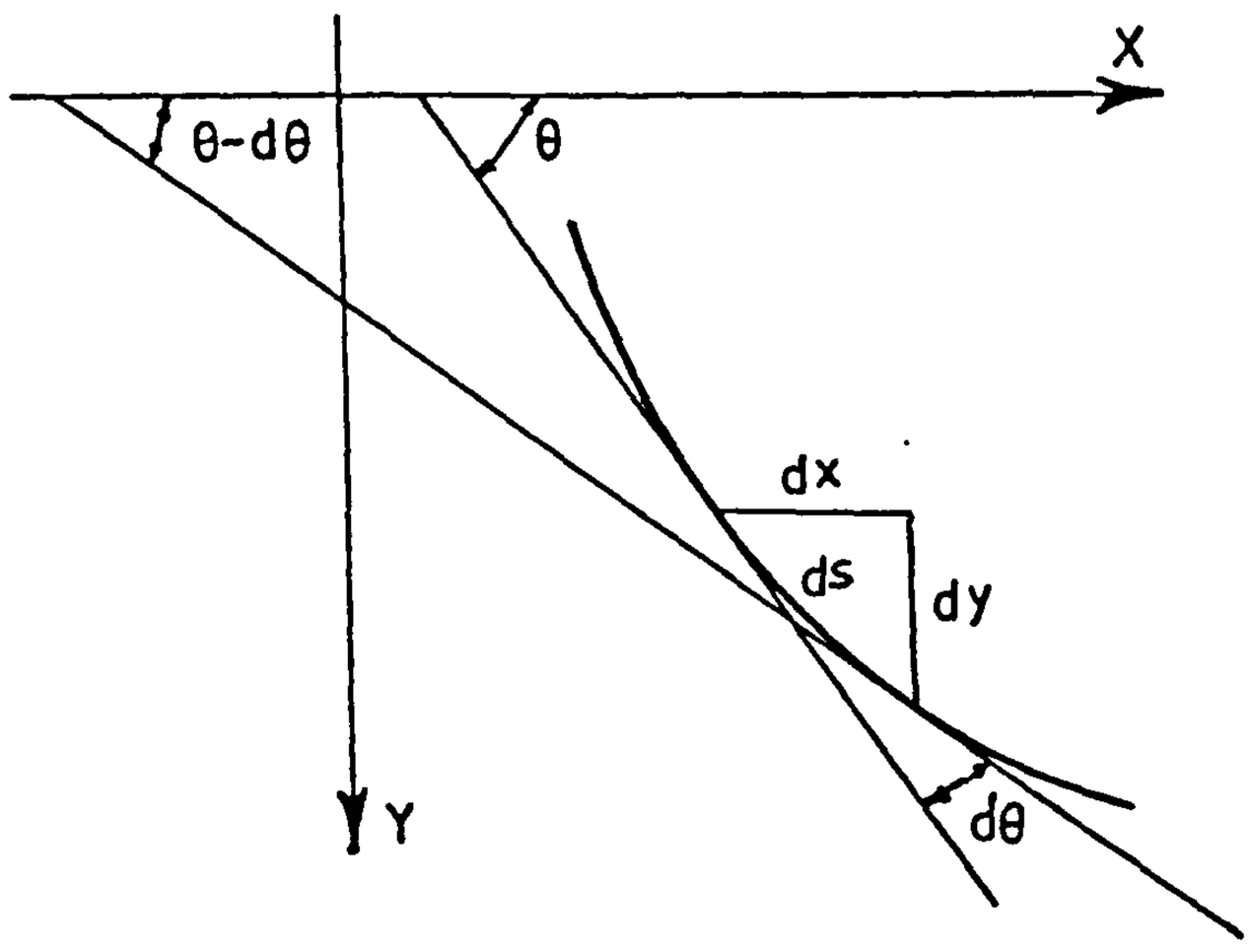

(b)

Fig.(2-6) : Geometry of Axially Loaded Ties

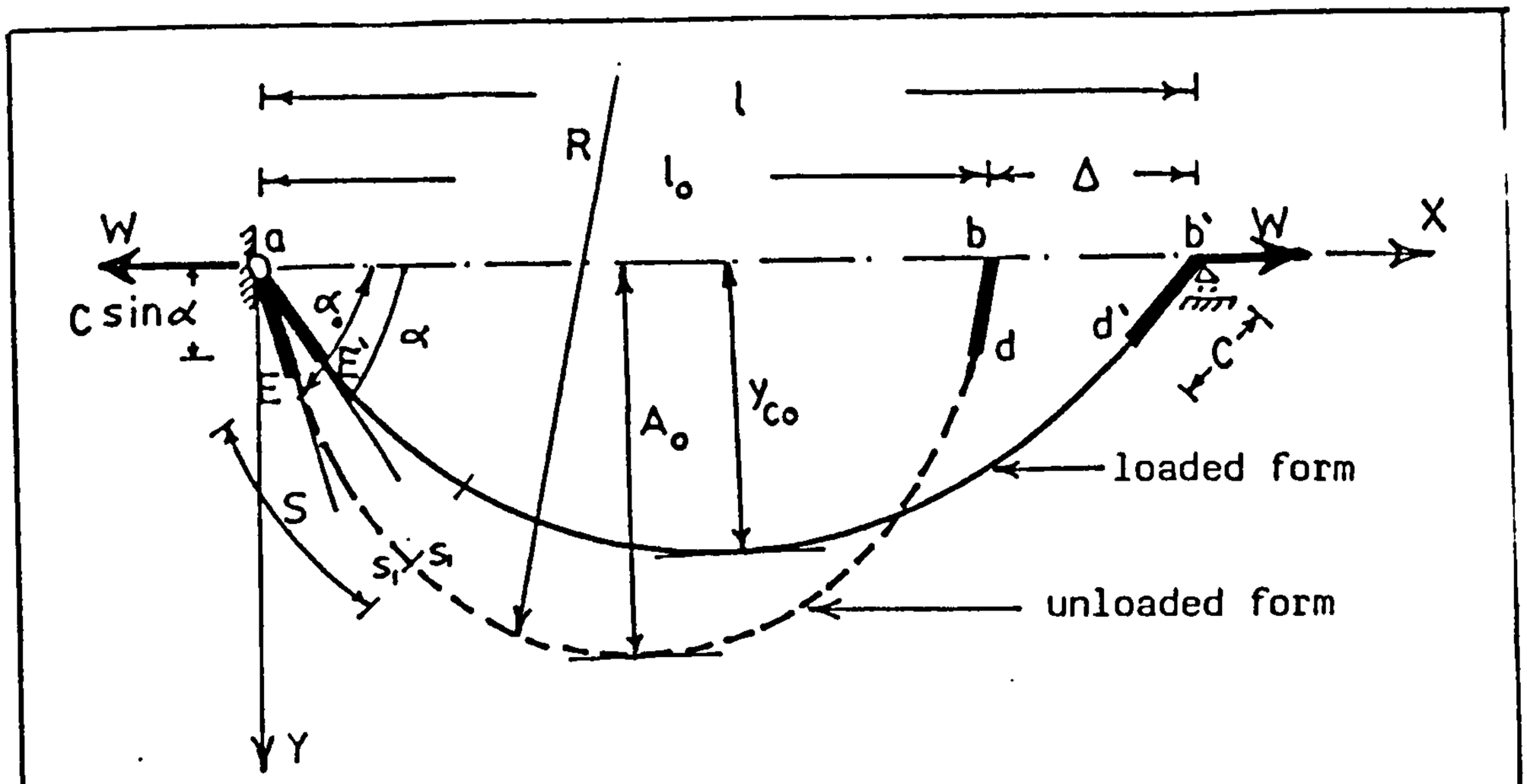

(a) Initially curved tie under eccentric loading

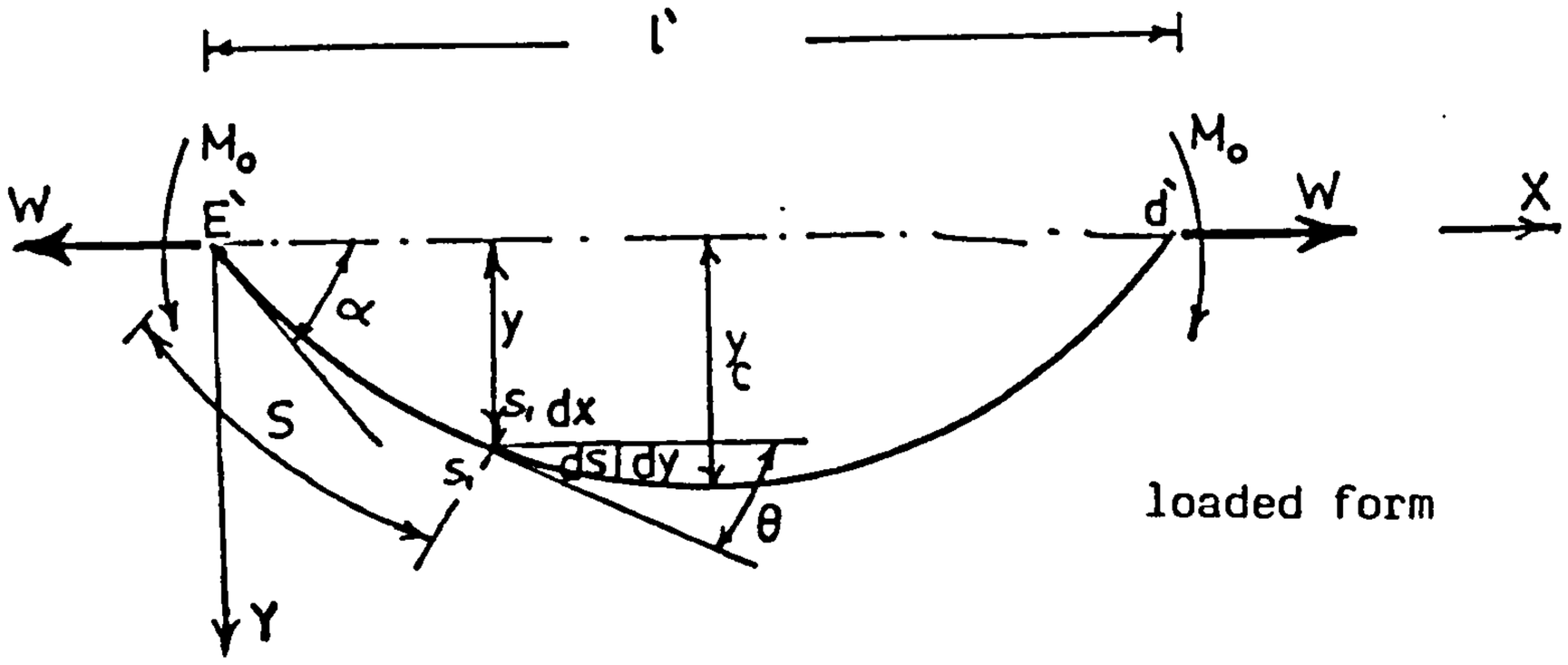

(b) Curved part of the tie after deformation

Fig.(2-7): Geometry of Eccentrically Loaded Tie

NON-DIMENSIONAL
LOAD-DISP. RELATIONSHIP
FOR CURVED TIE
THEORY OF LARGE DEFORMATION

FIG.(2.8)

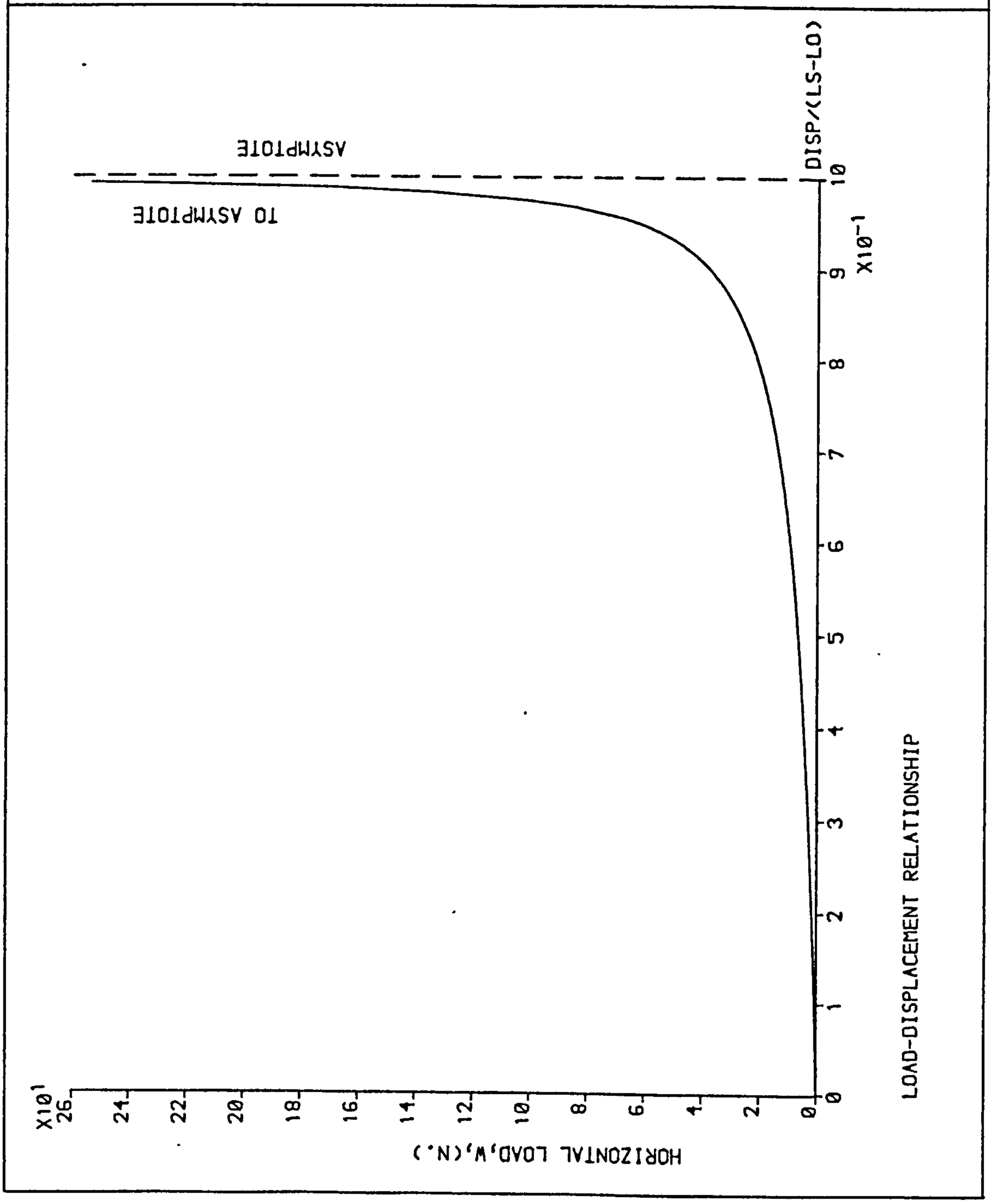

AXIAL STIFFNESS OF CURVED TIE

THEORY OF LARGE DEFORMATION

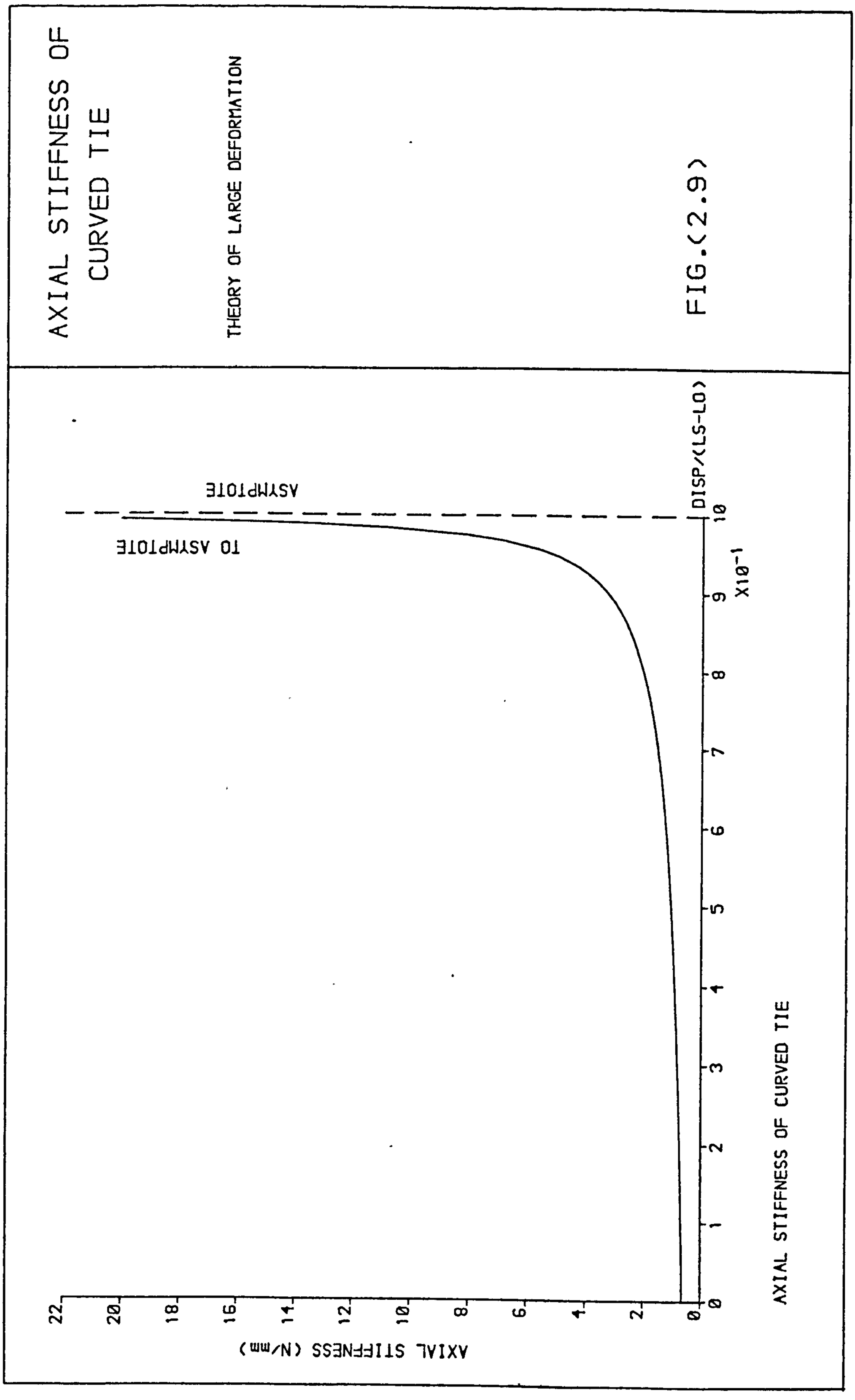

FIG.(2.9)

CHAPTER THREE

ELASTIC STABILITY OF FRAMEWORKS WITH NONLINEAR RESTRAINTS

3.1 Introduction

The previous chapter was concerned with those members which were capable of being isolated from the adjacent structure, for the purposes of analysis. In this chapter the analysis will deal with bent members (struts or ties) which need to be regarded as components of frameworks.

Generally most of the steel frame types of structures, especially tall building frames, need bracing to prevent them from excessive lateral deflection and also to brace the frame against instability. All structural frames can be classified into two basic types, the first is no-sway frames, where it is assumed that the ends of members are not free to move relative to each other e.g. triangulated frames or multi-storey portal frames with sway bracing. The second type is sway frames, where the resistance to lateral loads is provided by sway moments induced in the columns. Therefore the determination of elastic critical load depends on the type of frame. This elastic critical load is an important quantity in many framework calculations, and it is useful to have the means to evaluate it.

In this chapter the elastic non-linear behaviour of frames, consisting of columns or columns and beams (portal frames), stiffened by curved bracing is examined. Methods are described also for the calculation of the elastic critical loads.

3.2 The Stability of a Column with Nonlinear Lateral Restraints

To illustrate what happens when a column in a typical framework becomes unstable owing to sidesway, a simple model of a column together with a bracing member or members has been set up. The column is pinned at end "A" and loaded by horizontal and vertical loads "W and P," respectively, as shown in Fig. (3.1). Also the end of the column "B" is restrained against lateral movement in either direction by a pin ended curved bracing member or members, as shown in Fig. (3.1.a) or (3.1.b).

Since the bracing is normally made from a very light member compared to the column, it can be assumed to be a spring of non-linear stiffness "K" in the analysis. It is important to investigate the stability of the equilibrium of this model.

The behaviour of this system is used to illustrate the method of calculation the elastic critical load of a frame structure which has been discussed in great detail by Bolton [3]. Further discussions in this section are mainly concerned with a particular type of instability encountered.

3.2.1 The Stability of a Column Restrained by a Spring with Non-Linear Stiffness, K.

Fig. (3.2) shows a column pinned at one end and restrained by a spring of stiffness K at the other end. The column is subjected to lateral and axial forces "W & P",respectively, as shown. For any combination of loads P and W the spring will be deflected by an amount Δ. This means that under the combined influence of the

vertical load "P" and the horizontal load "W" lateral motion of joint "B" will occur until equilibrium, if possible, is attained. It will be observed that two distinct actions are operating on the system, such as,

i) The vertical load "P" acting at a sway eccentricity "Δ", causing an overturning action about the base of the column "A" (this is frequently referred to as the P-Δ effect). Also the horizontal load "W" will increase the overturning action about the base of the column.

ii) The restoring force "F" due to the horizontal displacement "Δ" of the equivalent spring which results in a restoring moment; M_R = F.H" about the base of the column.

It is possible to take moments about "A" and observe that the net restoring moment "M_A" is given by:

$$M_A = FH" - P\Delta - WH" = 0 \qquad (3.1)$$

where, $H" = H.\cos(\alpha_1)$

in which α_1 is the rotation of the column about the base "A".

The spring force "F" is equal to the spring stiffness "K" multiplied by the horizontal deflection "Δ" , thus, the spring force "F" may be written as K. Δ, and equation (3.1) becomes:

$$M_A = K\Delta H" - P\Delta - WH" = 0 \qquad (3.2)$$

i.e.

$$\Delta = \frac{W.H"}{KH"-P} \qquad (3.3)$$

when KH" = P in Eq. (3.3) then the horizontal displacement "Δ" tends to infinity and this means that the structure is in unstable condition. This defines the elastic critical load to be P_{cr} = K.H". This is the usual result for elastic critical load when the spring stiffness is constant [3]. The column will be in stable equilibrium up to a critical value of P equal to K.H" and then it becomes unstable once this load is reached.

3.2.2 The Elastic Critical Loads of a Column With Non-Linear Spring

It should be realized that the value of P_{cr} = KH", based on equation (3.2),is dependent on the assumptions that K is constant and also P remains constant with Δ. Essentially it is a mathematical device for calculating the critical value "P_{cr}" . If the fact that P may be a function of Δ is introduced in Eq. (3.2), because the stiffness of the spring is non-linear, then the relationship between the applied load "P" and its displacement "Δ" may be extremely complicated. The loads on the structure are likely to be a function not only of the distance through which it acts, but also of the rate of displacement. This rate is dependent on the non-linear stiffness of the equivalent spring and of the loads, because these affect the speed with which the loads can follow the movement of the column. Such dynamic effects are often very important in particular cases.

Now, the behaviour of a column restrained by an equivalent spring (for curved bracing) with non-linear stiffness "K" is studied as loading are applied from zero, the load being applied in specified increments. In this system the displacement "Δ" occurs as soon as the load set "P & W" is given a value, and the general stiffness-

displacement response to be expected may be seen in Figs. (3.3.a) and (3.4.a).

Fig. (3.3.a) shows the stiffness variation of an equivalent spring, for a curved compression bracing. It is seen that the stiffness "K_c" is decreasing as the displacement "Δ" increases.

Fig. (3.4.a) shows the stiffness variation of the equivalent spring for a curved tension bracing. As shown in the figure, the stiffness "K_t" is increasing as the displacement "Δ" increases.

It is necessary, now, to represent the relationship between the load P and the value KH". The graphs of the values KH" and P against Δ are plotted in Figs. (3.3.b) and (3.4.b) in cases of the spring subjected to compressive and tensile forces respectively, where, the upper curve (i) in the figures, represents the variation of the value KH" and the lower curve (ii) represents the variation of the vertical applied load P. These plots show that the value of P = KH" will occur at $\Delta=\infty$ (the same limit as indicated in Eq. (3.3)). This means that the condition of P = KH" is not sufficient for the calculation of the elastic critical load P_{cr}.

The response of the system to a given set of applied loads "P & W" is investigated, in which, under the combined influence of P and W, the structure will deflect by an amount "Δ" until equilibrium is attained.

Equation (3.2) gives the static equilibrium of the system. This equation involves the considerations of overturning action due to the applied loads ($WH'' + P\Delta$) and the restoring moment in the equivalent spring ($K\Delta H''$).

Making use of the assumptions that:

$$F_1 = K \Delta H'' \tag{3.4}$$

and

$$F_2 = WH'' + P\Delta \tag{3.5}$$

Then, Eq. (3.2) can be written in the form :

$$M_A = F_1 - F_2 = 0 \tag{3.6}$$

Now, it should be realized that the solution of Eq. (3.6) will be achieved when the net restoring moment, "M_A" is equal to zero, i.e. when the function F_1 is equal to the function F_2.

The relationship between the function "F_2" and the displacement "Δ" is represented by a straight line, as shown in Figs. (3.5.a) and (3.6.a) , with slope "P" and an intercept WH" on the vertical axis at Δ=0.

Also the relationship between the function "F_1" and the displacement "Δ" is shown in Figs. (3.5.b) and (3.6.b) for a spring loaded by a compressive and a tensile force respectively.

3.2.2.1 The Elastic Critical Load of a Column With a Non-Linear Spring Loaded by a Compressive Force

If the two figures (3.5.a) and (3.5.b) are superimposed the two lines, represent F_1 and F_2, intersect as shown in Fig. (3.5.c) and the column will be stable under the action of the given set of applied loads, and the corresponding configuration is represented by the points E'and E" , Fig. (3.5.c) , where Δ is equal to $\Delta_{E'}$ and $\Delta_{E''}$ respectively. Actually, as seen from Fig. (3.5.c), if the system is slightly displaced from E' (i.e. the equilibrium is altered from point E') by increasing the displacement "Δ", then the restoring moment "F_1" in the equivalent spring will increase more slightly than the overturning action "F_2" and the net restoring moment M_A in Eq. (3.6) will be positive. Therefore, the system will tend to revert to its initial undistorted position E'. This means that the stable equilibrium of the system will be at point E'. Point E" represents another equilibrium configuration but can only be reached by applying additional loads and then removing these gradually.

If the values of the applied loads are increased, the corresponding straight line in the diagram, Fig. (3.5.c) shifts upwards. Points E' and E", therefore, tend to draw nearer together and, at the limit, to coincide when the straight line is tangential to the curve "F_1" of the restoring moment in the spring. The value of the vertical load "P" corresponding to this limit condition provides the first elastic instability critical load "P_{cr1}" for a column restrained by a compressive initially curved bracing.

3.2.2.2 The Elastic Critical Load of a Column with a Non-Linear Spring Loaded by a Tensile Force

To determine the critical load for the system of a column restrained by a non-linear spring subjected to a tensile force, consider the two figures (3.6.a) and (3.6.b) which are superimposed in Fig. (3.6.c). The two lines, represent the functions F_1 and F_2, intersect as shown in Fig. (3.6.c) and the column will be stable under the action of the given set of the applied load. The corresponding configuration is expressed by point E'(Fig. (3.6.c)), where $\Delta = \Delta_{E'}$. If the values of the applied loads are increased, the value of F_2 also will increase, then the corresponding straight line in the diagram shifts upwards and the structure will be stable at another point G, where Δ_G is greater than $\Delta_{E'}$, and the spring at this point will be stiffer than at E'(as defined from the stiffness-displacement curve Fig. (3.4.a)). Hence the critical value of P provides the instability critical load P_{cr}, in this case, when P = KH" where K at this limit is equal to the stiffness when the curved tie becomes straight (i.e. $K = \frac{A_c E}{L_s}$). Therefore,the value of the critical load "P_{cr}" according to this condition can be written as:

$$P_{cr} = \left(\frac{A_c E}{L_s}\right) \cdot H" \qquad \text{at } \Delta = \infty \tag{3.7}$$

3.2.2.3 The Elastic Critical Loads for a Column Restrained By a Combined Bracing System

In this case consider the simple model shown in Fig. (3.1.b) which consists of a pin ended column "A-B" and restrained against lateral movement in the horizintal (X,Y) plane in either direction by pin

ended curved bracing members.

The column is loaded by horiziotal and vertical loads W and P respectively at joint B, this means that, once the loads are applied, one of the curved bracing will be under a compressive force and the other under a tensile force. The bracing members are replaced by springs of non-linear stiffness, K_c and K_t respectively, as shown in Fig. (3.7.a) where, K_c is the non-linear spring stiffness in compression and K_t is the non-linear spring stiffness in tension.

For the purpose of this research assume initially, at $\Delta = 0$ $K_c >> K_t$.

Figure (3.7.b) shows the forces acting on the column in the displaced position, where Δ is the lateral displacement of joint B. The restoring force "F_c"in the equivalent spring for bracing in compression is equal to $K_c.\Delta$. Also the restoring force" F_t " in the equivalent spring for bracing in tension is equal to $K_t.\Delta$. Therefore the total restoring force "F " can be written in the form:

$$F = F_c + F_t = K.\Delta \qquad (3.8)$$

where $$K = K_c + K_t \qquad (3.9)$$

K is the global stiffness of the whole combined bracing system.

Fig. (3.8.a) shows the variation in the global stiffness "K" of the system. The horizontal axis represents the lateral displacement Δ. The vertical axis represents the global stiffness K. It is seen that, at the beginning the stiffness decreases very rapidly as the variation in the lateral displacement Δ is small. As the displacement Δ, increases more, the variation in the stiffness is very small until the structure starts to retake its stiffness by the tensile spring stiffness, and becomes much stiffer. This means that, at the

beginning, the loading is mostly sustained by the spring in compression. If the loading is increased, and therefore the lateral deflection increases, then the stiffness of the spring in compression reduces and the stiffness of the spring in tension rises. Eventually the loading is sustained finally by the spring in tension.

Now, the equation of static equilibrium of the structure can be obtained by taking moments about the pin end "A" of the column, such as:

$$M_A = F.H'' - W.H'' - P.\Delta = 0$$

or

$$M_A = K\Delta.H'' - (W.H'' + P.\Delta) = 0 \qquad (3.10)$$

or

$$\Delta = \frac{WH''}{K.H'' - P} \qquad (3.11)$$

Again, the structure becomes unstable as $P = KH''$ at $\Delta=\infty$. Fig. (3.8.b) shows the relationship between the variation in KH'' and the applied load "P" against Δ, the upper curve (i) represents the variation in KH'' and the lower curve (ii) represents the variation in P. It is seen that, the value of $P = KH''$ at $\Delta=\infty$, and this gives the higher value the elastic critical load applied to the system.

Now,Eq. (3.10) can be simplified to the form:

$$M_A = F_1 - F_2 = 0 \qquad (3.12)$$

where,

$$F_1 = K\Delta.H'' \qquad (3.13)$$

which represents the restoring moment in the combined system of the springs about the pin end "A",

and $$F_2 = WH'' + P.\Delta \quad . \tag{3.14}$$

which represents the overturning action due to the applied loads about the hinged base "A".

The function F_2 in Eq. (3.14) represents a straight line with slope P and intercept W.H" to the vertical axis at $\Delta = 0$. This means that the function F_2 depends on two terms. The first is WH", the effect of this term is shown in Fig. (3.9.a) where the lateral load "W"is increasing, while the applied vertical load "P"is constant. It is seen from this figure that the straight line, which represents F_2 shifts upwards parrallel to its original position.

The second term is P.Δ, the effect of this term on F_2 is shown in Fig. (3.9.b) where the lateral load "W" is constant and the applied vertical load "P" is increased. It is seen from this figure that this is a straight line turning anticlockwise with a new slope equal to the new load "P".

The function F_1, Eq. (3.13), is dependent essentially on the characteristics of the non-linear springs stiffnesses. Fig. (3.9.c) shows the relationship between the function F_1 and the displacement "Δ" where, in this figure, F_1 is dependent on Δ as K is also dependent on Δ.

Now for any given load set "P & W" the equilibrium diagram is sketched in Fig. (3.10). This figure shows the relationship between

the functions F_1 and F_2 respectively against the lateral displacement "Δ."

It is seen from the figure that the straight line (i), which represents F_2, intersects the curve F_1 at point x_1 only. The column will be stable under the action of the given loads at this point x_1, where $\Delta = \Delta_{x1}$.

If the values of the applied loads "W & P" are increased, the corresponding straight line in the diagram shifts upwards and intersects the curve F_1 at points x_2, x_3 and x_4 respectively, as shown in Fig. (3.10), line (ii). These three points represent the static equilibrium of the structure, i.e. the net restoring moment "M_A" in Eq. (3.12) is equal to zero. The column will be stable under the action of the applied loads and the corresponding configuration is represented by the point x_2, where $\Delta = \Delta_{x2}$.

Points x_3 and x_4 represent other equilibrium configurations, where $\Delta = \Delta_{x3}$ and Δ_{x4} respectively. At point x_3 the equilibrium is unstable. Also at x_3 an increase in load leads to a reduction in deflection. Actually, as seen from the figure (3.10), if the system is slightly displaced laterally from point x_2, by increasing the displacement Δ, by a small amount u, in this case there are two possibilities:

<u>The first</u> is, if $\Delta_{x2} + u < \Delta_{x3}$, then the restoring moment "F_1" increases more than the overturning action "F_2", hence, the net restoring moment M_A in Eq. (3.12) will be positive and the system will tend to revert to its initial undistorted position x_2.

The second is, if $\Delta_{x2} + u > \Delta_{x3}$, then the overturning action "F_2" increases more than the restoring moment "F_1", hence the net restoring moment "M_A" will be negative and the structure will move forward until the new equilibrium position x_4 is reached. This second case explains why the structure, at x_3, is unstable and not at x_4.

If the system of the applied loads (P & W) are increased more, then the straight line will shift upwards more, therefore points x_2 and x_3 tend to draw nearer together and at the limit, to coincide at point x, when the straight line is tangential to the curve of F_1, as shown in Fig. (3.10) line (iii). The value of P corresponding to this limit condition provides the first instability critical load "P_{cr1}".

A small increase in the load at this limit will lead to a sudden change in the deflection "Δ "until the new equilibrium position at y is reached, and the dynamic effects are often very important in this case. Between x and y the stiffness "K" of the structure reaches its minimum value and, therefore, the value of function F_1 is lesser than the value of function F_2, so that the static equilibrium cannot be achieved. This stage represents the region of unstable equilibrium. In this research this will be called the region of "transient instability".

However, further increase in the set of the applied loads than the first elastic critical values (i.e. $P > P_{cr1}$) increases the lateral displacement"Δ" and the straight line represents F_2, shifts upwards more and more, and the structure will move directly to the stable equilibrium x_5, as shown in Fig. (3.10), line (iv). The structure at

this point is stable, where the equivalent spring stiffness "K" is increased. This means that there is a critical value of P which is defined as P_{cr} = KH" at $\Delta=\infty$ (as explained in the case of a tensile spring).

From the above discussion it is seen that the critical load, for a column restrained by a combined curved bracing, depends essentially on the characteristics of the structure, hence on the relationship between functions "F_1" and "F_2".

3.2.2.3.1 Influence of the Ratio R_i = P/W on the Phenomenon of Transient Instability

For any given set of applied load "P & W" consider an arbitrary ratio "R_i" between P and W (i.e. R_i = P/W) which is relatively low. Once this system of the load is applied to the structure, then it will be displaced by an amount "Δ" until stable equilibrium is achieved.

Fig. (3.11) shows the equilibrium position of the structure where, the corresponding configuration is represented by point x. Now if the ratio R_i between P and W is kept constant as the set of the applied load "P & W" is increased, then the structure will be stable at another equilibrium position. Points x_1, x_2 and x_3 represent the positions of the stable equilibrium of the structure according to the successive increment in the applied loads P and W respectively.

It is seen from Fig. (3.11) that the structure has only one position of equilibrium, this means that there is only one solution to the equilibrium equation (Eq. (3.12)). According to this case,

the phenomenon of transient instability does not appear and the overall behaviour of the structure is in stable equilibrium until the applied loads reach the critical values dependent on the limiting stiffness at $\Delta=\infty$ as explained in the previous article.

3.2.2.3.2 The Relationship Between the Applied Loads and The Displacement "Δ"

It is seen from the previous articles that the lateral displacement "Δ" is dependent on the applied loads "P & W" and also on the characteristics of the non-linear bracings.

The relationship between the vertical load "P" and the displacement, "Δ" where R_i = P/W = constant, is illustrated graphically in Fig. (3.12.a). It is seen from this figure that the variation of the vertical load "P", where P=F(Δ) is dependent on the ratio "R_i".

In Fig. (3.12.a) curve (i) represents the non-linear relationship between P and Δ in case of no transient instability, where the ratio R_i is relatively low. The elastic critical load, in this case, is equal to P_{cr}, as explained previously. Curve (ii) represents the relationship between "P" and "Δ" where, in this case, the phenomenon of transient instability arises. It is seen from the curve (ii) that at point x (i.e. at the onset of the transient instability, see also Fig. (3.12.b)), the slope of the tangent to the load-displacement curve is equal to zero.

Thus, at point x,

$$\frac{dP}{d\Delta} = 0 \quad , \quad \Delta = \Delta_1 \quad \text{and} \quad P = P_{cr1} \tag{3.16}$$

It is of interest to consider the solution for the load P_o in Fig. (3.12.a). At point B" the slope of the load-displacement curve is equal to zero, i.e. $\frac{dP}{d\Delta} = 0$, and the value of the vertical load is equal to P_o. Also, in Fig. (3.12.b) the straight line representing the function "F_2", at vertical load equal to P_o, is tangential to the curve "F_1" at point B". At this load "P_o" the structure has two equilibrium positions i.e. at points B and B". Point B represents the stable equilibrium of the structure. There is no path to point B", where in the region B-B" the net restoring moment M_A, Eq. (3.12), is positive, and the structure will be stable only at point B as explained before. Point B" can only be reached by applying additional loads and then removing these gradually. Thus at point B":

$$\frac{dP}{d\Delta} = 0 \quad , \Delta = \Delta_{11} > \Delta_1 \quad \text{and} \quad P = P_o < P_{cr1} \tag{3.17}$$

It is seen from Eq. (3.17) that the displacement "Δ_1" at the onset of transient instability can be defined as the lowest displacement at $dP/d\Delta = 0$. Also the elastic critical load P_{cr1} is the highest vertical load at $dP/d\Delta = 0$.

This analysis may be useful to the determination of the elastic critical load "P_{cr1}" at the onset of transient instability region, numerically.

3.3 Numerical Solutions to Determine the Transient Instability Region and the Corresponding Critical Load P_{cr1}

It is necessary to determine the value of the critical load "P_{cr1}"

at a specified ratio "R_i", where the onset of transient instability is encountered, by numerical methods rather than graphically.

It is seen from the relationship between the functions F_1 and F_2 and the lateral displacement "Δ", which is depicted graphically in Fig. (3.12.b) that, at point x, i.e. at the onset of transient instability region, the displacement "Δ" becomes close to the tangent point deflection "Δ_1" and the vertical load "P" approaches the critical value "P_{cr1}". Once this point has been reached the critical value "P_{cr1}" will be obtained.

It is obvious that the critical value "P_{cr1}" depends on the ratio "R_i" between the system of the applied loads "P & W" and also on the lateral displacement "Δ" .

Two numerical methods for calculating the theoretical value of the critical load "P_{cr1}" and also the relationship between the load "P" and the corresponding displacement "Δ" are adopted. The two methods are described in the next sections.

3.3.1 Tangent Slope Method

The critical value of the applied vertical load "P_{cr1}" and the corresponding lateral displacements, at the onset and the end of transient instability, may be obtained directly by calculating the slope of a line between two successive points on the load-displacement curve. The critical load "P_{cr1}" and the corresponding lateral displacement "Δ_1" will be obtained when the slope of the line tends to zero and the increment in the displacement between the two successive points tends also to be very small. The steps of

the calculation may be summarized as follows:

1. A small value of the lateral displacement "Δ" is chosen.

2. The corresponding stiffness of each equivalent spring, (i.e. K_c and K_t) for this value of Δ, is calculated hence the global stiffness "K" is obtained (Eq. (3.9)).

3. The value of the function "F_1" is calculated (Eq. (3.13)).

4. The values of the applied loads "P & W" can be obtained from Eq. (3.12), which can be written in the following form:

$$F_1 - \left(\frac{P}{R_i} \cdot H'' + P.\Delta \right) = 0$$

or

$$P = \frac{F_1}{H''/R_i + \Delta} \qquad (3.18)$$

where, $W = P/R_i$.

5. The steps 1 to 4 are repeated for higher values of Δ, without changing the chosen ratio "R_i". The increment in the displacement "δ" between two successive points is chosen relatively small, where $\delta = \Delta_i - \Delta_{i-1}$.

6. The slope of the line "S" between two successive points, on the load-displacement relationship, can be calculated from the following equation:

$$S = \frac{P_i - P_{i-1}}{\delta} \qquad (3.19)$$

The slope "S" is positive if the value of the assumed displacement is less than or equal to the displacement at the onset of transient instability region "Δ_1" .

7. If the slope "S" tends to be zero or negative, then the value

of the displacement will reduce to $\Delta = \Delta_i - 2\delta$, where Δ_i is illustrated in Fig. (3.13). At this stage the increment in the displacement is reduced to half of the previous increment, then the procedure is repeated again until the slope "S" tends to zero and also the increment "δ" tends to be very small. Once this condition is reached, the lateral displacement Δ_1, at the onset of transient instability, and the corresponding critical load P_{cr1} are obtained.

8. The processes of the calculation are repeated for a larger value of Δ than Δ_1 with an increment in the displacement equal to the original increment "δ". The corresponding values of the vertical load "P" and the slope "S" are obtained. The vertical load "P" in this case, will be smaller than the critical load "P_{cr1}" and hence the slope "S" will be negative. If the displacement is increased more and more, then the results of the corresponding vertical loads and the slopes will start to increase also. The lateral displacement at the end of the transient instability, Δ_2, will be obtained when the corresponding load P reaches P_{cr1} again (as shown in Fig. (3.13)).

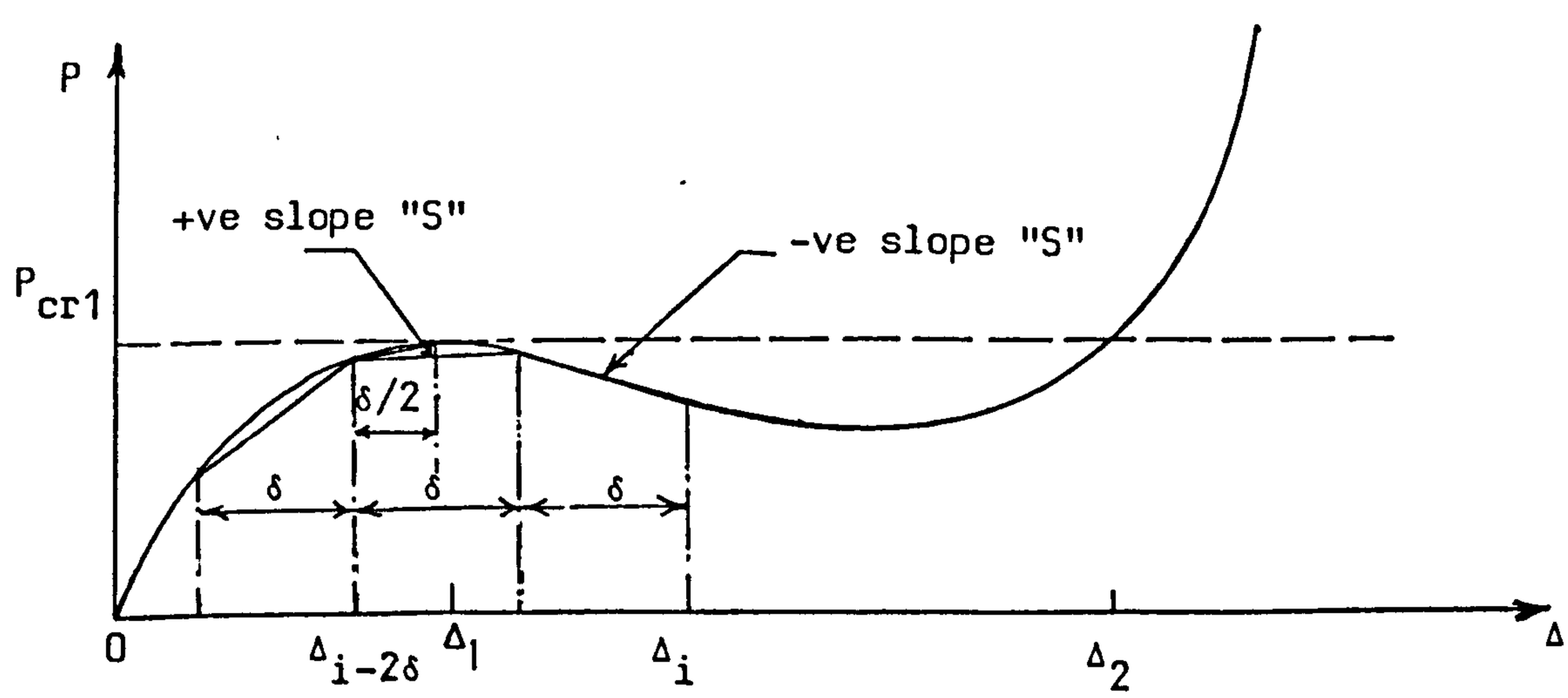

Fig.(3.13): Illustration of Tangent Slope Method

3.3.2 Influence Coefficient Method

The values of the lateral displacement "Δ" and the corresponding values of the vertical load "P" can be represented by a mathematical equation using a numerical method of Chebychev mathematical approximation for curve fitting [17,24,38,39]. In this research a NAG Computer library routine (E02ACF) [67] was used to calculate a polynominal to fit this set of data points. The aim of this routine is to approximate the set of data points as closely as possible with a specified function $P = f(\Delta)$, this means that there is a dependent variable "P" and independent variable "Δ". Therefore the routine determines a polynomial of given degree which is a minimax fit to data points with equal weights. The data points have been presented by the values of P and Δ . These values are calculated by repeating the steps 1 to 5 explained in the previous article (3.3.1), with equal increments in the displacement "Δ". The end of the calculation of Δ and P will be reached when the curved tensile bracing is straight i.e. when $\Delta = L_s - L_o$ for tensile bracing member. To arrive at a satisfactory degree of the polynomial it will be necessary to try several different degrees and examine the results graphically. Initial guidance can be obtained from the value of the maximum residual between the set of data points and the function f(Δ). This will vary with the degree of the polynomial. The residual of a single data point (Δ_i, P_i) to the function can simply be taken as $\xi_i = P_i - f(\Delta_i)$, this residual "ξ" was considered as a very small value $(0.001\% P_i)$.

Now the value of the critical load "P_{cr1}" and the values of the

displacement defining the region of the transient instability can be determined by following the next steps:

1. The general form of the polynomial can be written such as:

$$P = f(\Delta) = \sum_{i=0}^{i=n} a_i \Delta^i \qquad (3.21)$$

where, a_o and a_n are the coefficients of the polynomial, and n is the degree of the polynomial.

2. The critical value P_{cr1} and the value of the displacement Δ_1 at the onset of the transient instability region can be obtained when, $P' = dP/d\Delta = f'(\Delta) =$ zero.

or

$$P' = f'(\Delta) = \sum_{i=1}^{i=n} a_i \Delta^{i-1} = \text{zero} \qquad (3.22)$$

The roots of equation (3.22) can be calculated using the NAG library routine E02AEF [67]. This routine evaluates the roots of a polynomial in its Chebychev-series form [24,38], which interpolates (passes exactly through) data at a special set of points. The solution of the formula $P' = f'(\Delta) = 0$ using E02AEF [67] will give the roots of this equation. Some of these roots will be imaginary and the others are real. Some of the real roots will be negative and the others will be positive. The imaginary and the negative roots of the equation are neglected. The two positive roots which represent the solution of the true curve (i.e. within the range of data points) are selected. The lower positive root represents the value of the displacement "Δ_1" at the onset of the transient instability region. The corresponding vertical load $P = f(\Delta_1)$ represents the elastic critical load "P_{cr1}".

3. The value of the lateral displacement "Δ_2" at the end of the transient instability region can be obtained by computing the roots of the function $P = f(\Delta) = P_{cr1}$, where the value P_{cr1} is obtained from step 2. The NAG library routine E02AEF was used again to compute the roots of this function. The imaginary and the negative roots are neglected. The two positive roots which represent the solution of the true curve are selected. Thus the solution of the equation, $P = f(\Delta) = P_{cr1}$, will give two values. The lower represents the lateral displacement Δ_1, this value Δ_1 can be checked with that obtained from step 2. The higher value represents the lateral displacement Δ_2 at the end of the transient instability region.

3.4 The Stability of Multistorey Framework Stiffened by Curved Diagonal Bracing

Many types of bracing have been used in steel frames. These types normally take the form of inclined members, having small cross-sectional area in comparison with columns and beams of the frame. The most commonly used is diagonal bracing as shown in Fig. (3.14.a). Assuming all joints of the frame are pinned connections and the columns have the same cross-sectional area, then Fig. (3.14.a) can be transformed to Fig. (3.14.b) with cross bracing. If the loadings are only applied at the joints and the columns are sufficiently stiff, then it is reasonable to assume just a typical one storey of the frame with cross bracings as shown in Fig. (3.14.c). For further analysis it is seen from the above discussion that the sway deflection characteristics of a single story portal frame can be used to obtain the corresponding characteristics of a

particular family of multi-bay multi-storey portals [2,34].
Thus for all these portals the equivalent single storey portal frame may be obtained by the application of the following rules:

1. In the single storey frame the sum of column stiffnesses is equal to the sum of column stiffnesses of the original frame.

2. In the single storey frame the sum of the columns loads is equal to the sum of the columns loads of the original frame multiplied by an equivalence factor.

3. The stiffness of the cross bracing in the single storey frame is the sum of the stiffnesses of the equivalent diagonal bracing in the original frame, as shown in Fig. (3.14).

4. The beam stiffness in the single storey frame is equal to the sum of the beams stiffnesses of the original frame.

An analysis of the frame shown in Fig. (3.14.c) shows that, the cross bracing is subjected to a compressive force and tensile force. Since all joints are pinned connections and the cross section of the columns and the beam are much stiffer than the bracing members, therefore a fairly close estimate of the critical load and the behaviour of the frame can be obtained if the equivalent single framework shown in Fig. (3.14.c) is simplified judiciously to a simple column with inclined equivalent non-linear springs as shown in Fig. (3.15). Consequently in calculating the critical load,attention

may be confined to the simpler problem in Fig. (3.15.c), in which there is no bending in the column even when loaded.

This simpler column approach (Fig. (3.15.c) is identical to the previous structure explained before in section 3.2.2.3. The only difference is the equivalent springs (for bracings in compression and in tension) take the inclined position instead of the horiziontal position. Therefore a similar analysis to that explained in section 3.2.2.3 will be considered here.

Now, if the structure in Fig. (3.15.c) is disturbed from its vertical position under equivalent applied loads P_Q and W_Q then it will deflect by an amount Δ until equilibrium is attained, as shown in Fig. (3.15.d). In this figure the external loads P_Q and W_Q are the equivalent vertical and lateral loads applied at the column respectively. Also the forces F_c and F_t are the restoring forces in the equivalent springs for compression and tension bracing respectively, and these are dependent on the displacement Δ.

The equation of static equilibrium for the structure can be obtained by taking moment about the pin ended "A", Fig. (3.15.d) such as:

$$M_A = F_c.H \cdot \sin\alpha_{cc} + F_t \cdot H. \sin\alpha_{tc} - P_Q.\Delta - W_Q.H. \cos\alpha_1 = 0$$

or

$$M_A = F_1 - F_2 = 0 \qquad (3.20)$$

where, $F_1 = F_c \cdot H \cdot \sin\alpha_{cc} + F_t.H. \sin\alpha_{tc}$ (3.21)

F_1 is the restoring moment in the equivalent springs,

α_{cc} is the angle between the chord line of the compression bracing and the column after deformation, Fig. (3.15.d)

and α_{tc} is the angle between the chord line of the tension bracing and the column after deformation,Fig. (3.15.d).

Also, $$F_2 = P_Q \cdot \Delta + W_Q . H . \cos\alpha_1 \qquad (3.22)$$

where, F_2 is the overturning action, due to the equivalent system of the applied load, about the hinge "A", in which:

$$\alpha_1 = \sin^{-1} \left(\frac{\Delta}{H}\right) \qquad (3.23)$$

is the rotation angle of the column.

Equation (3.20) is identical with Eq. (3.12), therefore the relationship between the functions F_1 and F_2 is identical to the relationship explained before in section 3.2.2.3 and Fig. (3.10).

The remainder of this section is devoted to methods of determining the critical values of the applied loads and also the steps in the calculation of the restoring moment F_1 and the overturning action F_2.

One consequence of this simplification, described above , is that the axial deformation and the stiffnesses of the curved bracing members have to be estimated separately, before the calculation of the restoring moment in the springs "F_1". Another consequence of the equivalent model,(Fig. 3.15.c) is that the applied loads P_Q and W_Q have to be calculated first, before the calculation of the overturning action F_2.

To illustrate this,consider the pin jointed two storey portal framework with initially curved cross bracings, as shown in Fig. (3.16.a). In any storey "i" the stiffnesses of the initially curved bracing (i.e. the bracing in compression and in tension) are K_{ci} and K_{ti} respectively. Also in the same storey the values of the axial deformation in the bracings in compression and in tension are δ_{ci} and δ_{ti} respectively.

Suppose that the framework sways an amount Δ at the first storey level under a suitable loading. Now, the two storey framework can be replaced,first,by the equivalent single storey frame, Fig. (3.16.b) and then it may be replaced by an equivalent single column with inclined non-linear springs as shown in Fig. (3.16.c). (N.B. This simplification of the single storey frame can be made, only,in the case of constant height of the storeys of the original framework. If the height of the storeys of the original framework are not constant , then,the procedure for the general behaviour of the structure will be discussed in the next section).

Now the methods described in section 3.2.2.3 may be used to check the stability of this equivalent structure, (Fig. 3.16.c) and to determine the critical values of the applied loads.

It is instructive to review the steps of analysis in two stages:

Stage 1

i) The stiffnesses of the equivalent springs of bracings in compression and in tension can be calculated from the following formulas:

$$K_c = \sum_{i=1}^{i=N} K_{ci} \qquad (3.24)$$

$$K_t = \sum_{i=1}^{i=N} K_{ti} \qquad (3.25)$$

where, K_c is the stiffness of the equivalent spring of compression bracings,

K_t is the stiffness of the equivalent spring of tension bracings,

and N is the number of storeys of the original framework (N=2 in the example shown in Fig. (3.16.a)).

ii) The axial deformation of the equivalent springs for bracings in compression and in tension can be written as:

$$\delta_c = \frac{Z}{\sin(\alpha_o)} - \frac{Z-\Delta}{\sin(\alpha_c)} \qquad (3.26)$$

and

$$\delta_t = \frac{Z+\Delta}{\sin(\alpha_t)} - \frac{Z}{\sin(\alpha_o)} \qquad (3.27)$$

where,

Z is the span of the framework.

Δ is the horizontal displacement at the top of the equivalent single storey frame.

$$\alpha_o = \tan^{-1}\left(\frac{Z}{h}\right) \qquad (3.28)$$

is the angle between the chord line of the curved bracing and the vertical position in the undeformed shape (Fig. (3.16.a)),

h is the height of each storey (assumed to be constant),

$$\alpha_c = \tan^{-1}\left(\frac{Z-\Delta}{h\cos\alpha_1}\right) \qquad (3.29)$$

is the angle between the chord line of the deformed bracing in compression and the vertical position, Fig. (3.16.b).

α_1 is defined before in Eq. (3.23).

and $$\alpha_t = \tan^{-1}\left(\frac{Z+\Delta}{h\cos\alpha_1}\right) \qquad (3.30)$$

is the angle between the chord line of the deformed tensile bracing and the vertical position.

iii) The restoring forces in the equivalent springs F_c and F_t can be calculated as:

$$F_c = K_c \cdot \delta_c \qquad (3.31)$$

$$F_t = K_t \cdot \delta_t \qquad (3.32)$$

iv) The value of the restoring moment (i.e. the function F_1) can be easily obtained by taking the moments about the hinged base of the column "A" (the moment will be taken for the restoring forces F_c and F_t only, Fig. (3.16.c) and the resulting formula is obtained as follows:

$$F_1 = F_c \cdot H \cdot \sin\alpha_{cc} + F_t \cdot H \cdot \sin\alpha_{tc} \qquad (3.33)$$

where, $H = h$ is the height of the equivalent single column,

$$\alpha_{cc} = \alpha_c + \alpha_1 \qquad (3.34)$$

is the angle between the chord line of the compression bracing and the column after deformation, Fig. (3.16.c)

and $$\alpha_{tc} = \alpha_t - \alpha_1 \qquad (3.35)$$

is the angle between the chord line of the deformed tensile bracing and the column.

v) It is necessary to calculate the equivalent loads P_Q and W_Q needed to produce a convenient arbitrary sway displacement "Δ" at the top of the equivalent single column, Fig. (3.16.c). Suppose that the original framework sways an amount "Δ" at the top level of the first storey, so that the sway at the top of the frame is equal to N.Δ . Now the moment at the base of the original framework due to the external applied loads, only, must be equal to the moments at the pin end of the equivalent single column due to the equivalent external applied loads P_Q and W_Q i.e.

$$2PN.\Delta + W.Nh\cos\alpha_1 = W_Q.h\cos\alpha_1 + P_Q.\Delta$$

therefore,

$$W_Q = W.N \qquad (3.36)$$

and

$$P_Q = 2P.N \qquad (3.37)$$

Equations (3.36) and (3.37) give the equivalent applied loads W_Q and P_Q applied at the top of the equivalent single column shown in Fig. (3.16.b) and (3.16.c).

vi) The overturning action (i.e. the function F_2) can be easily determined from Eq. (3.22).

Stage 2

The elastic critical load "P_{cr1}", causing the transient instability can be estimated accurately, using one of the methods derived previously in articles (3.2.2.3) and (3.3), i.e. the graphical or numerical methods. The critical load P_{cr1}, i.e. the value of the vertical

applied load at the onset of the transient instability, can be defined when the straight line representing the function F_2 becomes tangential to the curve "F_1" as explained before in Fig. (3.12.b) or when $dP/d\Delta = 0$ at $\Delta=\Delta_1$, Fig. (3.12.b).

The elastic critical load "P_{cr}" is dependent on the limiting stiffness at $\Delta=\infty$, where at this limit the structure is unstable.

Therefore, there are four possibilities for the overall behaviour of the framework, and can be summarized as follows:

1. At $P_Q < P_{cr1}$, the structure is in stable equilibrium
2. At $P_Q \equiv P_{cr1}$, the equilibrium of the structure is unstable and this is represented by the phenomenon of transient instability.
3. At $P_{cr} > P_Q > P_{cr1}$, the structure will be in stable equilibrium again.
4. At $P_Q \equiv P_{cr}$, the equilibrium of the structure is unstable, where P_{cr} is dependent on the limiting stiffness at $\Delta=\infty$

3.4.1 The General Behaviour of a Multi-Storey Framework With Different Storey Height

The technique just described assumes the height "h" of each storey of the original multi-storey framework to be constant. If this height is not constant, then the equivalent single column with inclined springs will be as shown in Fig. (3.17) and the original framework cannot be simplified to a single storey frame. In Fig. (3.17.a), h_i is the height of the i^{th} storey, also α_{oi} is the angle between the chord line of the curved bracing and the vertical position, in any

storey i, in the original framework before deformation.

Suppose that the framework sways an amount "Δ" at the top of the first storey level, under a combined system of loading "P & W", Fig. (3.17.b). The deformation of any storey differs from any other, therefore, the characteristics of each storey are calculated separately. The lateral displacement at the top of any storey "i" can be represented as follows:

$$\Delta_i = \sum_{i=1}^{i=i} h_i \cdot \frac{\Delta}{h_1} - \sum_{j=1}^{j=i-1} \Delta_j \qquad (3.38)$$

where Δ is the lateral displacements at the top of the first storey.

and h_1 is the height of the first storey.

The sum of the storey displacement to the top of the framework is equal to:

$$\Delta_T = \sum_{i=1}^{i=N} \Delta_i \qquad (3.39)$$

where,

N is the number of the storeys.

The restoring forces in the equivalent springs, F_{ci} and F_{ti}, in any storey "i" can be written as:

$$F_{ci} = K_{ci} \cdot \delta_{ci} \qquad (3.40)$$

$$F_{ti} = K_{ti} \cdot \delta_{ti} \qquad (3.41)$$

where K_{ci} and K_{ti} are the stiffnesses of the equivalent springs for compression and tension bracing respectively, in any storey "i".

Also, δ_{ci} and δ_{ti} are the axial displacements in the equivalent springs for struts and ties, respectively, in any storey "i".

The values of K_{ci}, K_{ti}, δ_{ci} and δ_{ti} depend on the geometry of the storey "i" and also on the lateral displacement "Δ_i" at the top level of this storey.

The axial displacements δ_{ci} and δ_{ti} can be written according to the geometry of the storey "i" such as:

$$\delta_{ci} = \frac{Z}{\sin(\alpha_{oi})} - \frac{Z-\Delta_i}{\sin(\alpha_{ci})} \qquad (3.42)$$

and

$$\delta_{ti} = \frac{Z+\Delta_i}{\sin(\alpha_{ti})} - \frac{Z}{\sin(\alpha_{oi})} \qquad (3.43)$$

where,

α_{ci} and α_{ti} are the angles between the chord line of the bracings and the vertical position, in the i^{th} storey after deformation. Fig. (3.17.d).

and Z is the span of the frame.

Finally the values of the functions F_1 and F_2 can be written as follows:

$$F_1 = \sum_{i=1}^{i=N} \{[F_{ci}\cdot\sin\alpha_{cci} + F_{ti}\cdot\sin\alpha_{tci}][h_i]\} \qquad (3.44)$$

where,

α_{cci} and α_{tci} are the angles between the chord line of the compressive, tensile bracing, and the column after deformation respectively, Fig. (3.17.d).

Also,

$$F_2 = W \cdot \sum_{i=1}^{i=N} h_i \cdot \cos\alpha_1 + P_Q \cdot \Delta_T \qquad (3.45)$$

where α_1 is the rotation of the column.

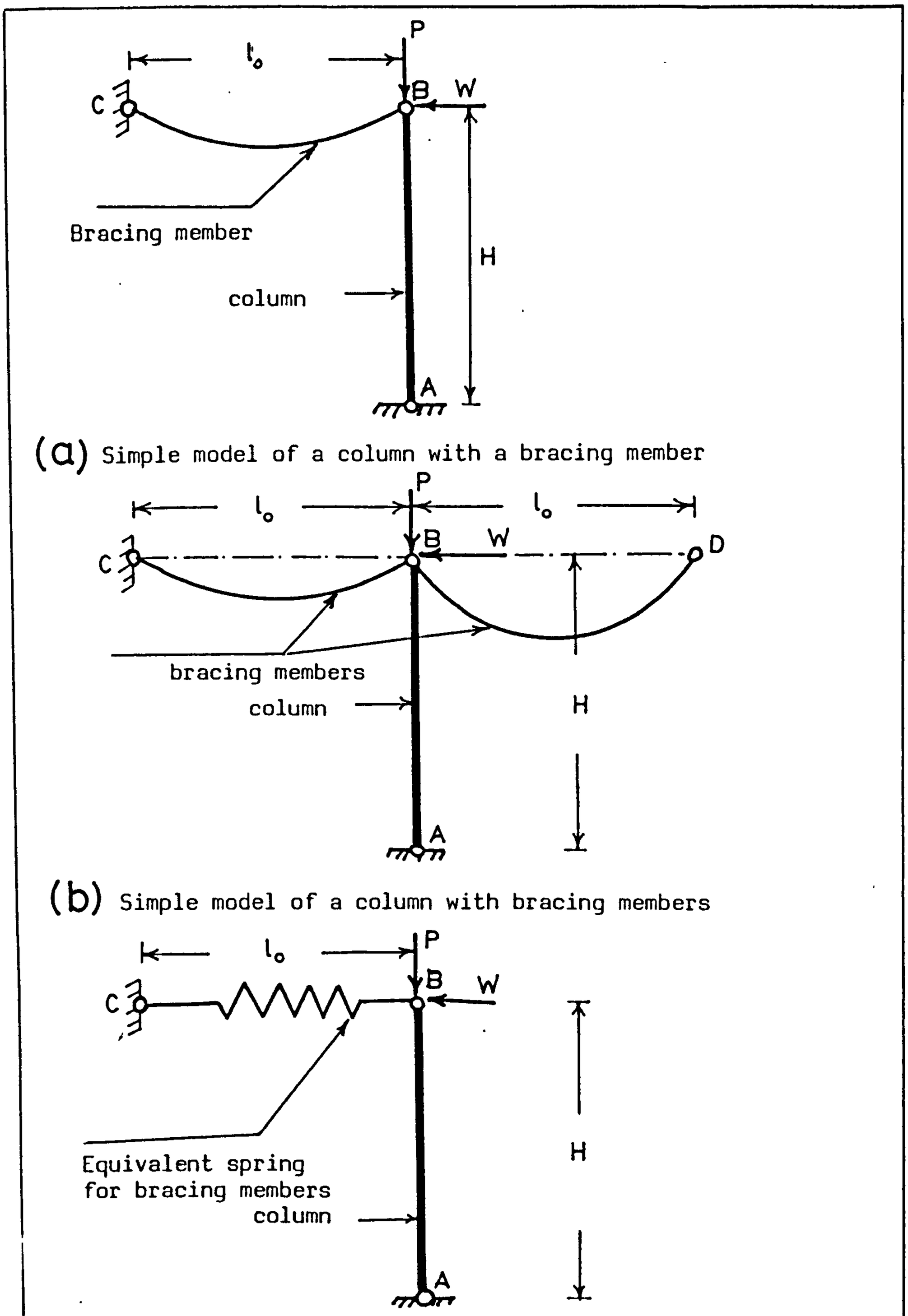

(a) Simple model of a column with a bracing member

(b) Simple model of a column with bracing members

(c) Simple model of a column with an equivalent spring

Fig.(3-1)

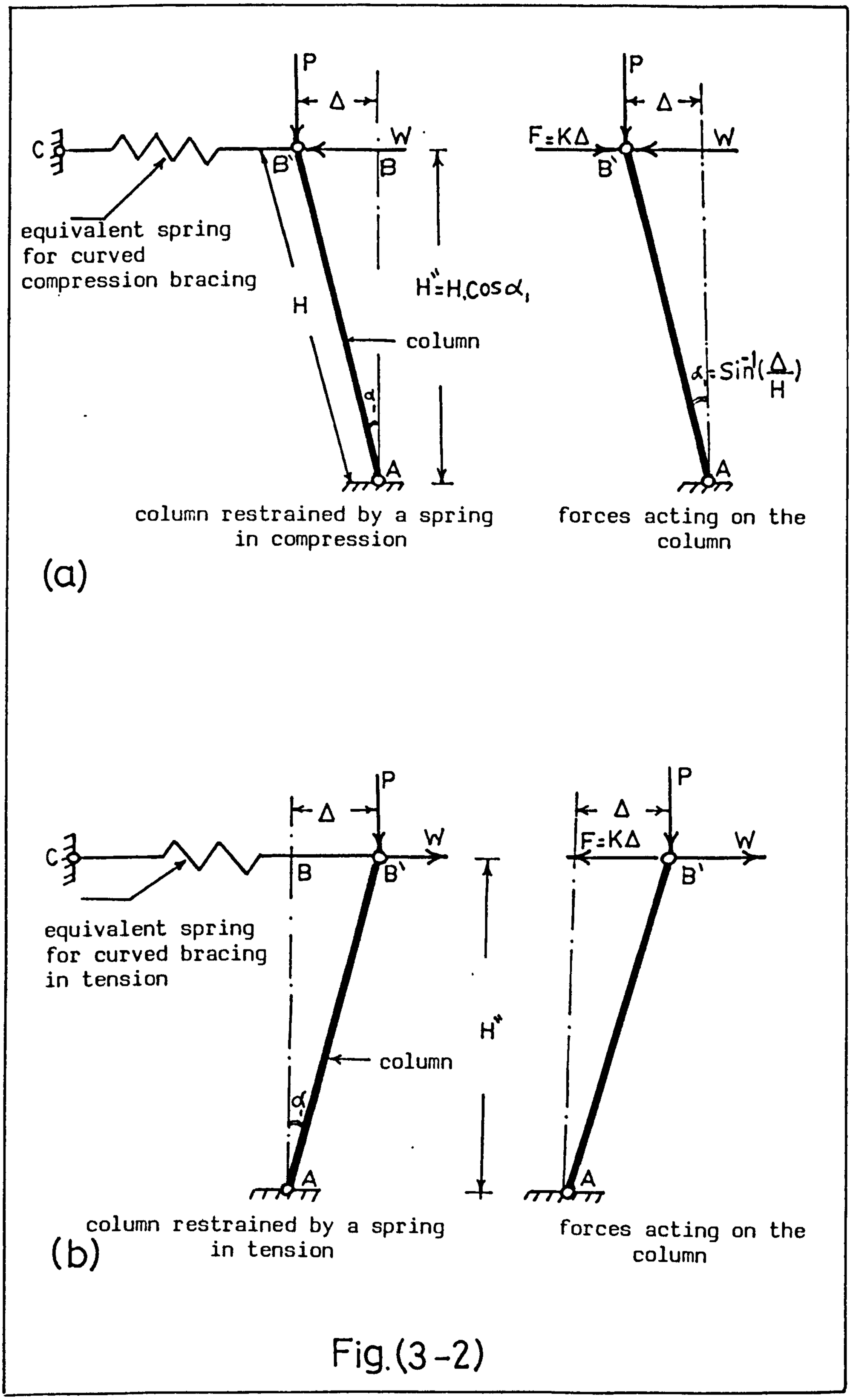

column restrained by a spring in compression

forces acting on the column

(a)

(b)

Fig.(3-2)

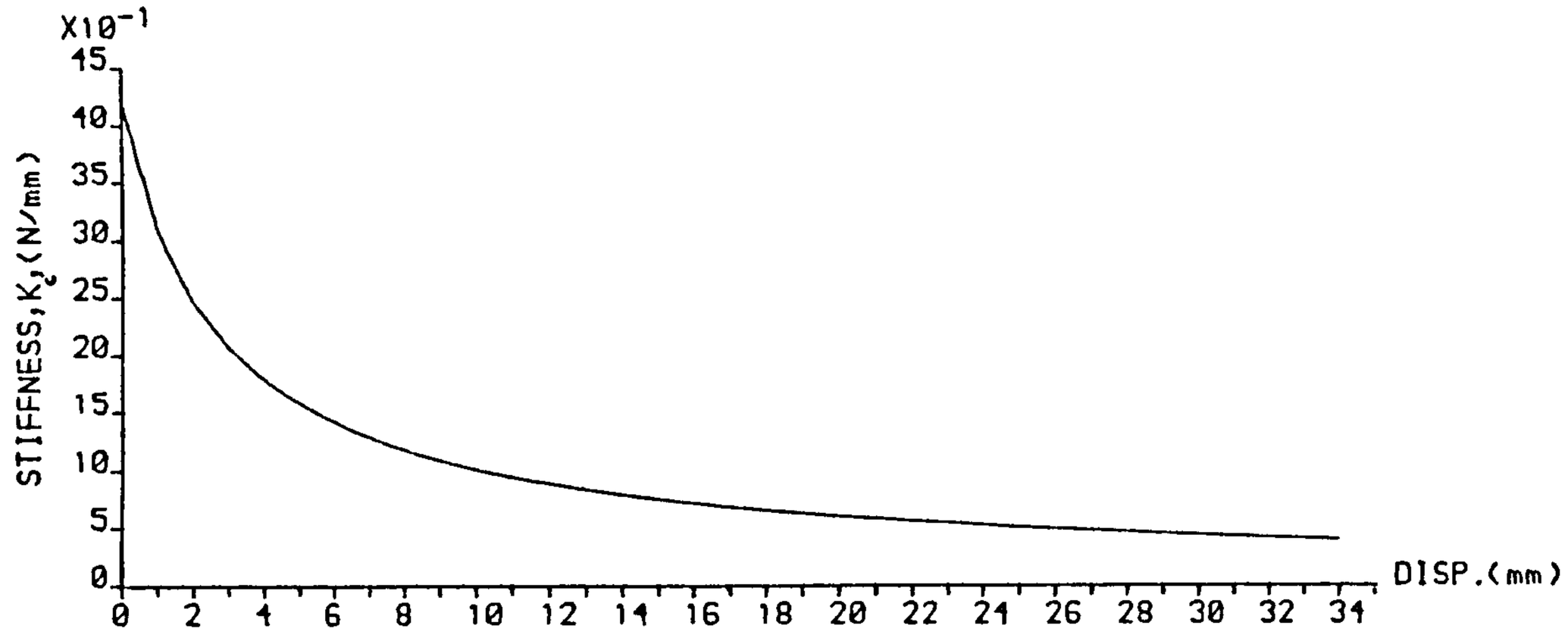

(a) STIFFNESS OF EQUIVALENT SPRING, FOR COMPRESSION BRACING.

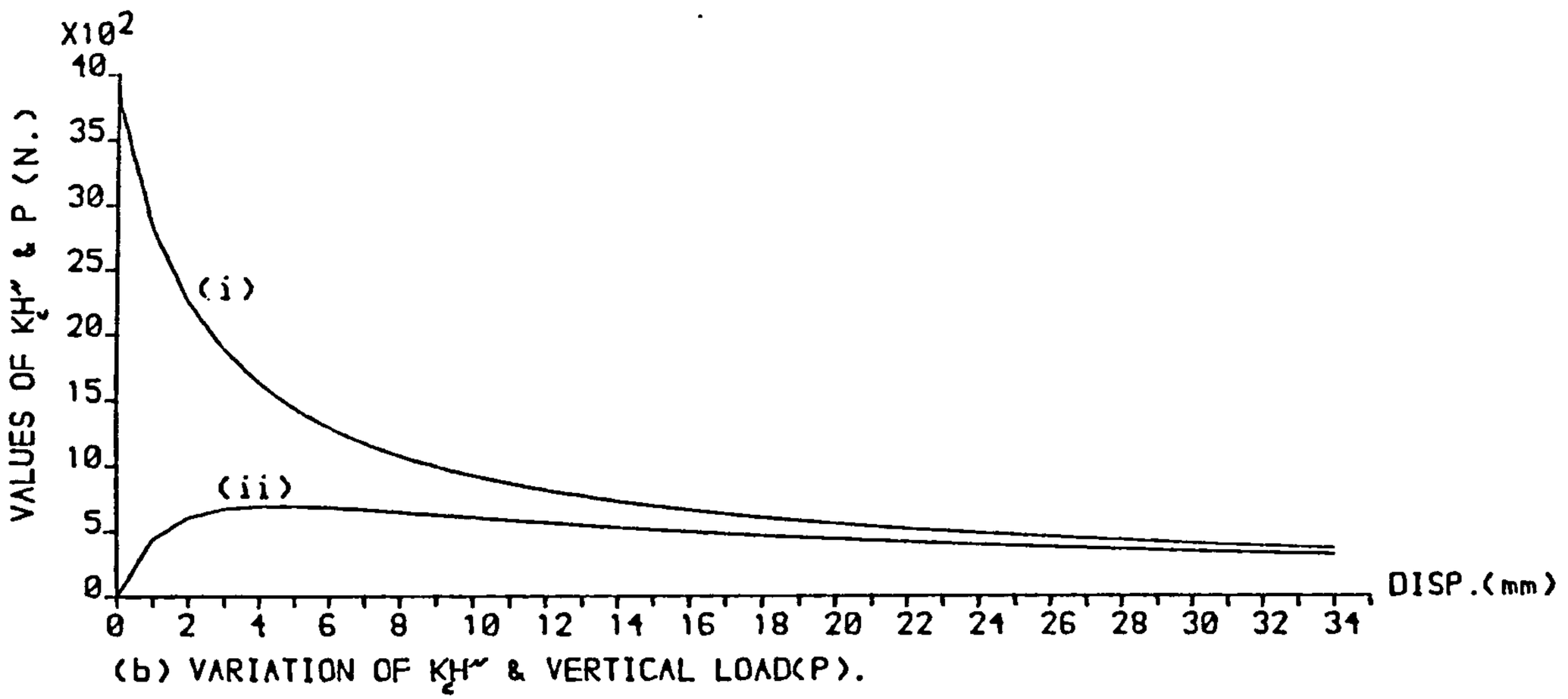

(b) VARIATION OF $K_c H^{\nu}$ & VERTICAL LOAD(P).

STABILITY OF COLUMN

RESTRAINED BY A COMPRESSION

BRACING SYSTEM

THE CRITICAL LOAD Pc IS

DEFINED AS $K_c.H^{\nu} = P$ AT $\Delta = \infty$

FIG.(3-3)

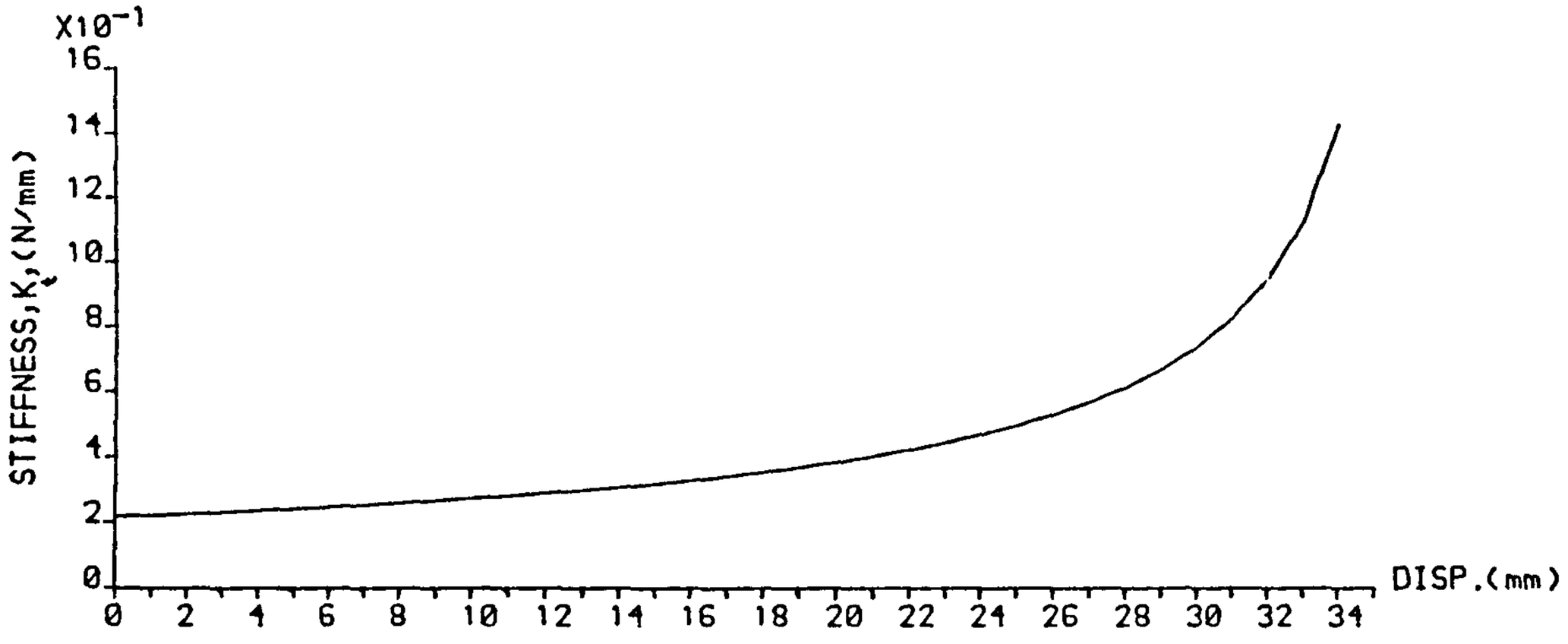

(a) STIFFNESS OF EQUIVALENT SPRING, FOR TENSION BRACING.

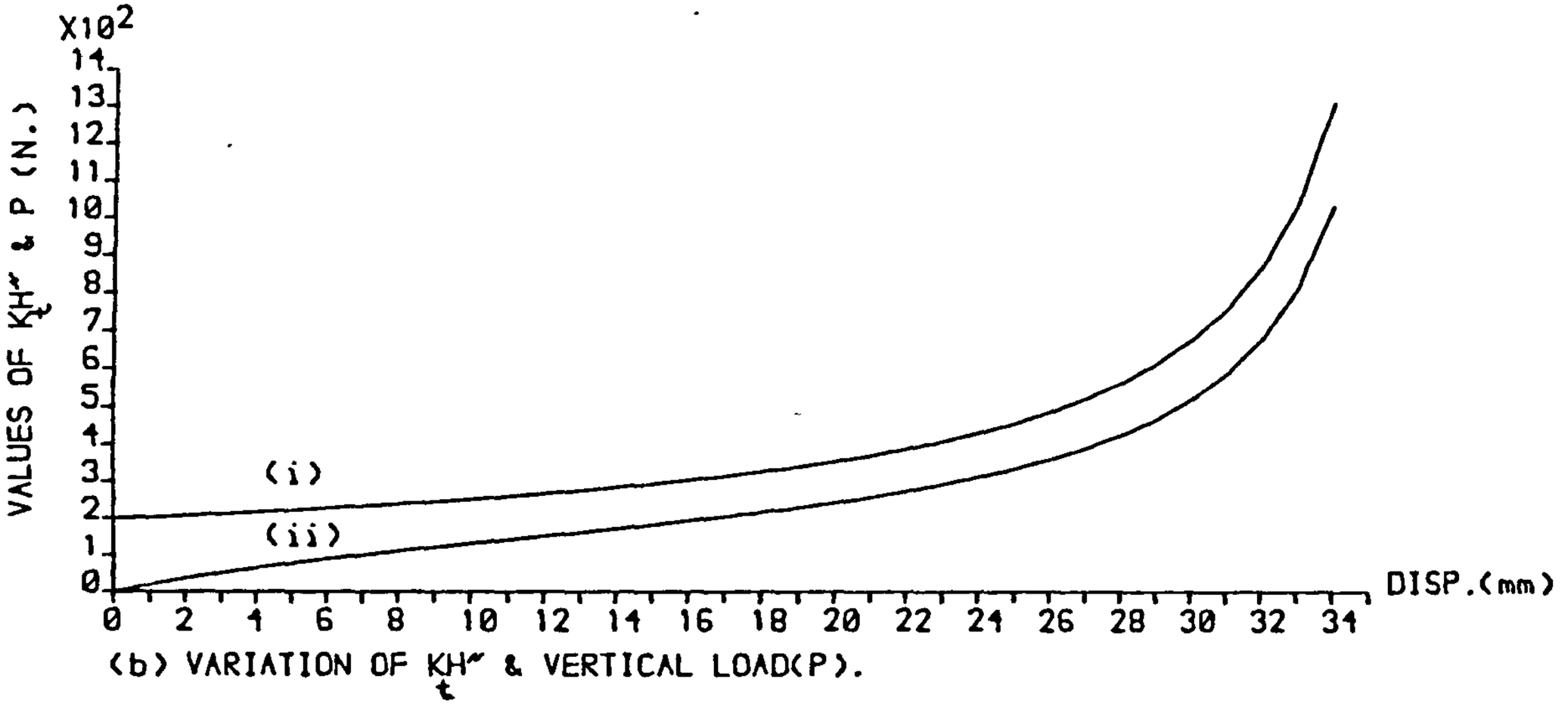

(b) VARIATION OF $KH^{\sim}_t$ & VERTICAL LOAD(P).

STABILITY OF COLUMN

RESTRAINED BY A TENSION

BRACING SYSTEM

THE CRITICAL LOAD Pc IS

DEFINED AS $K_t.H^{\sim} = P$ AT $A = \infty$

FIG.(3-4)

STABILITY OF COLUMN

RESTRAINED BY A COMPRESSION

BRACING SYSTEM

FIG.(3-5)

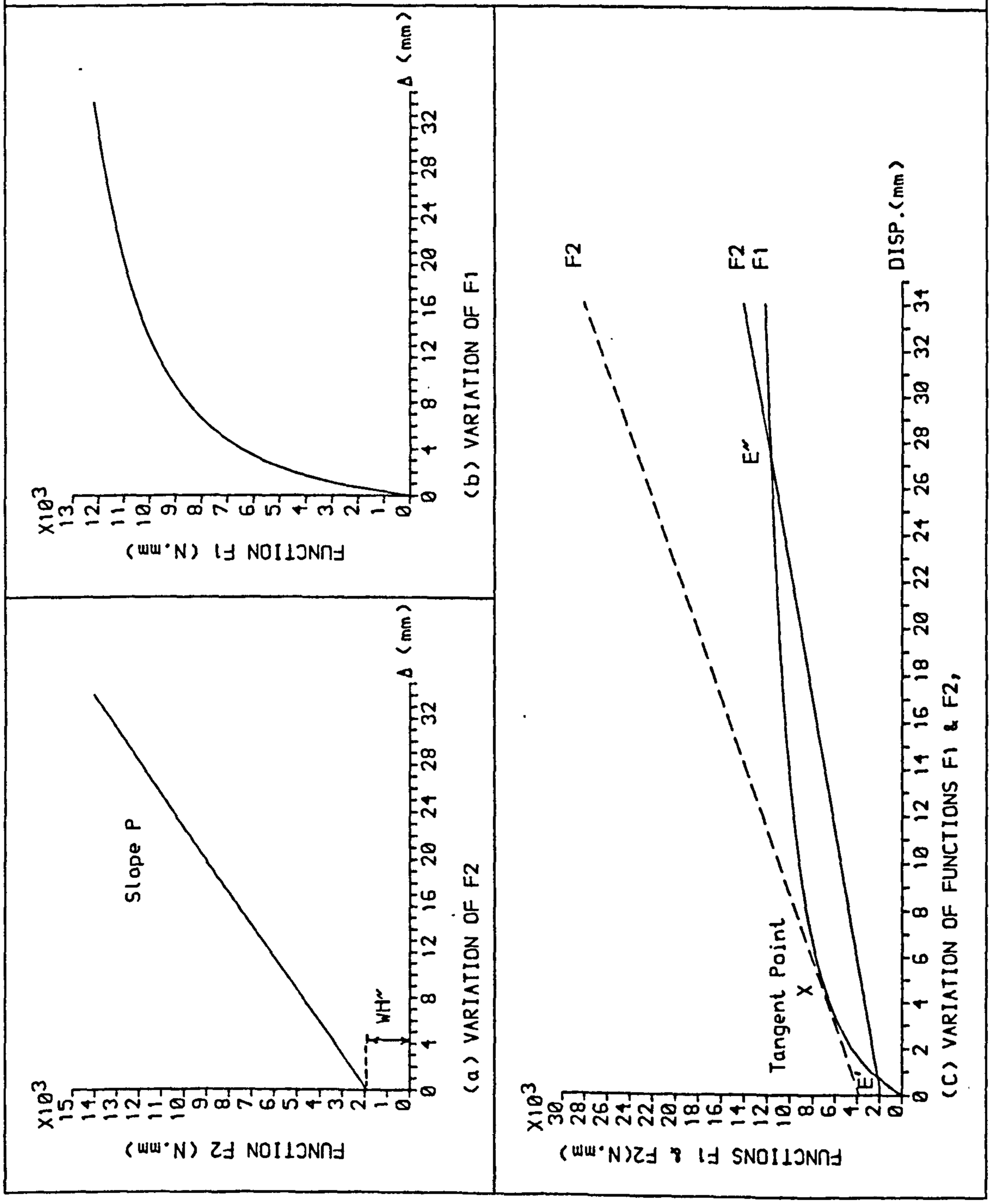

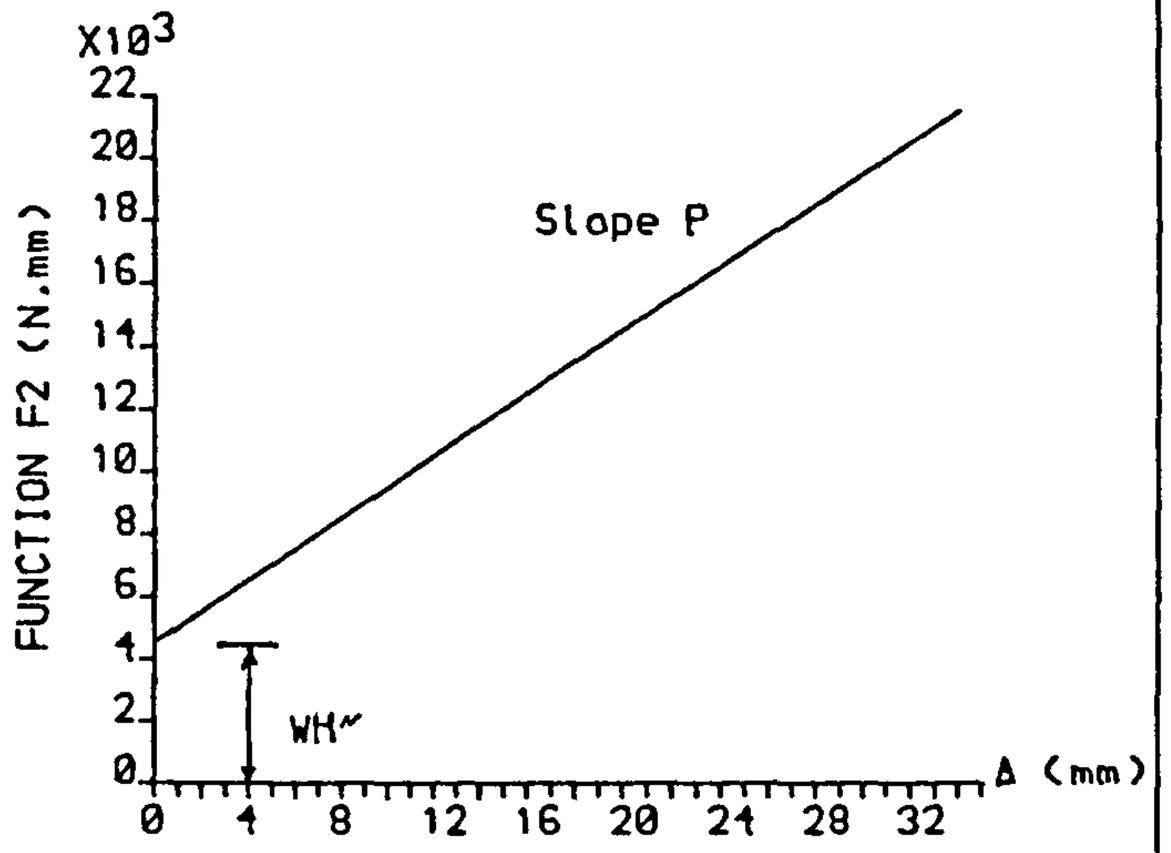

(a) VARIATION OF F2

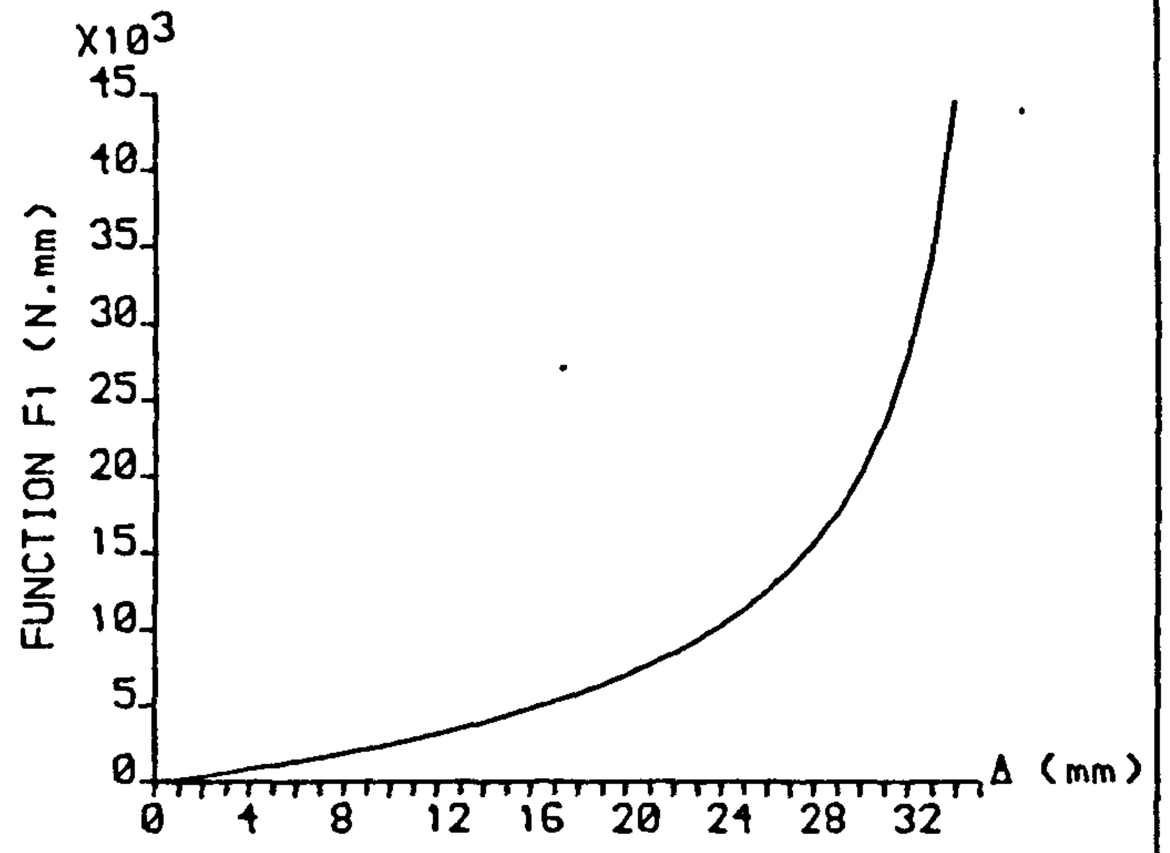

(b) VARIATION OF F1

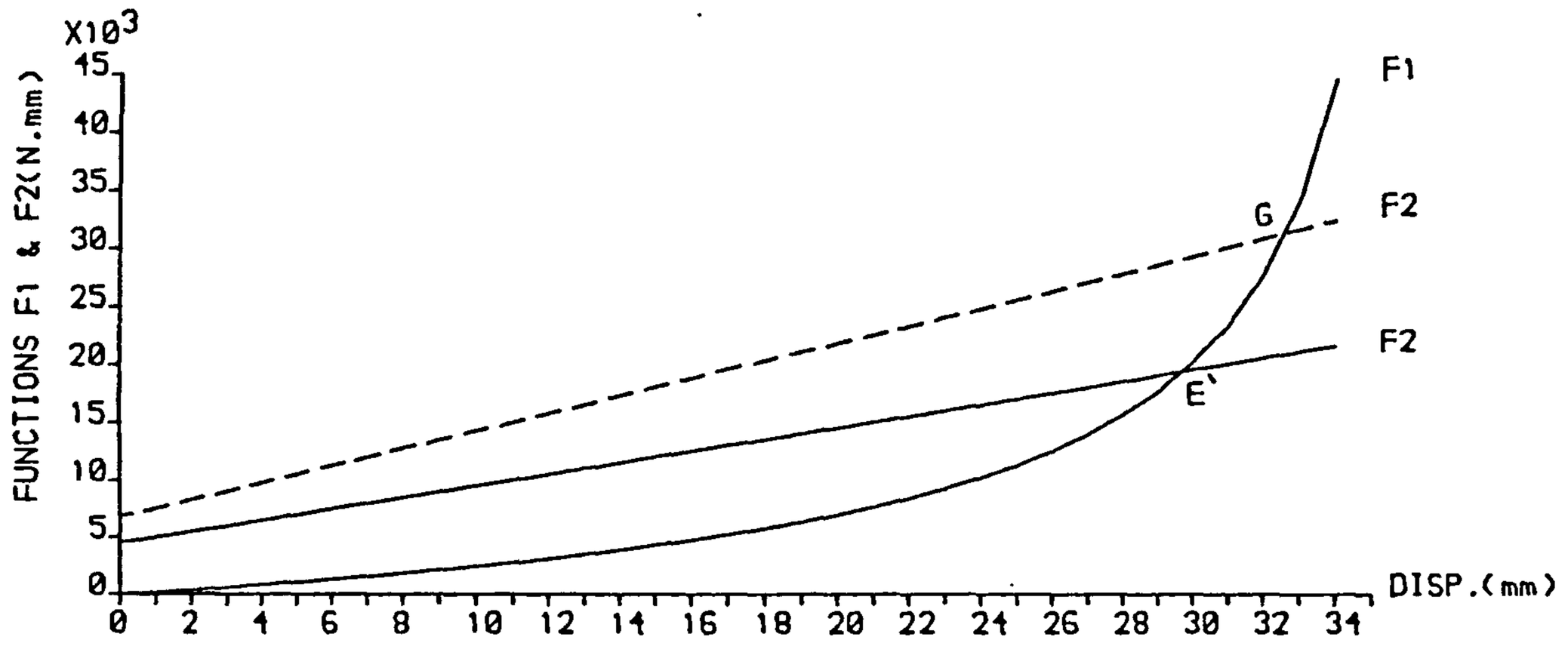

(C) VARIATION OF FUNCTIONS F1 & F2,

STABILITY OF COLUMN

RESTRAINED BY A TENSION

BRACING SYSTEM

FIG.(3-6)

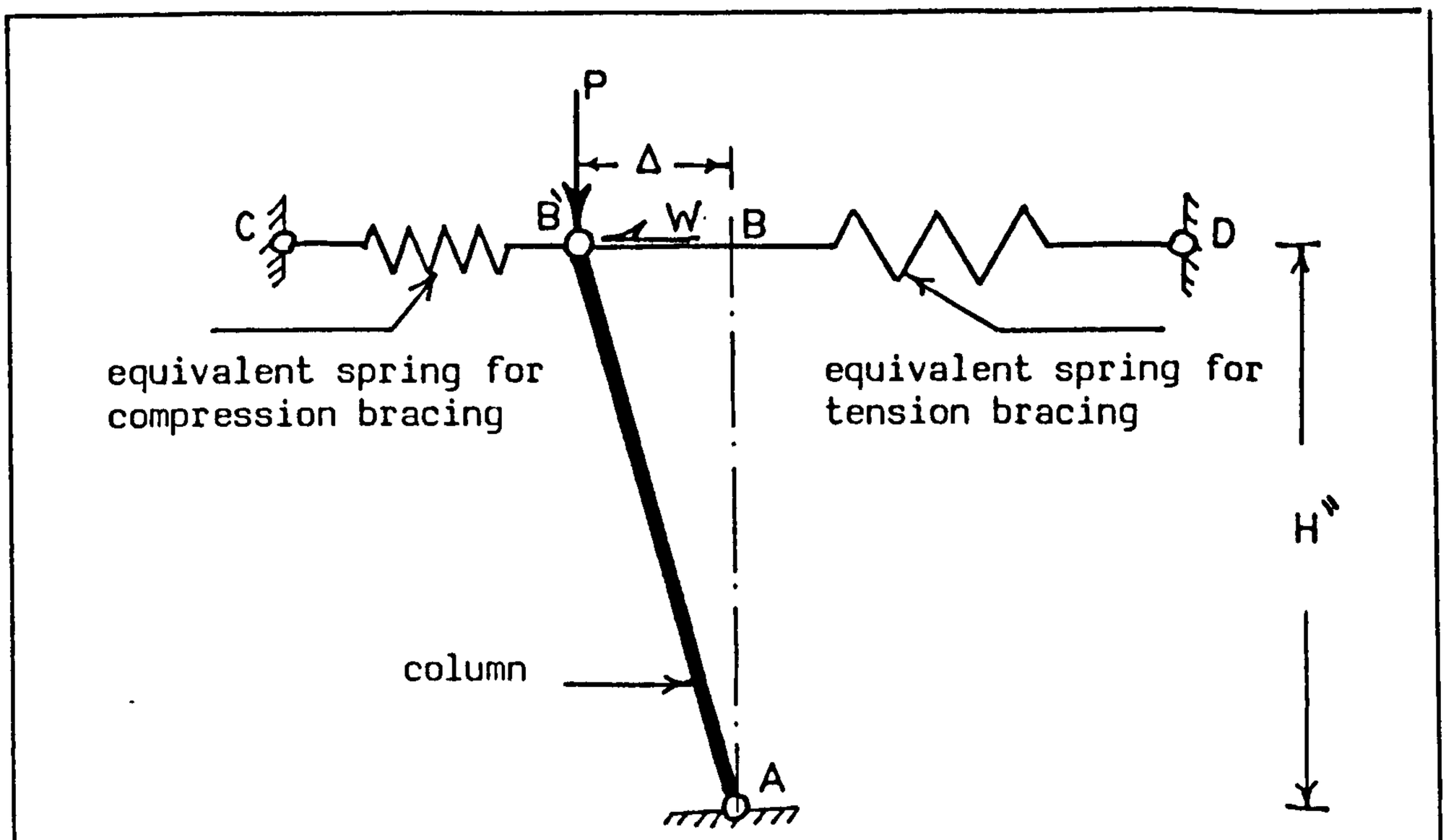

(a) Column restrained by combined equivalent spring systems

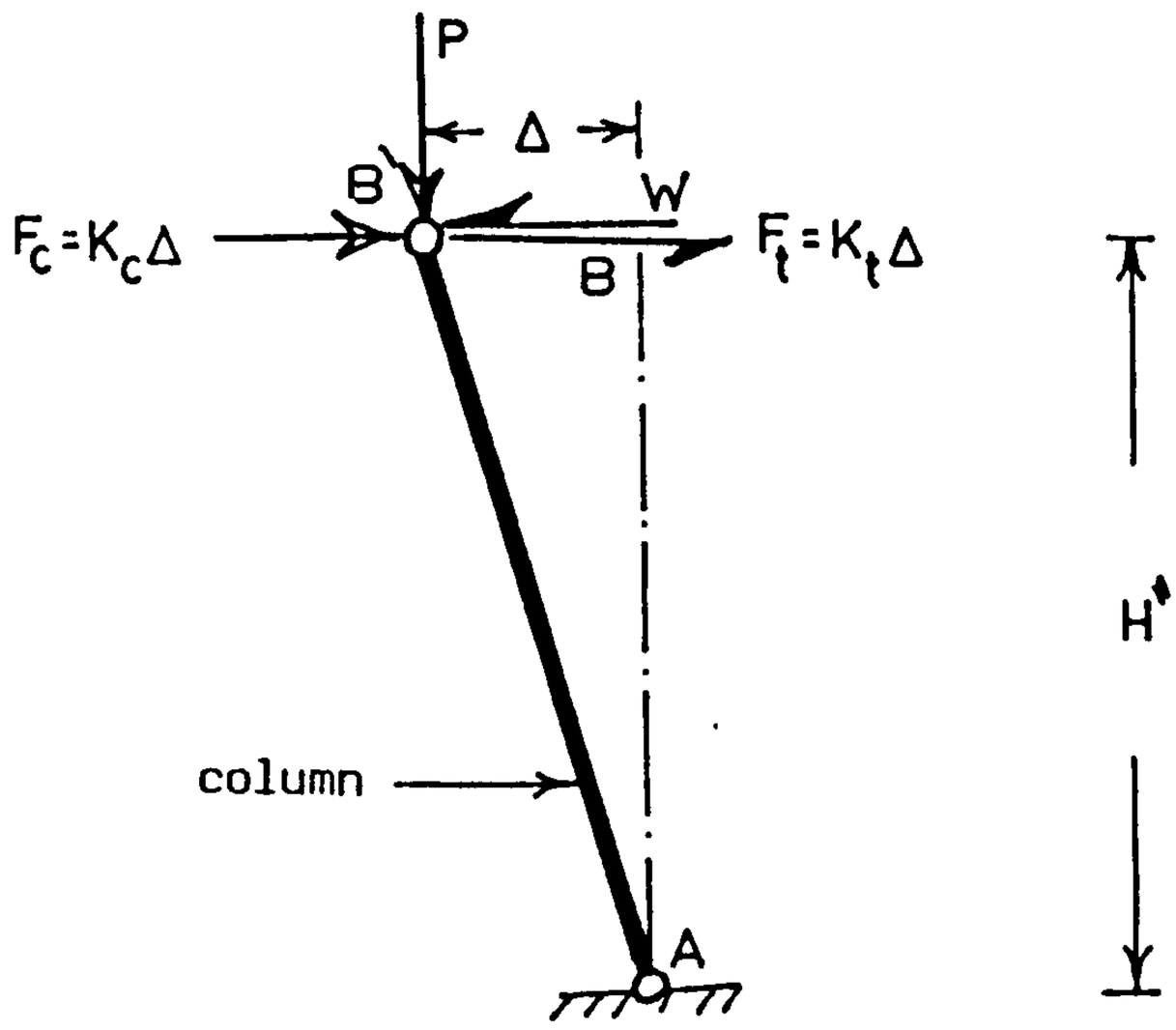

(b) Forces acting on the column

Fig.(3-7)

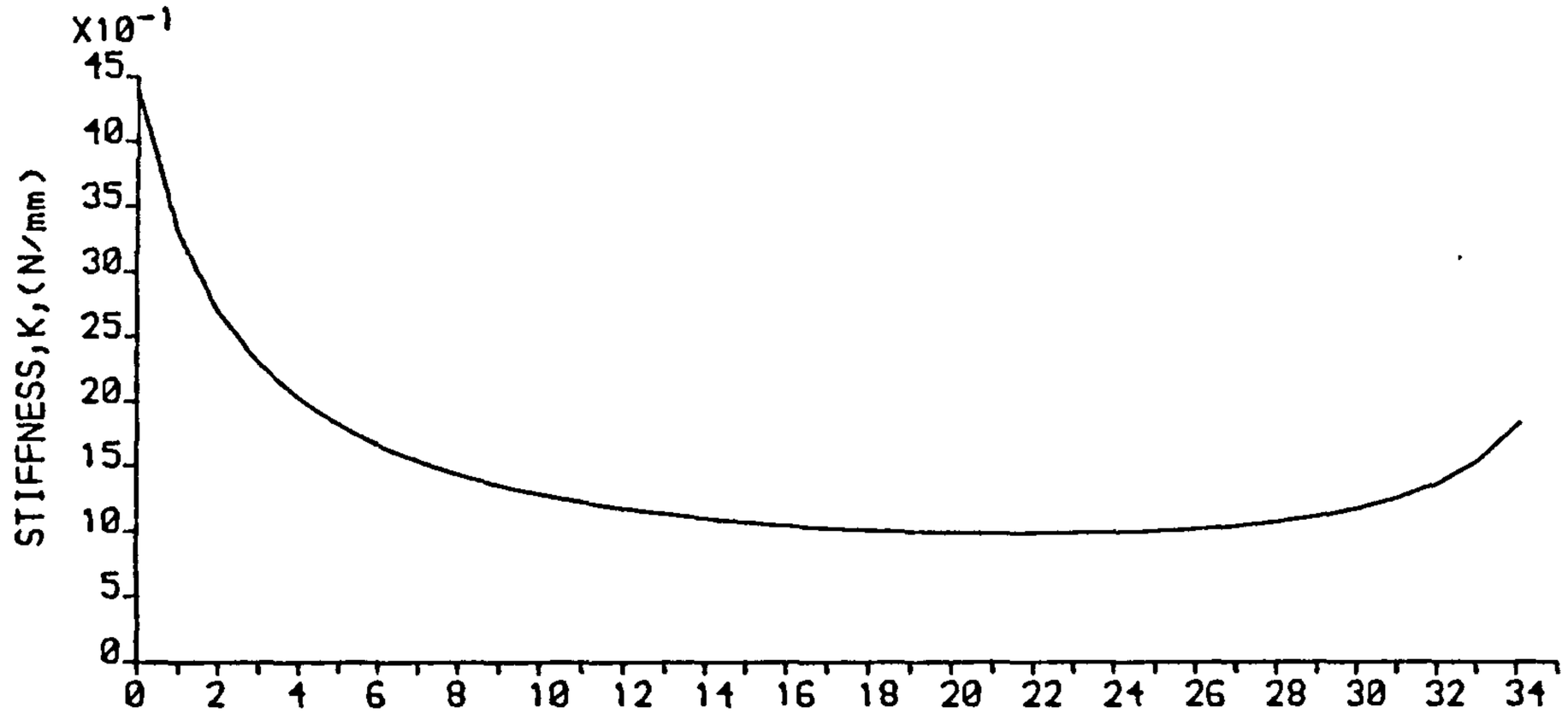

(a) STIFFNESS OF EQUIVALENT SPRING,FOR A COMBINED BRACING SYSTEM

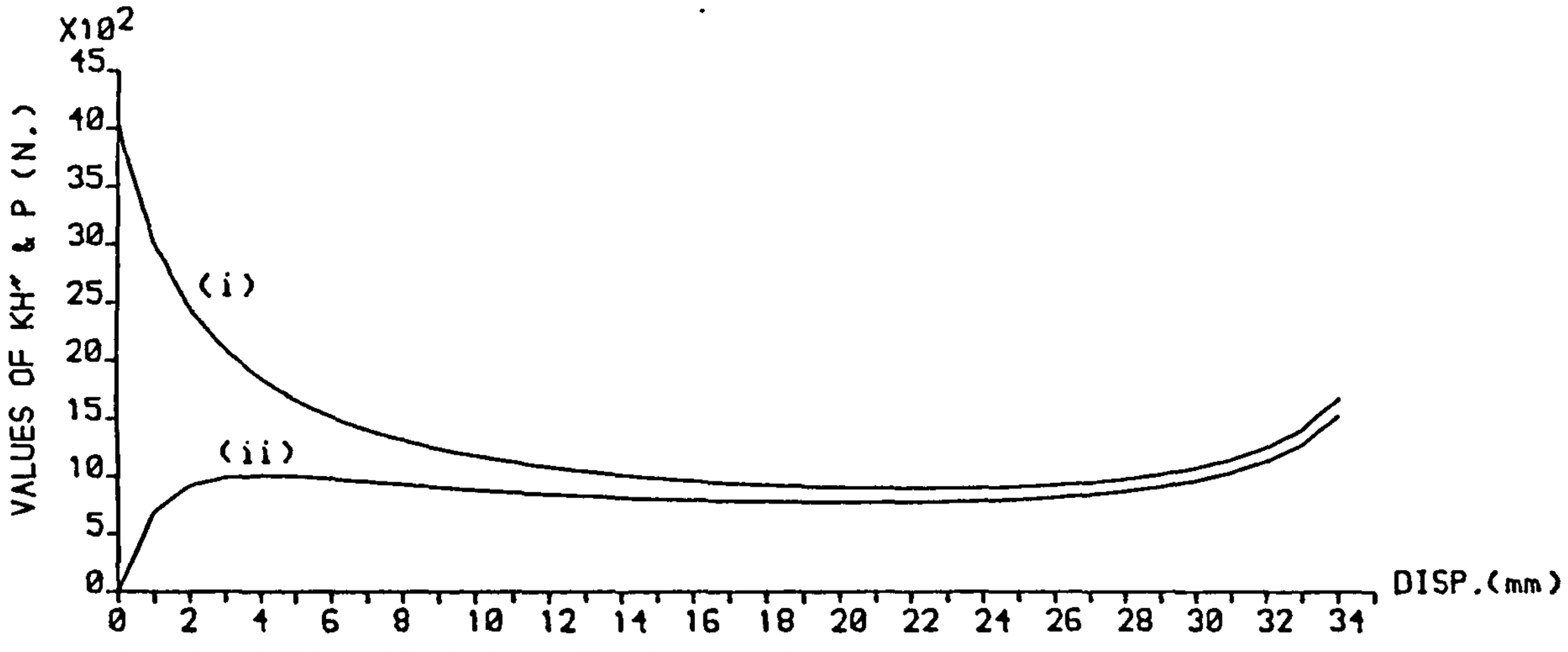

(b) VARIATION OF KH" & VERTICAL LOAD(P).

STABILITY OF COLUMN

RESTRAINED BY A COMBINED

BRACING SYSTEM

THE CRITICAL LOAD Pc IS

DEFINED AS K.H"= P AT $\Delta=\infty$

FIG.(3-8)

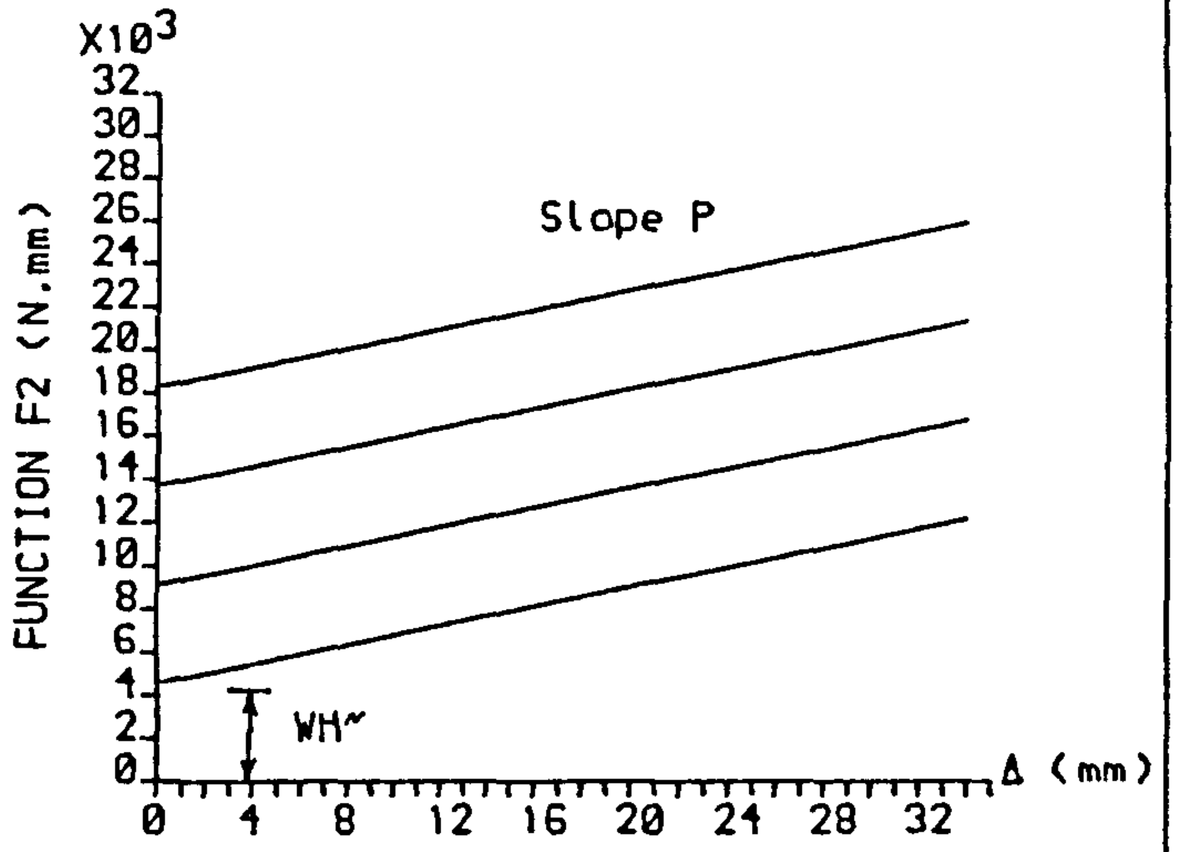

(a) VARIATION OF F2 AT CONSTANT P

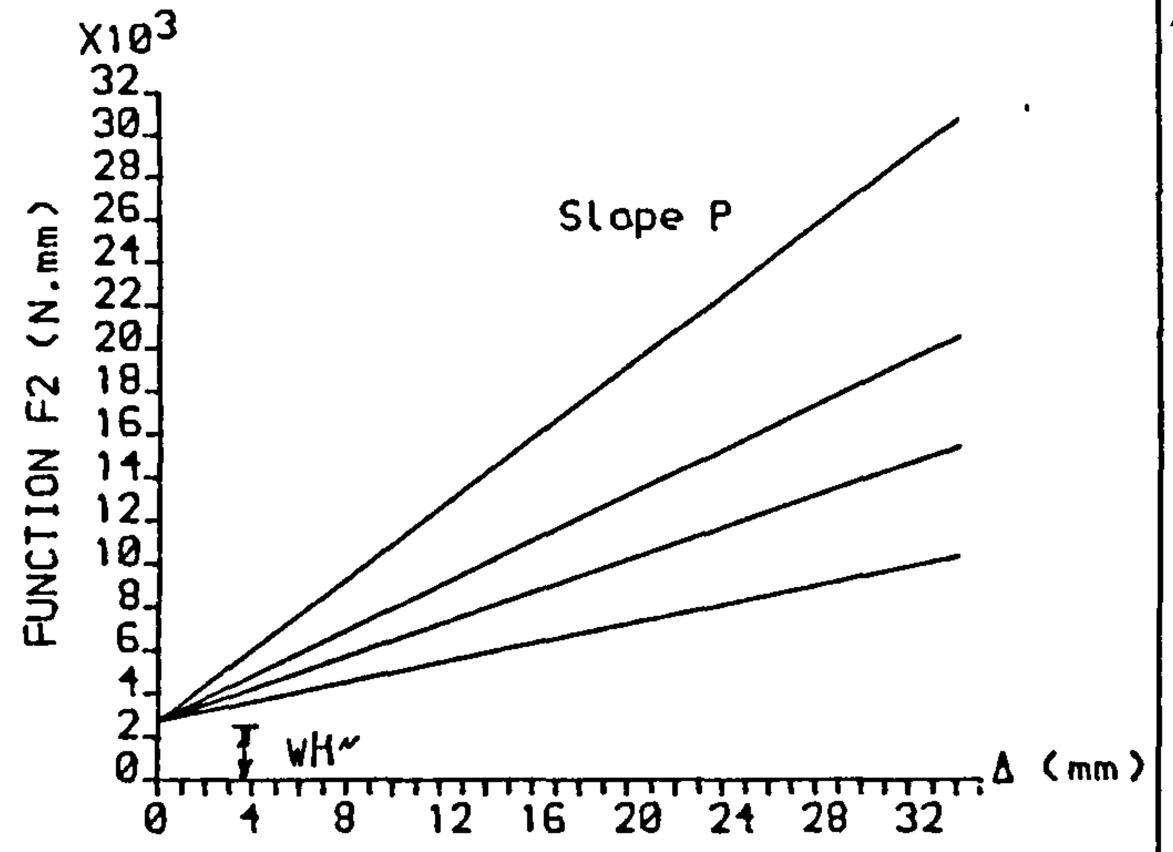

(b) VARIATION OF F2 AT CONSTANT W

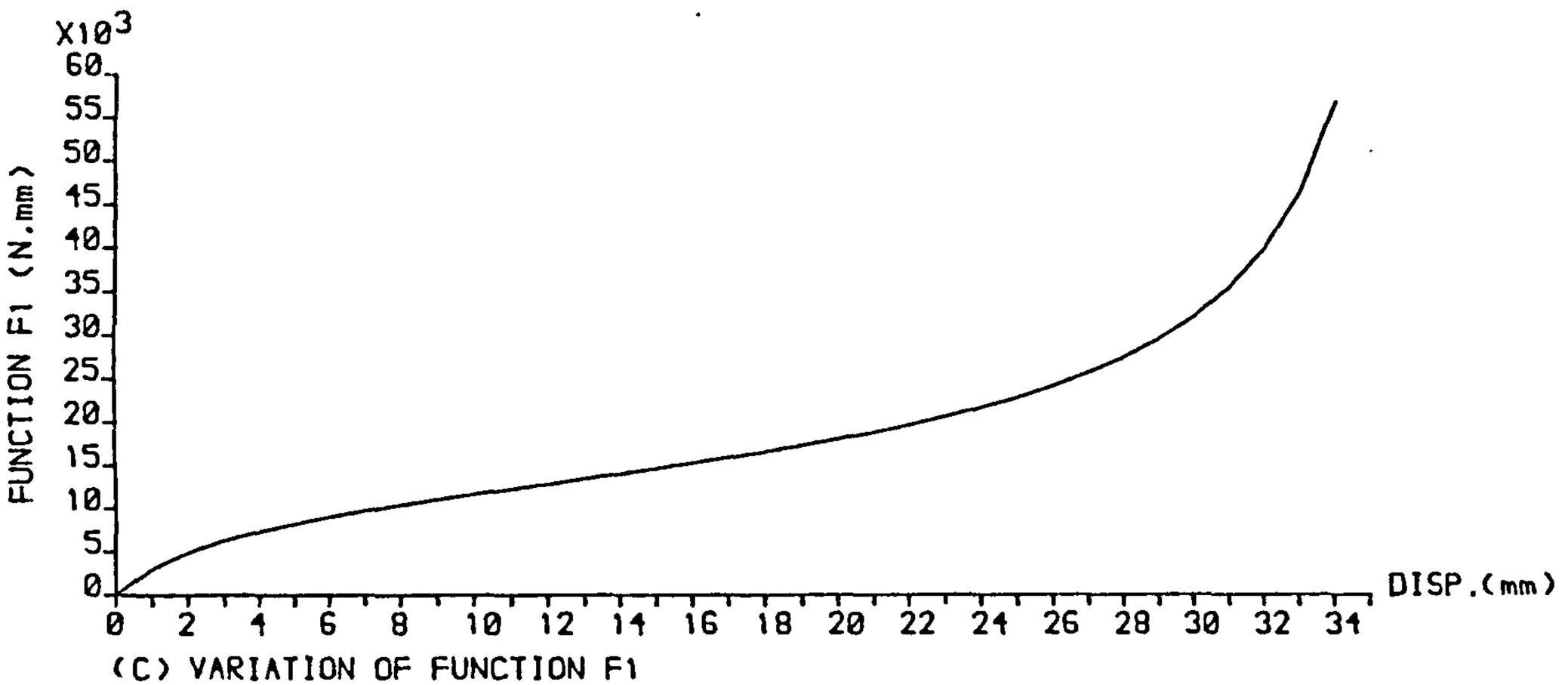

(C) VARIATION OF FUNCTION F1

STABILITY OF COLUMN

RESTRAINED BY A COMBINED

BRACING SYSTEM

FIG.(3-9)

STABILITY OF COLUMN

RESTRAINED BY A COMBINED

BRACING SYSTEM

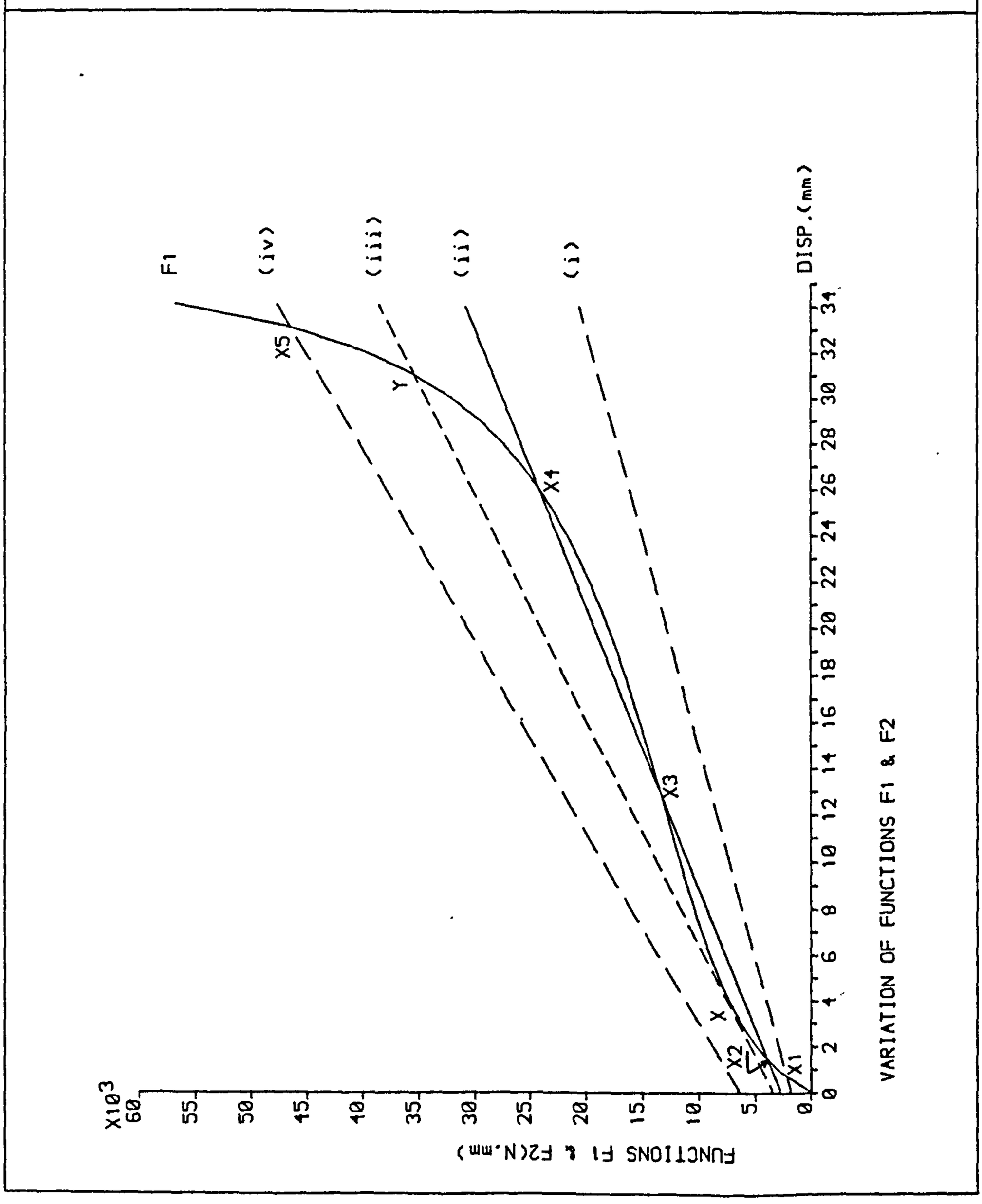

FIG.(3-10)

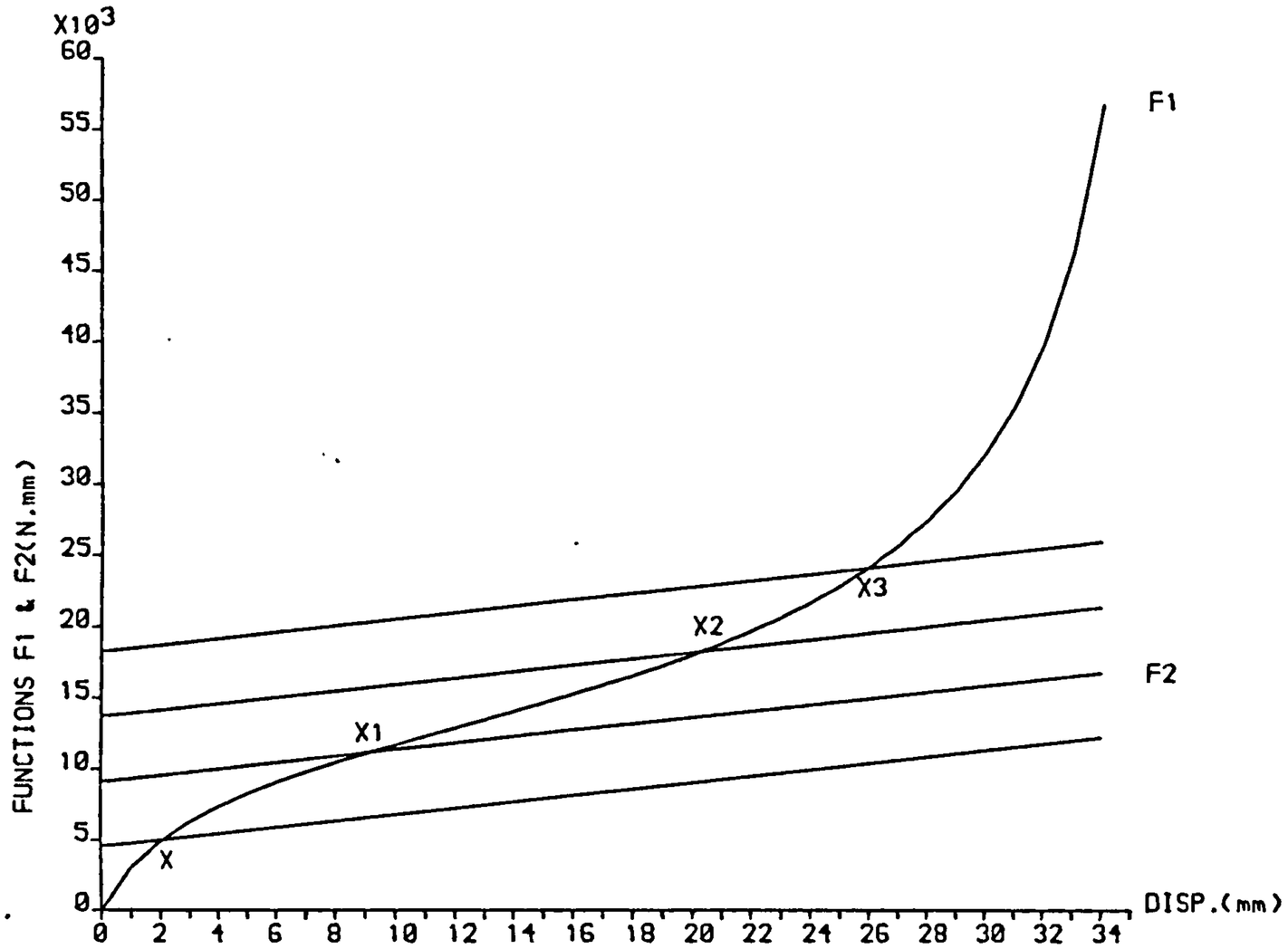

VARIATION OF FUNCTIONS F1 & F2 AT NO TRANSIENT INSTABILITY

STABILITY OF COLUMN

RESTRAINED BY A COMBINED

BRACING SYSTEM

FIG.(3-11)

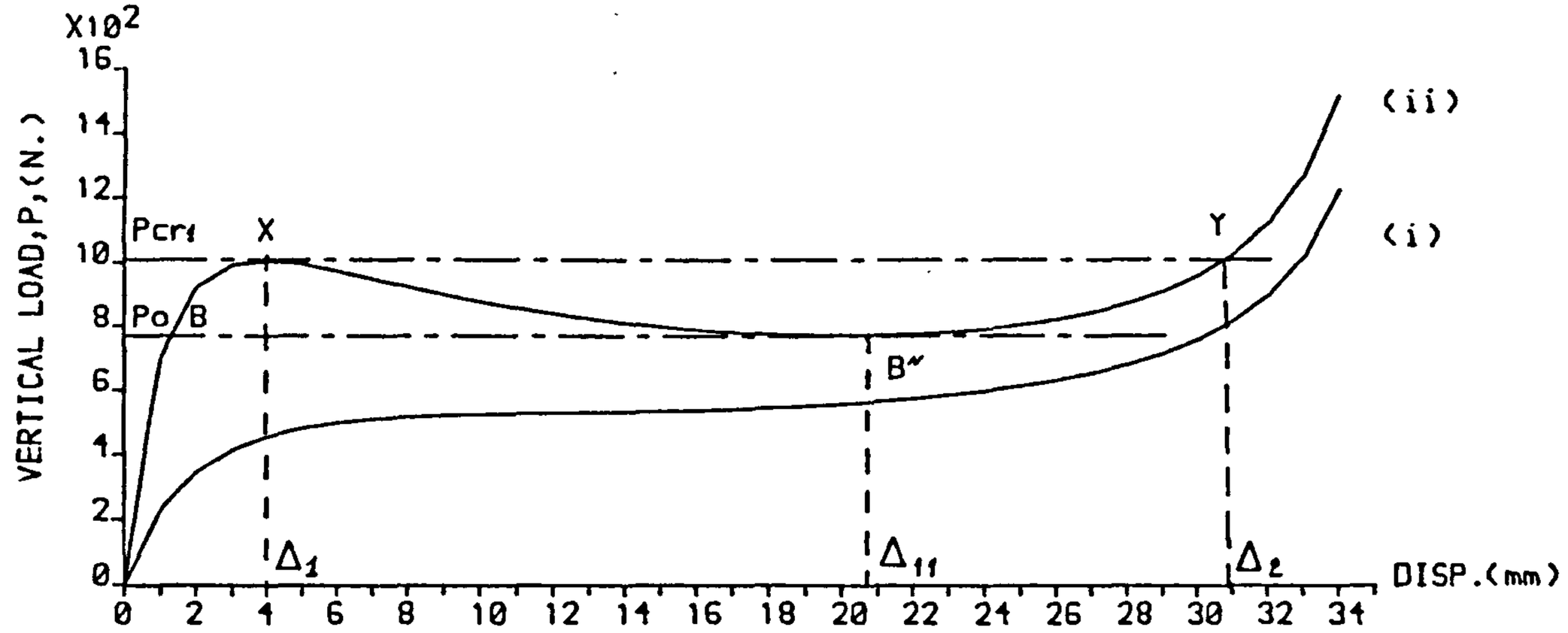

(a)RELATIONSHIP BETWEEN VERTICAL LOAD & DISPLACEMENT

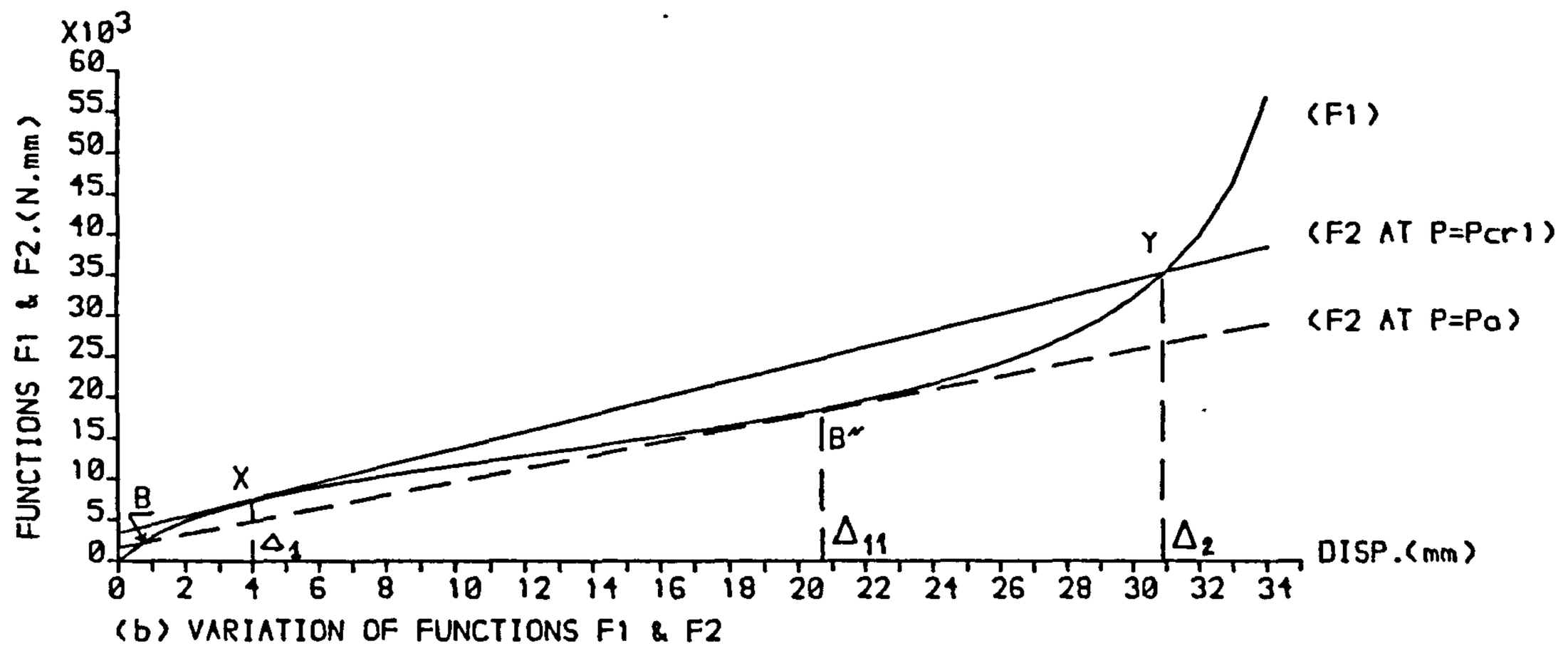

(b) VARIATION OF FUNCTIONS F1 & F2

STABILITY OF COLUMN

RESTRAINED BY A COMBINED

BRACING SYSTEM

FIG.(3-12)

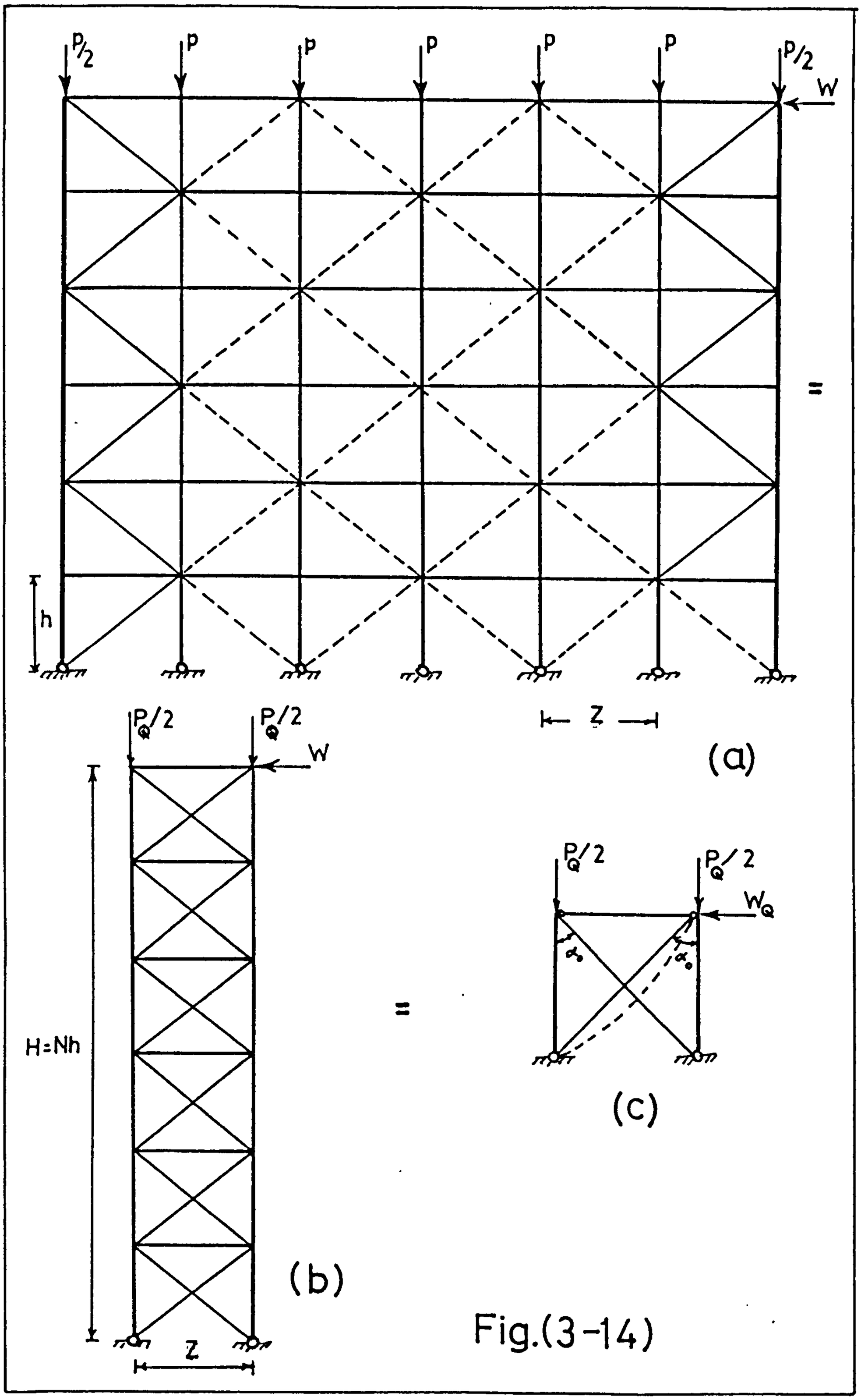

Fig.(3-14)

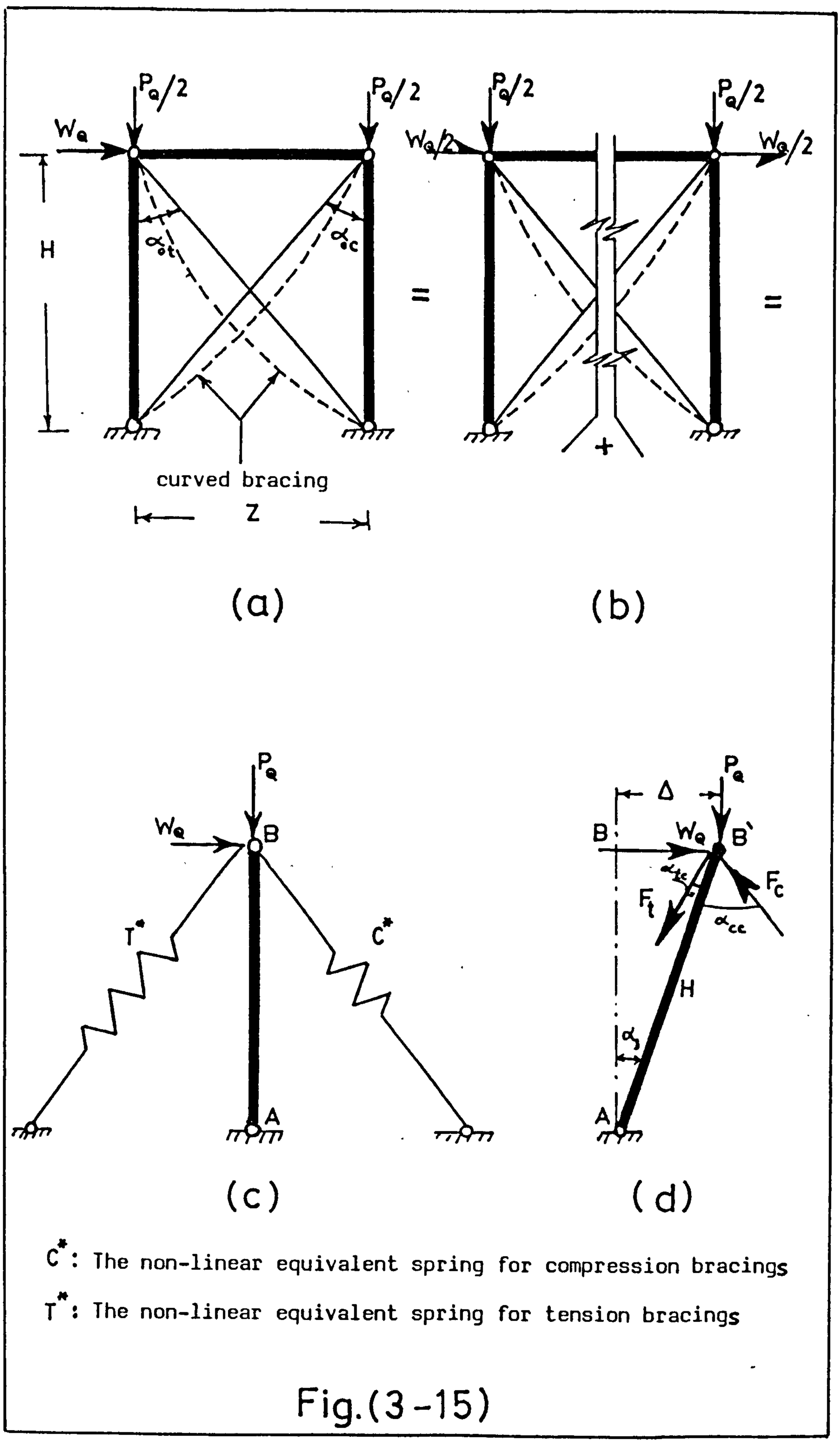
$P_Q/2$
$P_Q/2$
W_Q
H
α_t
α_c
curved bracing
Z
=
$P_Q/2$
$P_Q/2$
$W_Q/2$
$W_Q/2$
=
+
(a)
(b)
P_Q
W_Q
B
T*
C*
A
P_Q
Δ
B
W_Q
B'
α_{tc}
F_t
F_c
α_{cc}
H
α_3
A
(c)
(d)
C*: The non-linear equivalent spring for compression bracings
T*: The non-linear equivalent spring for tension bracings

Fig.(3-15)

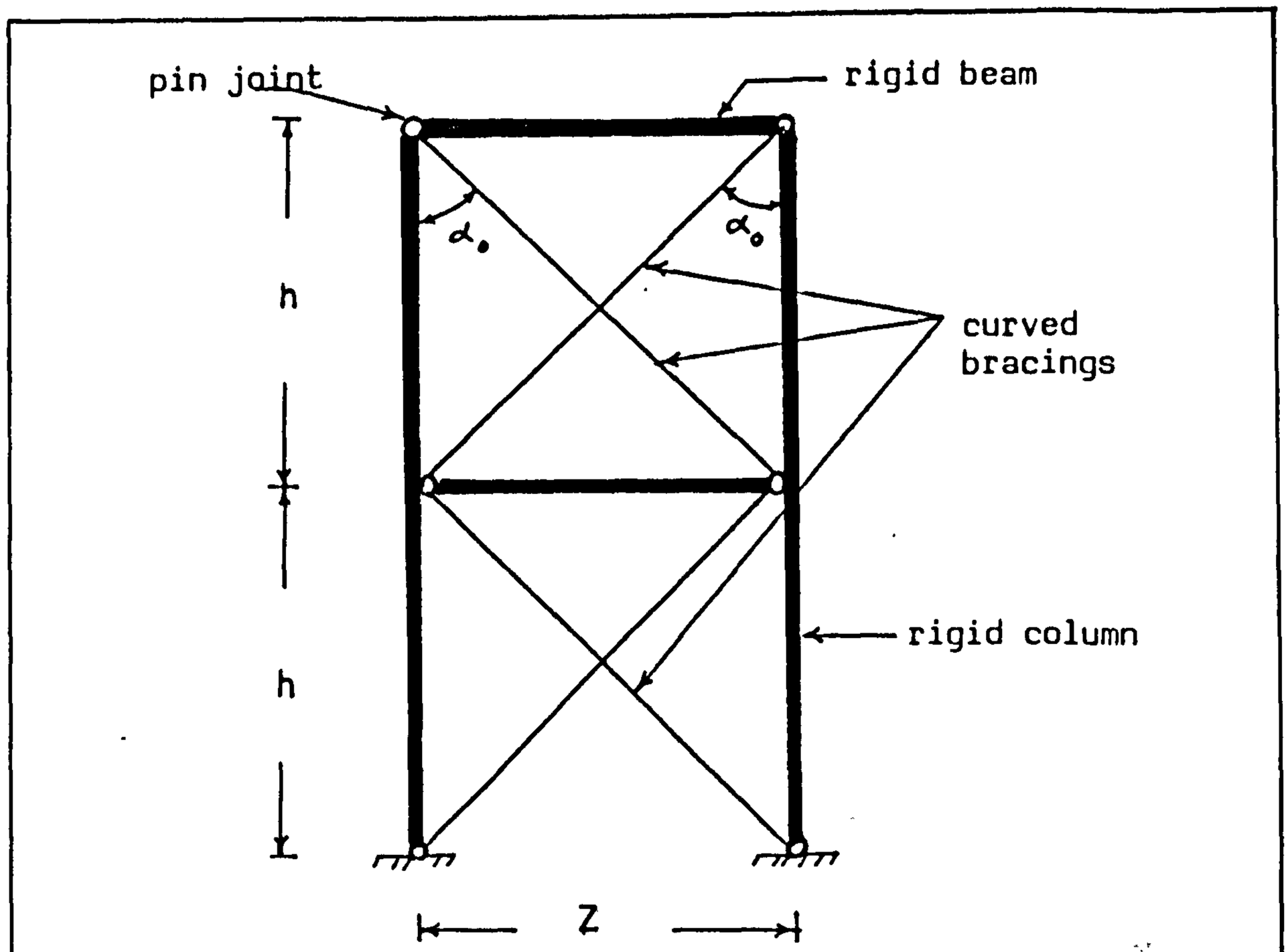

(a) Original pin jointed framework

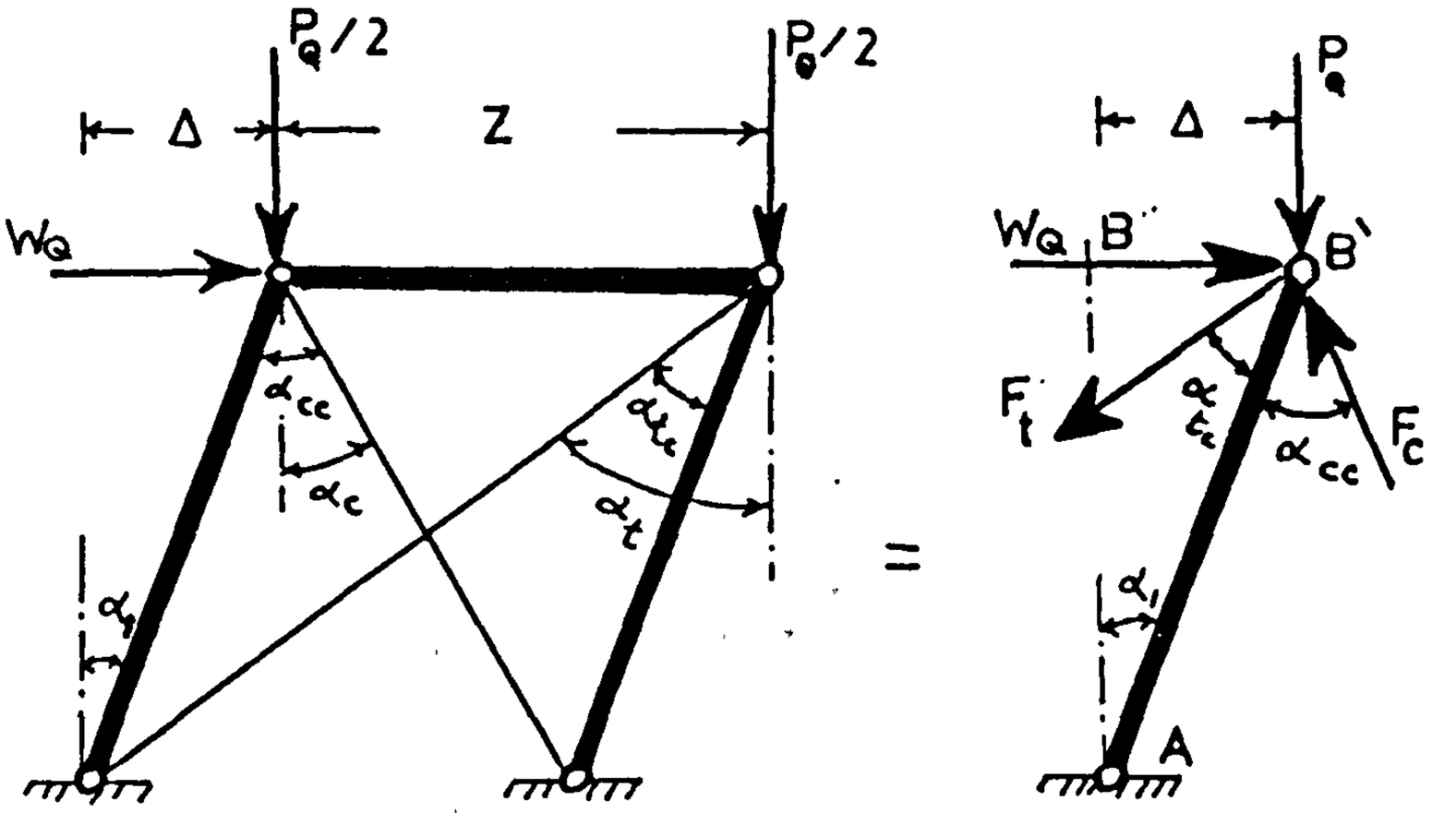

(b) Equivalent single storey frame(after deformation)

(c) Forces acting on equivalent single columns

Fig.(3-16)

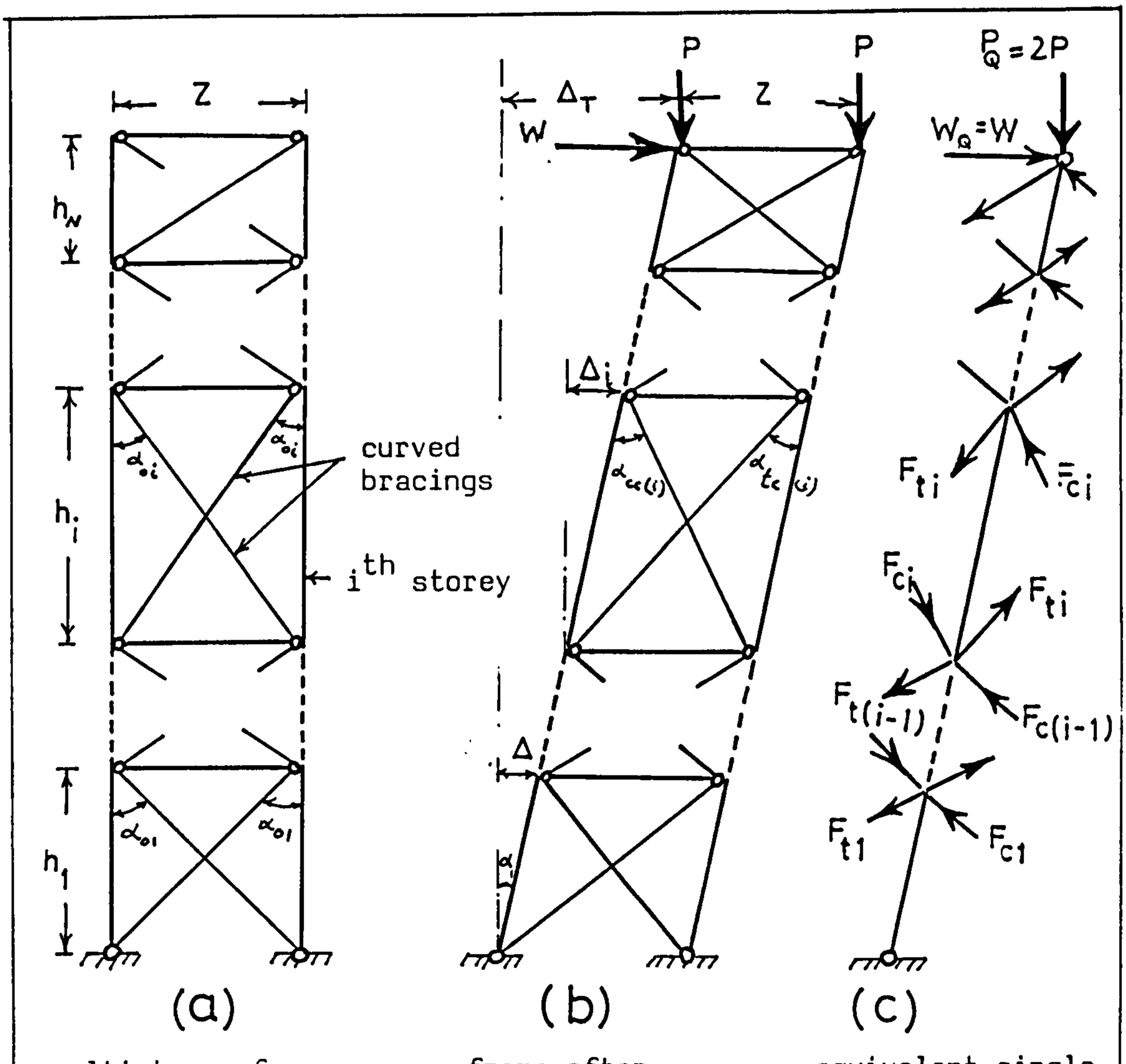
Z
h_N
h_i
h_1
α_oi
α_oi
α_o1
α_o1
curved bracings
i^th storey
(a)
multistorey frame before deformation
P
P
Δ_T
Z
W
Δ_i
Δ
α_cc(i)
α_tc(i)
α
(b)
frame after deformation
P_Q = 2P
W_Q = W
F_ti
F_ci
F_ci
F_ti
F_t(i-1)
F_c(i-1)
F_t1
F_c1
(c)
equivalent single column

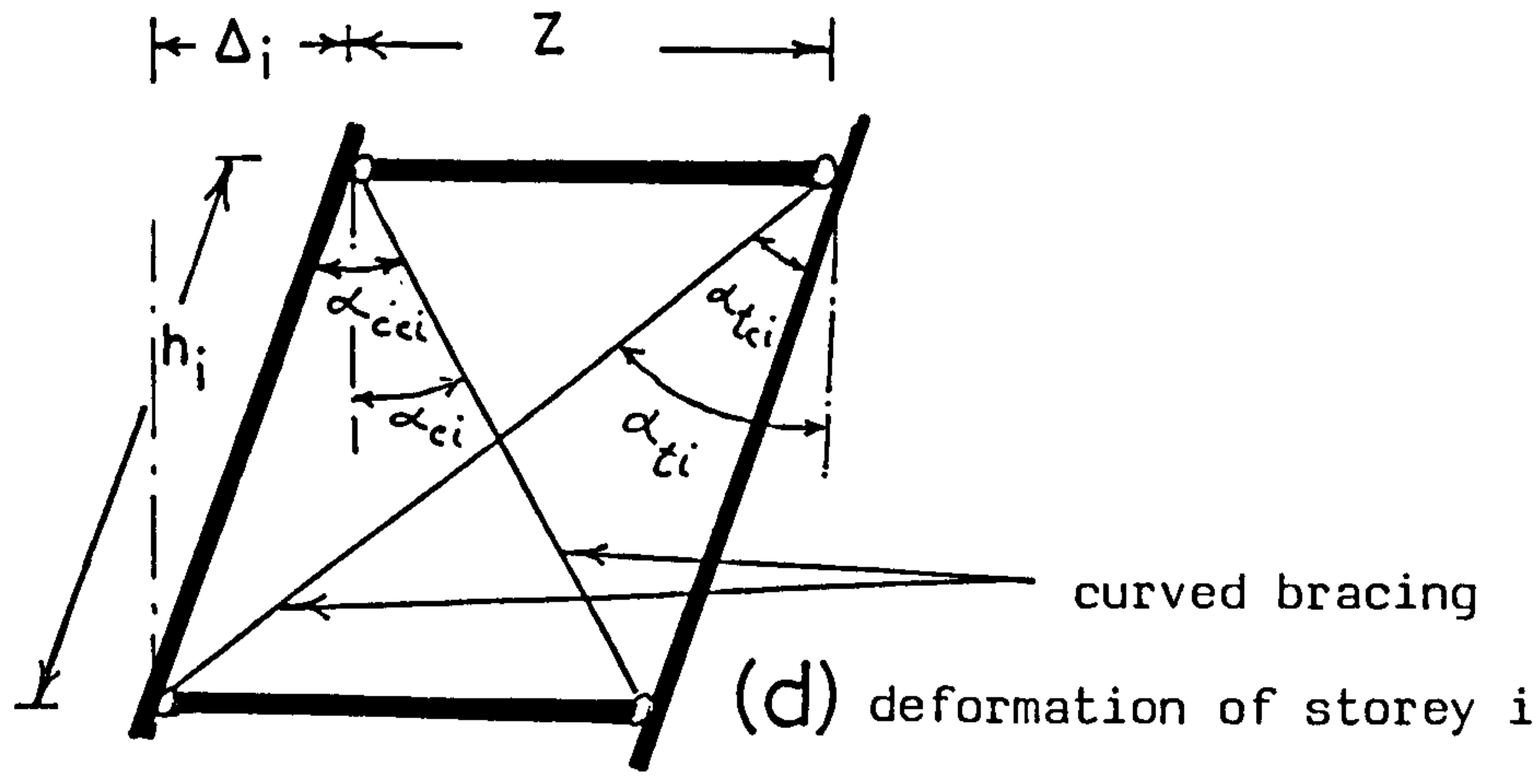
Δ_i
Z
h_i
α_cci
α_ci
α_tci
α_ti
curved bracing
(d) deformation of storey i

Fig.(3-17)

CHAPTER FOUR
EXPERIMENTAL INVESTIGATION UNDER STATIC LOADING

4.1 Introduction

In order to verify the accuracy of the methods of the analyses which have been presented in Chapters 2 and 3, tests have been performed on a small scale for single column , with non-linear bracing member or members, and also for a two storey framework, with non-linear cross bracings. The experimental results obtained have been compared with the corresponding numerical results evaluated by the theoretical methods of analyses. Three separate groups of tests have been carried out. The first series have been conducted to substantiate the methods of analysis employed in Chapter Two, for calculating the axial stiffnesses of initially curved struts and ties. The second series of tests have been carried out to verify the methods of analyses which have been presented in Chapter 3 and consider the behaviour of single columns restrained by compressive and tensile bracings.

The third series of tests have been carried out to verify the methods of analysis which represent the elastic behaviour of frame structures employed in Chapter 3, article (3.4).

4.2 Choice of Materials and Setting Out of the Models

Two types of models were used to carry out these experiments. The first consisted of a single column and bracing member or members, to determine the axial stiffnesses of initially curved bracings. The same model was used to carry out the stability tests on a single

column. The second model consisted of a two storey framework with cross, initially curved, bracing members. All joints of this framework were hinged joints and the bracings were perfectly pin connected to the main frame elements. Further the columns,as well as beams, were very stiff relative to the bracing to resist the applied loads acting on the framework. Therefore, the columns and the beams remained straight even when the frame was loaded, i.e. no significant bending deformation occurred in these main elements of the framework, and all deformation was attributable only to the cross bracings.

The bracing members which were used in the first and second groups of tests were strips of curved annealed mild steel with various chord lengths and initial rises. While the bracing members which were used in the third group of tests, i.e. with the framework test, were curved steel strips with constant chord length and various initial rises. The chord length of these bracings was constant to fit the dimension of the frame model.

The thicknesses of the bracings were 1.22 and 1.2 mm and the breadths were 12.4 and 15.0 mm. These were cut into strips from steel plates. Table (4.1) shows the chord lengths "L_o" and the initial rises "A_o" as well as the breadths and the thicknesses of the bracings which have been used in the groups of tests. The initial rise "A_o", shown in Table (4.1) was the rise at the centre of the bracing member. The bracing members were bent into an arc of a circle with radius "R". The radius of the circle depended on the value of the initial rise "A_o" and the chord length "L_o" and can be written as follows:

$$R = \frac{4A_o^2 + L_o^2}{8A_o} \qquad (4.1)$$

The bracing members used with the framework model were from a different type of annealed steel. Therefore, these bracings had different Young's Modulus "E" to those bracings used in the first and second group of tests.

Generally, all groups of tests were carried out by adopting a rigorous procedure of testing whereby all necessary precautions were taken to minimise the adverse effects.

4.3 Determination of Modulus of Elasticity "E" for the Bracing Members

The value of the elastic modulus "E" for the bracing material was required for the theoretical analysis of the model. This was determined from tests made on specimens cut from the same steel sheets used to make the bracing members. There are at least two methods for determining this value. The first is a tensile test which has been adopted in this experiment. Three samples of steel strips were tested in this way. The tests were carried out on a tensile machine with an automatic recording.. The slope of the straight part of the stress-strain diagram was used to calculate the E value from the following equation;

$$E = \frac{\sigma}{\epsilon} \quad \text{or} \quad E = \frac{P}{A_c \epsilon} \qquad (4.2)$$

where, E is the Young's modulus

σ is the stress

ϵ is the strain

P is the applied load

A_c is the cross sectional area of the specimen.

The value of the strain was obtained from an extensometer with a gauge length of 50 mm about the centre of the tested specimen. The thickness of each specimen was measured by a micrometer at different points along the specimen for calculating the cross sectional properties "A_c". Generally, the specimen properties and the values of Young's Moduli obtained from this test are shown in Table (4.2). The average value of this modulus is 186.32 kN/mm^2. This value conforms well with that expected for thin steel sheet. The standard value of Young's modulus for a mild steel is 207 kN/mm^2.

Other tests were carried out especially for the specimens which were used with the framework behaviour, i.e. in the third series of tests. Again three samples of steel strips were tested. On these occasions the strain was measured using electrical resistance strain gauges located at the centre of length of the specimens.

The properties and the values of Young's moduli are shown in Table (4.2). The average value of elastic Young's modulus is 214.59 kN/mm^2. This value conforms well with the standard value of mild steel.

Typical load-strain curves for each type of steel are given in Fig. (4.3)

4.4 First Series of Tests (Stiffness Tests)

These types of tests were carried out especially to determine the axial stiffnesses of initially curved bracings in compression and in tension.

4.4.1 Design and Construction of Model

The design of the model, and the test procedure was adopted to be suitable to evaluate directly the change in the chord length of the initially curved bracings, due to the axial applied load, and hence the axial stiffnesses. In these series of tests the bracings were tested singly in compression and in tension with various initial rises.

The model used in these experiments consisted essentially of a single column, of height 915 mm, made up from, 25 mm square, mild steel hollow section, and a curved bracing member. The model was set up as shown in Fig. (4.1). The base of the column model was situated on a rail such that the solumn could be plumbed prior to each test, and then secured in position at the base. At the top of the column the pinned connection joining the bracing member to the column was made as frictionless as possible as were the connections of the bracing members to the I beam. All the connection details are shown in Fig. (4.2). A means of controlling deflection during the loading operations was made by the use of an adjustable screw. This screw was necessary to reduce the disturbances during applying the weights to the hanger. After each load increment the screw, which is positioned to the face of the column, was unwound slowly until the equilibrium point was reached and the bracing was able to support the loading. At this point the lateral deflection was recorded from a dial gauge positioned at the face of the column, at the same level as the column-bracing connection.

Since the model was quite small with especially flexible

bracing, it was possible to use wieghts which were applied manually rather than using a hydraulic system of loading. The column was designed such that it would not buckle throughout the experiments.

4.4.2 Test Programme for Bracing Properties

All together, twenty specimens were tested - twelve of them to determine the axial stiffnesses of curved bracings in compression and the others to determine the axial stiffnesses of curved bracings in tension. The specimens were cut into three different lengths and bent into nine different initial curvatures as shown in Table (4.1). A 3.5 mm diameter hole was drilled in each end of the specimen such that it could be positioned in the model.

4.4.3 Test Procedure and Evaluation of Test Results

4.4.3.1 Compressive Loading

The column was set in a vertical position by adjusting the base plate as shown in Fig. (4.2.c). This was checked by making use of a plumb bob which hung from the centre of the steel rod at the top of the column. The initial curved bracing member was connected to the model where one end was fixed to the pinned connection at the top of the column, i.e. at joint c, which could move laterally and the other end to the hinged bearing fixed to the I beam, i.e. at joint B, as shown in Fig. (4.1).

The deflection gauge was positioned at the top of the column and zeroed.

In these tests, only a horizontal load "W" was applied. At each load increment the deflection screw at the top end of the column was unwound such that the load was transferred to the bracing member. Once satisfied that the model was in a stable condition, the horizontal deflection was recorded from the dial gauge. As the load was applied in increments, the procedure was continued until the bracing member failed by buckling. Throughout the procedure a record of horizontal load "W" and lateral displacement "Δ" was kept. Values of "W" and deflection "Δ" were recorded as accurately as possible when the bracing was approaching failure conditions. With the record of horizontal load "W" and displacement "Δ" the stiffness of the bracing member could be worked out from the equation,

$$WH'' + P_{o.w} \cdot \frac{\Delta}{2} = K_{\Delta} H''$$

or

$$K = \frac{W}{\Delta} + \frac{P_{o.w}}{2.H''} \qquad (4.3)$$

where $P_{o.w}$ is the self weight of the column model.

4.4.3.2 Tensile Loading

The procedure here was exactly the same as for the previous section (4.4.3.1) except that the bracing member did not fail, the test being completed when the displacement "Δ" between consecutive movements of loading was becoming very small. The stiffness of the member was again worked out using the formula $K = \frac{W}{\Delta} + \frac{P_{o.w}}{2.H''}$

4.4.3.3 Interaction Diagrams for Final Results

The results obtained from the experiments outlined above for both the cases of bracing in compression and in tension can be conveniently incorporated into displacement-stiffness interaction diagrams (i.e. Δ-K diagrams). Also the load-displacement interaction diagram i.e. W.H" against Δ for each bracing member can be plotted, where H" is the height of the column after deformation. The diagrams are illustrated in Chapter Five.

4.5 Second Series of Tests (Stability Tests)

The graphs of KΔH" viz Δ for all the bracing members were then scrutinized such that a pair of members, one compressive and one tensile,could be combined satisfactorily to give a good result in terms of transient instability for stability tests.

The characteristics of the members chosen for the stability tests were then combined graphically to give a plot of $F_1 = K\Delta H"$ v Δ . In order to assess a suitable combination of loading for these tests which involve horizontal and vertical loading "W" and "P" respectively at the top of column, a second graph was drawn on the F_1 v Δ plot. This graph was in the form of a straight line described by the equation $F_2 = WH" + P\Delta$. Its position in relation to the F_1 v Δ plot was such that it lay tangential to this curve at a point somewhere in the region where the compression bracing member began to lose its strength. This tangential point represent, theoretically, the onset of the transient instability region. The straight line was then continued to intersect the F_1 curve at another point where the tensile bracing member was providing stability. This point

represents the end of instability region.

The critical value of the horizontal load "W_{cr1}" applied to the system as the column became unstable could be determined from the following equation,

$$W_{cr1} = \frac{F_2}{H''} \quad \text{at} \quad \Delta=0 \tag{4.4}$$

where,

$$F_2 = WH' + P\Delta \tag{4.5}$$

Also the critical load P_{cr1} could be obtained, according to this case, by calculating the slope of the straight line representing F_2. The ratio between the vertical and horizontal loads was then, equal to $R_i = P_{cr1}/W_{cr1}$.

In order that these loads do not become too large, the straight line was drawn as flat as possible. The important criterion was that there must be as clear a value as possible of the tangent point so that in the experiment, well defined results were obtained.

4.5.1 Test Programme for Column Stability

Bracings with the same length "L_o" and different initial rise "A_o" as the stiffness tests were used again in these types of experiments. Two different combinations were considered for these series of tests.

The best loading ratio "R_i" and the dimensions of the two combinations are illustrated in Table (4.3).

4.5.2 Test Procedure and Evaluation of Test Results

In this type of test the model was set up as shown in Fig. (4.1). The experimental procedure was the same as for the stiffness test except that vertical load "P" was introduced such that the ratio "R_i" between P & W remained constant throughout the test.

As the loads P & W approached the critical values "P_{cr1}" and "W_{cr1}", i.e. as the displacement "Δ" became close to the tangent point displacement, the increments of loading were greatly reduced, such that an accurate value of deflection could be recorded at the onset of the transient instability. Once this point has been reached a careful record of vertical load "P" and horizontal load "W" are now available. With no more loadings added the deflection screw was unwound slowly and carefully to avoid disturbances until the bracing member in tension became sufficiently stiff to resist the loadings which initially caused instability. Again a reocrd was kept the value of displacement when stability was returned. Next, the applied loads"P" and "W" were increased until the displacement "Δ" between consecutive movements of loadings was becoming very small.

From the results of these experiments a comparison can be made with the results obtained from the theoretical investigation presented in Chapter Three, article (3.3).

4.6 Third Series of Tests (Framework Stability Tests)

These types of tests were carried out to examine the stability, or lack of it, for framework structures with non-linear cross bracings, having initial curvatures.

4.6.1 Design and Construction of Model

In the first and second series of tests described, the single column was assumed infinitely stiff in comparison with the bracing members, and it was possible to treat these bracings in the theoretical analysis as non-linear springs. Also in the third series of tests the columns and the beams of the framework were considered infinitely stiff in comparison with the bracing members for the purpose of verification of the method of the analysis.

The model used in these types of tests consisted of a single bay two storey framework. The dimensions of this model are shown in Fig. (4.4). The ratio of span to storey-height was chosen as unity. The columns and the beams of the framework model were made from the same material and the same cross-sectional area as the column used in the first and the second series of tests. Double beams were used at each storey to ensure that the frame was symmetrical about the vertical plane. Each connection between the columns and the beams was designed as a hinged joint. Each joint comprised commercially manufactured needle bearings. The bearing shaft, of 6 mm diameter,was run through these needle bearings, as shown in Fig. (4.5.a). The needle bearings were used to reduce the possibility of friction between the beam-column joints to an acceptable level. It was considered necessary to avoid the possibility of other errors, such as manufacturing errors, confusing the net dimensions of the framework, therefore, a variable screwed joint with left and right hand thread was made at the middle of each beam and column of each storey to adjust the net dimensions of the framework, the details of these joints are shown in Fig. (4.5.b).

The only variable in this type of test was the initial rise of the bracing members, where different combinations were arranged between bracings in compression and in tension. The pinned connections joining the bracing members to the main frame elements were made as frictionless as possible. The connections were designed to allow the bracings to bend out of the plane of the framework, so that the bracings would not touch each other. The chord line of each bracing member passed through the beam-column joint connecting this member. The positions of the bracing members are shown in Fig. (4.4).

The frame had two hinged bases which were situated on a flat plate fixed to an I beam rigid support. The hinged base comprised commercially manufactured needle bearings to reduce the possibility of friction. The hinged shaft of 12.7 mm diameter was run through these needle bearings. The need to restrict the movement of the frame out of its own plane was considered in the design of the bases. Therefore the hinged shaft at the bottom of the column was made sufficiently long so that, when inserted in the needle bearing assemblies, it was rigid enough to give support to the frame column, to minimise the movement of the frame out of its own plane. In this way the frame was rigidly held in its own plane while still being capable of free sidesway within its plane. The details of the hinged base are shown in Fig. (4.5.c).

The horizontal load was applied through a system of pulleys and thin strong string. The latter being attached to the frame by hooks into the top joint of the frame. Horizontal load was applied to the top of the frame panel point. The system of pulleys were fixed into a stanchion welded to the rigid I beam support, as shown

in Fig. (4.4). The system of pulleys were designed to work with ball bearings to reduce the friction as far as possible. The vertical loads were applied at the top of the column, where the columns were extended with vertical load carriers. The length of each carrier was adjusted to be suitable for the maximum applied load.

A means of controlling lateral displacement during the loading operations was made by the use of an adjustable screw. This screw was necessary to reduce the disturbances during placing the loads on the structure.

The lateral deflection of the frame was measured by a dial gauge during the test procedure. Independent trials showed appreciable force applied by the gauge to the frame. Consequently the spring of the dial gauge was taken out. As the result of this no appreciable force remained.

4.6.2 Test Programme for Frame Stability

Owing to the many variables present in the behaviour of the multistorey framework with non-linear cross bracing members, different combinations of initially curved bracings were considered. Five tests were carried out for this framework, to provide sufficient variety in the parameters for the general verification of the accuracy of the theoretical analysis mentioned in Chapter Three, Art. (3.4). Table (4.4) illustrates the different combinations considered in this type of test.

4.6.3 Experimental Procedure

Details of the experimental techniques employed and actual test procedure will be discussed in this section. The complete frame was placed in the test position and the base flat plate clamped onto the fixed rigid I beam which had been adjusted to a horizontal level. The adjustable screw deflection rod was then attached and adjusted so that the frame was as near as possible to being in a true vertical plane. This was checked by using a plumb bob which hung from the centre of the top joint of the frame. Then the verticality of the columns within their own plane was checked by measuring the diagonals and pitches between joints of each storey, and adjusted to as close a figure as possible. Adjustment was made by using the pitch setting gauges.

Next, the bent bracing members, horizontal weight hanger and dial gauge were attached. The dial gauge was zeroed and the initial rise "A_o" for each bracing member was adjusted exactly.

After adjusting the test proceeded in a regular manner, horizontal and vertical loads being applied to horizontal and vertical positions, such that the ratio of vertical to horizontal loads remained constant throughout, and deflection readings were taken for each increment. Load increments were decreased as the transient instability condition was approached such that accurate values of critical loads and deflection could be recorded. With no more loading added the deflection screw was unwound slowly and carefully to avoid disturbances until the bracing members in tension became sufficiently stiff to resist the loading which initially caused the

instability. Again a record was kept of the value of deflection when stability returned. Next, increments in the applied loads "P" and "W" were added until the deflection "Δ" between consecutive movements of loadings became very small.

The test was repeated again with another combination of bracing members (as shown in Table (4.4)) using the procedure just described.

Finally the results obtained from this type of experiment were conveniently incorporated into F_2 against Δ interaction diagrams where F_2 is equal to WH"+PΔ. Discussions and illustrations of these diagrams are presented in Chapter Five.

Table (4.1) : Dimensions of Tested Bracing Members

Length, L_o (mm)	310	450	520
Initial Rise, A_o (mm)	10 30 50 65	10 30 50 65	20 30 50 65 75 85 95 105
Breadth, b_s (mm)	12.4	12.4	15
Thickness, t_s (mm)	1.22	1.22	1.2

Table (4.2) : Properties and Young's Moduli of Tested Specimens

Specimen No.	Thickness t_s (mm)	Breadth b_s (mm)	Young's Modulus $E(kN/mm^2)$	Notes
1	1.22	12.4	188.03	specimens
2	1.22	12.35	185.92	used in
3	1.22	12.31	185.00	stability tests
1	1.2	15.05	202.23	specimens
2	1.2	14.85	207.92	used in
3	1.2	14.92	233.63	frame tests

Table (4.3) : Combinations of Bracings in Stability Tests

Test No.	Initial Rise "A_o"(mm)		Length "L_o"(mm)	Ratio"R_i=P/W"
	Compression	Tesnsion		
1	10	65	310	72.0
2	10	65	450	145.6

Table (4.4) : Combinations of Bracings in Frame Test

Test No.	Initial Rise "A_o"(mm)				Dimension of bracing member with end connection
	1st Storey		2nd Storey		
	Comp.	Tens.	Comp.	Tens.	
1	20	85	20	85	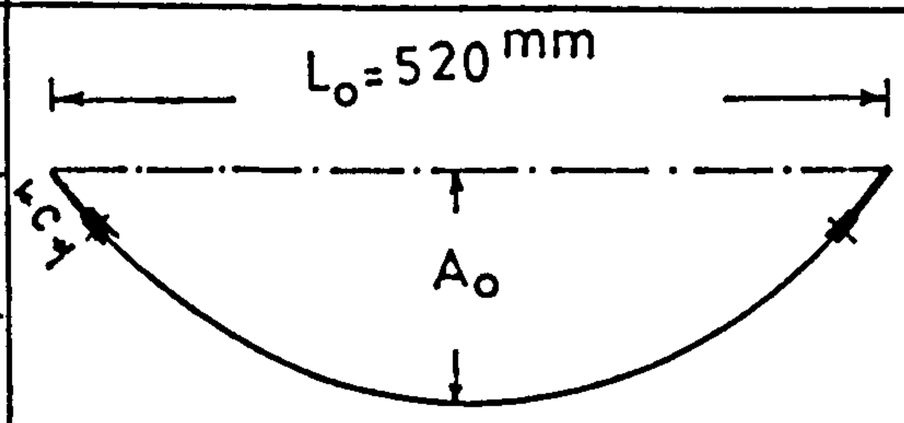 n.b. The ratio "R_i" kept constant and = 40. c = 24 mm
2	20	95	20	85	
3	20	95	20	95	
4	20	95	30	95	
5	30	95	30	95	

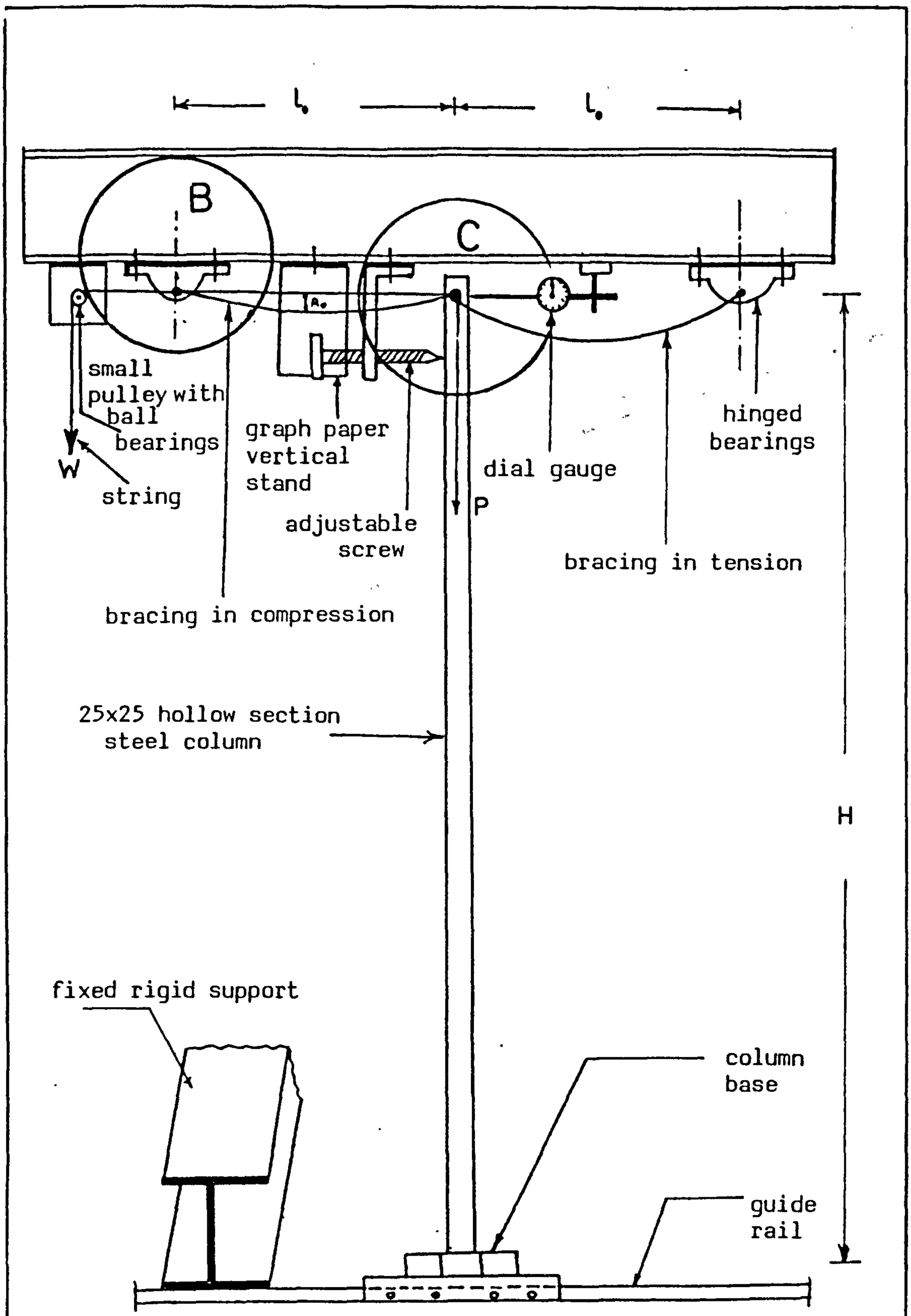

Fig.(4-1): Single Column Model

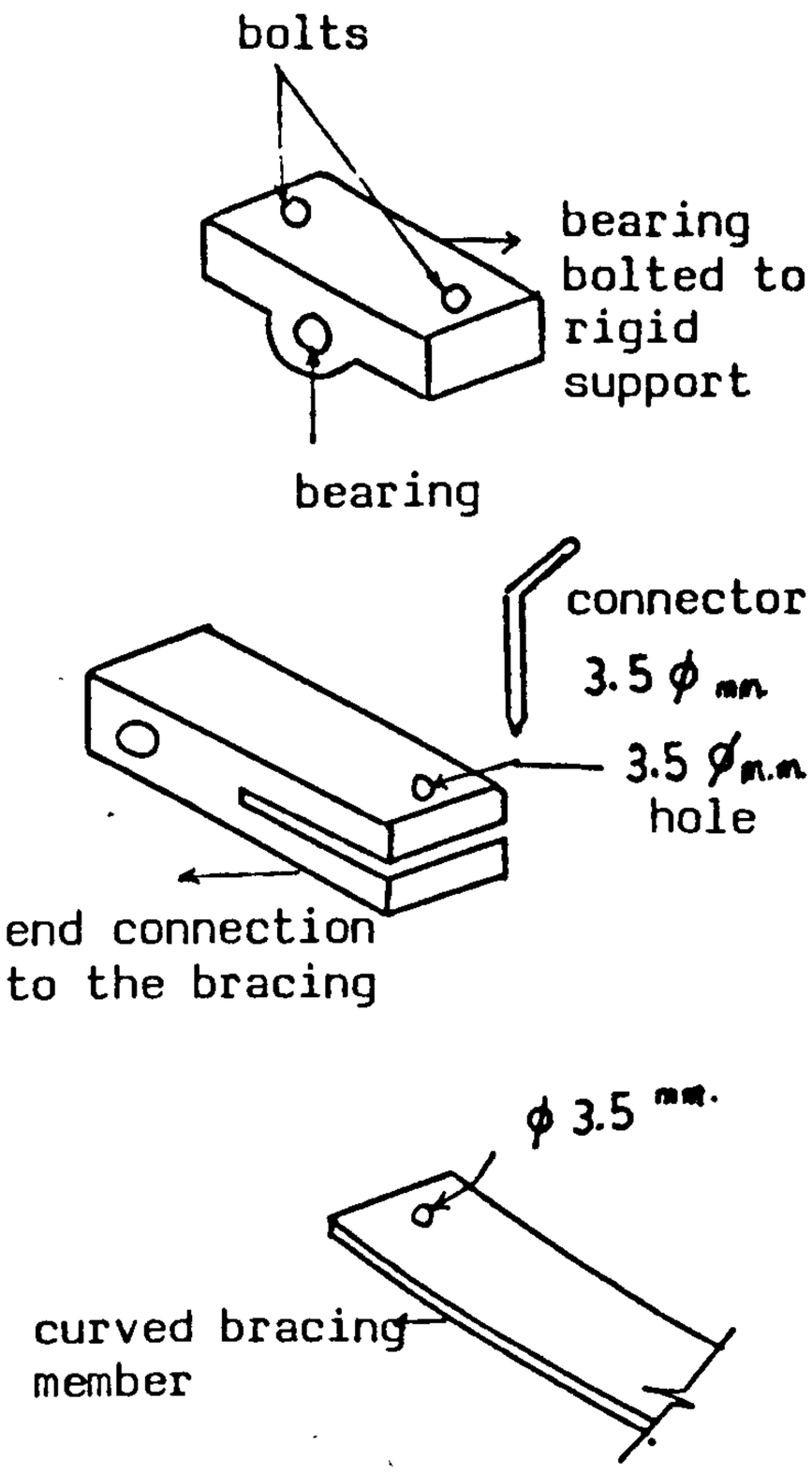

Fig.(4-2a): Connection at B

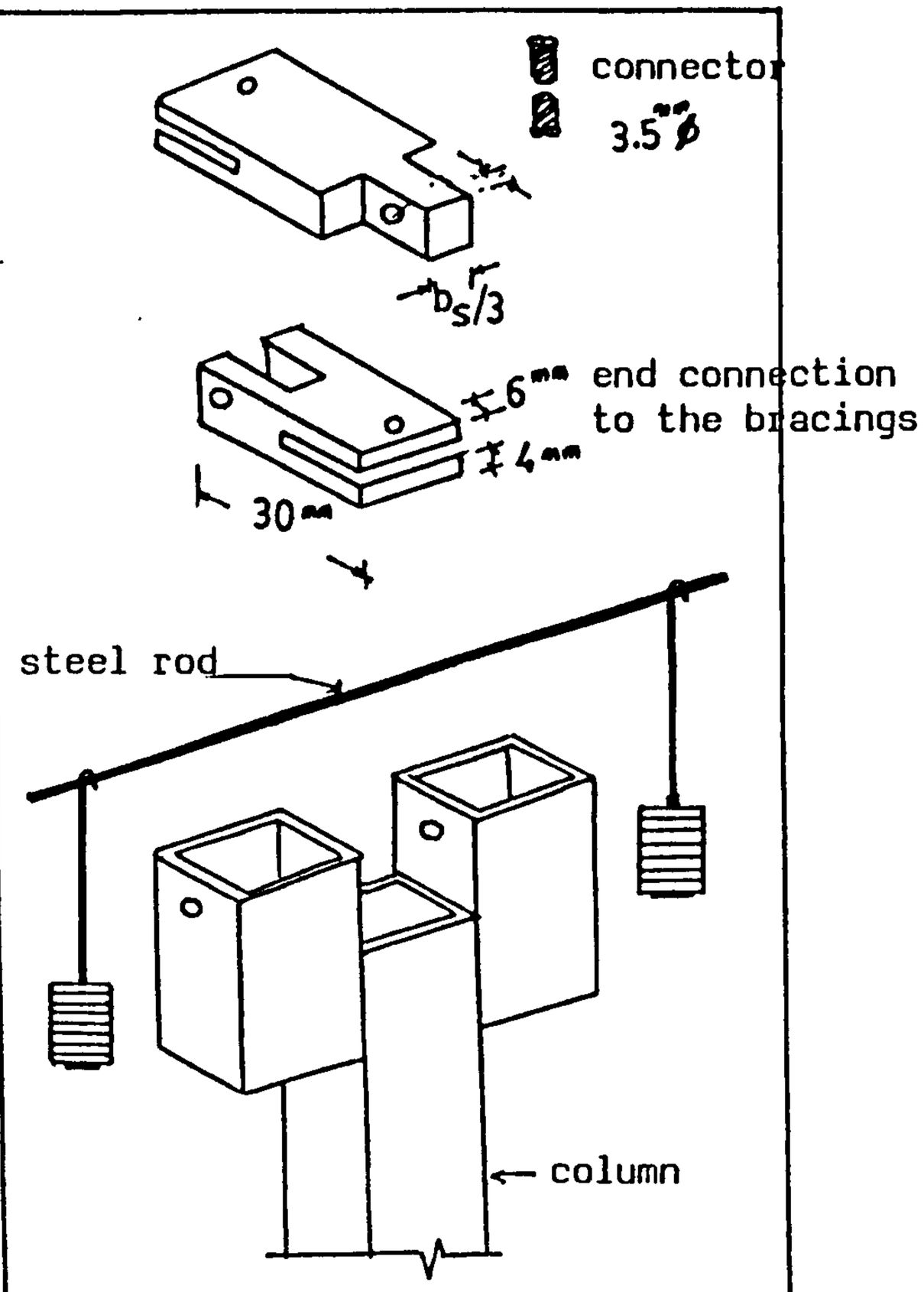

Fig.(4-2-b): Connection at C

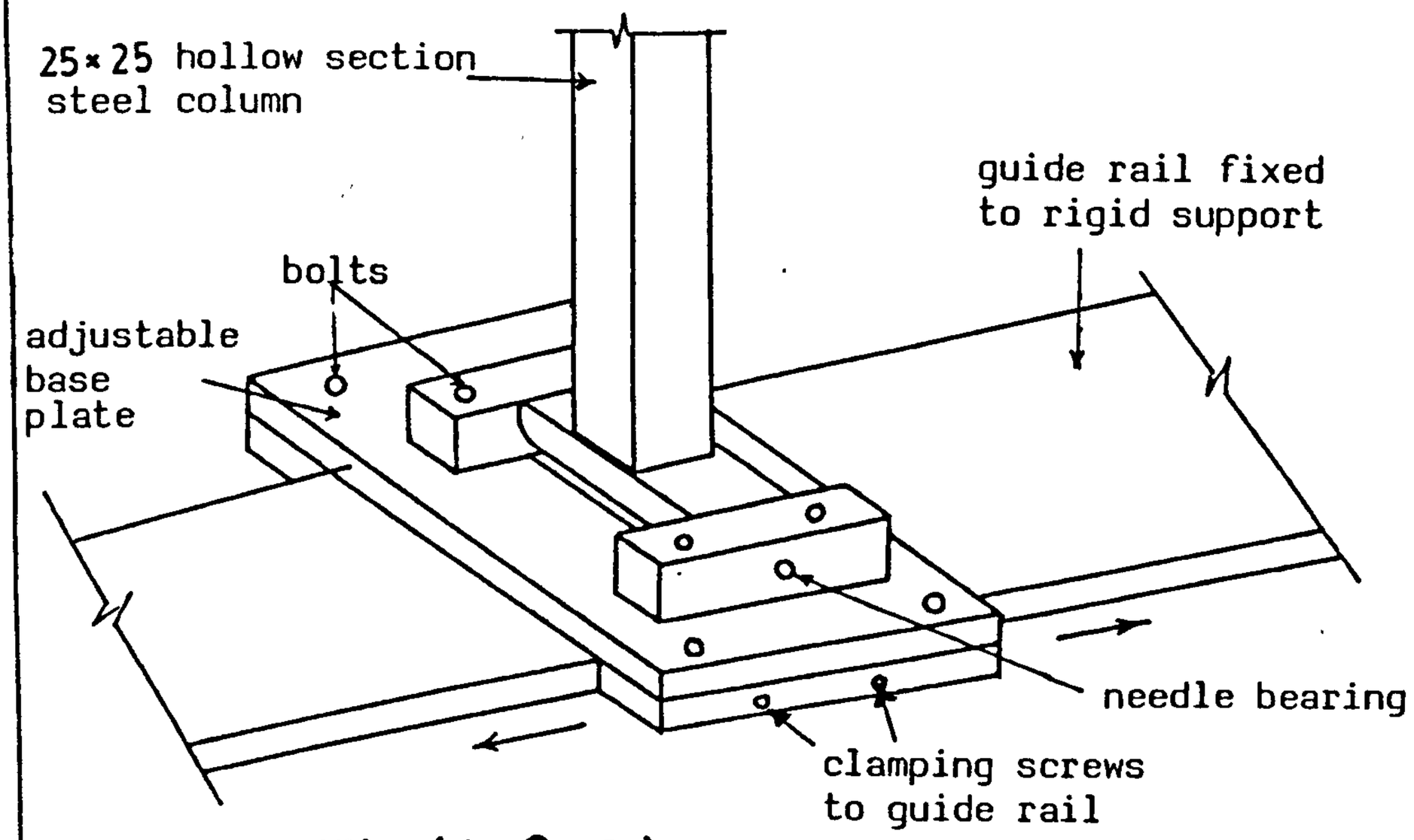

Fig.(4-2-C).: Connection at Column Base

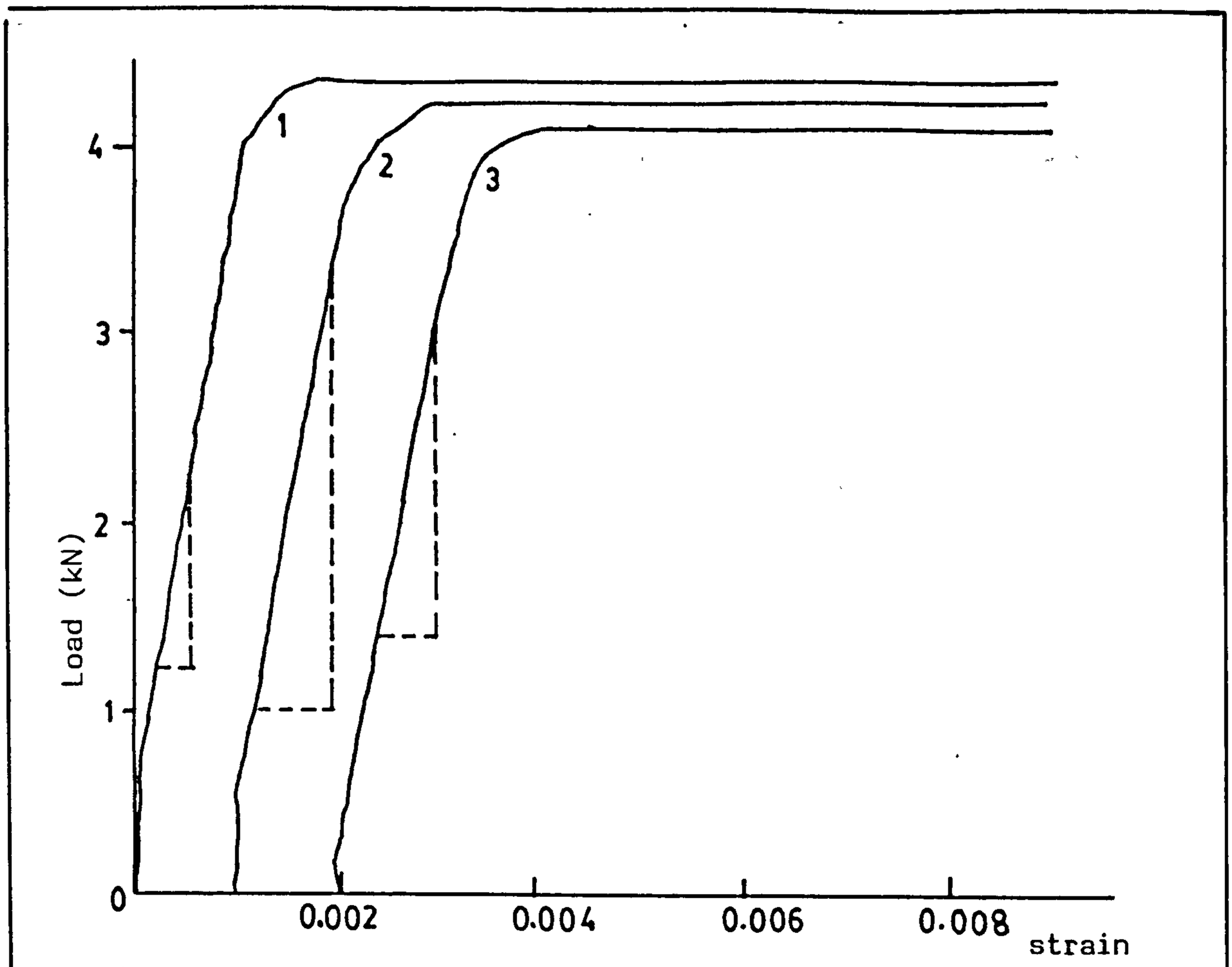

Fig.(4-3-a): Load-strain curve for tensile specimens used in stiffness and stability tests

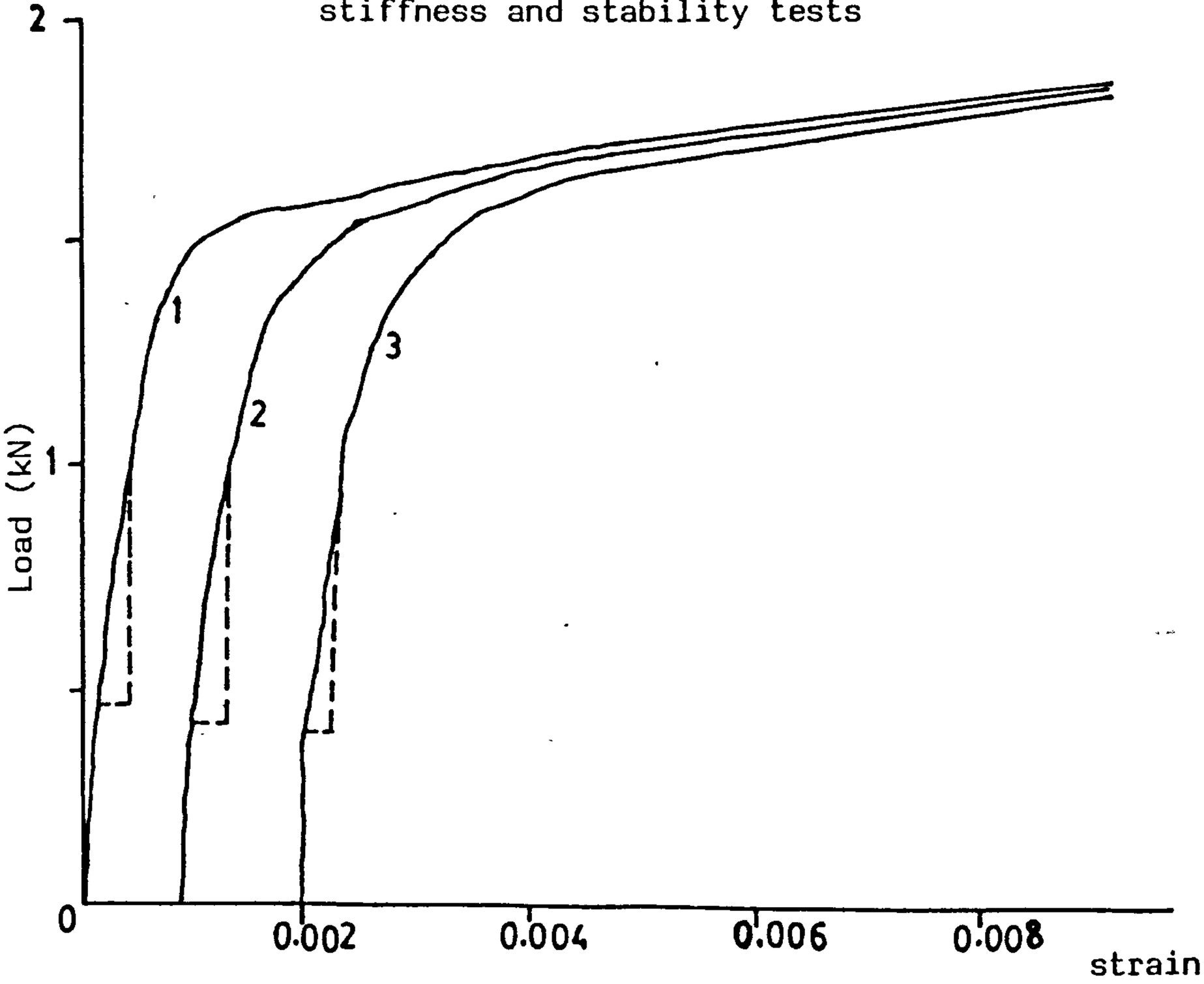

Fig.(4-3-b): Load-strain curve for tensile specimens used in frame tests

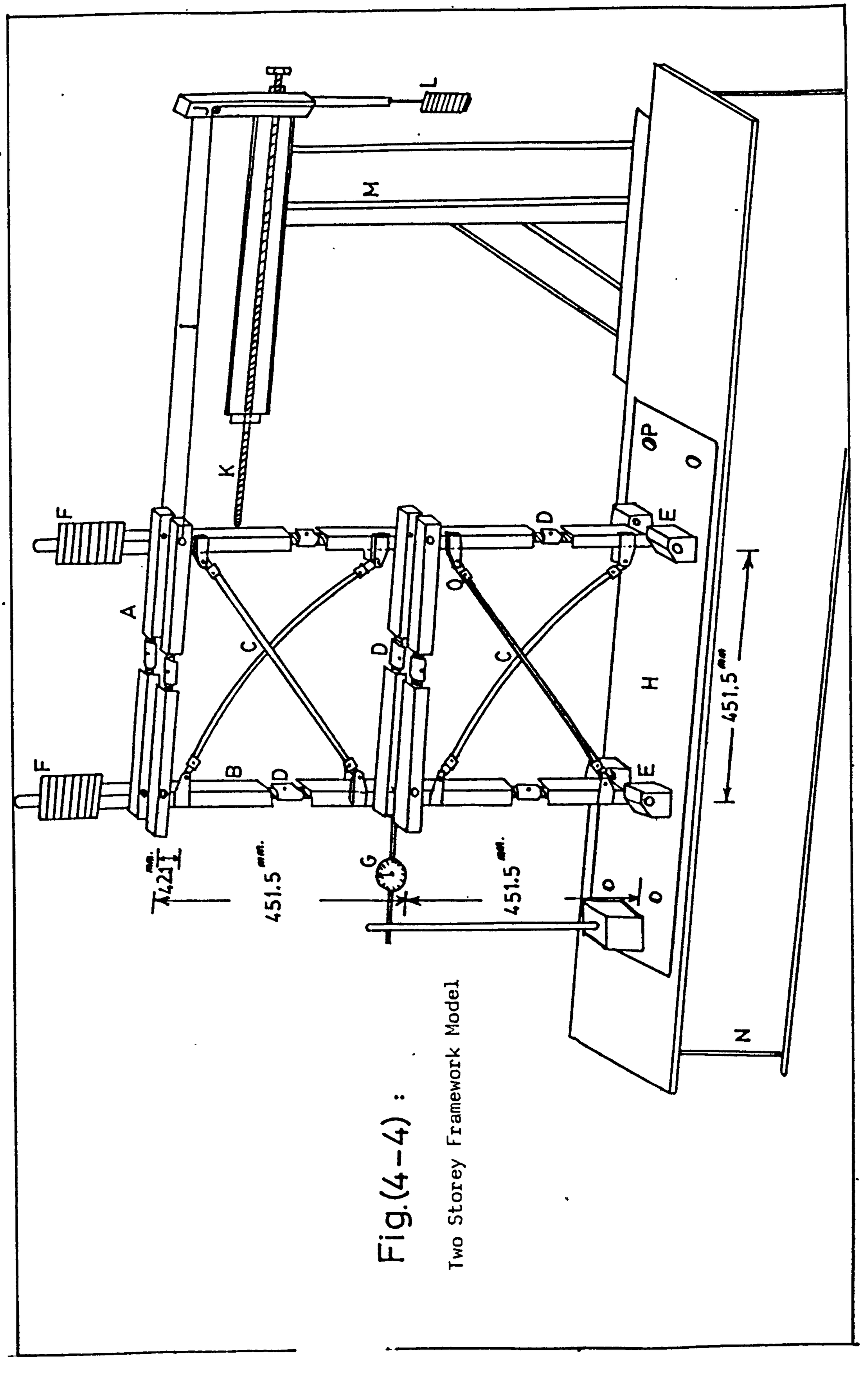

Fig.(4-4) : Two Storey Framework Model

Key to Fig. (4.4)

A - Frame beams

B - Frame columns

C - Curved bracings

D - Variable screwed joints

E - Frame base

F - Vertical loads

G - Dial gauge

H - Flat plate

I - String

J - Pulleys

K - Adjustable screw

L - Horizontal load

M - Rigid vertical stantion

N - I beam rigid support

O - End connections for bracing

P - Bolts

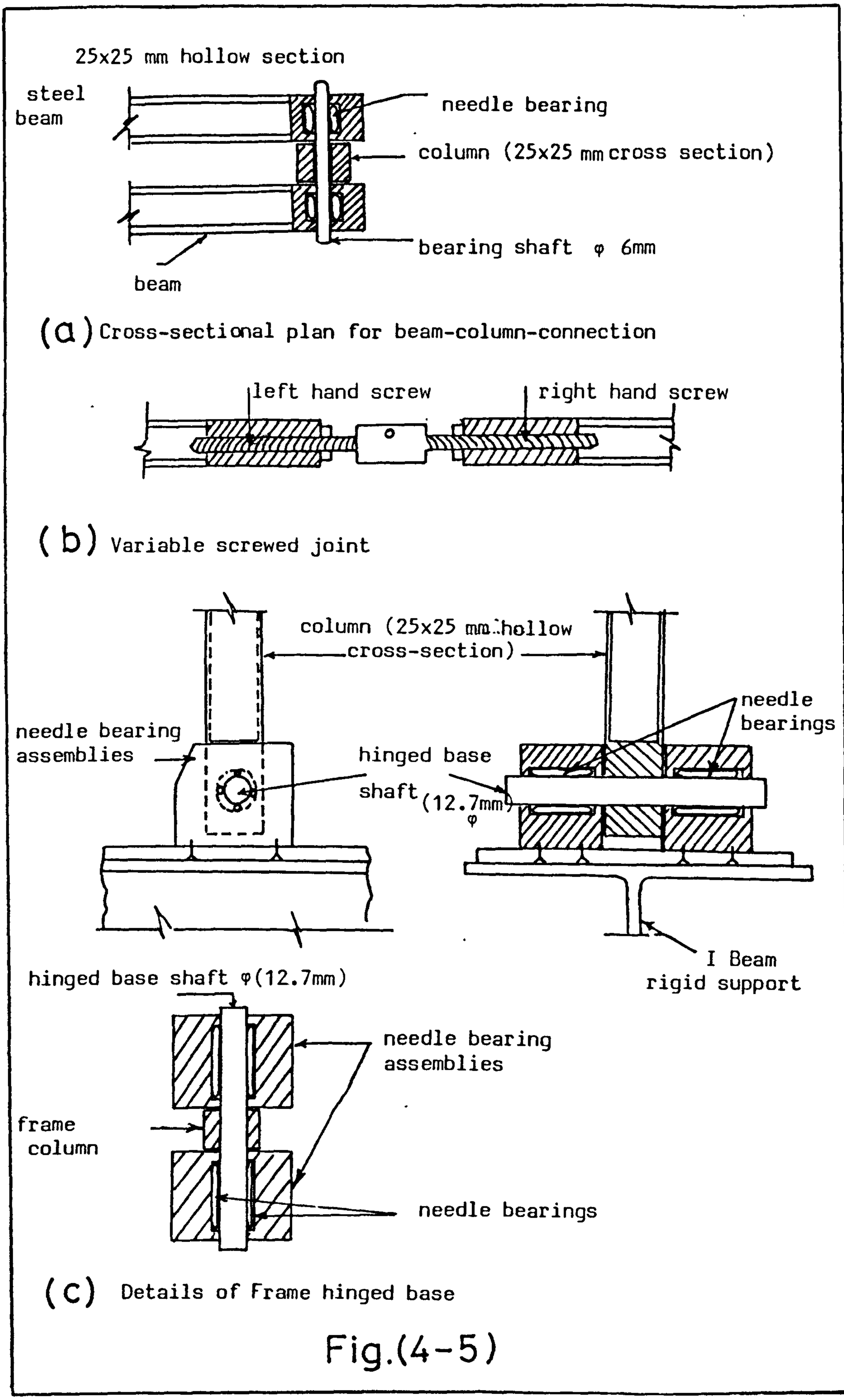
25x25 mm hollow section
steel beam
needle bearing
column (25x25 mm cross section)
bearing shaft φ 6mm
beam
(a) Cross-sectional plan for beam-column-connection
left hand screw
right hand screw
(b) Variable screwed joint
column (25x25 mm hollow cross-section)
needle bearing assemblies
hinged base shaft (12.7mm φ)
needle bearings
I Beam rigid support
hinged base shaft φ(12.7mm)
needle bearing assemblies
frame column
needle bearings
(C) Details of Frame hinged base

Fig.(4-5)

CHAPTER FIVE

COMPARISON OF THEORETICAL AND EXPERIMENTAL STATIC RESULTS

5.1 Introduction

The results of the experimental work, in chapter four, are presented and will be discussed in this chapter. The behaviour observed during testing was noted and a discussion of experimental shortcomings is included.

The theoretical analyses presented in chapters two and three have been applied to those structures investigated experimentally. Satisfactory comparisons between the theoretical results with those obtained experimentally have been achieved. The theoretical results, of struts and ties obtained from the analyses presented in chapter two (using the theory of large deformation), have been compared with those from Swannell [77] (using the theory of small deformation).

It must be noted that all the loads and dimensions quoted here are in 'Newtons' and 'Millimeters' respectively. The loads used in the experiments were in kilograms and for the purpose of comparison in this chapter have been converted to Newtons by multiplying them by 9.806.

5.2 Comparison of Theoretical Results Obtained From the Theory of Large Deformation with Those From the Theorey of Small Deformation (Swannell formula)

The theoretical results of struts obtained from the analysis presented in chapter two are compared with those obtained from the

formula which has been derived by Swannell [77] and later modified by Tsai [86] for a range of parameters.

The relationships between the ratio of axial displacement Δ/L_o and the load ratio W/P_E are shown graphically in Fig. (5.1), for several initial rises A_o/L_o, in which P_E is the Euler buckling load and is equal to $\pi^2 EI/L_o^2$.

The horizontal axis in this diagram represents the non-dimensional form Δ/L_o and the vertical axis represents the ratio W/P_E.

According to the Swannell formula (the small deformation theory), a load W greater than the Euler buckling load P_E cannot be applied to the strut and the load displacement curves approach the horizontal line $W=P_E$ asymptotically as shown by the dotted curves in Fig. (5.1). It is also seen from this figure that part of the Swannell curves for struts with $A_o/L_o \leqslant 5\%$ merge completely with the solid curves (obtained from the theory of large deformation) up to a load ratio $0.75\ W/P_E$, as shown by curves (i) and (ii). This means that the Swannell solution gives a good representation only for shallow struts up to this ratio of load. The discrepancy between the two theories increases when the ratio A_o/L_o is greater than 5%. As shown by curves (iii) and (iv).

Figure (5.2) shows the comparison between the theoretical stiffnesses of a strut with $A_o/L_o = 20\%$. In this figure the horizontal axis represents the ratio Δ/L_o and the vertical axis represents the axial stiffness "K(N/mm)". It is seen that the initial stiffness (i.e. K at W=0) calculated by the large deformation theory is much less than the stiffness calculated by Swannell formula,

this means that Swannell's solution is a very poor representation of K-Δ behaviour for struts with $A_o/L_o \geq 5\%$.

5.3 Stiffness-Displacement Interaction Diagrams

The relationship between the experimental and theoretical axial stiffness "K" and the lateral displacement "Δ" is obtained for various curved struts and ties. These struts and ties have three different lengths "L_o" and various initial rises "A_o" as shown in Table (4.1).

The stiffness-displacement relationship can be incorporated into K-Δ interaction diagrams which are divided into two groups. The first group is concerned with the investigation of curved struts as shown in Figs.(5.4) to (5.15), while the other group is devoted to the investigation of curved ties as shown in Figs. (5.16) to (5.23).

In both groups the theoretical interaction curves due to axial-loading and eccentric-loading are denoted by curves "L_a" and "L_e" respectively, in which "L_a" represents the theoretical curve in the case of axial loading and "L_e" represents the theoretical curve in the case of eccentric loading, with an eccentricity c=24.0 mm, the eccentric length "c" is equal to the length of the end connection used in the experimental model.

The experimental results of the stiffness "K" and the displacement "Δ" of these struts and ties are plotted also on Figs. (5.4) to (5.23).

The theoretical and the experimental results are compared with those obtained from Swannell formula. The Swannell curves have been plotted in Figs. (5.4) to (5.23) and are denoted by curves "S". In

Figs (5.4) to (5.23) the horizontal axes represent the axial displacements "Δ" and the vertical axes represent the axial stiffnesses "K".

5.3.1 Observations on Stiffness - Displacement Diagrams

From the diagrams shown in Figs. (5.4) to (5.15), concerning the group of curved struts, various observations have been made.

The stiffness of a curved strut decreases as the axial displacement increases, and this appears clearly from all curves shown in the figures.

The experimental stiffness values of the investigated struts, generally agree very well with the theoretical results from the large deformation theory with discrepancies in the stiffnesses varying from 0.5% to 10%. The larger discrepancies are associated with test results at high deflections, for which the measured displacements are larger than the predicted values. These appear to reflect the influence of inelastic material, where once this case is reached, the strut is less stiff than it would have been had it remained fully elastic, consequently displacements are greater than would be expected from the theoretical curves. For this reason the theoretical horizontal applied loads and the corresponding displacements of the struts, at the beginning and at the end of the inelastic behaviour, were calculated from the following formulas:

$$\frac{W_y}{\sigma_y . A_c} + \frac{W_y . y_y}{\sigma_y . Z_y} = 1 \qquad (5.1)$$

and $$\frac{W_p}{\sigma_y . A_c} + \frac{W_p . y_p}{\sigma_y . Z_p} = 1 \qquad (5.2)$$

where W_y is the applied load on the strut at the onset of plasticity

W_p is the applied load on the strut at the full plastic section

σ_y is the yield stress of the strut material (this stress was determined, for struts used in stiffness and stability tests from Fig. (4.3.a) and is equal to 261.199N/mm^2, while for struts used in the frame tests, the stress was determined from Fig. (4.3.b) and is equal to 107.095 N/mm^2),

A_c is the cross-sectional area of the strut,

Y_y is the lateral deflection at the centre line of the curved strut, at the onset of plasticity, where, the stress distribution on the cross-section of the strut at this stage is as shown in Fig. (5.3.b),

y_p is the lateral deflection of the curved strut at the full plasticity, where the stress distribution on the cross-section of the strut at this stage is as shown in Fig. (5.3.c).

$$Z_y = \frac{b_s . t_s^2}{6}$$

in which Z_y is the elastic modulus of the strut

$$Z_p = \frac{b_s . t_s^2}{4}$$

in which Z_p is the plastic modulus of the strut.

and b_s is the breadth of the strut while t_s is the thickness of the strut.

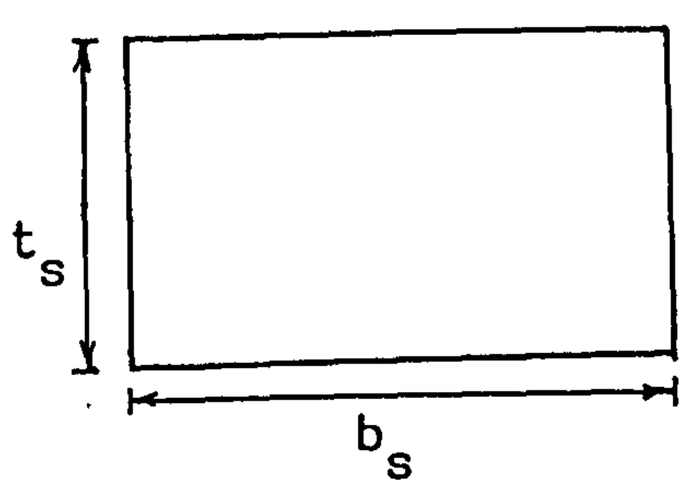

(a) cross-section of the strut

(b) stress distribution at yield

(c) stress distribution at full plasticity

Fig. (5.3)

The axial displacements at the onset and at the end of plasticity are plotted on Figs. (5.4) to (5.15), these displacements are denoted by "Δy" and "Δp" respectively. The axial displacements less than Δy represent the displacements of the full elastic behaviour of the strut, while the displacements in the range Δy to Δp represent the axial displacements of the partial plastic behaviour of the strut.

From Figs. (5.4) to (5.15), it is concluded that, the experimental stiffnesses in the region of full elasticity are very close to the theoretical results, while in the region of partial plasticity the experimental stiffnesses are generally lower than the theoretical results where the displacements in this region are larger than the theoretical values due to the inelastic material. Generally satisfactory results are obtained, despite the presence of some degree of plasticity.

The important point to notice from these figures is that the inelastic behaviour begins particularly early when the strut is relatively short. Conversely the beginning of the inelastic

behaviour is delayed when the strut is relatively long. A comparison between the maximum experimental displacement and the theoretical displacement at full plastic limit for different struts is shown in Table (5.1).

The theoretical curves of struts subjected to axial loading (curves L_a) are generally lower than the curves of struts subjected to eccentric loading (curves L_e). However the curves L_a and L_e are very close together as shown in the Figs (5.4) to (5.15) where the eccentricity c=24.0mm is small, if it is compared to the total length of the strut.

Swannell stiffness curves agree very well with the theoretical stiffness curves "L_a" when the ratio "A_o/L_o" is less than 5% as shown in the Figs. (5.4), (5.8) and (5.12), where the ratios "A_o/L_o" are 3.226%, 2.222% and 3.846% respectively. The discrepancy increases as the ratio "A_o/L_o" is greater than 5% as shown in the remaining figures. Generally the experimental and the theoretical stiffness curves are lower than the Swannell curves.

The stiffness-displacement interaction diagrams concerning the group of curved ties are shown in the Figs. (5.16) to (5.23). Various observations can be made.

The stiffnesses of curved ties increase as the axial displacements increase.

The experimental values of the stiffnesses of all investigated ties agree very well with the theoretical results. The experimental behaviour of the investigated ties was in fully elastic regions,

where the maximum applied loads were less than the yield loads of these ties. The yield load, for specimens used in stiffness and stability tests is shown in Fig. (4.3.a), while for specimens used in the frame tests is shown in Fig. (4.3.b).

The stiffness curves of the axially loaded ties are very close to those representing the eccentrically loaded ties, because the length of the end connection "c" is very small if it is comprared to the total length of the strut. Generally the curves "L_a", which represent the behaviour of axially loaded ties are lower than the curves "L_e",which represent the behaviour of the eccentrically loaded ties.

The experimental and the theoretical stiffness curves for the investigated ties are lower than those derived by Swannell. The discrepancy increases as the ratio "A_o/L_o" increases.

5.4 Load-Displacement Interaction Diagrams Concerning The Behaviour of Individual Bracings

Two types of stiffness tests were carried out as described in chapter four, i.e. for struts and ties.

The experimental and theoretical load-displacement relationship for both cases are shown graphically in the Figs. (5.24) to (5.43). The horizontal axes in all diagrams represent the axial displacement "Δ" while the vertical axes represent the moment about the base of the column model, due to the external applied loads on the struts or ties. The length "L_o" and the initial rise "A_o" of the bracings are shown on each plot. The theoretical load-displacement

relationships for axially and eccentrically loaded struts are shown graphically in the Figs. (5.24) to (5.35), where, the curves "L_a" and "L_e" represent the load-displacement diagrams, for axially and eccentrically loaded struts respectively. Also the load-displacement curves of Swannell, which are denoted by curves "S" have been plotted on the diagrams for the purpose of comparison.

The experimental horizontal load "W" for shallow strut ($A_o/L_o \leqslant 5\%$) rises quickly towards its maximum value levelling off at low displacement, as shown in the Figs. (5.24), (5.28) and (5.32). This means that the stiffness of the strut is at its greatest within this small region and then falls comparatively quickly as the loading and hence deflection is increased. In reality it is to be expected that a load will eventually be reached at which, somewhere in the strut, the material reaches its limit of proportionality. Further increase in the load leads to the development of a zone in which the material is partially plastic. The theoretical inelastic behaviour begins at a point on the curve which has a displacement "Δy", while the end of partial plastic behaviour is represented by a point which has a displacement "Δp", as shown in the figures.

Comparison between the experimental and theoretical maximum applied loads on the struts at the end of the partially plastic behaviours are shown in Table (5.1).

In Table (5.1) the important point to notice is that the maximum loads which the curved struts can carry, at the end of the partial plastic behaviours, are less than the Euler buckling loads "P_E".

The experimental loads and the corresponding axial displacements are in reasonable good agreement with the theoretical results obtained from the theory of large deformation. The experimental loads, at the beginning of each test, are very close to the theoretical loads in the fully elastic region (i.e. within a range of displacement lower than Δy). The experimental results for applied loads located in the partially plastic regions, in all the tests, showed discrepancies of less than 10% than the theoretical results. The struts are less stiff than they would have been had they remained fully elastic, consequently displacements are greater than would be expected from the theoretical calculations.

For struts with "A_o/L_o" relatively large the Swannell load-displacement curves lie above the theoretical and the experimental curves, especially within the range of the experimental values.

The load-displacement interaction diagrams for investigated ties are plotted in the Figs. (5.36) to (5.43). As can be seen the theoretical results agree very well with the experimental values. Also it is seen that the displacement increases at a slower rate than the load until the deformed tie form a straight tension member. Once this stage is reached the increment of the axial displacement will be proportional to the load increment.

5.5 Interaction Diagrams Concerning the Stability of a Column Restrained by a Combined Curved Bracing System

The results of the experimental work, concerning the stability tests (second series of tests article (4.5)), are presented and will be discussed in this section.

As numerical examples, the method of analysis explained in chapter three, articles (3.2.2.3) and (3.3) are applied to the combined bracing sets shown in Table (4.3). The eventual choice of the shallow rise (A_o = 10mm), for the compression bracing, and the deep rise (A_o = 65mm), for the tension bracing, was made after consideration of the form of K-Δ interaction diagrams, where the stiffness of the compression bracing, at the beginning, is greater than the stiffness of the tension bracing (see Figs. (5.4) and (5.17). This means that, at the beginning, if the applied load is increased gradually from zero, then the loading is mostly sustained by the compression bracing. If the load is increased more and more, then the lateral displacement "Δ" increases, the stiffness of the compression bracing reduces and the stiffness of the tension bracing rises. Eventually, the load is sustained mainly by the tensile bracing. Therefore the strut "A_o = 10mm", together with the tie "A_o = 65mm" formed a very good relationship when considered as a combined system.

The theoretical relationship between the restoring moment ($F_1 = K\Delta H"$) and the overturning action ($F_2 = WH"+ P\Delta$) against the lateral displacement "Δ", for the sets of the bracings illustrated in Table (4.3), are shown graphically in the Figs. (5.44) and (5.46). The horizontal axis, in each figure, represents the lateral displacement "Δ" at the top of the column and the vertical axis represents the functions F_1 and F_2.

The straight line, in these diagrams, shows the variation of the overturning action ($F_2 = WH"+ P_{cr1}.\Delta$). The slope of this line is equal to the vertical load P_{cr1} and intercept WH"on the vertical axis, i.e. at Δ=0. The ratio between the applied vertical load "P"

and the horizontal load "W" (R_i = P/W) is shown on each plot. The solid curve, in these diagrams shows the variation in the restoring moment (F_1 = KΔH") which is dependent essentially on the characteristics of the non-linear stiffnesses of the combined bracing system, therefore, the function F_1 is dependent on Δ, as K is also dependent on Δ.

The broken curve shows the variation in the restoring moment (F_{11} = K_tΔH") which is dependent on the characteristic of the non-linear stiffness of the tension bracing only. This curve is drawn in the region after the end of the theoretical transient instability region. This assumption is based on the fact that the compression bracing has failed by buckling after a plastic hinge has formed at the middle of the strut, hence at this condition the stiffness of the strut can be neglected. Therefore, in the region after the failure of the compression member, the column can be considered restrained by the tension bracing only.

The experimental values which represent the overturning action about the base of the column (i.e WH" + PΔ) were plotted on the figures for the purpose of comparison with the theoretical results.

With the ratio of loading shown on each plot, the transient instability is expected, theoretically, to begin at point B, where $\Delta=\Delta_1$, and cease at point c, where $\Delta=\Delta_2$. At point B, the straight line ABCD, which represents the overturning action "F_2",is tangential to the curve OBECF, which represents the restoring moment "F_1", i.e. $F_1=F_2$ at point B and this represents the onset of the phenomenon of transient instability. Between points B and C, the values of functions "F_2" are greater than the values of function "F_1", so that

static equilibrium cannot be achieved. This stage represents the expected region of transient instability. Point C represents the theoretical static equilibrium position of the column at the end of the instability region, where the function "F_1" is again equal to the function "F_2".

In Fig. (5.44), the experimental results shown in the region before the onset of the transient instability are close to the theoretical results of the combined system. In the region after the end of transient instability region, the experimental results are very close to the theoretical curve for the column restrained by tensile bracing only. This means that there is no influence from the actual stiffness of the compression member in this region. The experimental behaviour of the individual compression member used in this combined system (Figs. (5.4) and (5.24)) indicates that the behaviour of the member is elastic up to a displacement equal to 7mm approximately, and after this limit the member starts to loose some of its stiffness and a full plastic hinge will form at displacements higher than 14mm approximately. Thus since the displacement at the end of the transient instability region, Fig. (5.44), is greater than the displacement at the end of the partial plastic region of the compression member, therefore the experimental results after the end of transient instability region should agree more closely with the theoretical curve for the column restrained by tension bracing only, as the compression bracing has failed by buckling before this region of stability.

The experimental results shown in Fig. (5.46), which represent the plot of WH" + PΔ from the stability test, agree very well with the theoretical calculation of the combined bracing system,with discrepancies varying from ½% to 9.75%. The larger discrepancies are associated, only, with the results related to the higher displacements, i.e. in a range after the end of transient instability region. This appears to reflect the influence of the actual stiffness of the compression member. The test on the individual compression bracing member, Figs. (5.8) and (5.28) showed that the actual compression behaviour of the member started to loose some of its stiffness in the defined partial plastic region (i.e. in the region defined by Δy and Δp), and then the member started to fail by buckling at a displacement higher than 30.0mm approximately. As the total experimental behaviour of this combined system lies within a range less than 30.0mm, therefore it is to be expected that the experimental points will tend to agree with the theoretical solution which includes the stiffness of compression bracing. The last three points of the experimental results agree less well with the theoretical results, where the corresponding displacements in the compression member, at these points lie within the partial plastic region of this member and this causes some reduction in the compression stiffness. Therefore the actual stiffness of the combined bracing system is lower than the calculated stiffness from the theoretical investigation. This could be the reason for discrepancies between the experimental and the theoretical results at these last three points.

The theoretical and the experimental relationships between the vertical applied load "P" and the displacement "Δ", for the sets of bracing systems shown in Table (4.3), are shown graphically in the Figs. (5.45) and (5.47). The ratio "R_i = P/W" is kept constant in all cases of loading. The horizontal axis, in each figure, represents the lateral displacement "Δ" while the vertical axis represents the applied vertical load "P".

It is seen from the figures that, as the vertical load "P" increases the lateral displacement "Δ" increases up to point B, where $\Delta=\Delta_1$ and $P = P_{cr1}$. At a slightly higher load than P_{cr1}, a sudden increase in the lateral displacement "Δ" occurs until the structure becomes stable again at point c, where $\Delta=\Delta_2$. The region between the displacements Δ_1 and Δ_2 is defined as the transient instability region, for the combined bracing system.

The displacement "Δ_1" represents the lateral displacement, of the column, at the onset of the transient instability. The corresponding applied vertical load to this displacement represents the critical load "P_{cr1}" applied to the column.

The displacement "Δ_2" represents the lateral displacement at the top of the column, where the transient instability ends.

The slope of the tangent to the load-displacement curve at point B is equal to zero, i.e. $\frac{dP}{d\Delta} = 0$ at the onset of the transient instability region.

As the applied load "P" increases beyond P_{cr1} the displacement "Δ" is greater than Δ_2 and the structure is stable.

Generally, the experimental results agree reasonably well with those obtained theoretically for the column restrained laterally by the two sets of bracings as shown in Table (5.2).

In Table (5.2) the values Δ_1, Δ_{1e}, Δ_2, and Δ_{22} and Δ_{2e} can be defined as follows:

Δ_1 and Δ_{1e} are the theoretical and the experimental lateral displacements at the onset of the transient instability region, respectively,

Δ_2 is the theoretical displacement at the end of the instability region, where the solution includes the compression bracing,

Δ_{22} and Δ_{2e} are the theoretical and the experimental displacements at the end of the instability region respectively, where the theoretical solution includes the effect of plasticity in the compression member.

5.6 Interaction Diagrams Concerning the Stability of the Multistorey Framework Stiffened by Curved Diagonal Bracings

The techniques described previously in chapter three, article (3.4) were applied to study the behaviour of the two storey framework which was examined experimentally in chapter four, section (4.6). The dimensions of the frame are shown in Fig. (4.4). The ratio between the vertical and the horizontal applied loads "P & W" was kept constant in all cases of loading. The ratio $R_i = P/W = 40.0$ was chosen because it allows the phenomenon of transient instability to occur for all combinations of the curved bracing sets.

The relationships between the restoring moment "F_1" and the overturning action "F_2" against the lateral displacement "Δ" at the top of the framework are shown graphically in the Figs. (5.48) to (5.52). The combinations of bracings are shown on the figures. The function "F_2" is represented by the straight line ABCD, while the function "F_1", i.e. the restoring moment in the combined bracings, is represented by the solid curve OBECF. The broken curve, in each diagram, shows the variation of the restoring moment "F_{11}" in the tension bracing sets only. This curve is drawn in the region after the end of the transient instability region, where it is assumed that the compression bracings of each combination are ineffective at a displacement higher than the limit defining the end of the transient instability region.

5.6.1 Comparison Between Theoretical and Experimental Results

The experimental results obtained, from the third series of tests presented in chapter four, are compared with those from the theoretical results as shown in the Figs. (5.48) to (5.57).

It is seen from the figures that, with the ratio of loading shown in each plot, the onset of the transient instability region for the combined bracings is shown at point B where $\Delta=\Delta_1$ while the end of this region is at point c, where $\Delta=\Delta_2$. In the transient instability region, the values of function "F_2" are greater than the values of function "F_1", so that static equilibrium cannot be achieved. The ends of the transient instability region represents the theoretical static equilibrium position of the framework, where the function "F_1" is equal to the function "F_2".

The experimental results shown in all diagrams in the region before the onset of the transient instability are very close to the theoretical results, but in the region after the end of this transient instability the experimental results are closer to the theoretical results for frame restrained by the tensile bracing system only. This means that the influence of the stiffness of the compression bracing set has become negligible in this region.

The behaviour of the individual compression members, used in this combined systems, indicated that the compression bracing with an initial rise A_o=20mm , Fig. (5.12), failed at an axial displacement equal to 12mm approximately, while the compression member with an initial rise A_o=30mm, Fig. (5.13), failed at a displacement equal to 15mm approximately. Thus the corresponding displacements in the compression members at the ends of the transient instability regions are beyond the failure deflections.

It can be seen, also from the figures, that reasonable good agreement is obtained between the theoretical and the experimental results. A summary of the theoretical and the experimental results is given in Table (5.3).

5.6.1.1 Load-Displacement Interaction Diagrams Concerning the Stability of Frameworks

Values of the vertical applied load "P" on the framework are plotted against the corresponding lateral displacement "Δ" , at the top of the frame, for all combinations of the bracing sets, as shown in the Figs. (5.53) to (5.57). The horizontal axis, in each plot, represents the displacement "Δ" while the vertical

axis represents the vertical load "P".

It is seen from the figures that the displacement "Δ" increases with load "P" up to point B where, at B, $\Delta=\Delta_1$ and $P=P_{cr1}$. Thus at point B the frame becomes unstable and then snaps through to point c, where $\Delta=\Delta_2$. Further increase in the vertical load beyond P_{cr1} is associated with displacements greater than Δ_2 and the structure becomes stable again.

It can be shown that point B (onset of the transient instability region) corresponds to $\frac{dP}{d\Delta} = 0$.

In general the framework becomes unstable when the straight line, representing the function "F_2" is tangential to the curve representing the function "F_1" and this is associated with the zero slope of the load-displacement curve.

The experimental applied vertical loads causing the transient instability agree fairly well with the theoretical results at the onset of this instability region as shown in Table (5.3).

5.7 Effect of Initial Rise "A_o" of the Combined Bracing System On the Behaviour of the Framework

The numerical results presented in Table (5.3) indicate clearly that, with constant values of the initial rises of the tensile bracings, an increase in the initial rise of the compressive bracing has the effect of decreasing the critical load and, also, decreasing the range of the region of transient instability, (i.e. increasing the value of displacement at the onset of the instability region while decreasing the value of displacement at the end of this region). Also with constant values of the initial rises of the compressive bracings, an increase in the initial rise of the tensile bracing has

the effect of decreasing the values of the critical loads, and increasing the range of the transient instability region (i.e. decreasing the value of displacement at the onset of the instability region while increasing the value of displacement at the end of this region). This trend of results is to be expected, since increasing the initial rises of the combined bracing will reduce the resultant stiffness of these bracings and hence the value of function "F_1" and the critical loads respectively.

5.8 Comparison of Results Obtained by Tangent Slope and Influence Coefficient Methods

The results of the vertical loads "P" and the lateral displacements "Δ", obtained by the tangent slope method are compared, graphically, with those from the influence coefficient method, as shown in Fig. (5.58). The combination of the bracing system used for the comparison is shown in the figure.

Figure (5.58) shows, more convincingly, the remarkable accuracy of the influence coefficient method, by comparing the vertical loads "P" at different lateral displacements, calculated by the two different methods. The agreement between the two sets of results is so close that the small discrepancies are indiscernible on the curve plotted.

The comparison of displacements at the onsets and the ends of the transient instability regions and, also, the values of the critical loads "P_{cr1}" for different combinations of bracings, have shown equally good agreement between the two methods, as shown in Table (5.4). The influence coefficient results shown in the table

were obtained by using a degree of 20 for the polynomial representation. The results obtained by using a degree of 16 are slightly less than these results, in respect of the lateral displacements "Δ_1" and "Δ_2" , and have not been considered for comparison with the tangent slope method. The tangent slope results were obtained where the zero slope was taken as less than 1E-10 with an increment in the displacement equal to 1E-7mm. It is seen from the Table (5.4) that, very good agreement is, generally, obtained between the tangent slope and the influence coefficient results. The displacements at the onsets of the transient instability regions, obtained by the influence coefficient method, are slightly lower than those obtained by the tangent slope method, while the displacements at the ends of these regions, obtained by the influence coefficient method, are slightly higher than those obtained by the tangent slope method, for all combinations of the bracing systems. Although, the critical loads "P_{cr1}" obtained by the influence coefficient method are lower than those obtained by the tangent slope method does not mean that the influence coefficient results are more accurate because it depends on the chosen degree of the polynomial. A second source of inaccuracy in the influence coefficient method is that the results of this method are dependent on the number of data points. Since the precise results need a large number of these data points this will affect the computational time effort for the method. However the computational time effort for the tangent slope method is smaller than that for the influence coefficient method. Therefore, for all of these reasons the tangent slope method is preferred to the influence coefficient method.

Table 5.1 : Comparison Between Theoretical Results at the End of Partially Plastic Regions and Experimental Results

Initial chord length L_o (mm)	Initial Rise A_o (mm)	A_o/L_o	Central deflection y (mm)	Load(W) at full plasticity(N)		Axial displacement (Δ) (mm)		Euler load, P_E (N)	Theoretical Ratio W/P_E	Notes
				Theor.	Exp.(a)	Theor.	Exp.			
310	10	0.032	41.868	28.500	26.476 / 27.457	13.738	12.70	36.774	0.775	a: the second values represent the experimental failure buckling loads
	30	0.097	61.328	19.306	17.062 / 17.356	24.771	23.690		0.525	
	50	0.161	81.404	14.709	12.846 / 13.042	37.437	35.063		0.400	
	65	0.210	94.731	11.951	10.296 / 10.492	44.612	42.846		0.325	
450	10	0.022	75.593	15.706	14.219 / 14.415	32.539	29.50	17.452	0.900	
	30	0.066	95.569	12.652	11.277 / 11.473	49.564	45.150		0.725	
	50	0.111	113.569	10.471	8.678 / 8.825	64.871	59.240		0.600	
	65	0.144	126.442	9.162	7.060 / 7.207	75.404	65.820		0.525	
520	20	0.038	53.215	10.574	9.610 / 9.806	11.960	10.790	16.918	0.625	
	30	0.058	63.099	8.882	8.041 / 8.237	15.298	14.530		0.525	
	50	0.096	83.336	6.767	6.080 / 6.276	22.466	22.185		0.400	
	65	0.125	96.515	5.498	4.609 / 4.756	26.040	23.891		0.325	

Table (5.2) : The Theoretical and The Experimental Results of the Stability Tests

Length L_o (mm)	Ratio $R_i=\frac{P}{W}$	Initial rise, A_o (mm)		Displacements at partial plastic region (mm)		Cricital load P_{cr1}(N)		Displacement of transient instability region (mm)				
		Comp.	Tens.	Δ_y	Δ_p	(a) Theor.	(b) Exp.	Δ_1	Δ_{1e}	Δ_2	Δ_{22}	Δ_{2e}
310	72.0	10	65	6.884	13.738	1334.14	$\frac{1331.461}{1347.581}$	7.016	6.09	21.369	31.17	30.50
450	145.6	10	65	15.747	32.539	1141.088	$\frac{1140.336}{1172.150}$	3.494'	3.290	18.228	22.15	18.75

(a) Theor. : The theoretical results

(b) Exp. : The experimental results

Table 5.3 : Theoretical and Experimental Results for the Stability of Two Storey Framework Model

Chord length (L_o) mm	Initial rise (A_o) mm				Critical load (P_{cr1})N		Displacements of Transient Instability Regions						
	1st storey		2nd storey				onset (mm)			END (mm)			
	(a) Comp.	(b) Tens.	Comp.	Tens.	Theor. (c)	Exp (d)	Δ_1	Δ_c (e)	Δ_{1e}	Δ_2	Δ_c	Δ_{22}	Δ_{2e}
520	20	85	20	85	163.080	$\frac{160.818}{164.741}$	22.092	7.83	16.800	65.731	23.78	92.00	91.50
	20	95	20	85	159.760	$\frac{156.896}{160.818}$	20.69	7.45	15.689	79.113	28.57	98.80	97.00
	20	95	20	95	156.599	$\frac{156.296}{160.818}$	19.78	7.108	14.600	102.186	37.143	120.20	118.0
	20	95	30	95	137.482	$\frac{135.323}{139.245}$	24.977	8.90	19.00	89.147	32.6	117.70	116.0
	30	95	30	95	121.665	$\frac{121.594}{125.517}$	37.381	13.30	22.80	61.588	22.68	114.8	113.54

a) Comp. - compressing bracing
b) Tens. - tension bracing
c) Theor. - theoretical results
d) Exp. - experimental results
e) Δ_c - corresponding theoretical displacement in compression bracings

Table (5.4) : Comparison between tangent slope and influence coefficient results

Combinations of bracing system				Tangent Slope Method			Influence Coefficient Method		
1st storey		2nd storey		(a) P_{cr1} (N)	(b) Δ_1(mm)	(c) Δ_2(mm)	P_{cr1}	Δ_1(mm)	Δ_2(mm)
Comp.	Tens.	Comp.	Tens.						
20	85	20	85	163.080	22.092	65.731	163.032	22.025	65.848
20	95	20	85	159.760	20.69	79.113	159.718	20.601	79.604
20	95	20	95	156.599.	19.78	102.186	156.562	19.536	102.809
20	95	30	95	137.429	24.977	89.147	137.429	24.856	90.029
30	95	30	95	121.562	37.381	61.588	121.562	36.923	63.473

a) P_{cr1} : critical load causing the transient instability

b) Δ_1 : displacement at the onsets of transient instability regions $R_i = 40$

c) Δ_2 : displacement at the ends of transient instability regions

NON-DIMENSIONAL
LOAD DISP. RELATIONSHIP
OF CURVED STRUTS

COMPARISON BETWEEN THEORIES
OF LARGE & SMALL DEFORMATIONS

—— LARGE DEFORMATION THEORY

---- SMALL DEFORMATION THEORY

(i) : Ao/Lo=0.02

(ii) : Ao/Lo=0.04

(iii): Ao/Lo=0.10

(iv) : Ao/Lo=0.20

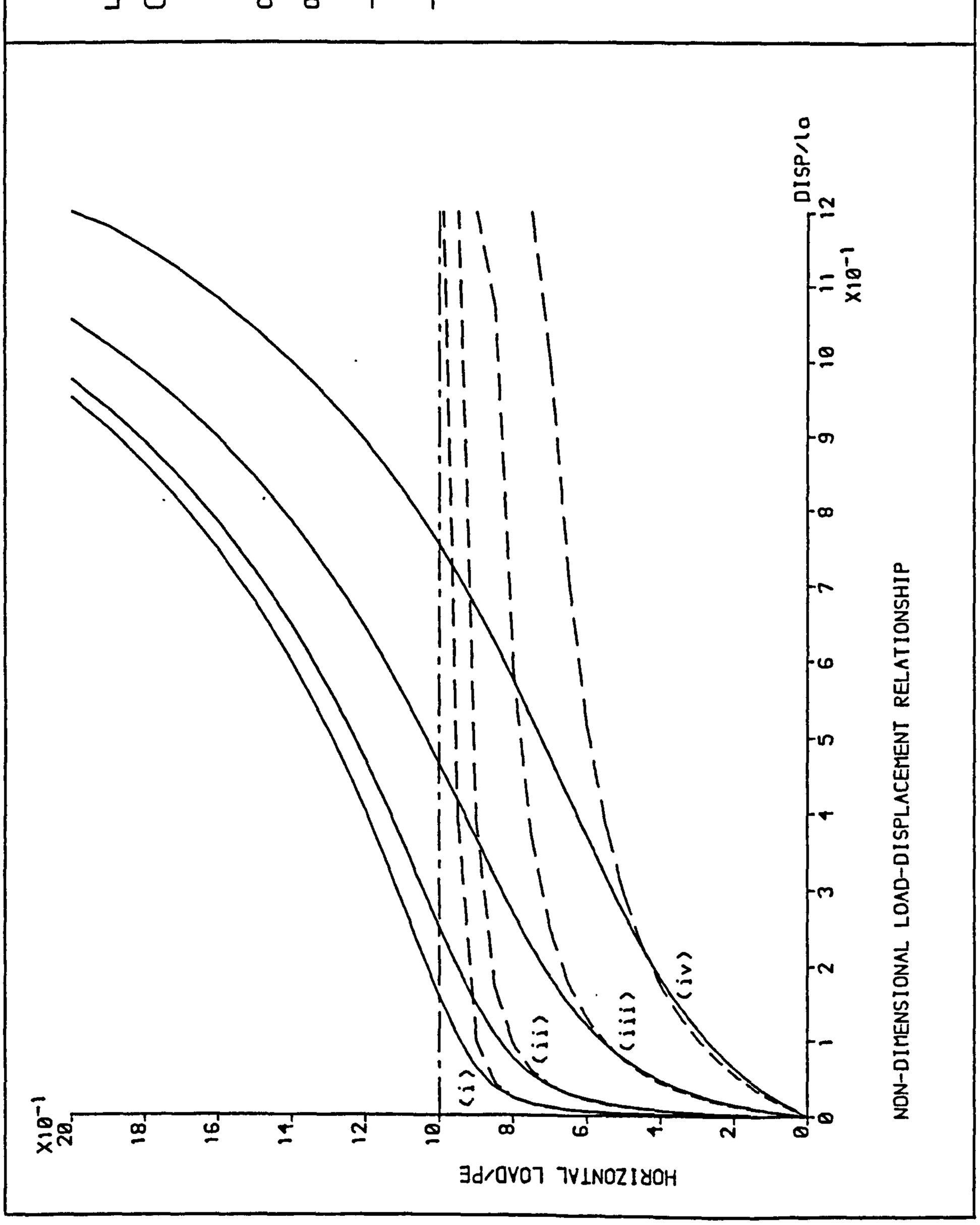

FIG.(5-1)

AXIAL STIFFNESSES OF CURVED STRUTS

COMPARISON BETWEEN THEORIES OF LARGE & SMALL DEFORMATIONS

—— LARGE DEFORMATION THEORY

---- SMALL DEFORMATION THEORY

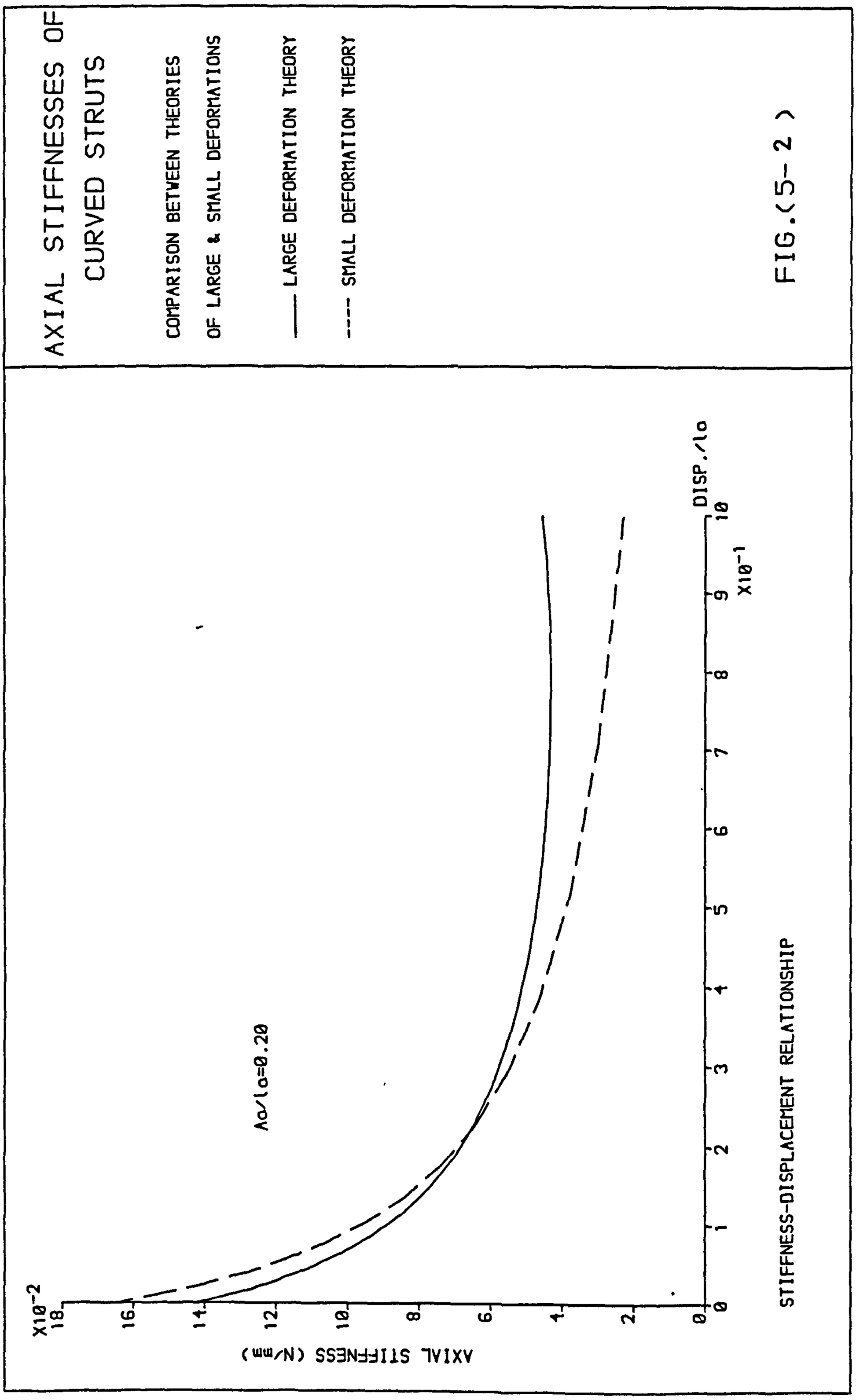

FIG.(5-2)

AXIAL STIFFNESSES OF STRUT

CHORD LENGTH(Lo) =310.0 (mm)

INITIAL RISE(Ao) = 10.0 (mm)

COMPARISON BETWEEN THEORETICAL AND EXPERIMENTAL STIFFNESSES

S :SWANNELL CURVE

Le:ECCENTRIC LOADING CURVE:C=24

Lo:AXIAL LOADING CURVE :C=0.

Δ_y:DISPLACEMENT AT YIELD

Δ_p:DISP. AT FULL PLASTICITY

* EXPERIMENTAL VALUES

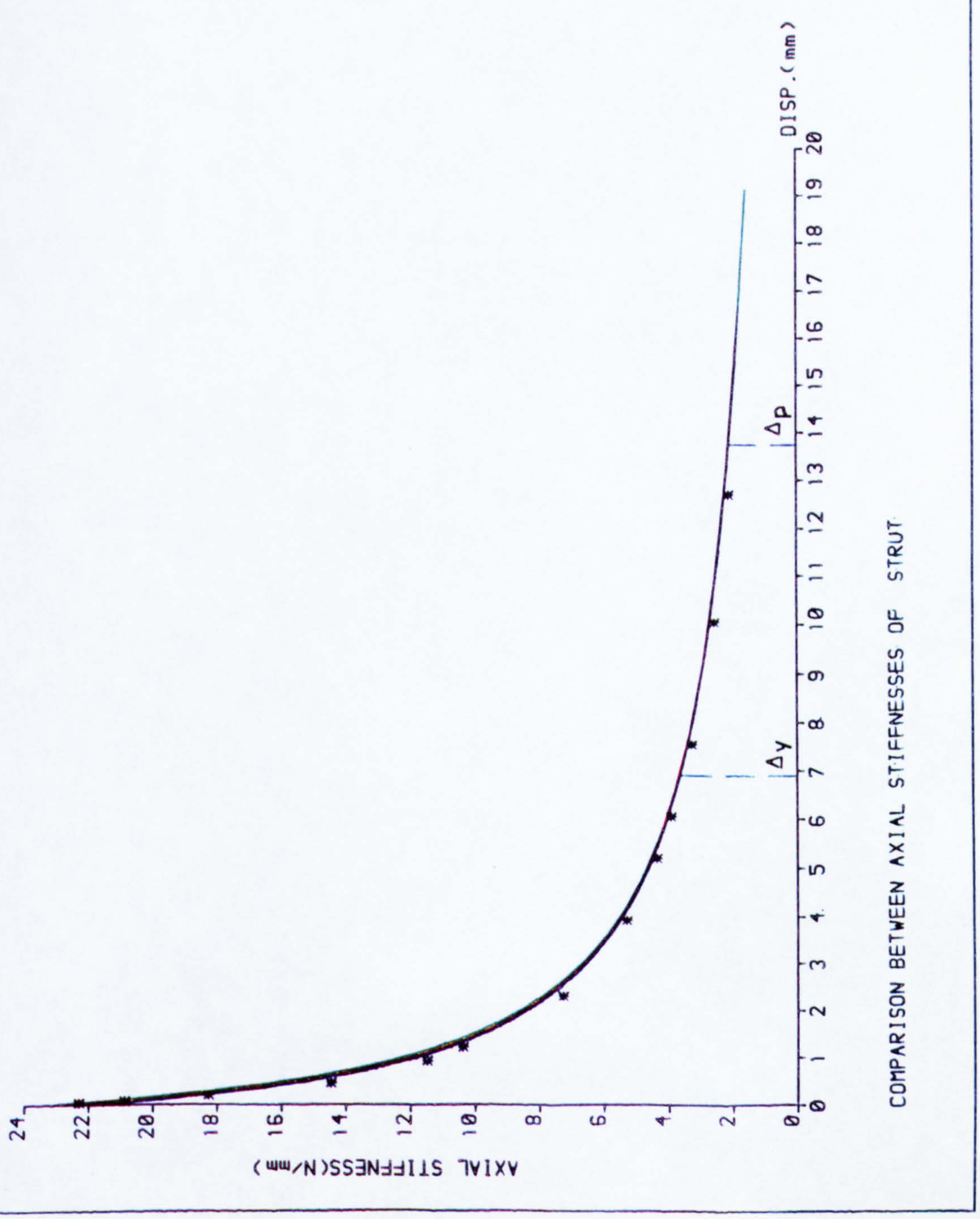

FIG (5- 4)

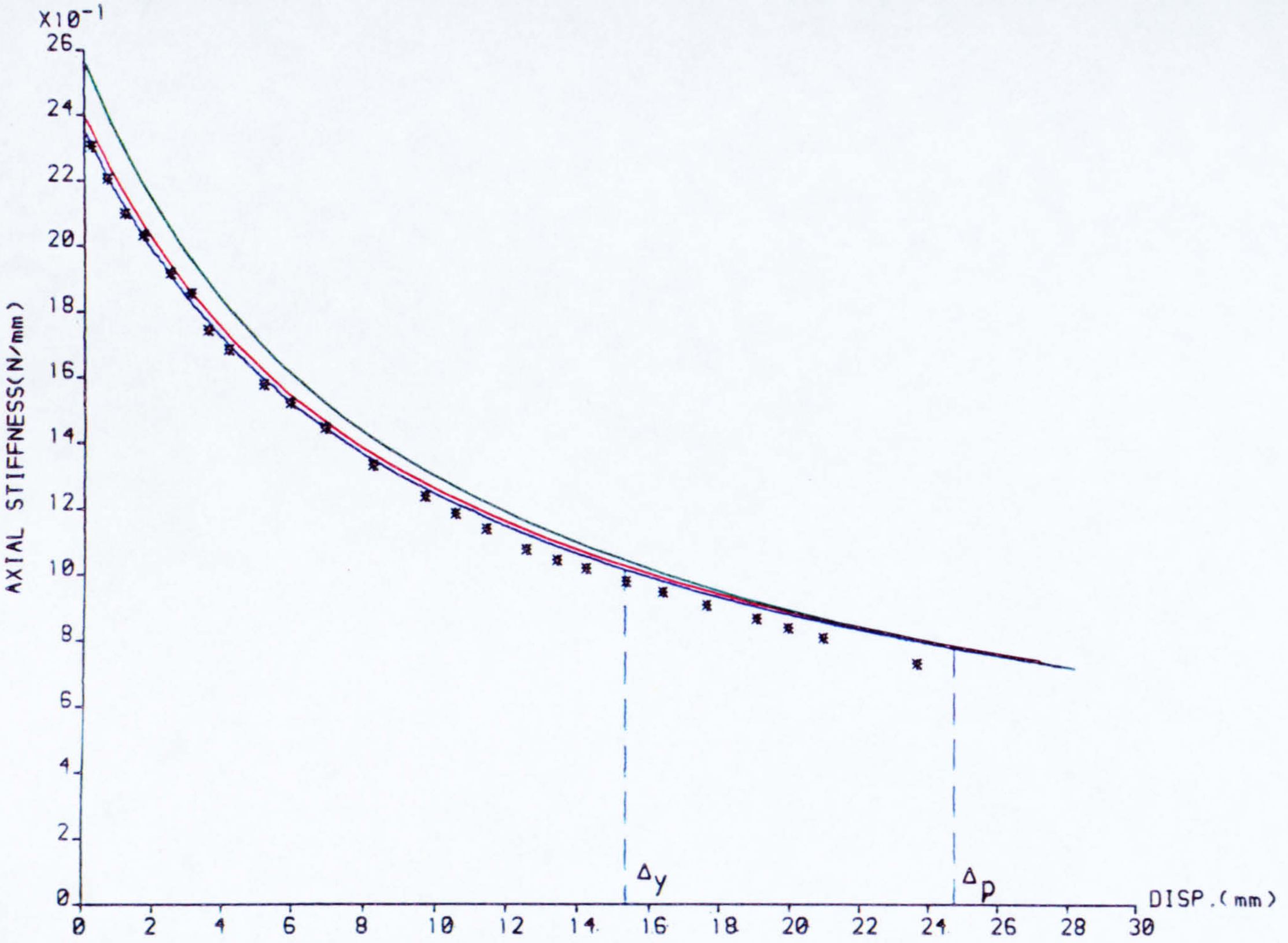

COMPARISON BETWEEN AXIAL STIFFNESSES OF STRUT

AXIAL STIFFNESSES OF STRUT

CHORD LENGTH(Lo) =310.0 (mm)

INITIAL RISE(Ao) = 30.0 (mm)

COMPARISON BETWEEN THEORETICAL AND EXPERIMENTAL STIFFNESSES

S :SWANNELL CURVE

Le:ECCENTRIC LOADING CURVE:C=24

La:AXIAL LOADING CURVE :C=0.

Δ y:DISPLACEMENT AT YIELD

Δ p:DISP. AT FULL PLASTICITY

* EXPERIMENTAL VALUES

FIG (5- 5)

AXIAL STIFFNESSES OF STRUT

CHORD LENGTH(Lo) =310.0 (mm)
INITIAL RISE(Ao) = 50.0 (mm)

COMPARISON BETWEEN THEORETICAL AND EXPERIMENTAL STIFFNESSES

S :SWANNELL CURVE
Le:ECCENTRIC LOADING CURVE:C=24
La:AXIAL LOADING CURVE :C=0.
Δ_y:DISPLACEMENT AT YIELD
Δ_p:DISP. AT FULL PLASTICITY
* EXPERIMENTAL VALUES

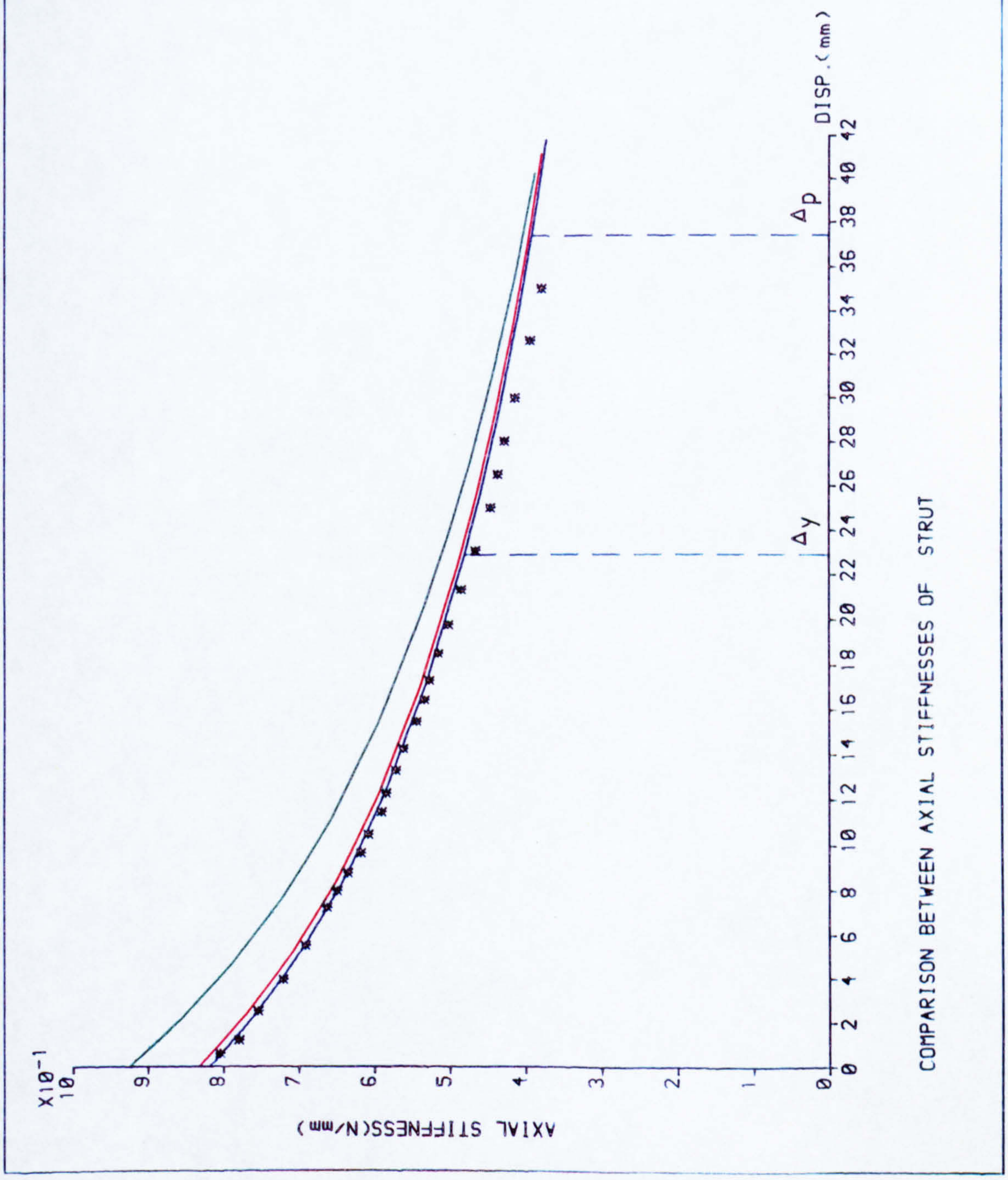

FIG (5- 6)

AXIAL STIFFNESSES OF STRUT

CHORD LENGTH(Lo) =310.0 (mm)

INITIAL RISE(Ao) = 65.0 (mm)

COMPARISON BETWEEN THEORETICAL AND EXPERIMENTAL STIFFNESSES

S :SWANNELL CURVE

Le:ECCENTRIC LOADING CURVE:C=24

Lo:AXIAL LOADING CURVE :C=0.

Δ_y:DISPLACEMENT AT YIELD

Δ_p:DISP. AT FULL PLASTICITY

* EXPERIMENTAL VALUES

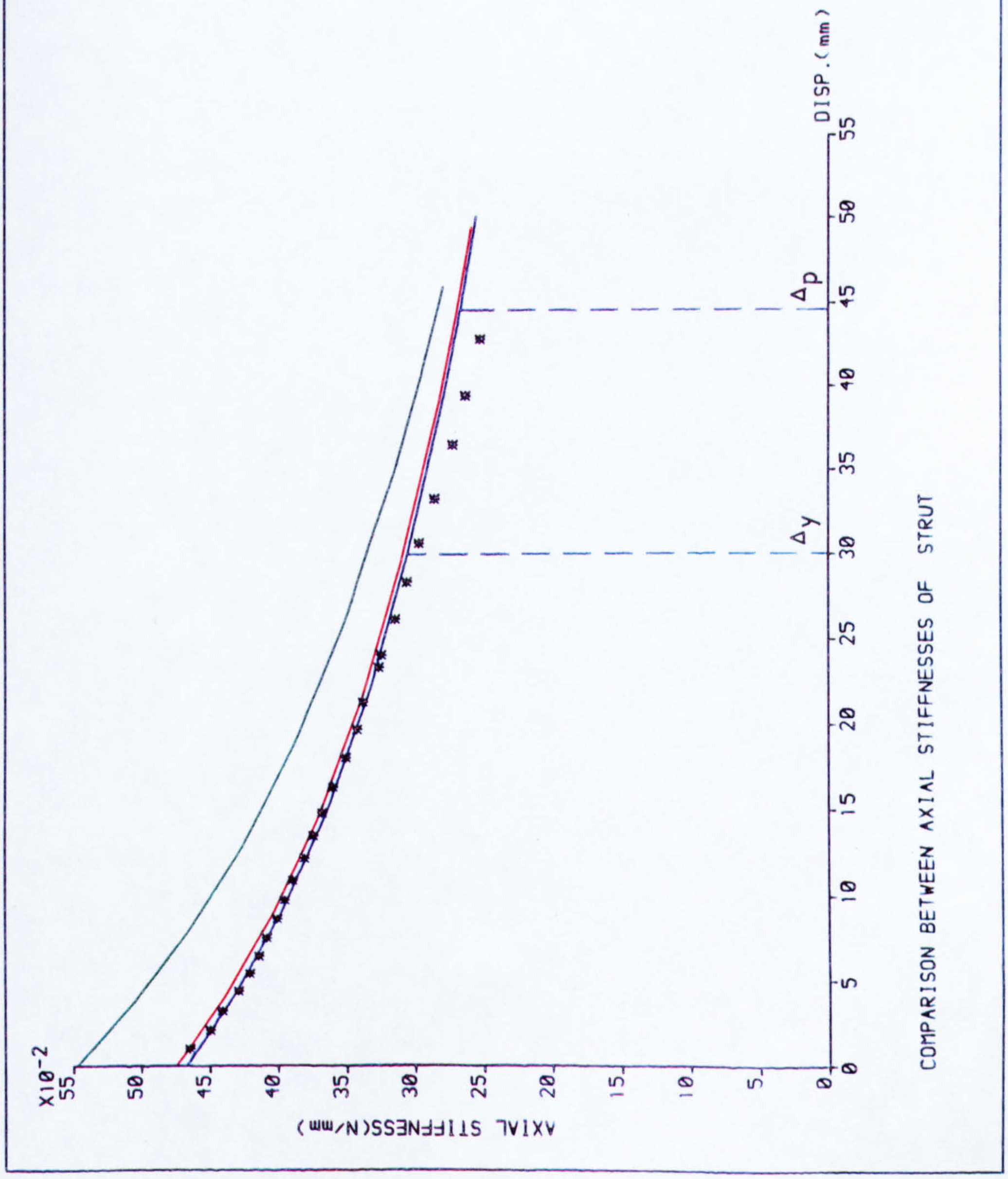

FIG (5- 7)

AXIAL STIFFNESSES
OF STRUT

CHORD LENGTH(Lo) =450.0 (mm)
INITIAL RISE(Ao) = 10.0 (mm)

COMPARISON BETWEEN THEORETICAL
AND EXPERIMENTAL STIFFNESSES

S :SWANNELL CURVE
Le:ECCENTRIC LOADING CURVE:C=24
La:AXIAL LOADING CURVE :C=0.
Δ y:DISPLACEMENT AT YIELD
Δ p:DISP. AT FULL PLASTICITY
* EXPERIMENTAL VALUES

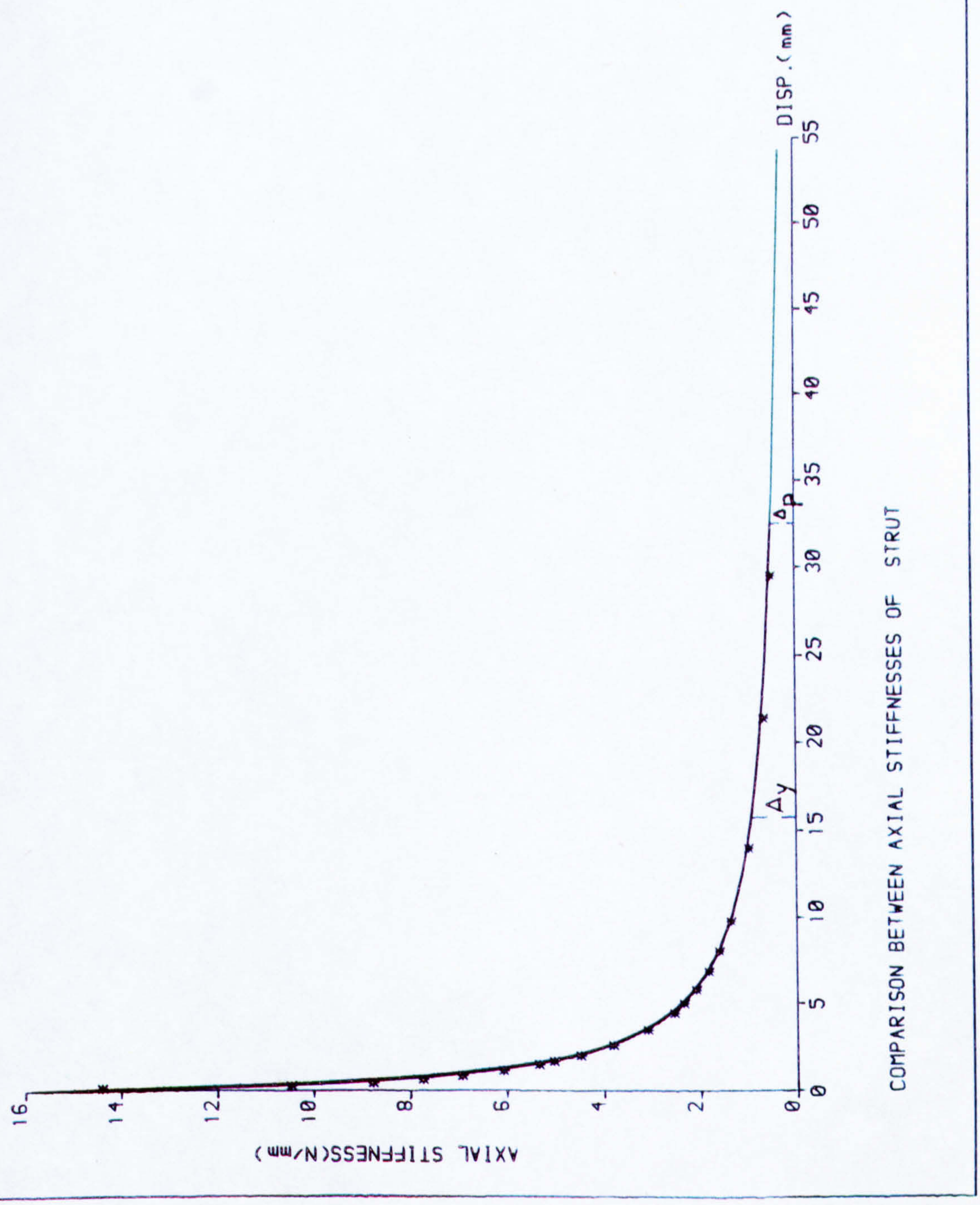

FIG (5-8)

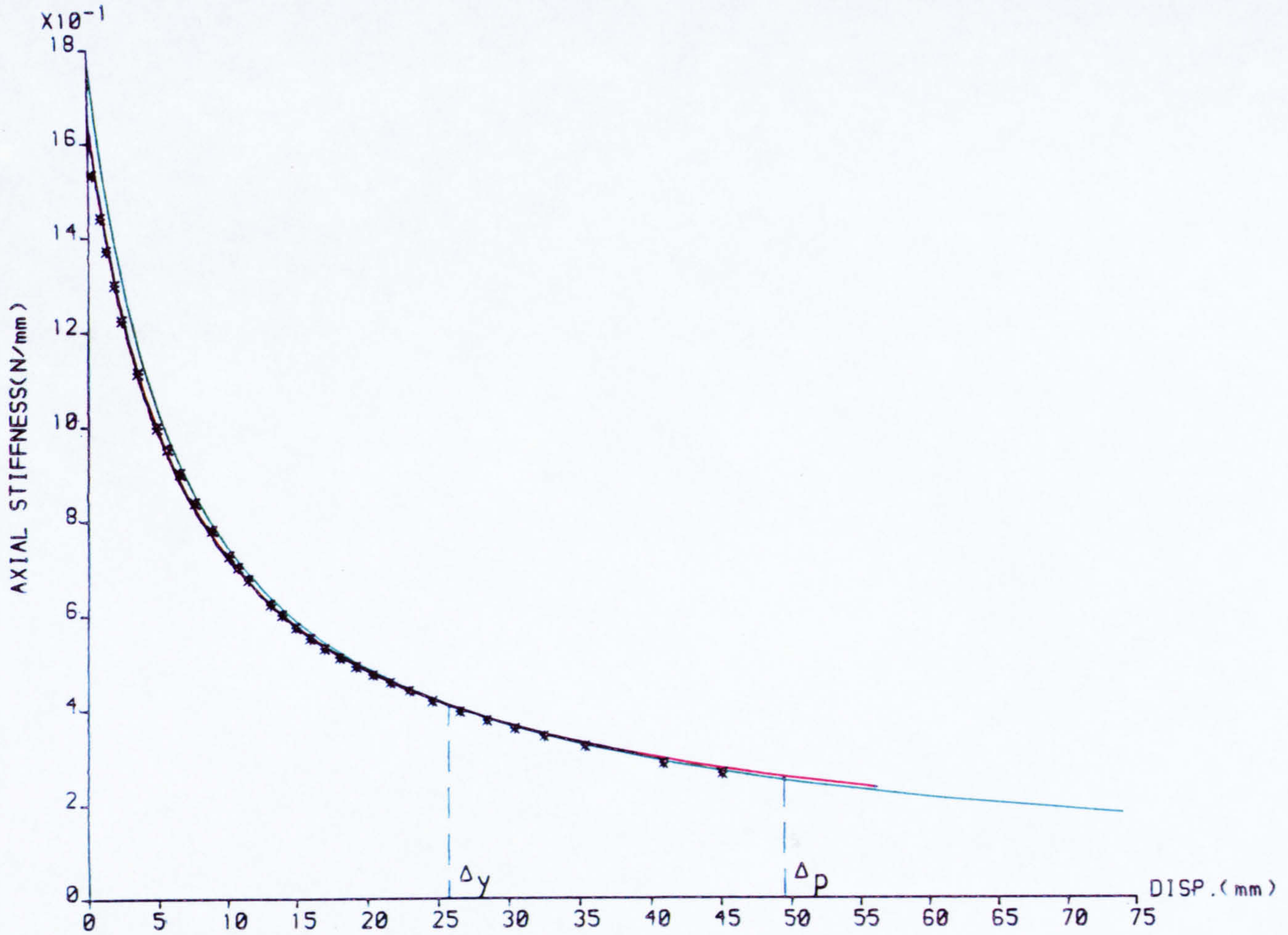

COMPARISON BETWEEN AXIAL STIFFNESSES OF STRUT

AXIAL STIFFNESSES OF STRUT

CHORD LENGTH(Lo.) =450.0 (mm)

INITIAL RISE(Ao) = 30.0 (mm)

COMPARISON BETWEEN THEORETICAL AND EXPERIMENTAL STIFFNESSES

S :SWANNELL CURVE

Le:ECCENTRIC LOADING CURVE:C=24

La:AXIAL LOADING CURVE :C=0.

Δ_y:DISPLACEMENT AT YIELD

Δ_p:DISP. AT FULL PLASTICITY

* EXPERIMENTAL VALUES

FIG (5- 9)

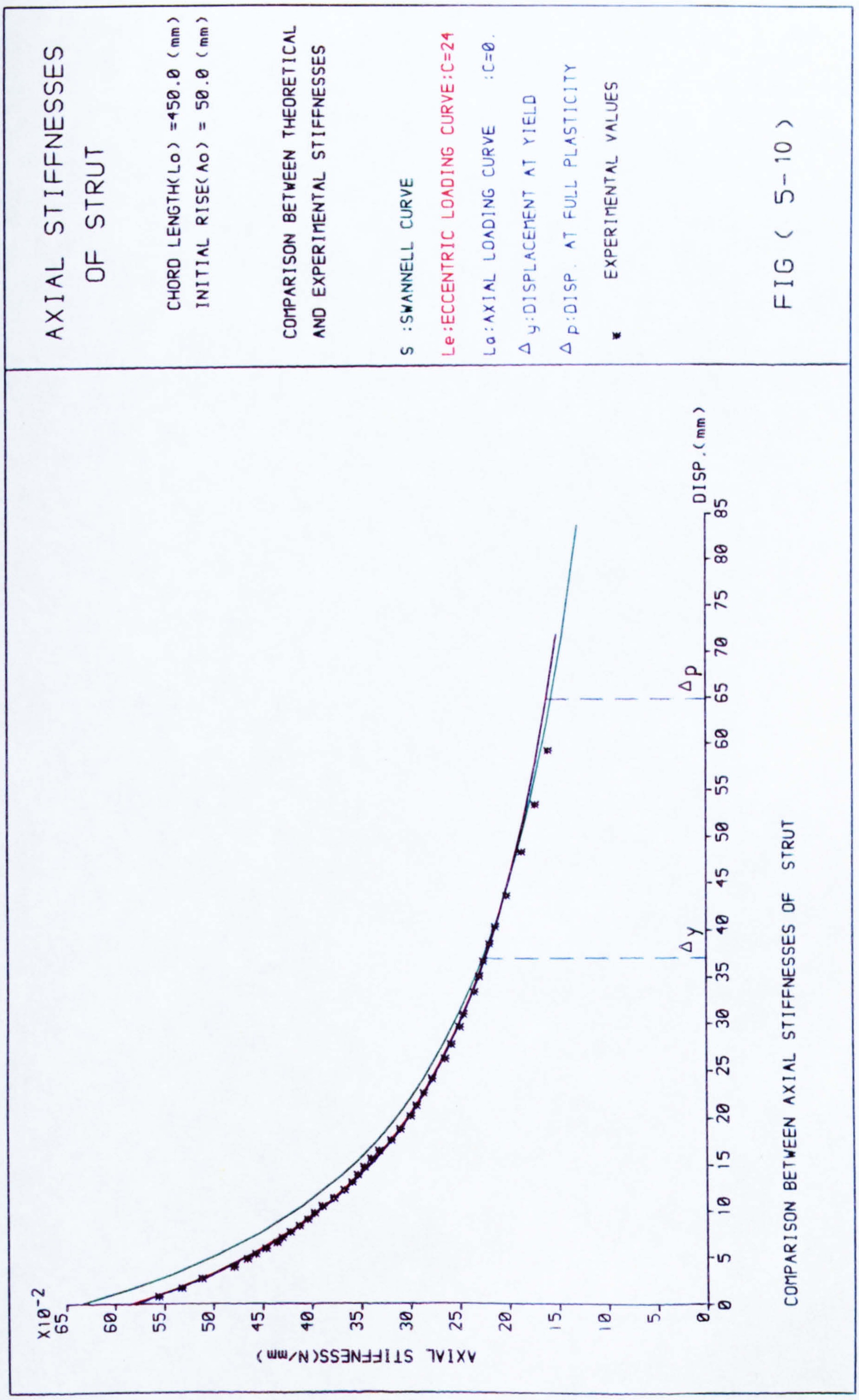
AXIAL STIFFNESSES
OF STRUT
CHORD LENGTH(Lo) =450.0 (mm)
INITIAL RISE(Ao) = 50.0 (mm)
COMPARISON BETWEEN THEORETICAL
AND EXPERIMENTAL STIFFNESSES
S :SWANNELL CURVE
Le:ECCENTRIC LOADING CURVE:C=24
La:AXIAL LOADING CURVE :C=0.
Δ y:DISPLACEMENT AT YIELD
Δ p:DISP. AT FULL PLASTICITY
EXPERIMENTAL VALUES
DISP.(mm)
Δp
Δy
AXIAL STIFFNESS(N/mm)
X10-2
COMPARISON BETWEEN AXIAL STIFFNESSES OF STRUT

FIG (5-10)

AXIAL STIFFNESSES OF STRUT

CHORD LENGTH(Lo) =450.0 (mm)
INITIAL RISE(Ao) = 65.0 (mm)

COMPARISON BETWEEN THEORETICAL AND EXPERIMENTAL STIFFNESSES

S :SWANNELL CURVE
Le:ECCENTRIC LOADING CURVE:C=24
La:AXIAL LOADING CURVE :C=0.
Δ y:DISPLACEMENT AT YIELD
Δ p:DISP. AT FULL PLASTICITY
* EXPERIMENTAL VALUES

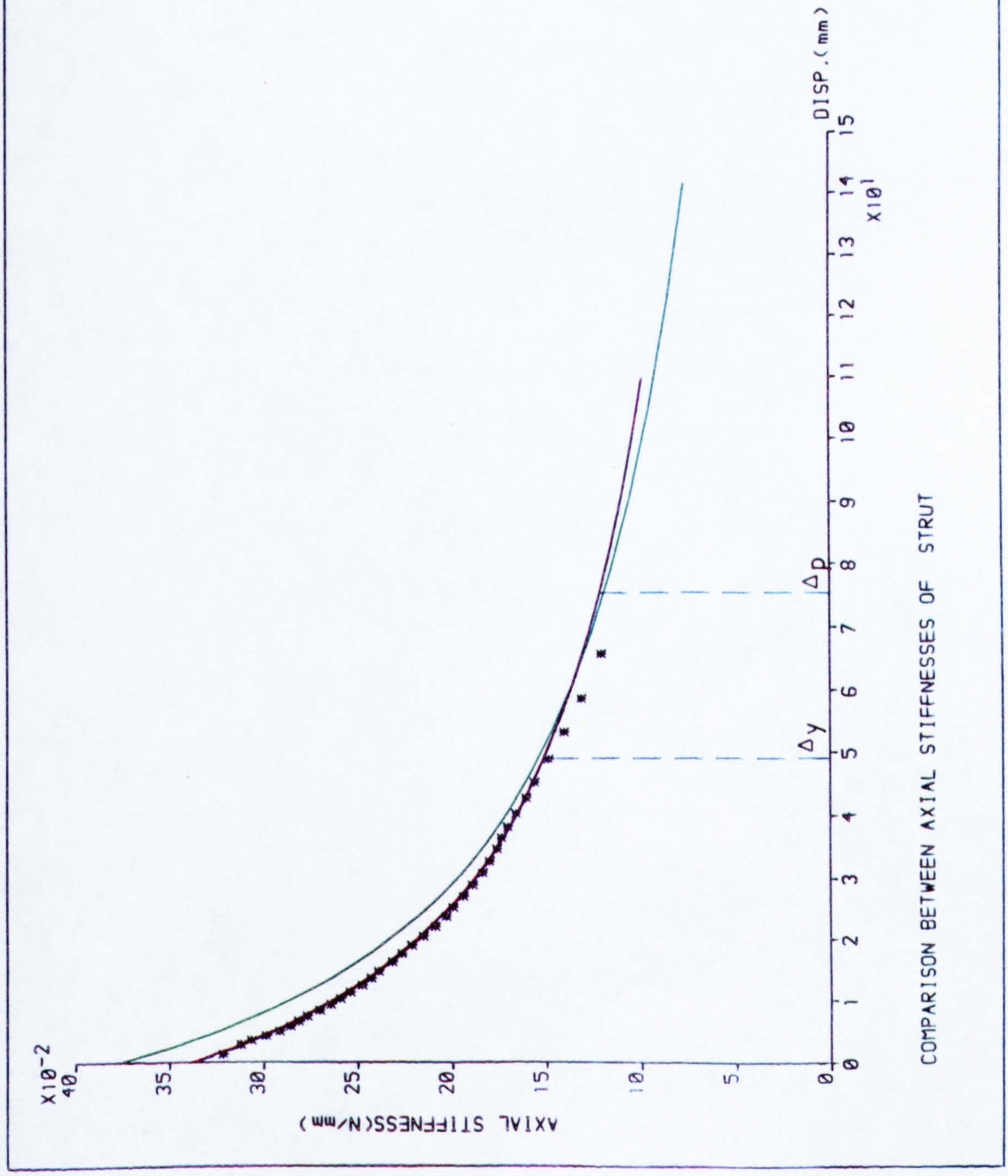

FIG (5-11)

AXIAL STIFFNESSES OF STRUT

CHORD LENGTH(Lo) =520.0 (mm)
INITIAL RISE(Ao) = 20.0 (mm)

COMPARISON BETWEEN THEORETICAL AND EXPERIMENTAL STIFFNESSES

S :SWANNELL CURVE
-e:ECCENTRIC LOADING CURVE:C=24
Lo:AXIAL LOADING CURVE :C=0.
Δ y:DISPLACEMENT AT YIELD
Δ p:DISP. AT FULL PLASTICITY
* EXPERIMENTAL VALUES

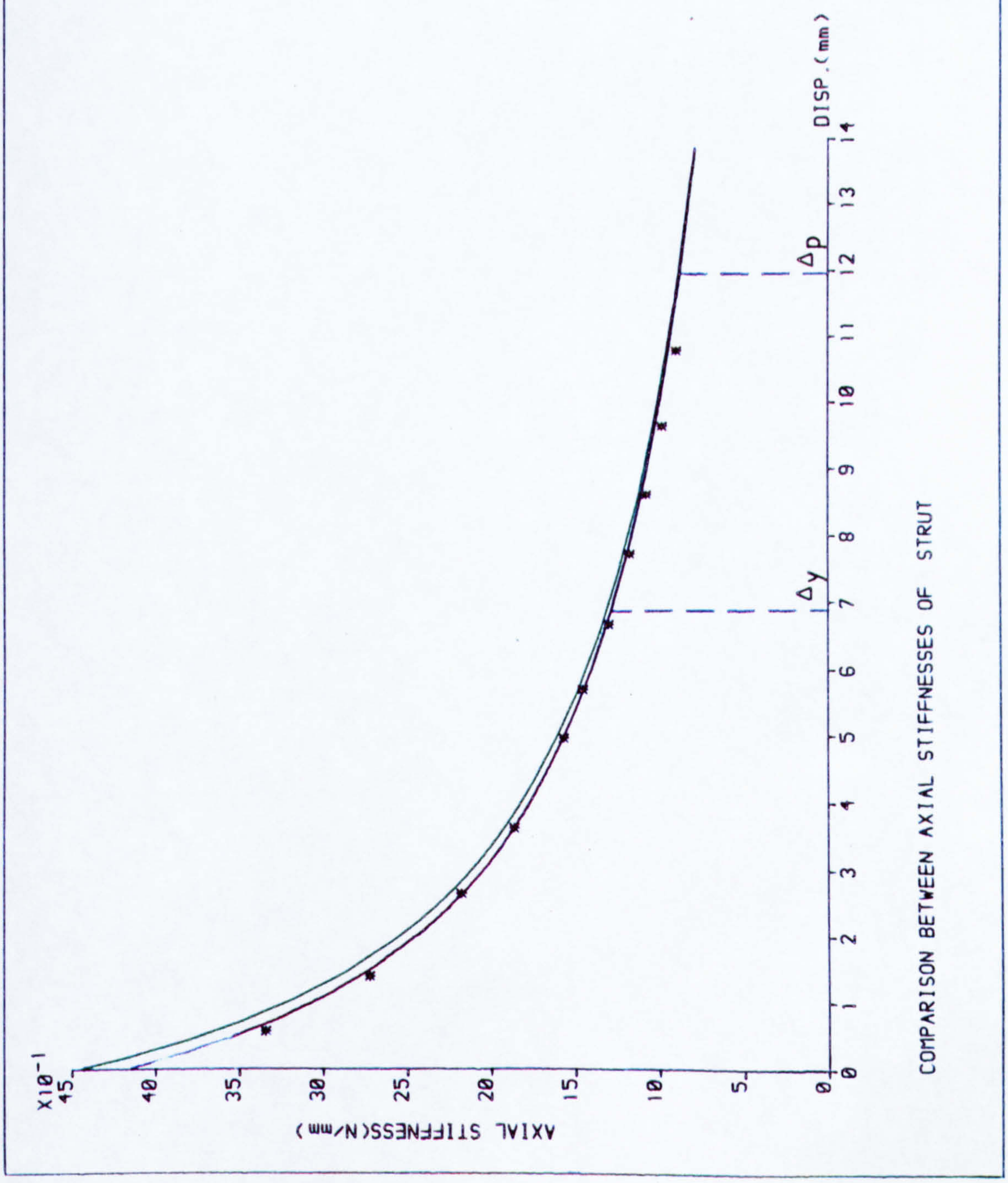

FIG (5-12)

AXIAL STIFFNESSES OF STRUT

CHORD LENGTH(Lo) =520.0 (mm)
INITIAL RISE(Ao) = 30.0 (mm)

COMPARISON BETWEEN THEORETICAL AND EXPERIMENTAL STIFFNESSES

S :SWANNELL CURVE
Le:ECCENTRIC LOADING CURVE:C=24
La:AXIAL LOADING CURVE :C=0.
Δ_y:DISPLACEMENT AT YIELD
Δ_p:DISP. AT FULL PLASTICITY
* EXPERIMENTAL VALUES

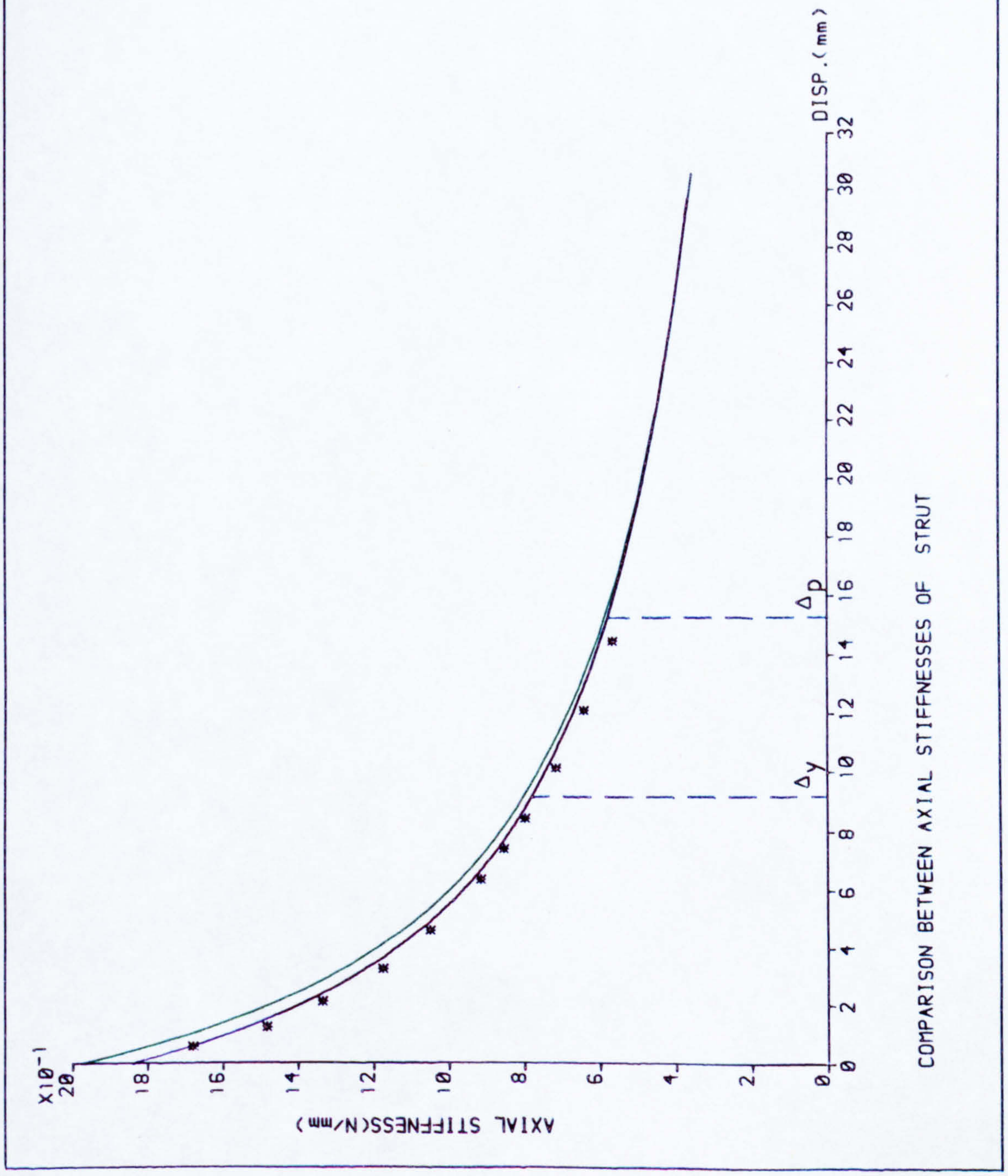

FIG (5-13)

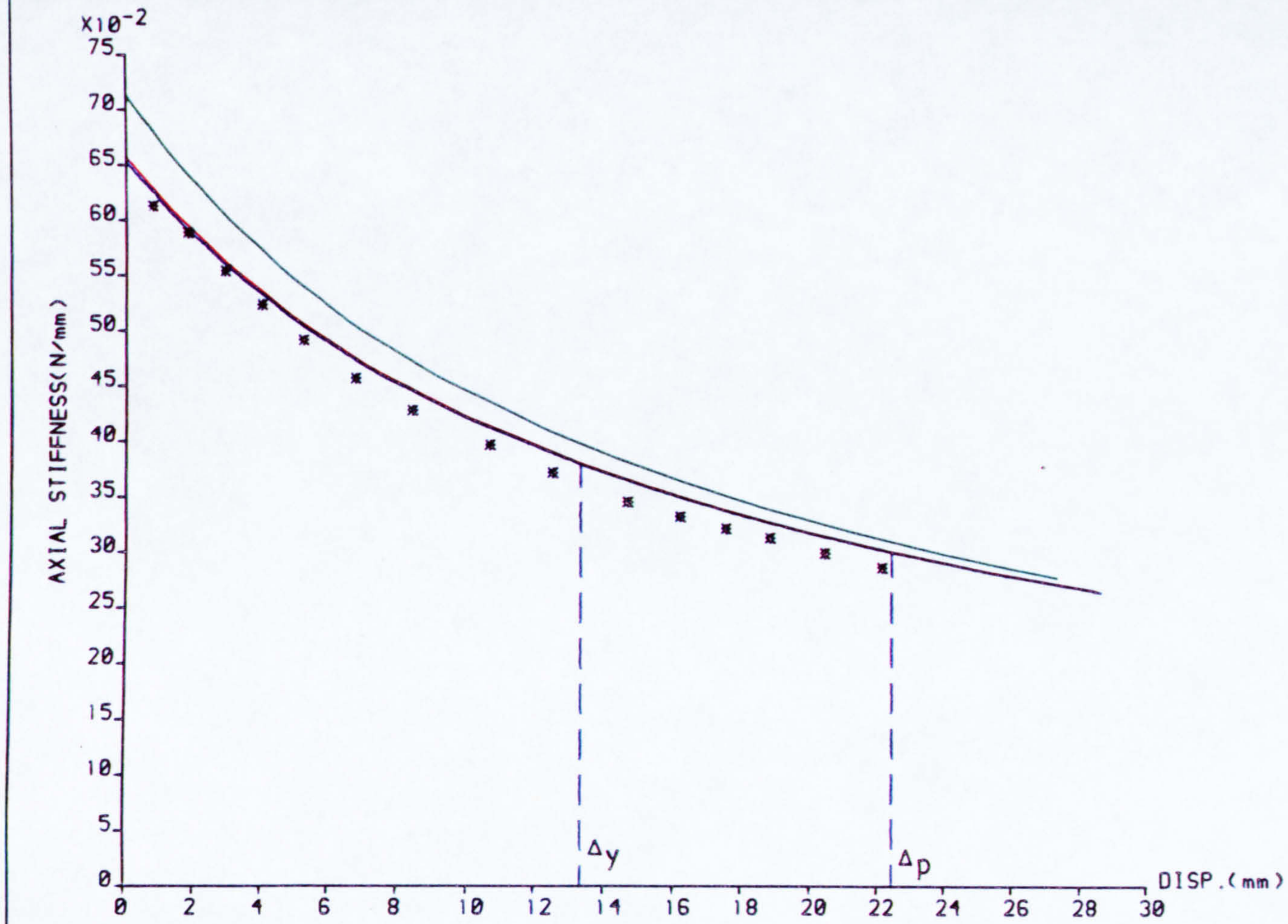

COMPARISON BETWEEN AXIAL STIFFNESSES OF STRUT

AXIAL STIFFNESSES OF STRUT

CHORD LENGTH(Lo) =520.0 (mm)

INITIAL RISE(Ao) = 50.0 (mm)

COMPARISON BETWEEN THEORETICAL AND EXPERIMENTAL STIFFNESSES

S :SWANNELL CURVE

Le:ECCENTRIC LOADING CURVE:C=24

La:AXIAL LOADING CURVE :C=0.

Δ y:DISPLACEMENT AT YIELD

Δ p:DISP. AT FULL PLASTICITY

* EXPERIMENTAL VALUES

FIG (5-14)

AXIAL STIFFNESSES
OF STRUT

CHORD LENGTH(Lo) =520.0 (mm)
INITIAL RISE(Ao) = 65.0 (mm)

COMPARISON BETWEEN THEORETICAL
AND EXPERIMENTAL STIFFNESSES

S :SWANNELL CURVE

-e:ECCENTRIC LOADING CURVE:C=24

La:AXIAL LOADING CURVE :C=0.

Δ_y:DISPLACEMENT AT YIELD

Δ_p:DISP. AT FULL PLASTICITY

* EXPERIMENTAL VALUES

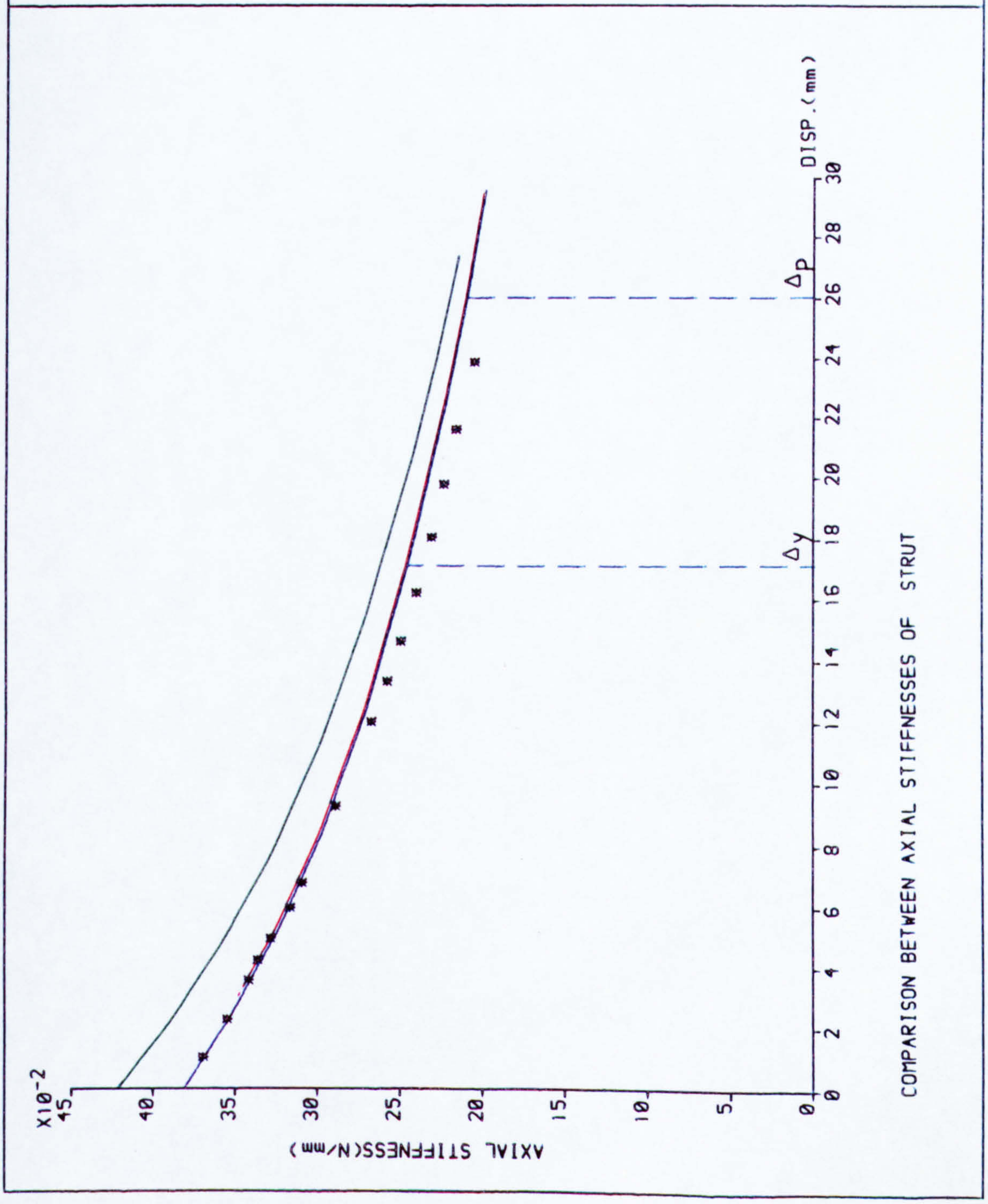

FIG (5-15)

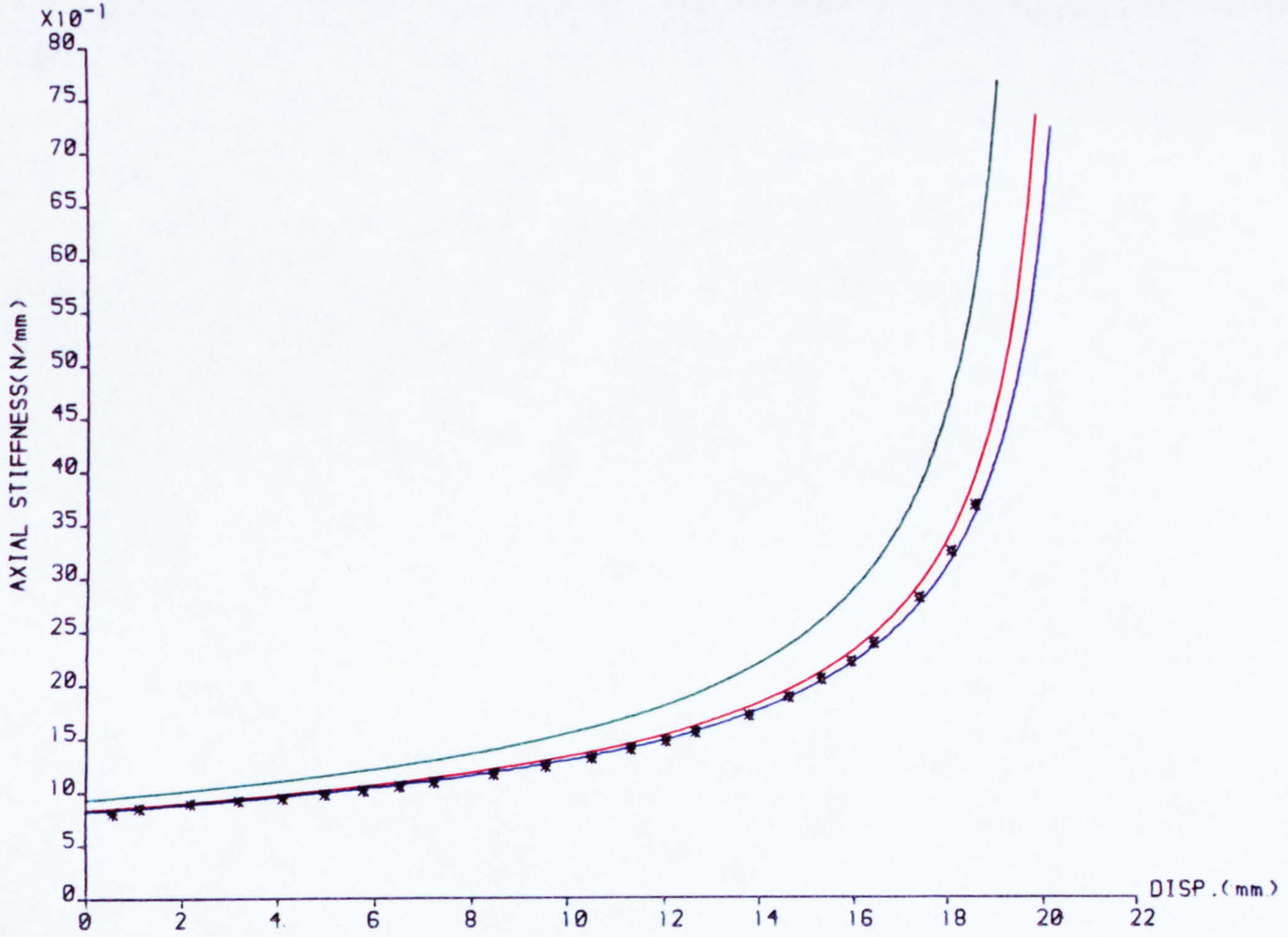

COMPARISON BETWEEN AXIAL STIFFNESSES OF TIE

AXIAL STIFFNESSES OF TIE

CHORD LENGTH(Lo) =310.0 (mm)

INITIAL RISE(Ao) = 50.0 (mm)

COMPARISON BETWEEN THEORETICAL AND EXPERIMENTAL STIFFNESSES

S :SWANNELL CURVE

Le:ECCENTRIC LOADING CURVE:C=24

La:AXIAL LOADING CURVE :C=0.

* EXPERIMENTAL VALUES

FIG (5-16)

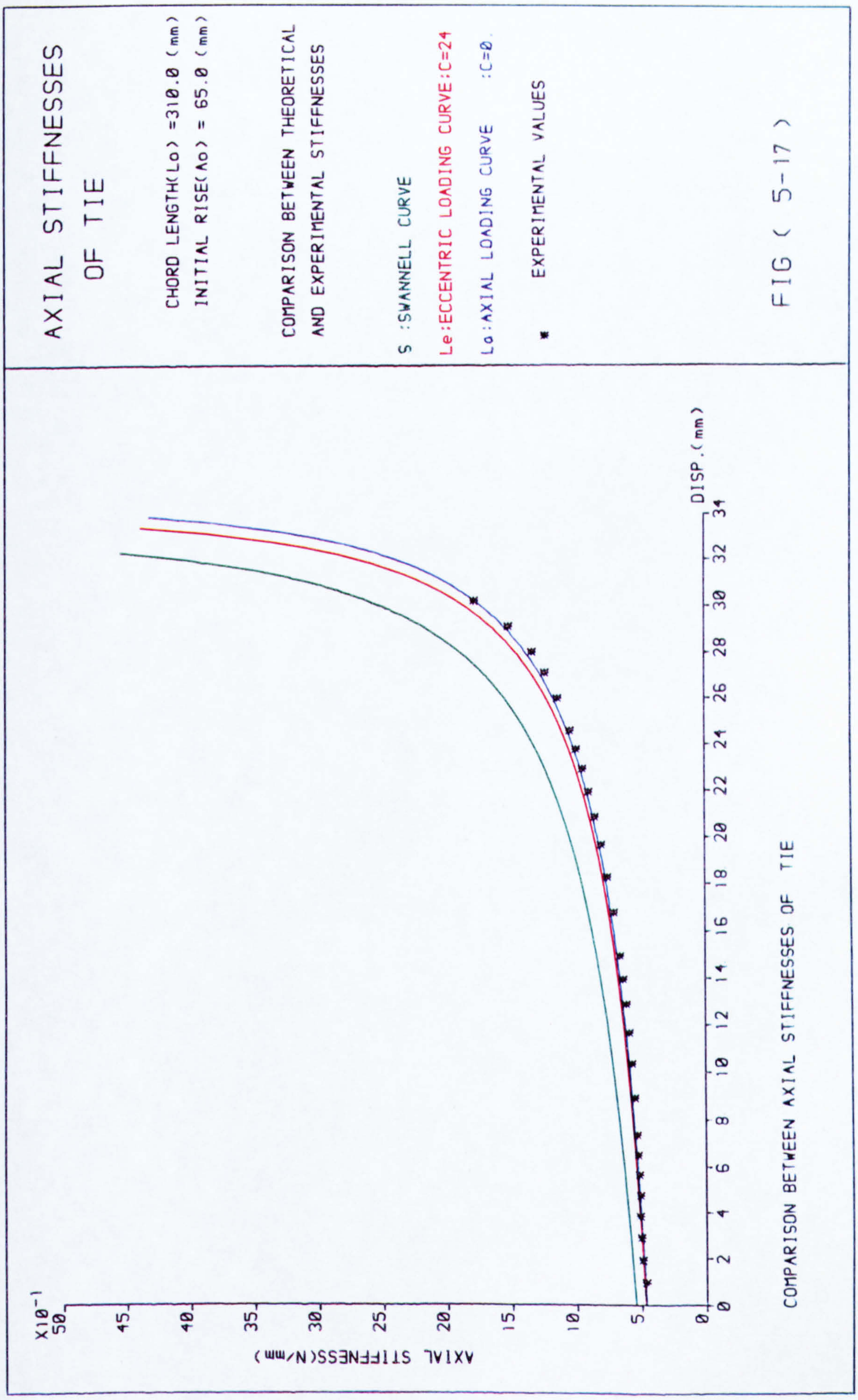
AXIAL STIFFNESSES
OF TIE
CHORD LENGTH(Lo) =310.0 (mm)
INITIAL RISE(Ao) = 65.0 (mm)
COMPARISON BETWEEN THEORETICAL
AND EXPERIMENTAL STIFFNESSES
S :SWANNELL CURVE
Le:ECCENTRIC LOADING CURVE:C=24
Lo:AXIAL LOADING CURVE :C=0.
* EXPERIMENTAL VALUES
DISP.(mm)
0 2 4 6 8 10 12 14 16 18 20 22 24 26 28 30 32 34
AXIAL STIFFNESS(N/mm)
X10⁻¹
0 5 10 15 20 25 30 35 40 45 50
COMPARISON BETWEEN AXIAL STIFFNESSES OF TIE

FIG (5-17)

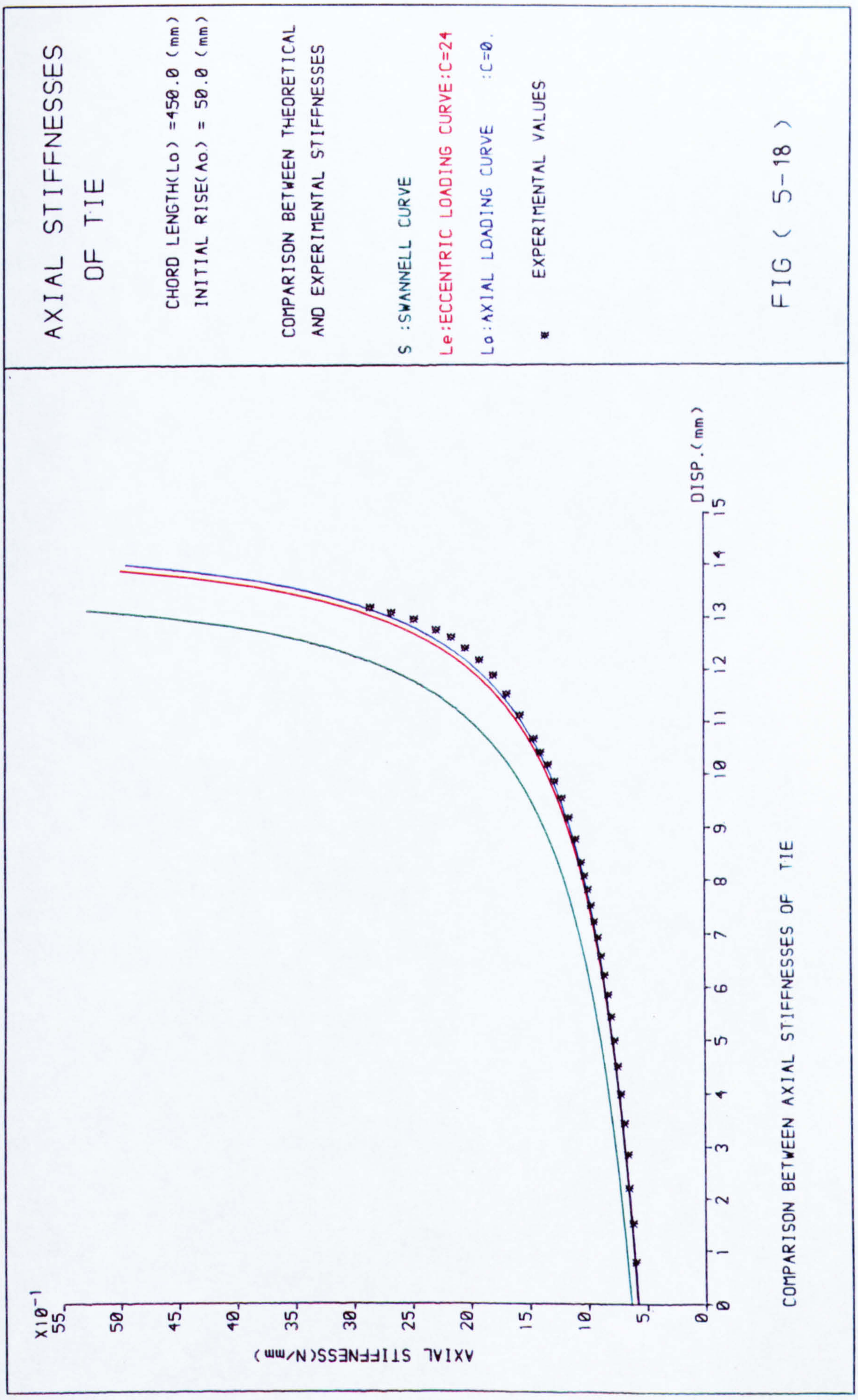
AXIAL STIFFNESSES
OF TIE
CHORD LENGTH(Lo) =450.0 (mm)
INITIAL RISE(Ao) = 50.0 (mm)
COMPARISON BETWEEN THEORETICAL
AND EXPERIMENTAL STIFFNESSES
S :SWANNELL CURVE
Le:ECCENTRIC LOADING CURVE:C=24
Lo:AXIAL LOADING CURVE :C=0.
* EXPERIMENTAL VALUES
DISP.(mm)
0 1 2 3 4 5 6 7 8 9 10 11 12 13 14 15
AXIAL STIFFNESS(N/mm)
X10⁻¹
0 5 10 15 20 25 30 35 40 45 50 55
COMPARISON BETWEEN AXIAL STIFFNESSES OF TIE

FIG (5-18)

AXIAL STIFFNESSES OF TIE

CHORD LENGTH(Lo) =450.0 (mm)
INITIAL RISE(Ao) = 65.0 (mm)

COMPARISON BETWEEN THEORETICAL AND EXPERIMENTAL STIFFNESSES

S :SWANNELL CURVE
Le:ECCENTRIC LOADING CURVE:C=24
Lo:AXIAL LOADING CURVE :C=0.
* EXPERIMENTAL VALUES

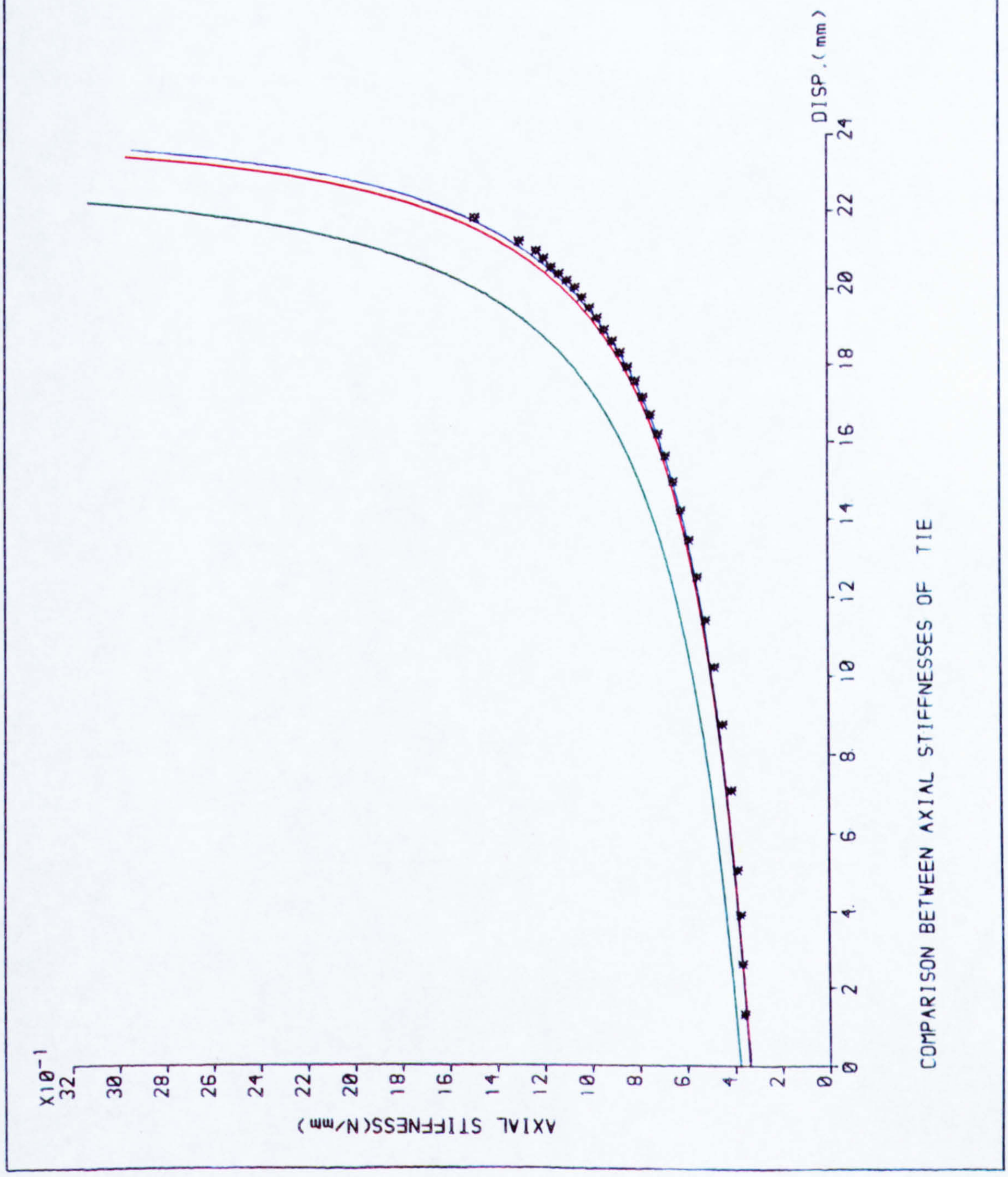

FIG (5-19)

AXIAL STIFFNESSES OF TIE

CHORD LENGTH(Lo) =520.0 (mm)
INITIAL RISE(Ao) = 75.0 (mm)

COMPARISON BETWEEN THEORETICAL AND EXPERIMENTAL STIFFNESSES

S :SWANNELL CURVE
e:ECCENTRIC LOADING CURVE:C=24
La:AXIAL LOADING CURVE :C=0.
* EXPERIMENTAL VALUES

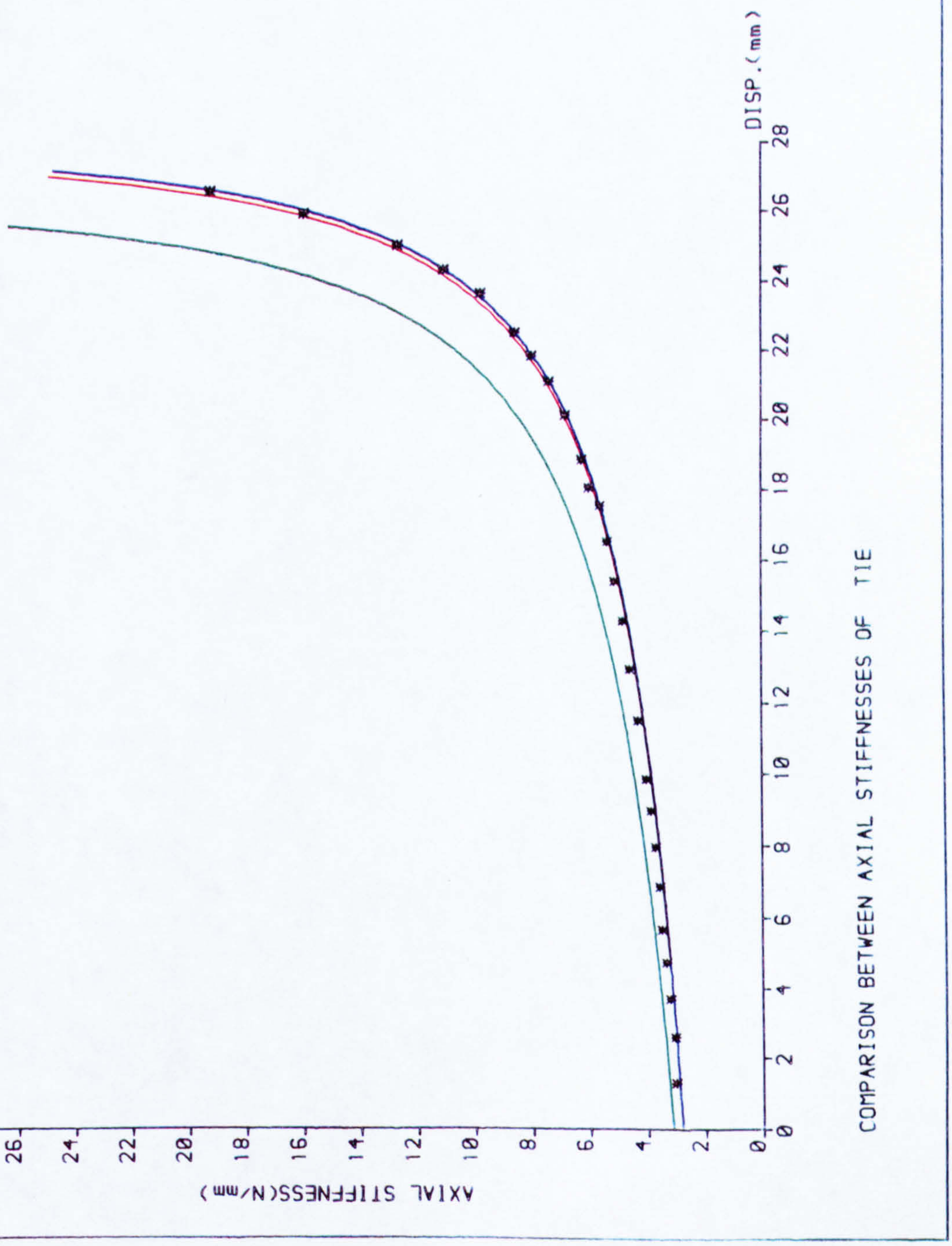

FIG (5-20)

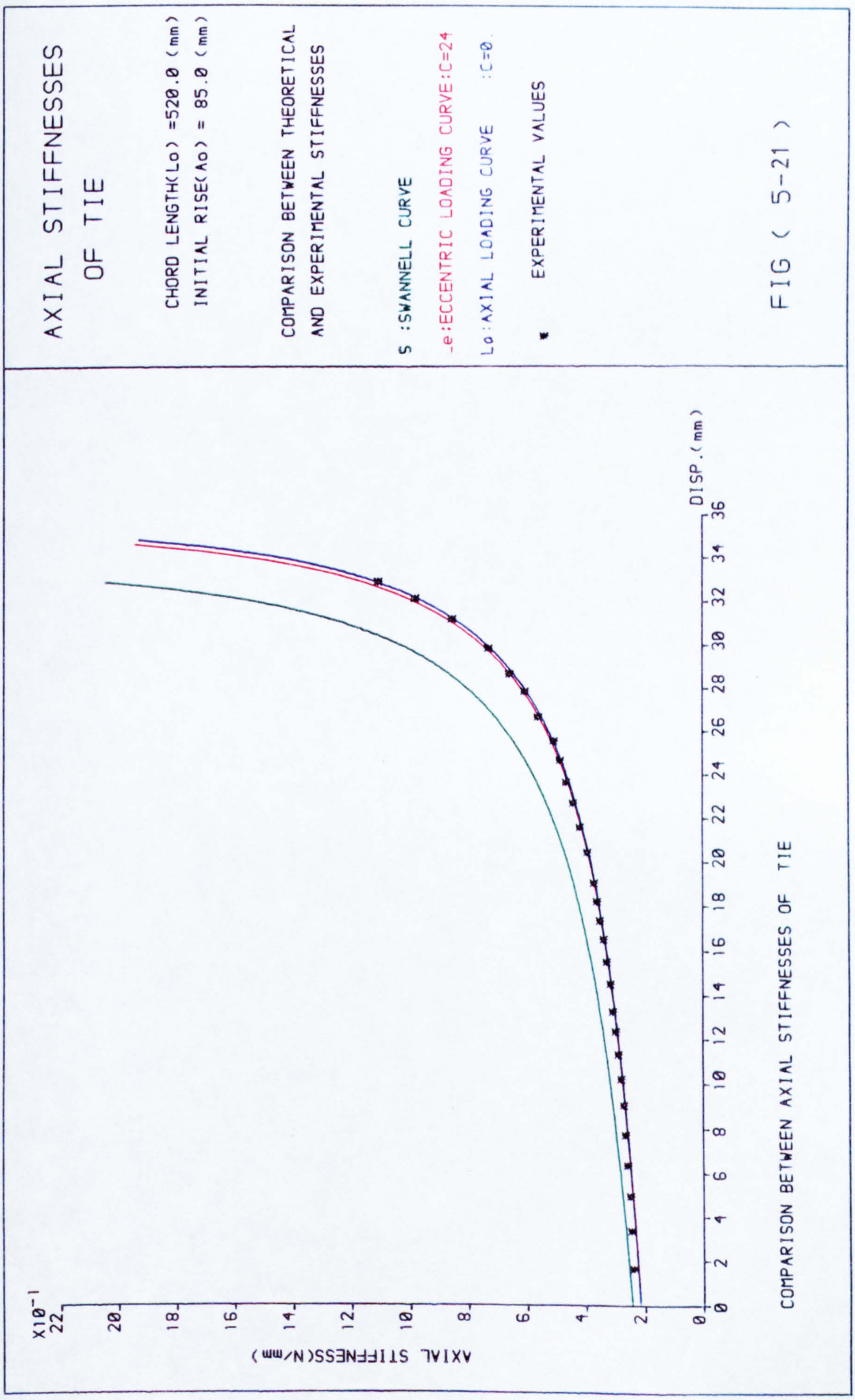
COMPARISON BETWEEN AXIAL STIFFNESSES OF TIE
AXIAL STIFFNESSES
OF TIE
CHORD LENGTH(Lo) =520.0 (mm)
INITIAL RISE(Ao) = 85.0 (mm)
COMPARISON BETWEEN THEORETICAL
AND EXPERIMENTAL STIFFNESSES
S :SWANNELL CURVE
-e:ECCENTRIC LOADING CURVE:C=24
Lo:AXIAL LOADING CURVE :C=0.
EXPERIMENTAL VALUES
AXIAL STIFFNESS(N/mm)
X10⁻¹
DISP.(mm)

FIG (5-21)

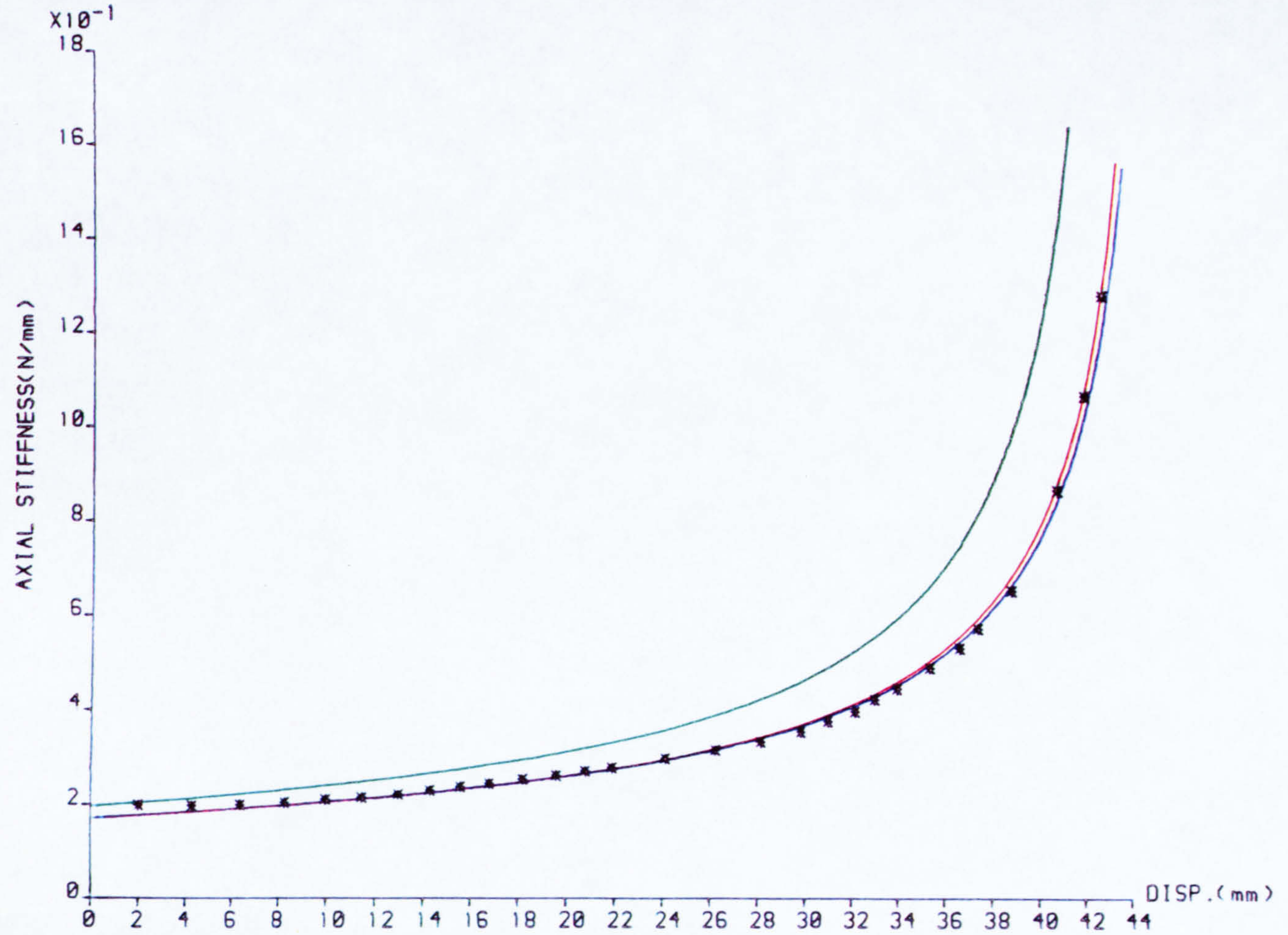

COMPARISON BETWEEN AXIAL STIFFNESSES OF TIE

AXIAL STIFFNESSES OF TIE

CHORD LENGTH(Lo) =520.0 (mm)
INITIAL RISE(Ao) = 95.0 (mm)

COMPARISON BETWEEN THEORETICAL AND EXPERIMENTAL STIFFNESSES

S :SWANNELL CURVE

Le:ECCENTRIC LOADING CURVE:C=24

La:AXIAL LOADING CURVE :C=0.

* EXPERIMENTAL VALUES

FIG (5-22)

AXIAL STIFFNESSES OF TIE

CHORD LENGTH(Lo) =520.0 (mm)
INITIAL RISE(Ao) =105.0 (mm)

COMPARISON BETWEEN THEORETICAL AND EXPERIMENTAL STIFFNESSES

S :SWANNELL CURVE
_e:ECCENTRIC LOADING CURVE:C=24
Lo:AXIAL LOADING CURVE :C=0.
* EXPERIMENTAL VALUES

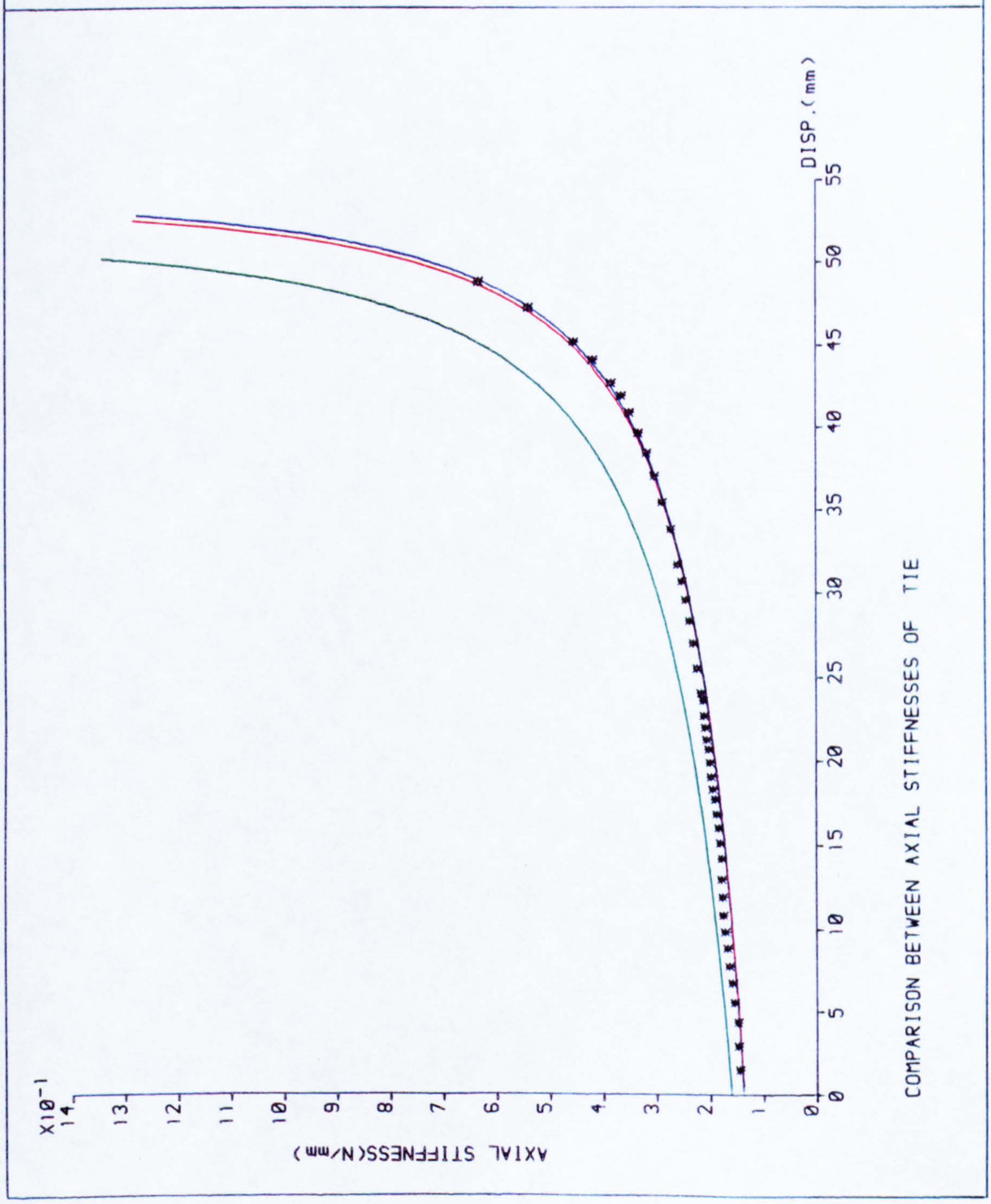

FIG (5-23)

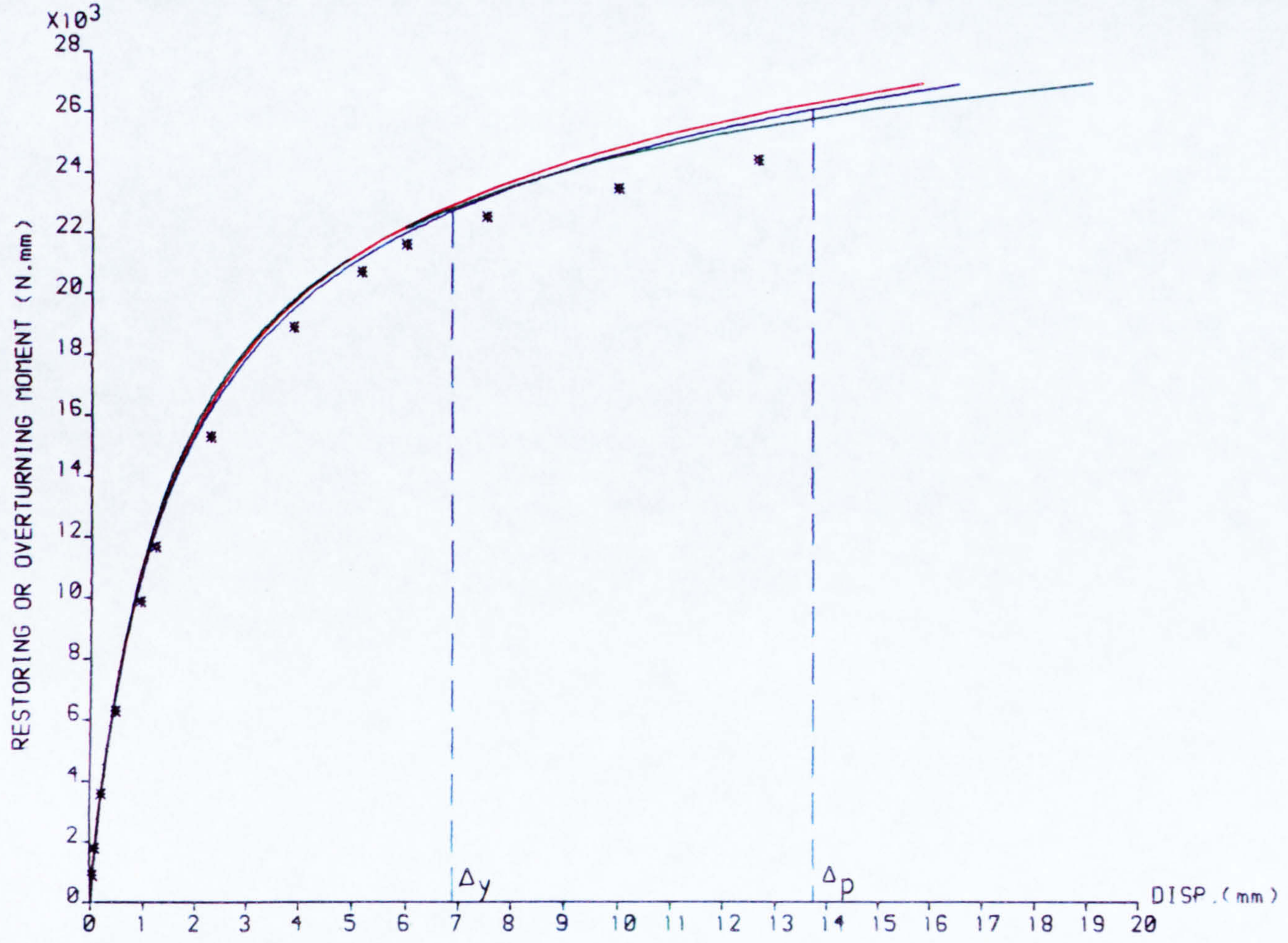

LOAD-DISPLACEMENT RELATIONSHIP

LOAD-DISPLACEMENT RELATIONSHIP OF STRUT

CHORD LENGTH(lo)=310.0 (mm)

INITIAL RISE(Ao)= 10.0 (mm)

COMPARISON BETWEEN THEORETICAL AND EXPERIMENTAL RESULTS

S :SWANNELL CURVE

Le:ECCENTRIC LOADING CURVE:C=24

La:AXIAL LOADING CURVE :C=0.

Δ_y:DISPLACEMENT AT YIELD

Δ_p:DISP. AT FULL PLASTICITY

* EXPERIMENTAL VALUES

FIG (5-24)

LOAD-DISPLACEMENT RELATIONSHIP OF STRUT

CHORD LENGTH(lo)=310.0 (mm)

INITIAL RISE(Ao)= 30.0 (mm)

COMPARISON BETWEEN THEORETICAL AND EXPERIMENTAL RESULTS

S :SWANNELL CURVE

Le:ECCENTRIC LOADING CURVE:C=24

Lo:AXIAL LOADING CURVE :C=0.

Δ_y:DISPLACEMENT AT YIELD

Δ_p:DISP. AT FULL PLASTICITY

* EXPERIMENTAL VALUES

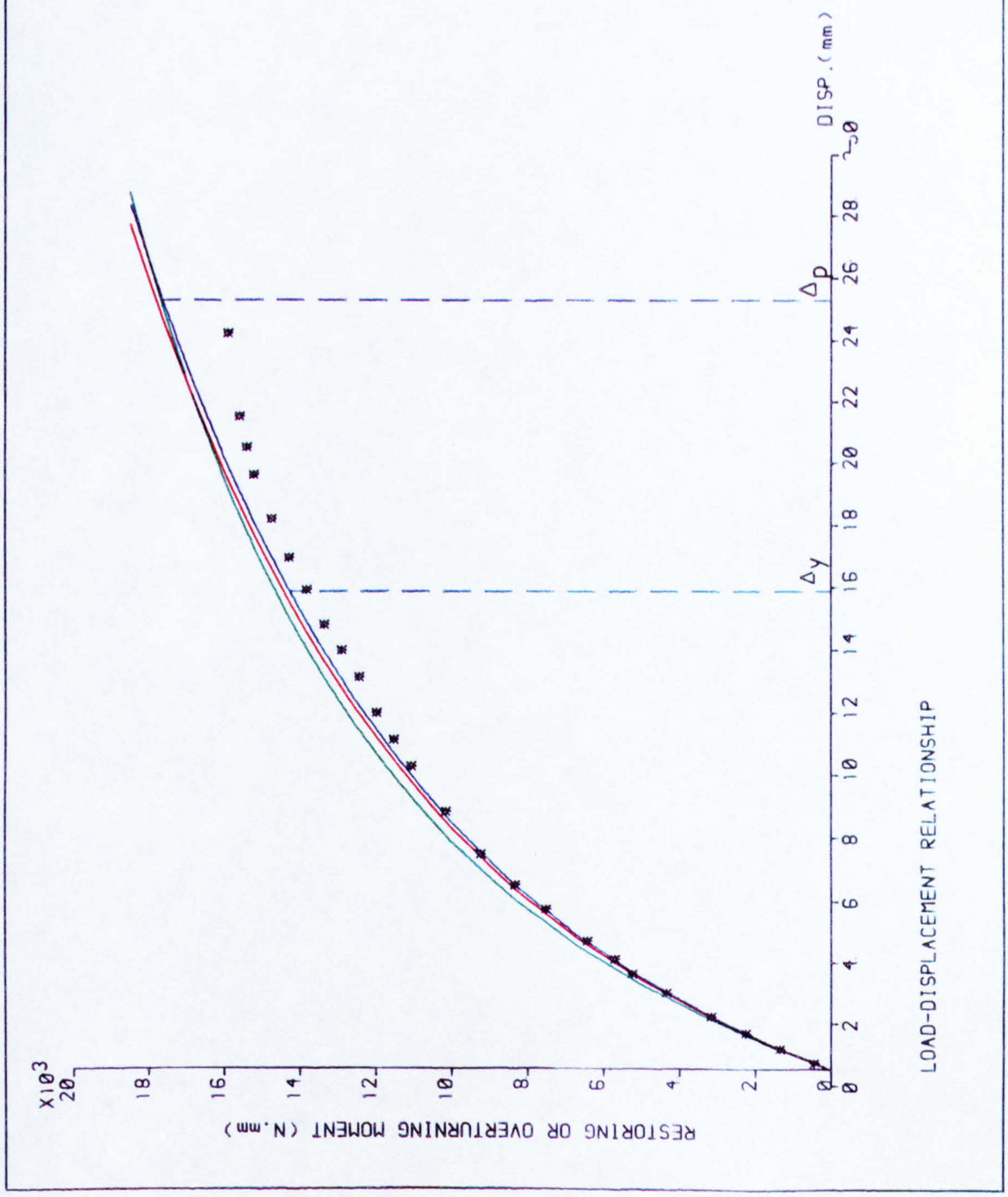

FIG (5-25)

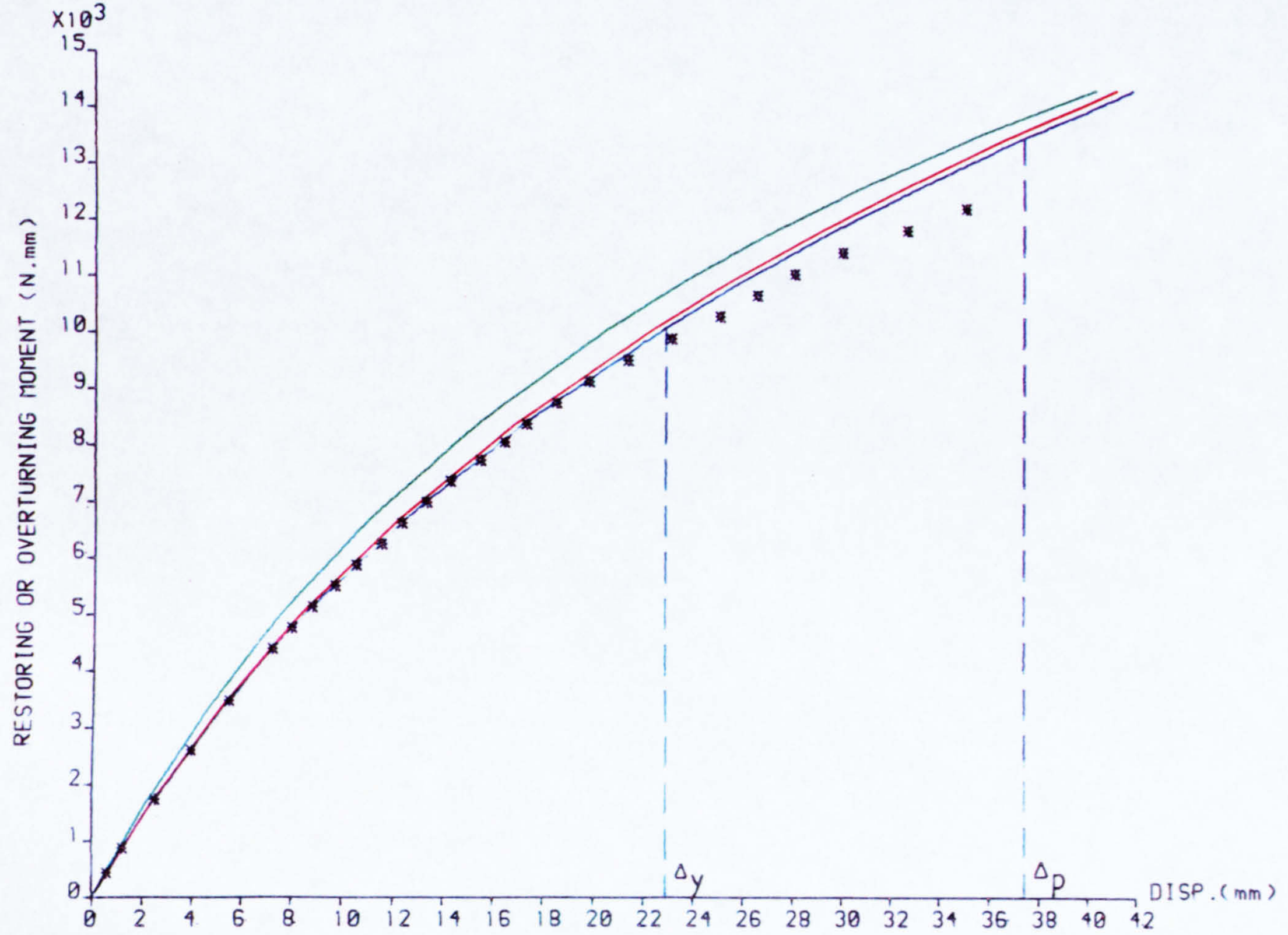

LOAD-DISPLACEMENT RELATIONSHIP

LOAD-DISPLACEMENT RELATIONSHIP OF STRUT

CHORD LENGTH(lo)=310.0 (mm)

INITIAL RISE(Ao)= 50.0 (mm)

COMPARISON BETWEEN THEORETICAL AND EXPERIMENTAL RESULTS

S :SWANNELL CURVE

Le:ECCENTRIC LOADING CURVE:C=24

La:AXIAL LOADING CURVE :C=0.

Δ y:DISPLACEMENT AT YIELD

Δ p:DISP. AT FULL PLASTICITY

* EXPERIMENTAL VALUES

FIG (5-26)

LOAD-DISPLACEMENT RELATIONSHIP OF STRUT

CHORD LENGTH(Lo)=310.0 (mm)

INITIAL RISE(Ao)= 65.0 (mm)

COMPARISON BETWEEN THEORETICAL AND EXPERIMENTAL RESULTS

S :SWANNELL CURVE

Le:ECCENTRIC LOADING CURVE:C=24

Lo:AXIAL LOADING CURVE :C=0.

Δ_y:DISPLACEMENT AT YIELD

Δ_p:DISP. AT FULL PLASTICITY

* EXPERIMENTAL VALUES

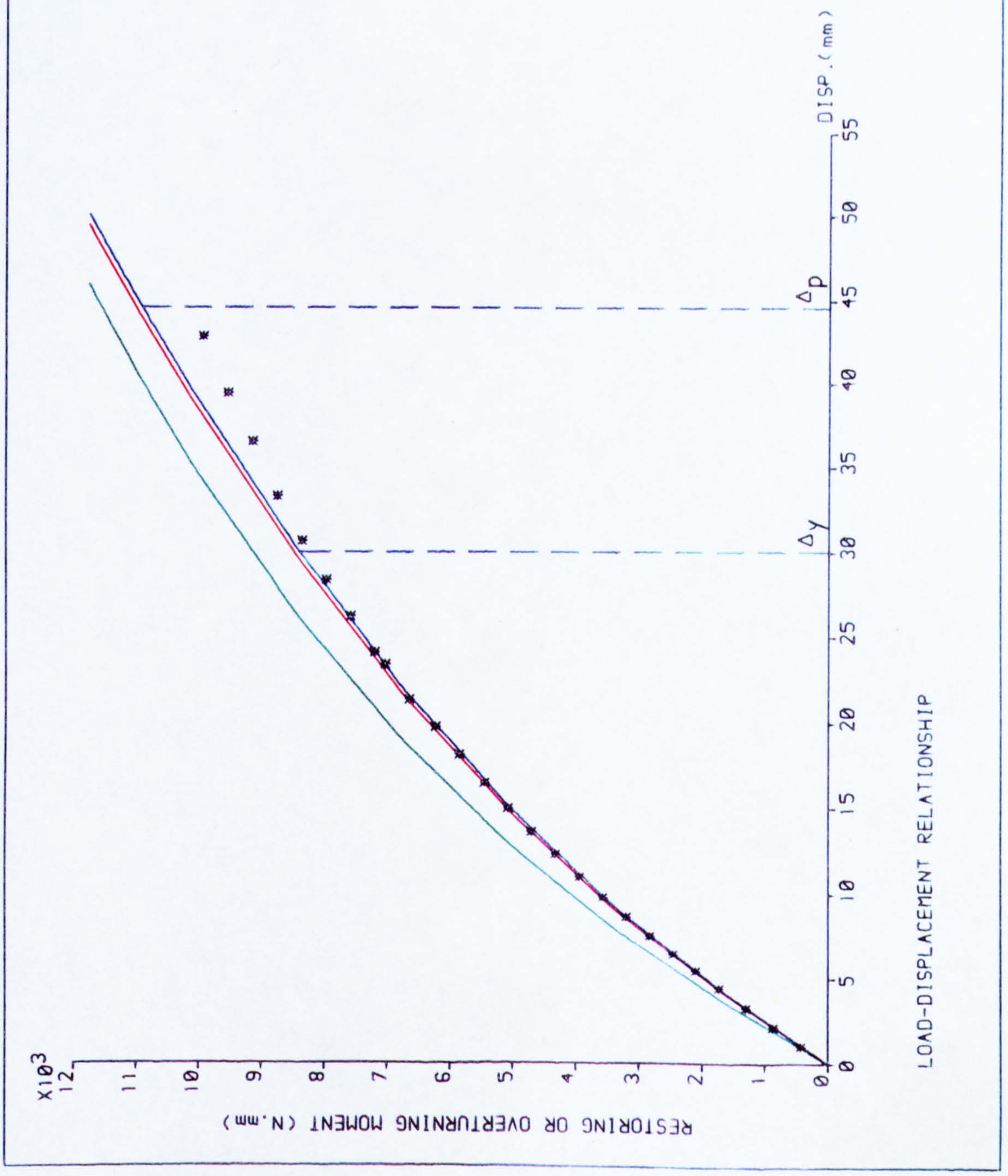

FIG (5-27)

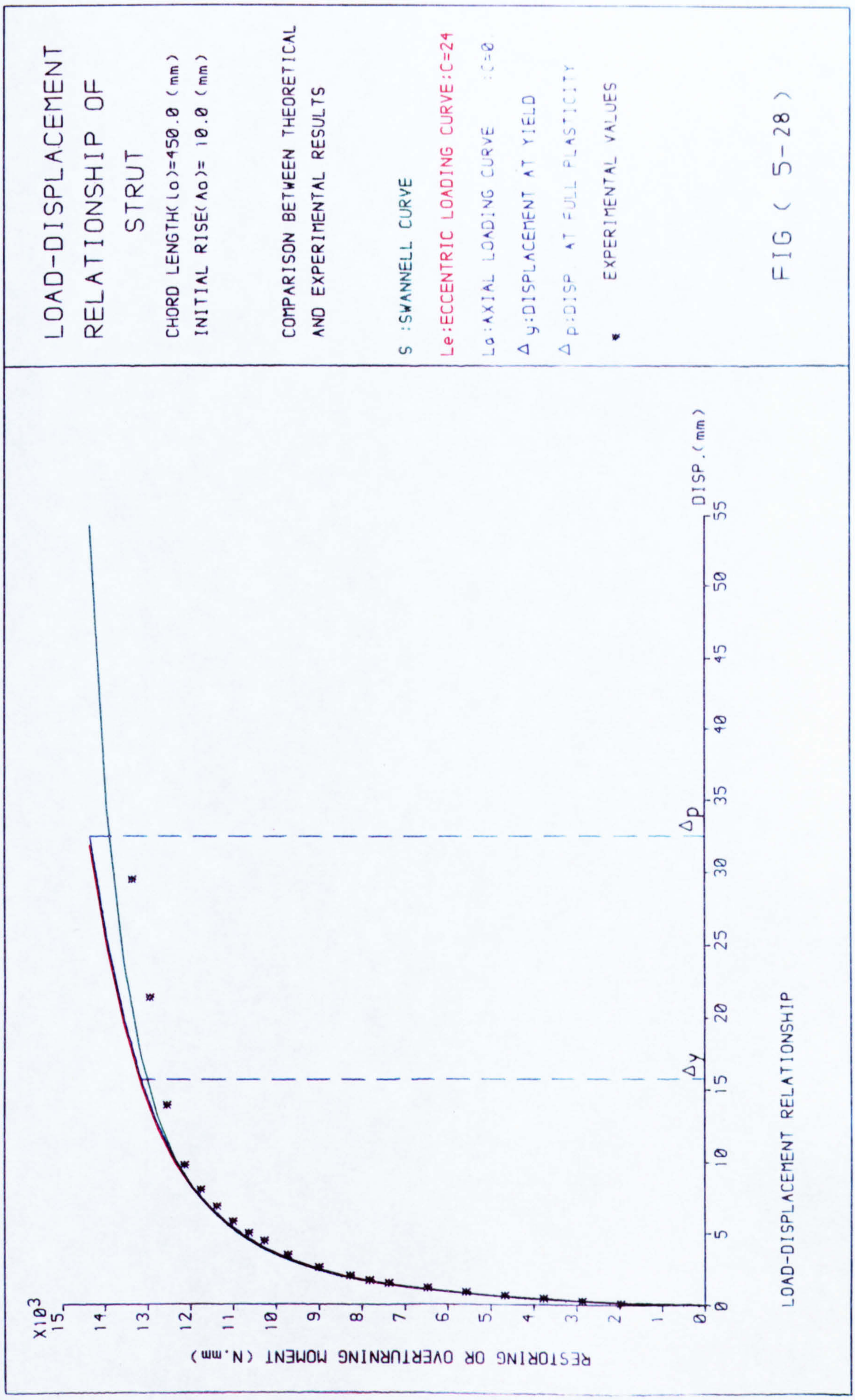
LOAD-DISPLACEMENT
RELATIONSHIP OF
STRUT
CHORD LENGTH(Lo)=450.0 (mm)
INITIAL RISE(Ao)= 10.0 (mm)
COMPARISON BETWEEN THEORETICAL
AND EXPERIMENTAL RESULTS
S :SWANNELL CURVE
Le:ECCENTRIC LOADING CURVE:C=24
Lo:AXIAL LOADING CURVE C=0
Δ y:DISPLACEMENT AT YIELD
Δ p:DISP AT FULL PLASTICITY
EXPERIMENTAL VALUES
DISP.(mm)
RESTORING OR OVERTURNING MOMENT (N.mm)
X10^3
LOAD-DISPLACEMENT RELATIONSHIP
Δy
Δp

FIG (5-28)

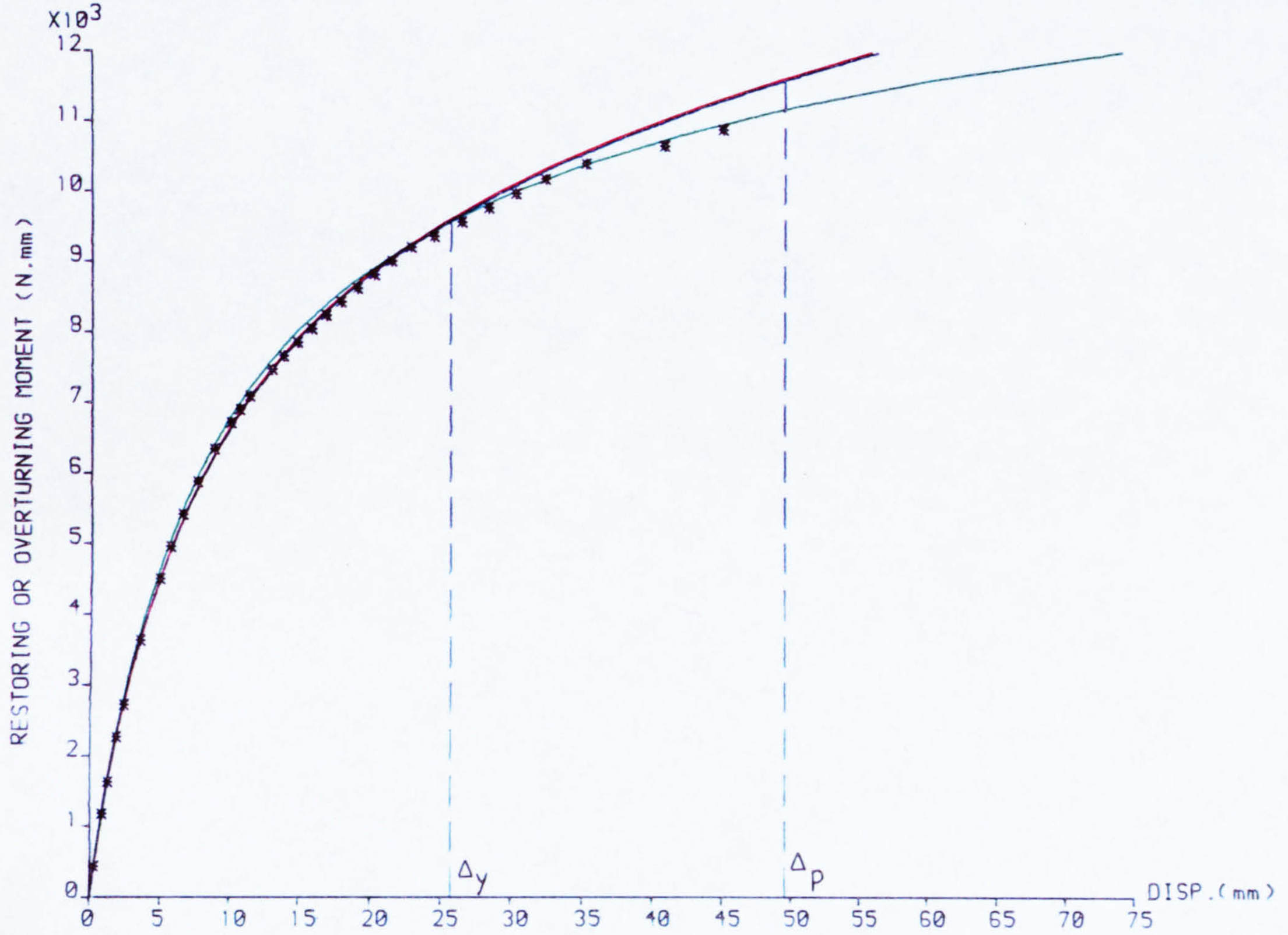

LOAD-DISPLACEMENT RELATIONSHIP

LOAD-DISPLACEMENT RELATIONSHIP OF STRUT

CHORD LENGTH(lo)=450.0 (mm)

INITIAL RISE(Ao)= 30.0 (mm)

COMPARISON BETWEEN THEORETICAL AND EXPERIMENTAL RESULTS

S :SWANNELL CURVE

Le:ECCENTRIC LOADING CURVE:C=24

La:AXIAL LOADING CURVE :C=8

Δ_y:DISPLACEMENT AT YIELD

Δ_p:DISP. AT FULL PLASTICITY

* EXPERIMENTAL VALUES

FIG (5-29)

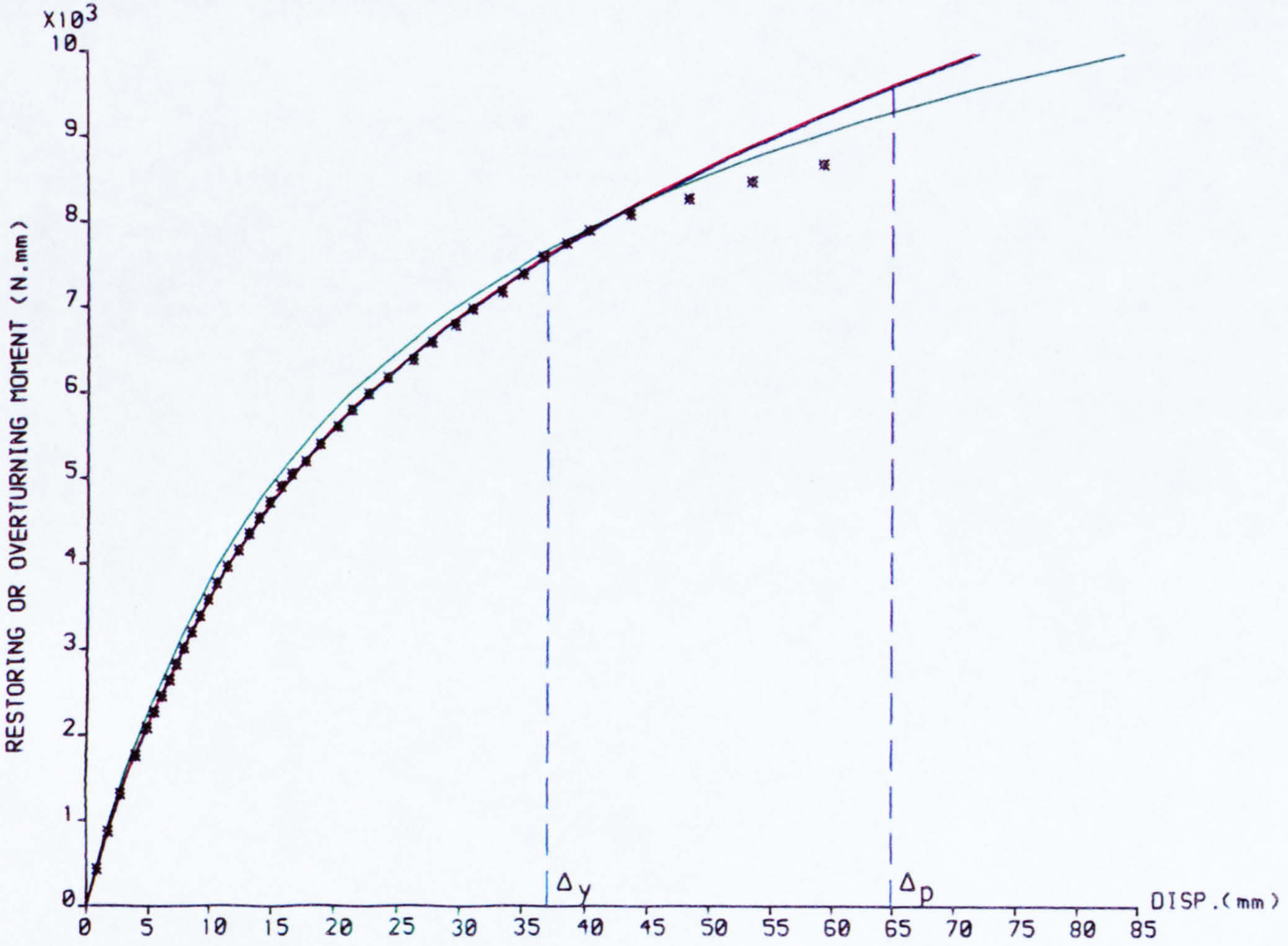

LOAD-DISPLACEMENT RELATIONSHIP

LOAD-DISPLACEMENT RELATIONSHIP OF STRUT

CHORD LENGTH(lo)=450.0 (mm)

INITIAL RISE(Ao)= 50.0 (mm)

COMPARISON BETWEEN THEORETICAL AND EXPERIMENTAL RESULTS

S :SWANNELL CURVE

Le:ECCENTRIC LOADING CURVE:C=24

La:AXIAL LOADING CURVE :C=0.

Δ_y:DISPLACEMENT AT YIELD

Δ_p:DISP. AT FULL PLASTICITY

* EXPERIMENTAL VALUES

FIG (5-30)

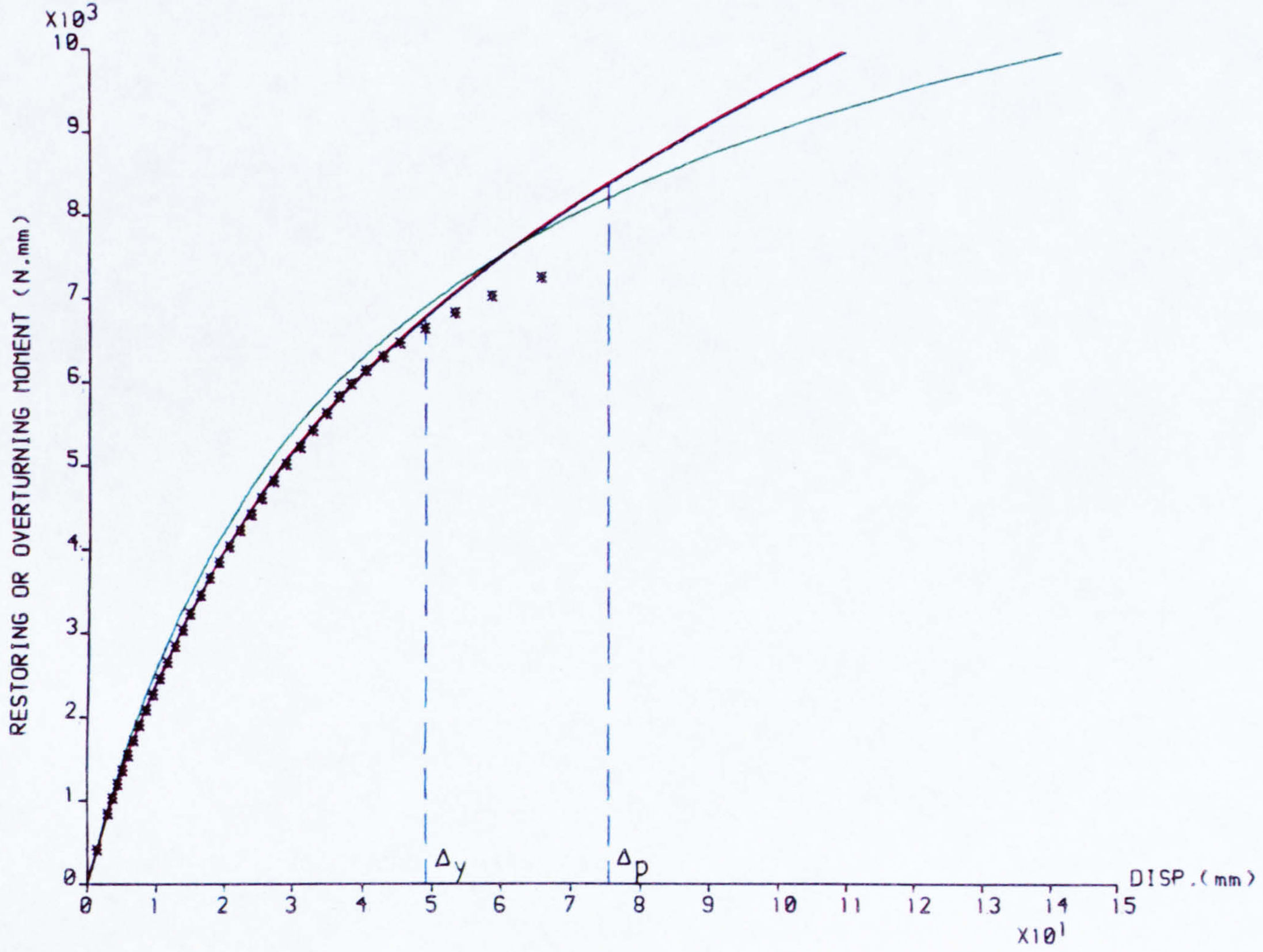

LOAD-DISPLACEMENT RELATIONSHIP

LOAD-DISPLACEMENT RELATIONSHIP OF STRUT

CHORD LENGTH(lo)=450.0 (mm)

INITIAL RISE(Ao)= 65.0 (mm)

COMPARISON BETWEEN THEORETICAL AND EXPERIMENTAL RESULTS

S :SWANNELL CURVE

Le:ECCENTRIC LOADING CURVE:C=24

La:AXIAL LOADING CURVE :C=0.

Δ_y:DISPLACEMENT AT YIELD

Δ_p:DISP. AT FULL PLASTICITY

* EXPERIMENTAL VALUES

FIG (5-31)

LOAD-DISPLACEMENT RELATIONSHIP OF STRUT

CHORD LENGTH(Lo)=520.0 (mm)
INITIAL RISE(Ao)= 20.0 (mm)

COMPARISON BETWEEN THEORETICAL AND EXPERIMENTAL RESULTS

S :SWANNELL CURVE
-e:ECCENTRIC LOADING CURVE:C=24
Lo:AXIAL LOADING CURVE :C=0.
Δ y:DISPLACEMENT AT YIELD
Δ p:DISP. AT FULL PLASTICITY
* EXPERIMENTAL VALUES

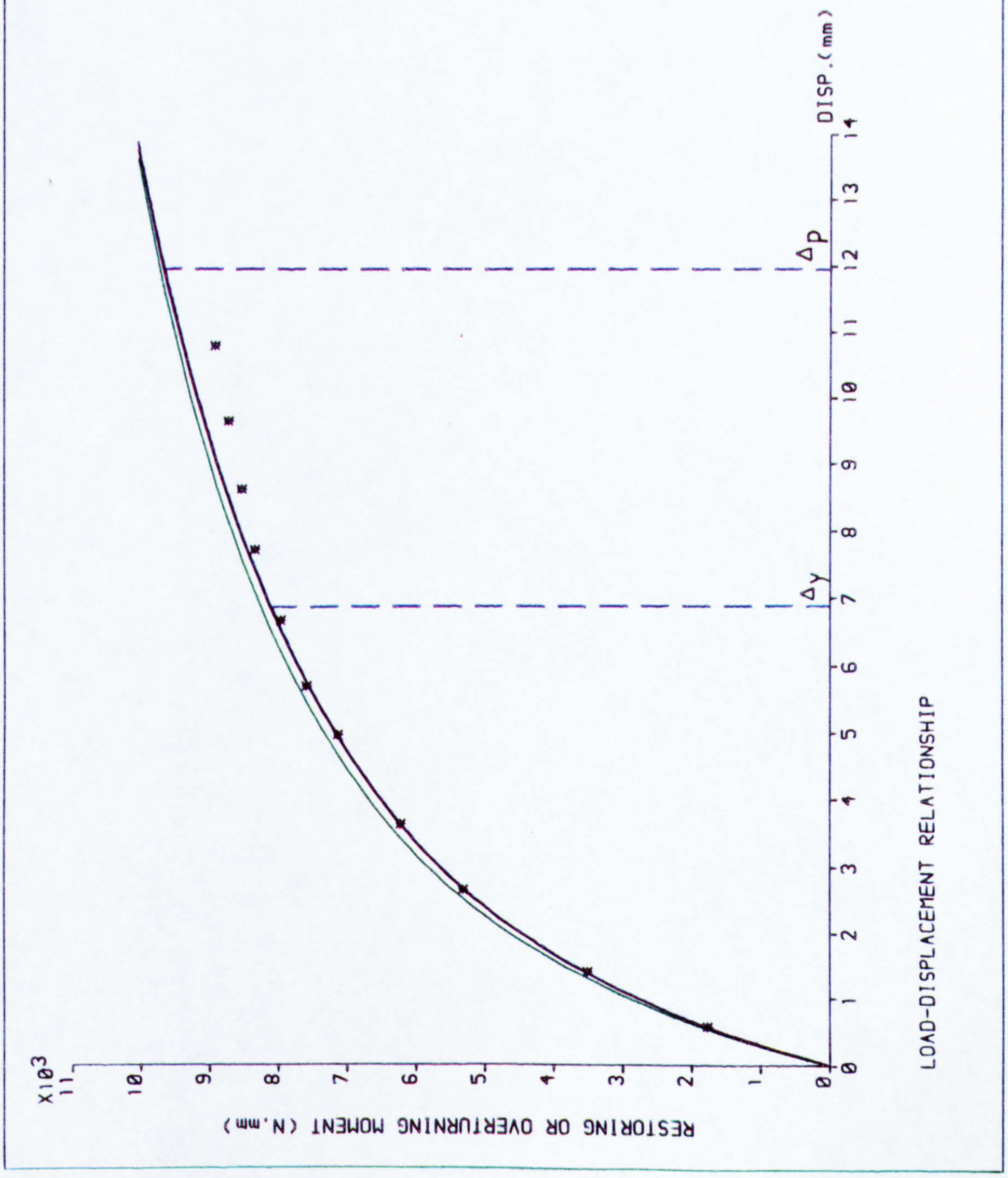

FIG (5-32)

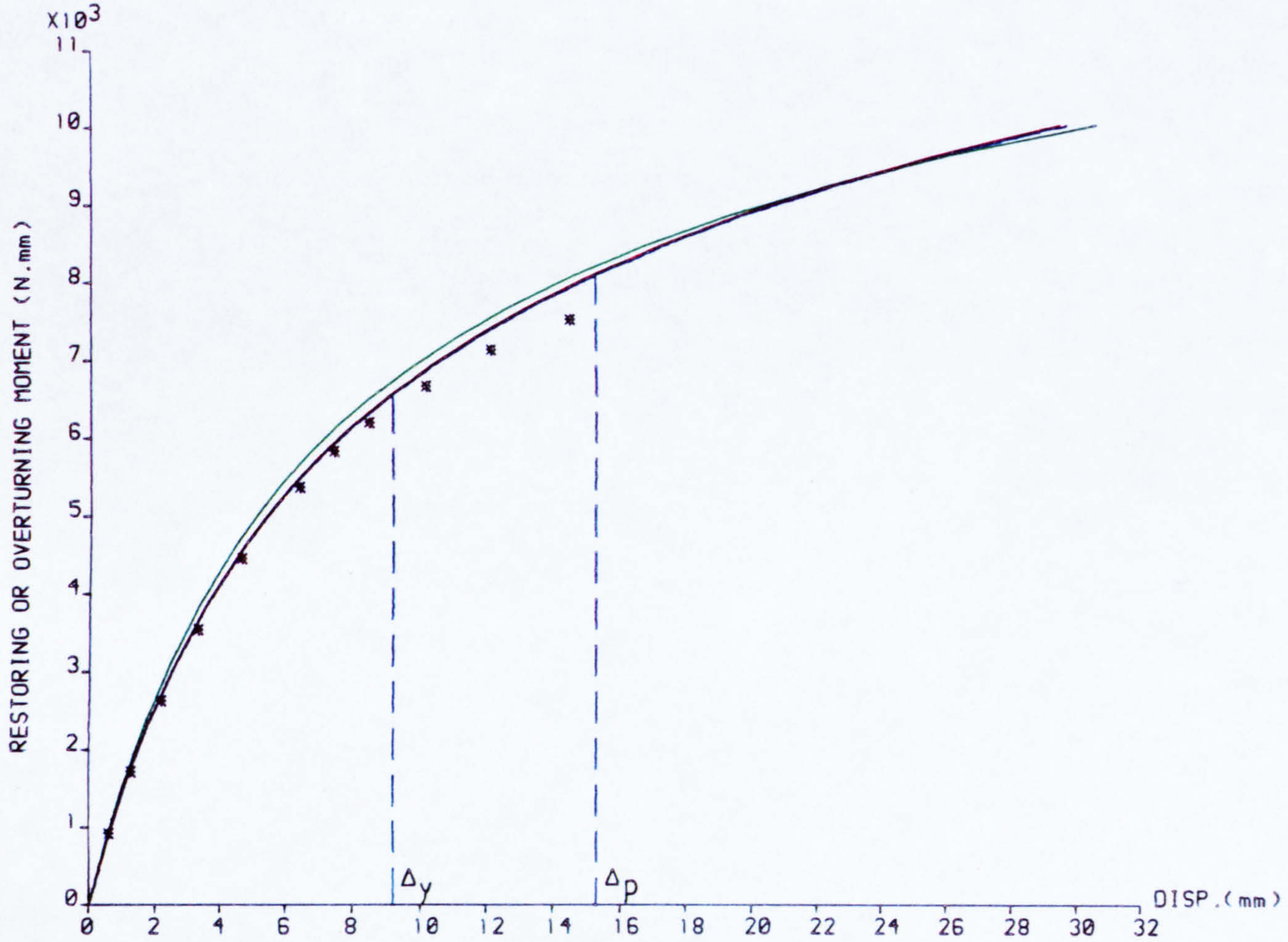

LOAD-DISPLACEMENT RELATIONSHIP

LOAD-DISPLACEMENT RELATIONSHIP OF STRUT

CHORD LENGTH(Lo)=520.0 (mm)

INITIAL RISE(Ao)= 30.0 (mm)

COMPARISON BETWEEN THEORETICAL AND EXPERIMENTAL RESULTS

S :SWANNELL CURVE

_e:ECCENTRIC LOADING CURVE:C=24

Lo:AXIAL LOADING CURVE :C=0.

Δ_y:DISPLACEMENT AT YIELD

Δ_p:DISP. AT FULL PLASTICITY

* EXPERIMENTAL VALUES

FIG (5-33)

LOAD-DISPLACEMENT RELATIONSHIP OF STRUT

CHORD LENGTH(lo)=520.0 (mm)
INITIAL RISE(Ao)= 50.0 (mm)

COMPARISON BETWEEN THEORETICAL AND EXPERIMENTAL RESULTS

S :SWANNELL CURVE
e:ECCENTRIC LOADING CURVE:C=24
Lo:AXIAL LOADING CURVE :C=0.
Δ_y:DISPLACEMENT AT YIELD
Δ_p:DISP. AT FULL PLASTICITY
* EXPERIMENTAL VALUES

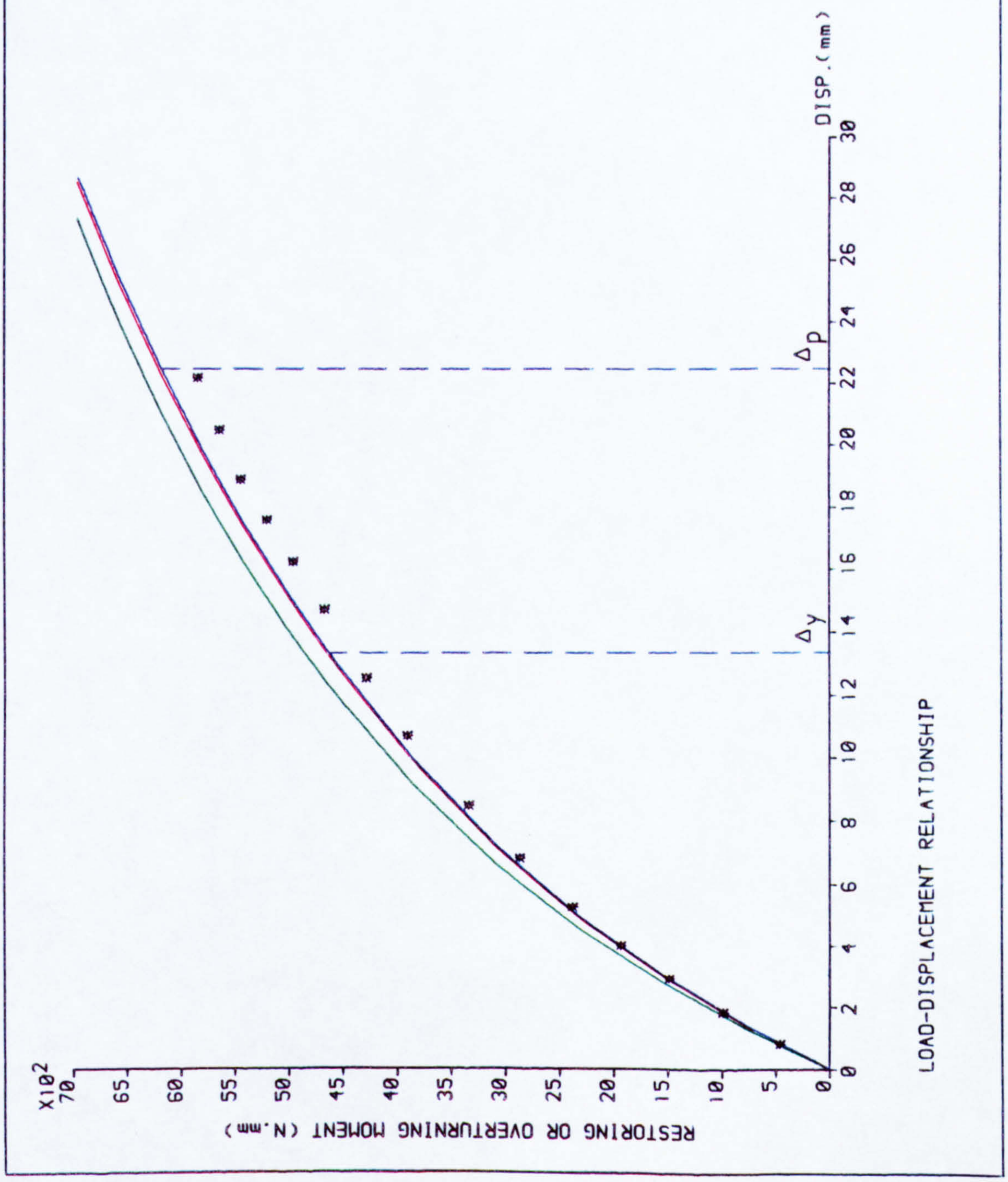

FIG (5-34)

LOAD-DISPLACEMENT RELATIONSHIP OF STRUT

CHORD LENGTH(Lo)=520.0 (mm)

INITIAL RISE(Ao)= 65.0 (mm)

COMPARISON BETWEEN THEORETICAL AND EXPERIMENTAL RESULTS

S :SWANNELL CURVE

e:ECCENTRIC LOADING CURVE:C=24

Lo:AXIAL LOADING CURVE :C=0.

Δ_y:DISPLACEMENT AT YIELD

Δ_p:DISP. AT FULL PLASTICITY

* EXPERIMENTAL VALUES

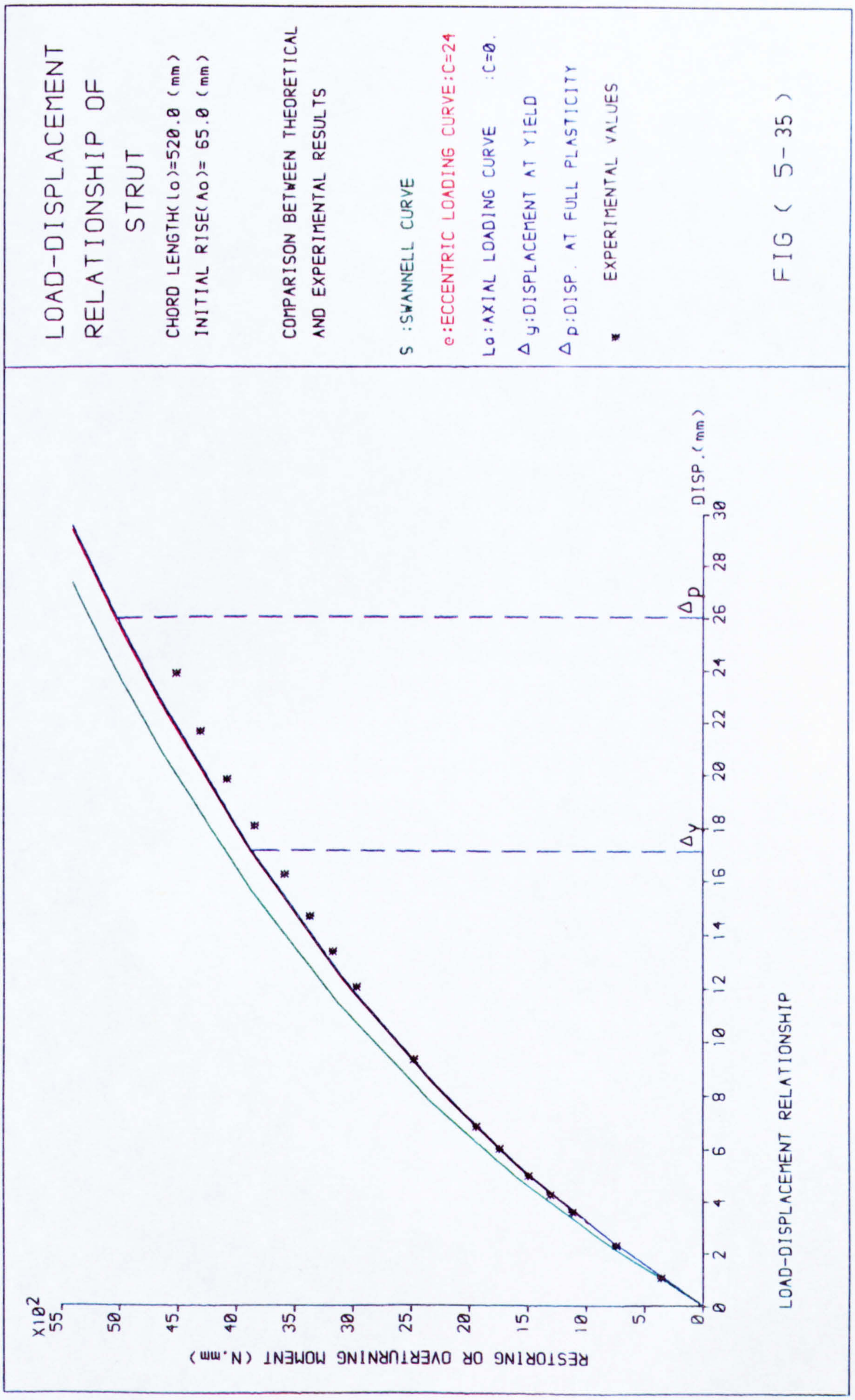

FIG (5-35)

LOAD-DISPLACEMENT
RELATIONSHIP OF
TIE

CHORD LENGTH(lo)=310.0 (mm)
INITIAL RISE(Ao)= 50.0 (mm)

COMPARISON BETWEEN THEORETICAL
AND EXPERIMENTAL RESULTS

S :SWANNELL CURVE
Le:ECCENTRIC LOADING CURVE:C=2
La:AXIAL LOADING CURVE :C=0.
* EXPERIMENTAL VALUES

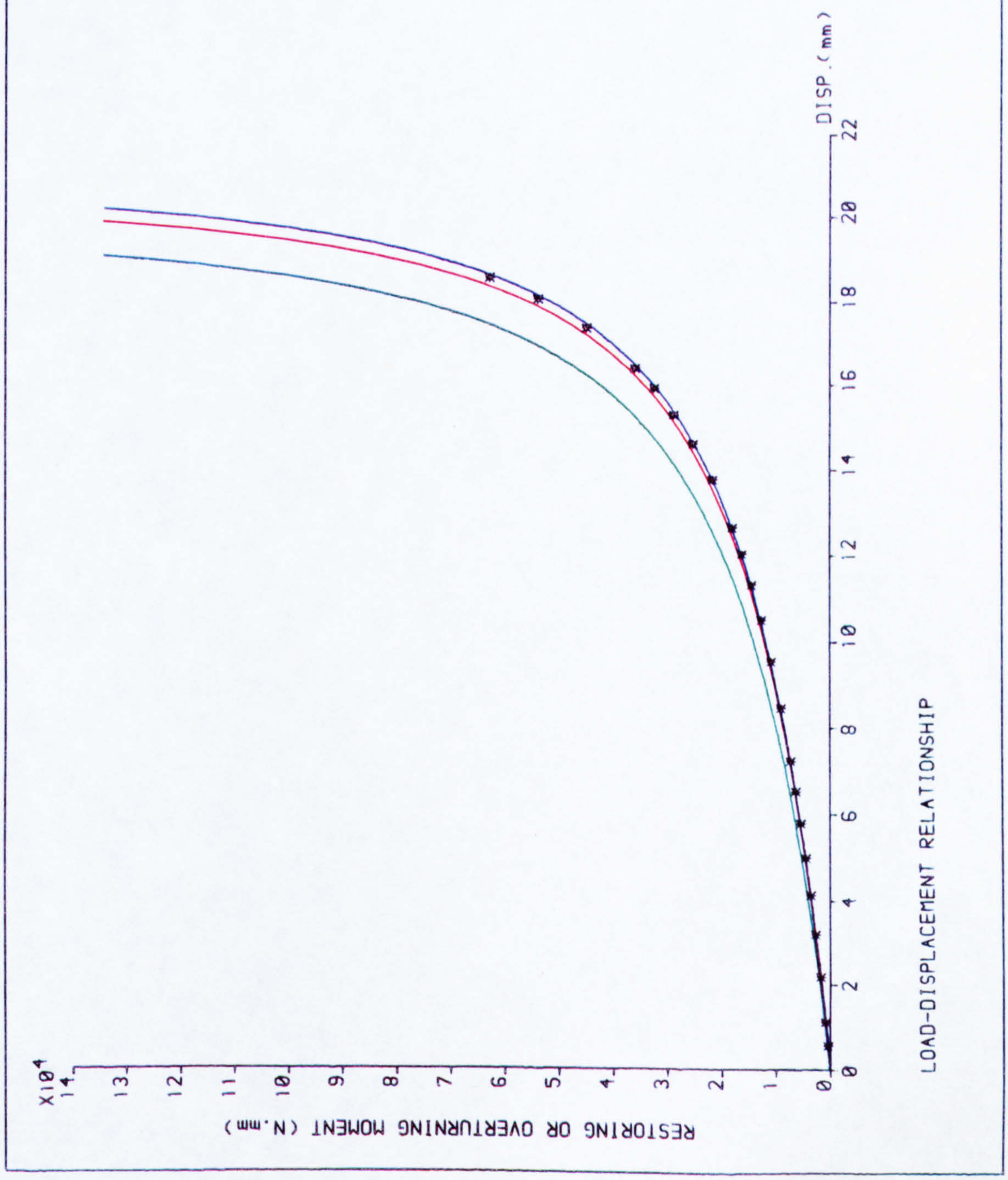

FIG (5-36)

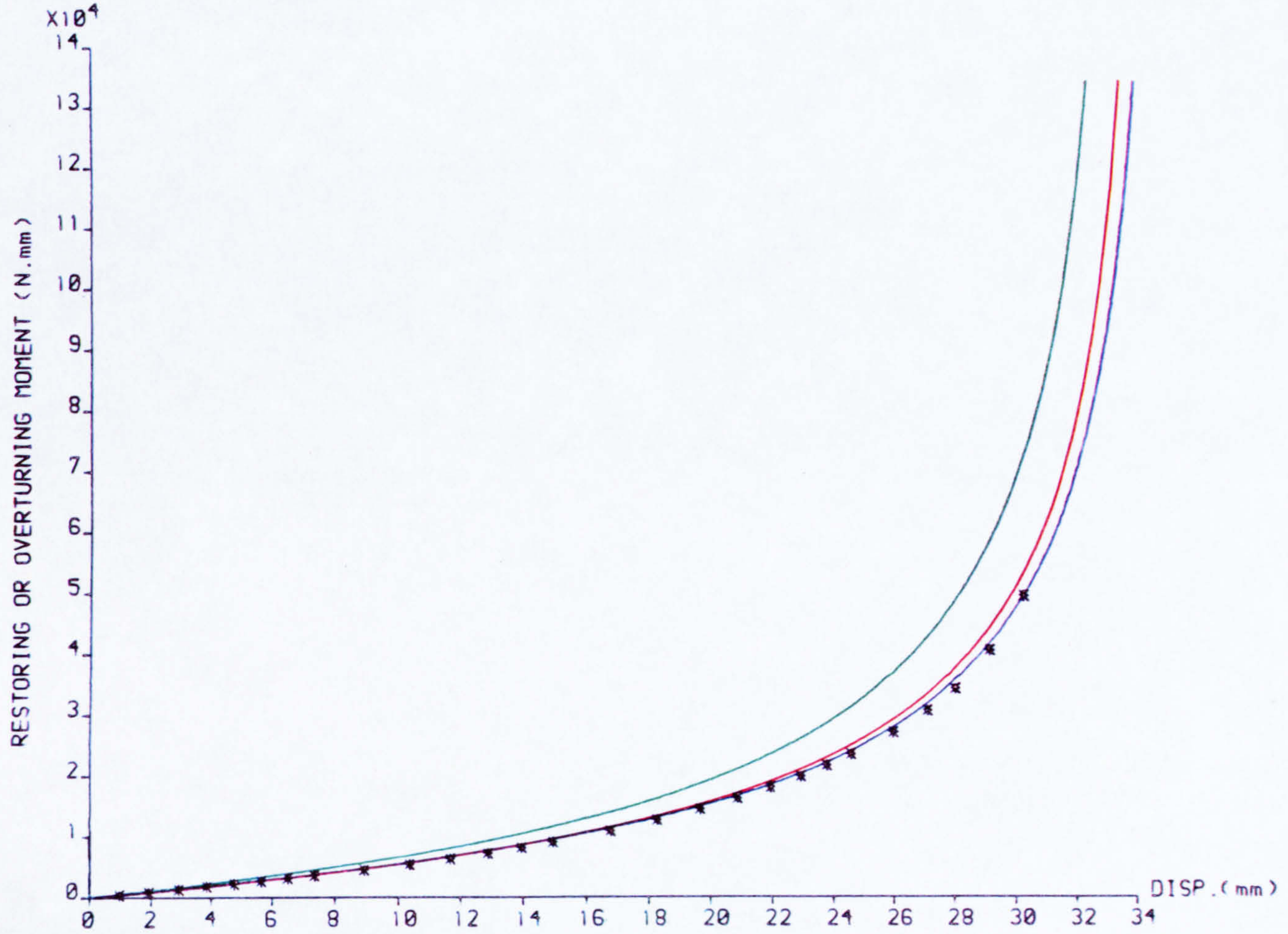

LOAD-DISPLACEMENT RELATIONSHIP

LOAD-DISPLACEMENT RELATIONSHIP OF TIE

CHORD LENGTH(lo)=310.0 (mm)

INITIAL RISE(Ao)= 65.0 (mm)

COMPARISON BETWEEN THEORETICAL AND EXPERIMENTAL RESULTS

S :SWANNELL CURVE

Le:ECCENTRIC LOADING CURVE:C=24

La:AXIAL LOADING CURVE :C=0.

* EXPERIMENTAL VALUES

FIG (5-37)

LOAD-DISPLACEMENT RELATIONSHIP OF TIE

CHORD LENGTH(lo)=450.0 (mm)

INITIAL RISE(Ao)= 50.0 (mm)

COMPARISON BETWEEN THEORETICAL AND EXPERIMENTAL RESULTS

S :SWANNELL CURVE

Le:ECCENTRIC LOADING CURVE:C=24

La:AXIAL LOADING CURVE :C=0.

* EXPERIMENTAL VALUES

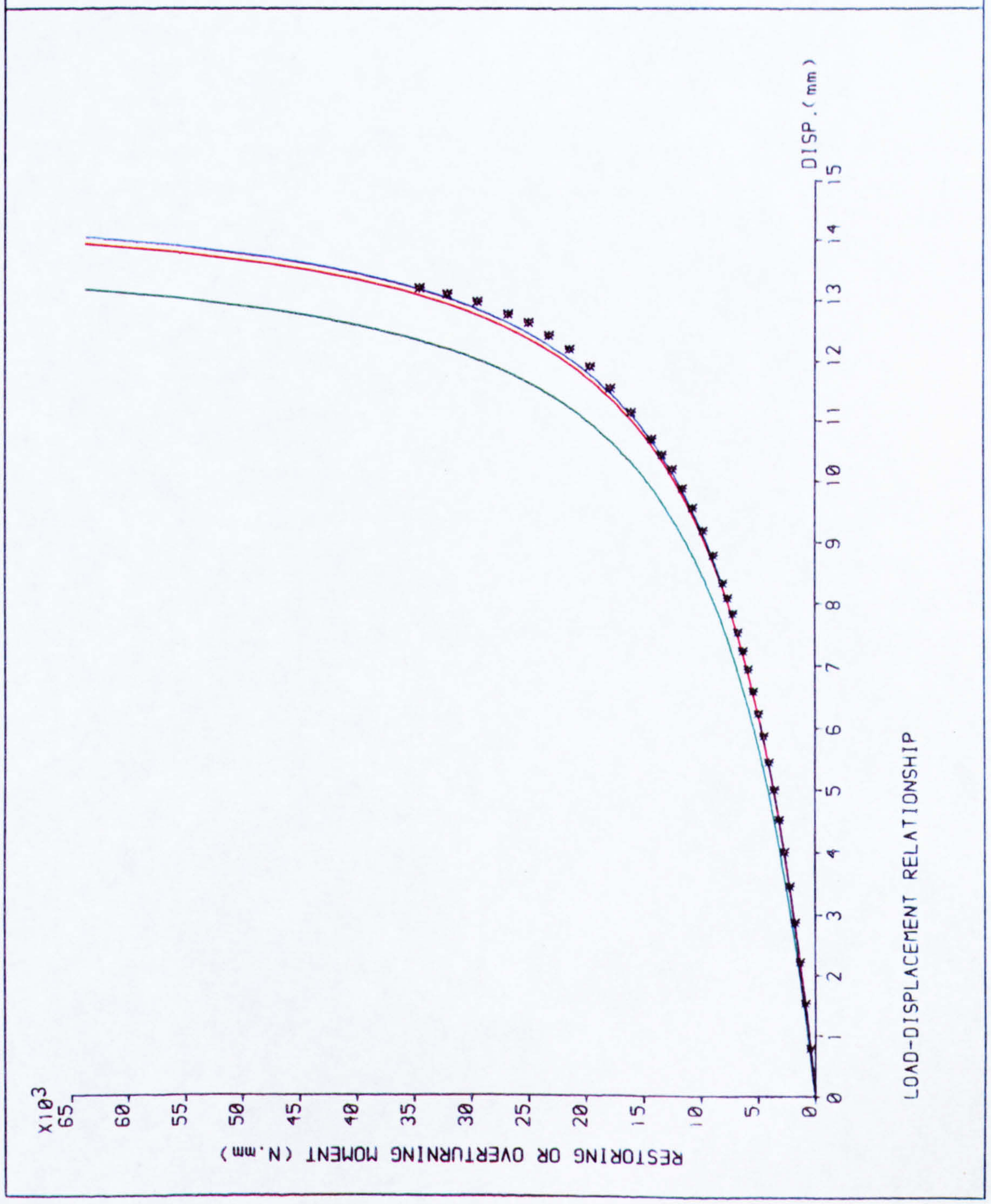

FIG (5-38)

LOAD-DISPLACEMENT
RELATIONSHIP OF
TIE

CHORD LENGTH(l_o)=450.0 (mm)
INITIAL RISE(Δ_o)= 65.0 (mm)

COMPARISON BETWEEN THEORETICAL
AND EXPERIMENTAL RESULTS

S :SWANNELL CURVE
Le:ECCENTRIC LOADING CURVE:C=24
La:AXIAL LOADING CURVE :C=0.
* EXPERIMENTAL VALUES

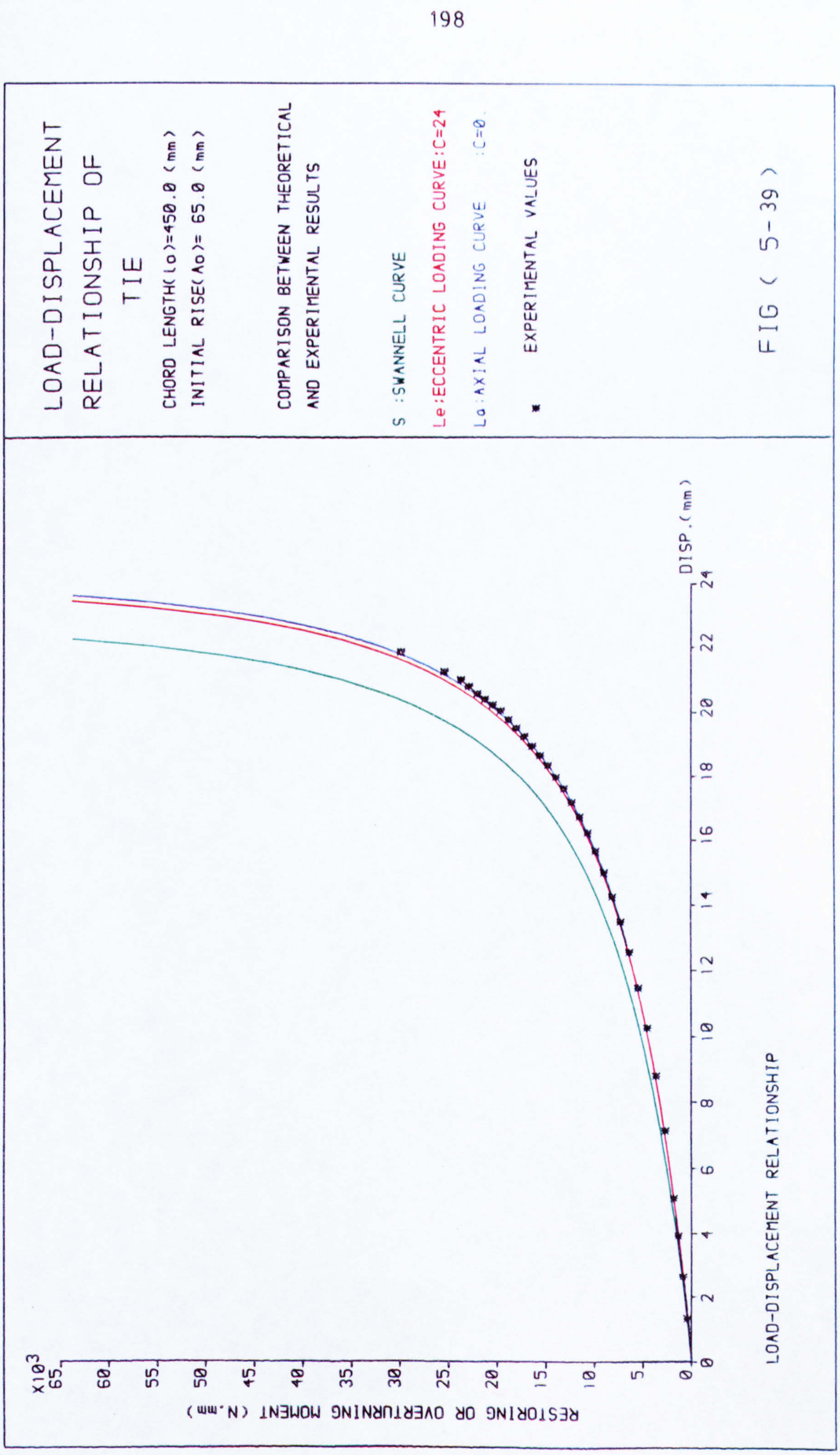

FIG (5-39)

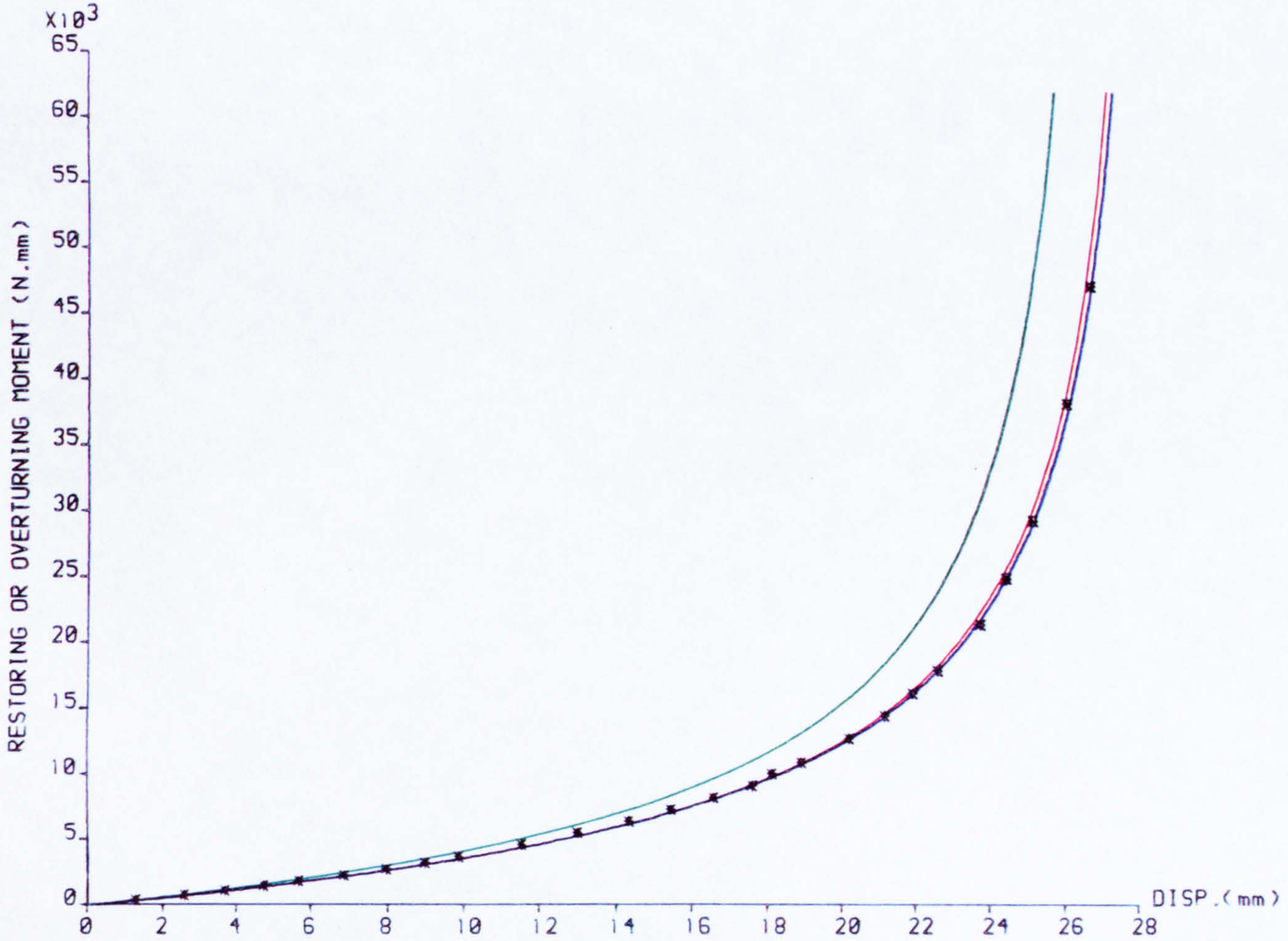

LOAD-DISPLACEMENT RELATIONSHIP

LOAD-DISPLACEMENT RELATIONSHIP OF TIE

CHORD LENGTH(lo)=520.0 (mm)

INITIAL RISE(Ao)= 75.0 (mm)

COMPARISON BETWEEN THEORETICAL AND EXPERIMENTAL RESULTS

S :SWANNELL CURVE

Le:ECCENTRIC LOADING CURVE:C=24

Lo:AXIAL LOADING CURVE :C=0.

* EXPERIMENTAL VALUES

FIG (5-40)

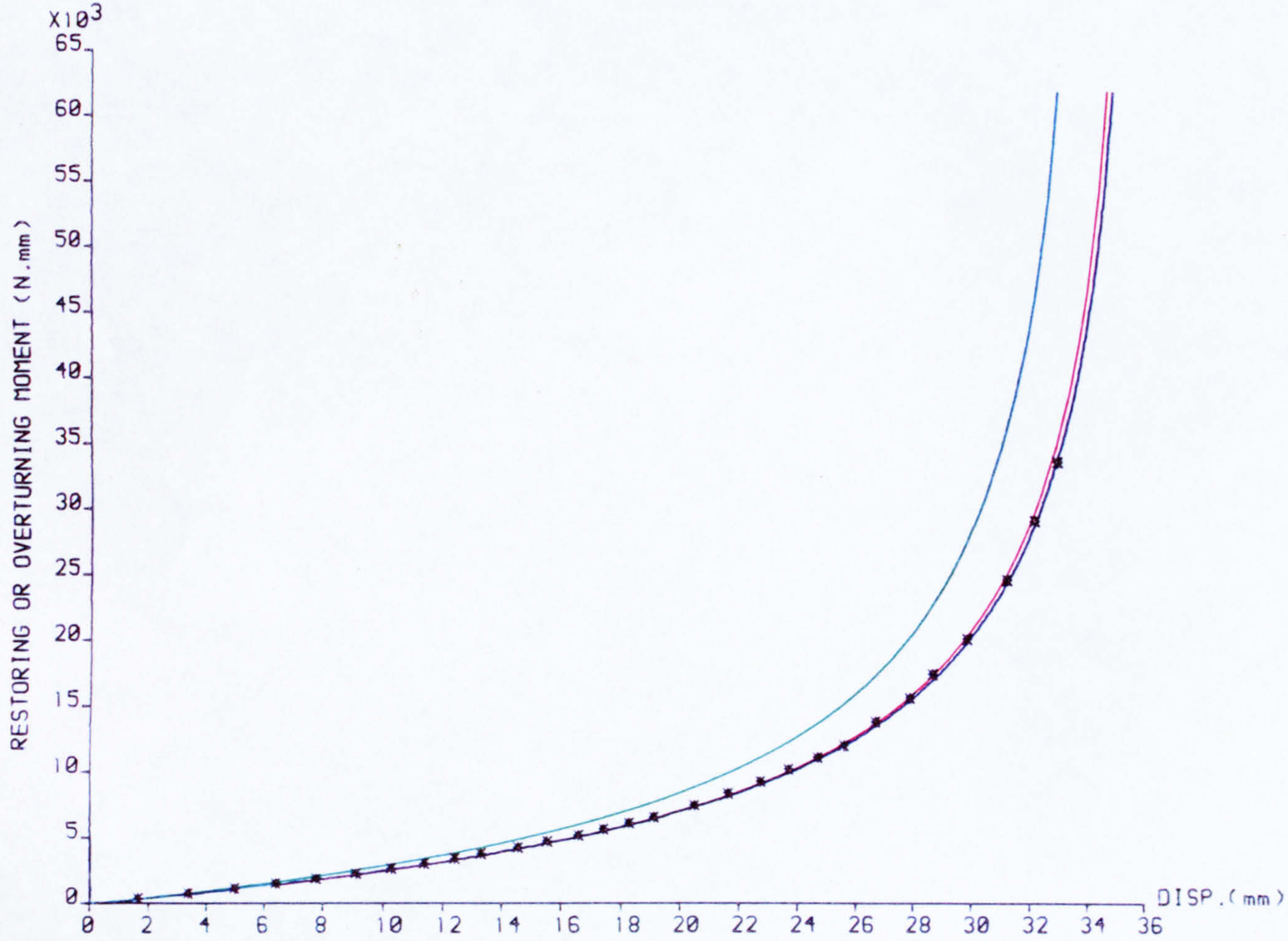

LOAD-DISPLACEMENT RELATIONSHIP

LOAD-DISPLACEMENT RELATIONSHIP OF TIE

CHORD LENGTH(lo)=520.0 (mm)

INITIAL RISE(Ao)= 85.0 (mm)

COMPARISON BETWEEN THEORETICAL AND EXPERIMENTAL RESULTS

S :SWANNELL CURVE

e:ECCENTRIC LOADING CURVE:C=24

La:AXIAL LOADING CURVE :C=0.

* EXPERIMENTAL VALUES

FIG (5-41)

007.200

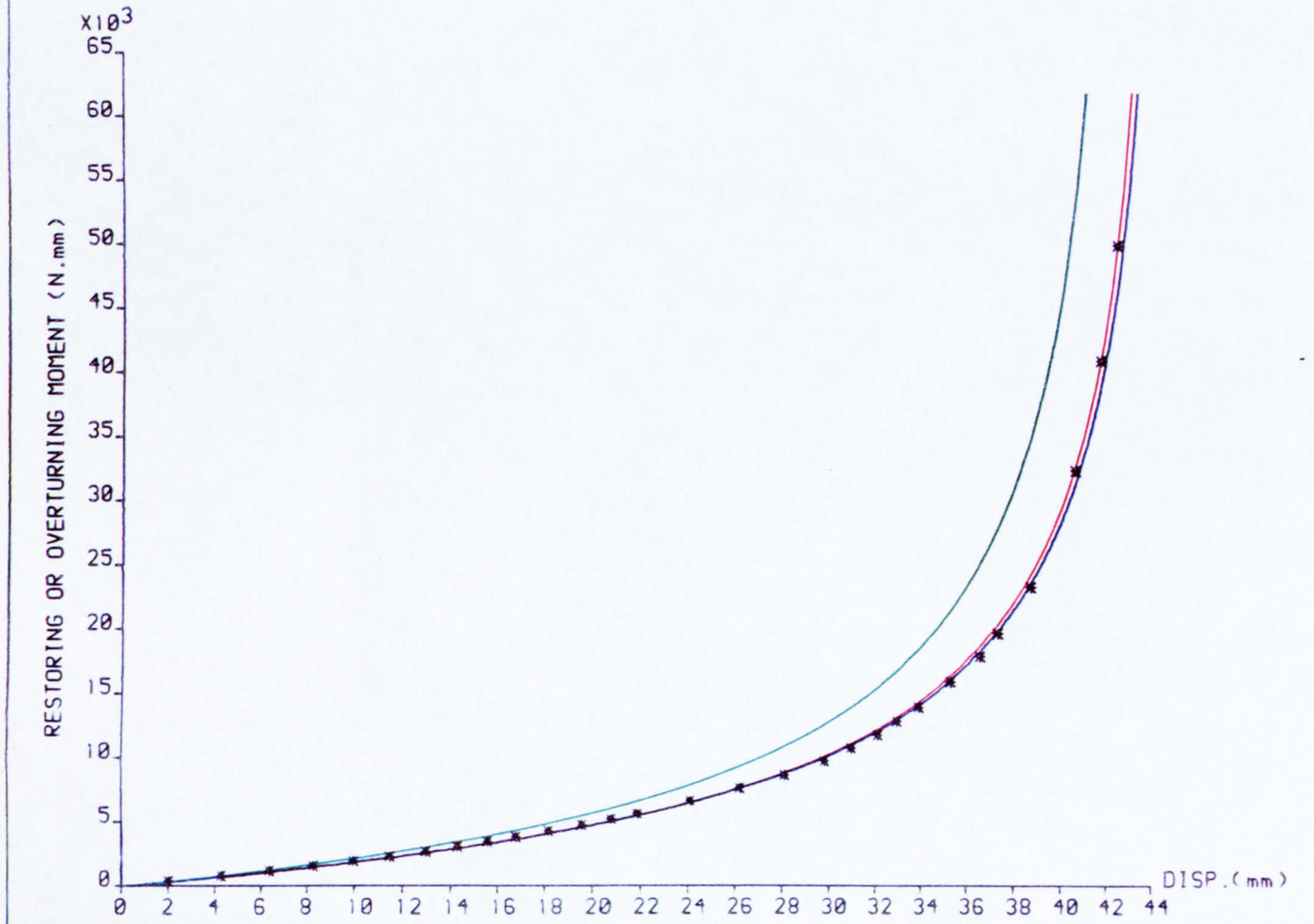

LOAD-DISPLACEMENT RELATIONSHIP

LOAD-DISPLACEMENT RELATIONSHIP OF TIE

CHORD LENGTH(lo)=520.0 (mm)

INITIAL RISE(Ao)= 95.0 (mm)

COMPARISON BETWEEN THEORETICAL AND EXPERIMENTAL RESULTS

S :SWANNELL CURVE

e:ECCENTRIC LOADING CURVE:C=24

La:AXIAL LOADING CURVE :C=0.

* EXPERIMENTAL VALUES

FIG (5-42)

LOAD-DISPLACEMENT
RELATIONSHIP OF
TIE

CHORD LENGTH(lo)=520.0 (mm)
INITIAL RISE(Ao)=105.0 (mm)

COMPARISON BETWEEN THEORETICAL
AND EXPERIMENTAL RESULTS

S :SWANNELL CURVE
Le:ECCENTRIC LOADING CURVE:C=24
La:AXIAL LOADING CURVE :C=0.
* EXPERIMENTAL VALUES

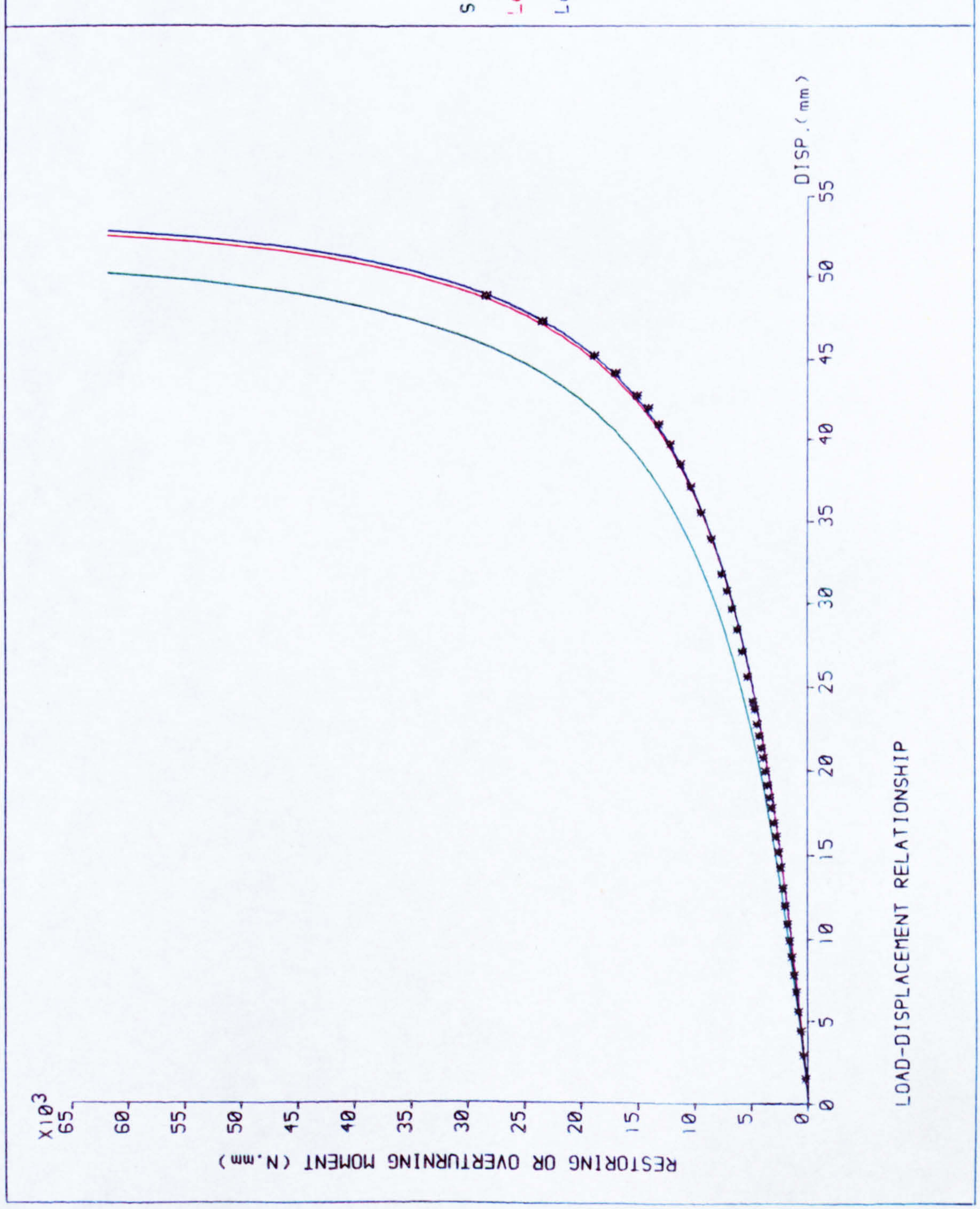

FIG (5-43)

STABILITY OF COLUMN

CHORD LENGTH(lo) =310.0 (mm)

INITIAL RISE:

(Aoc)= 10.0 (Aot) = 65.0 (mm)

COMPARISON BETWEEN THEORETICAL

AND EXPERIMENTAL RESULTS

——THEORETICAL RESULTS

* EXPERIMENTAL RESULTS

— —THEORETICAL RESULTS WITH

TENSILE BRACING ONLY

LOADS:

Wcr= 18.530 (N)

Pcr=1334.141 (N)

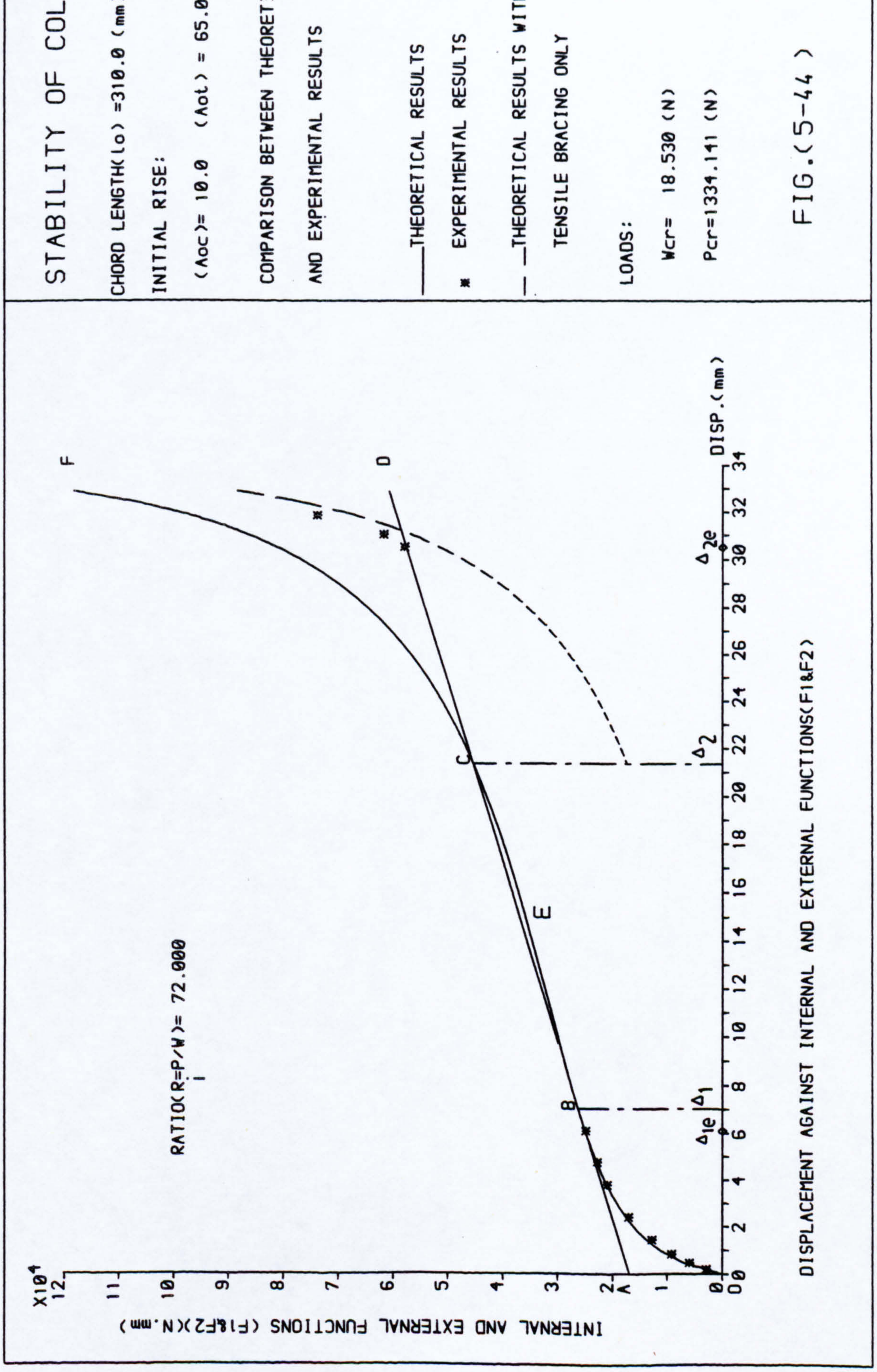

FIG.(5-44)

STABILITY OF COLUMN

CHORD LENGTH (lo) =310.0 (mm)

INITIAL RISE:

(Δoc)= 10.0 (Δot) = 65.0 (mm)

COMPARISON BETWEEN THEORETICAL

AND EXPERIMENTAL RESULTS

——THEORETICAL RESULTS

* EXPERIMENTAL RESULTS

— —THEORETICAL RESULTS WITH

TENSILE BRACING ONLY

LOADS:

Wcr= 18.530 (N)

Pcr=1334.141 (N)

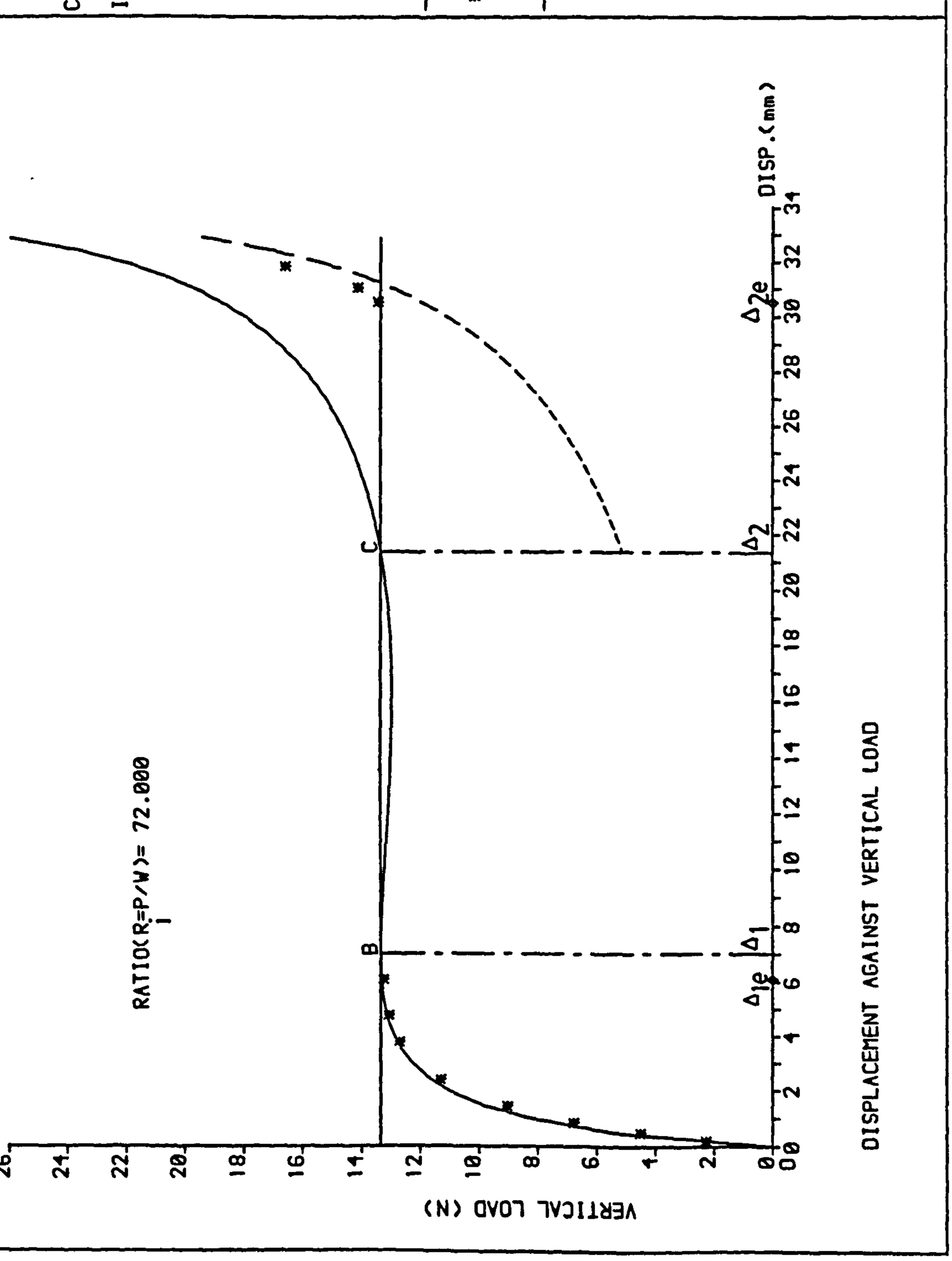

FIG.(5-45)

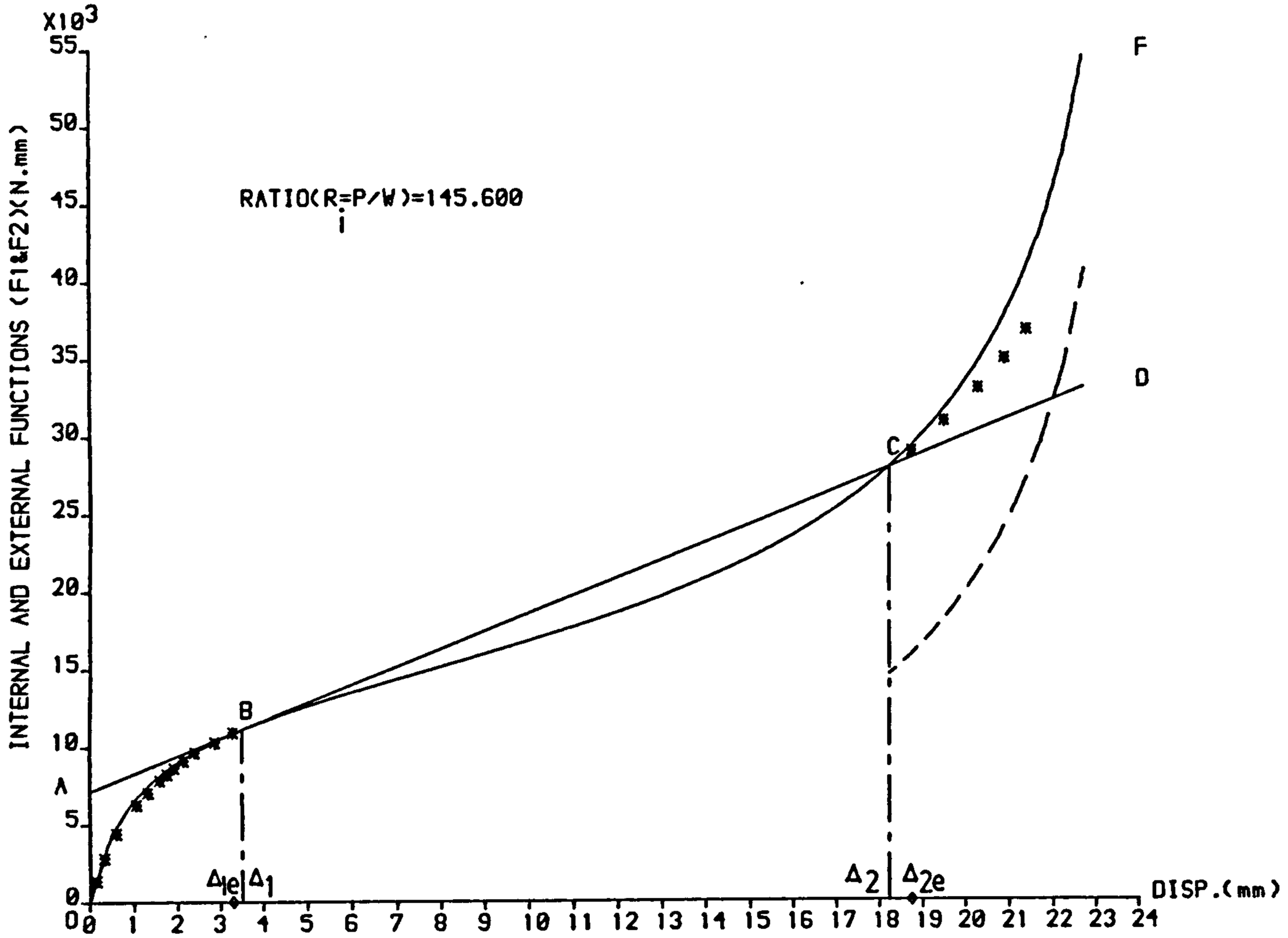

DISPLACEMENT AGAINST INTERNAL AND EXTERNAL FUNCTIONS(F1&F2)

STABILITY OF COLUMN

CHORD LENGTH(lo) =150.0 (mm)

INITIAL RISE:

(Δoc)= 10.0 (Δot) = 65.0 (mm)

COMPARISON BETWEEN THEORETICAL AND EXPERIMENTAL RESULTS

____THEORETICAL RESULTS

* EXPERIMENTAL RESULTS

_ _THEORETICAL RESULTS WITH TENSILE BRACING ONLY

LOADS:

Wcr= 7.837 (N)

Pcr=1141.088 (N)

FIG.(5-46).

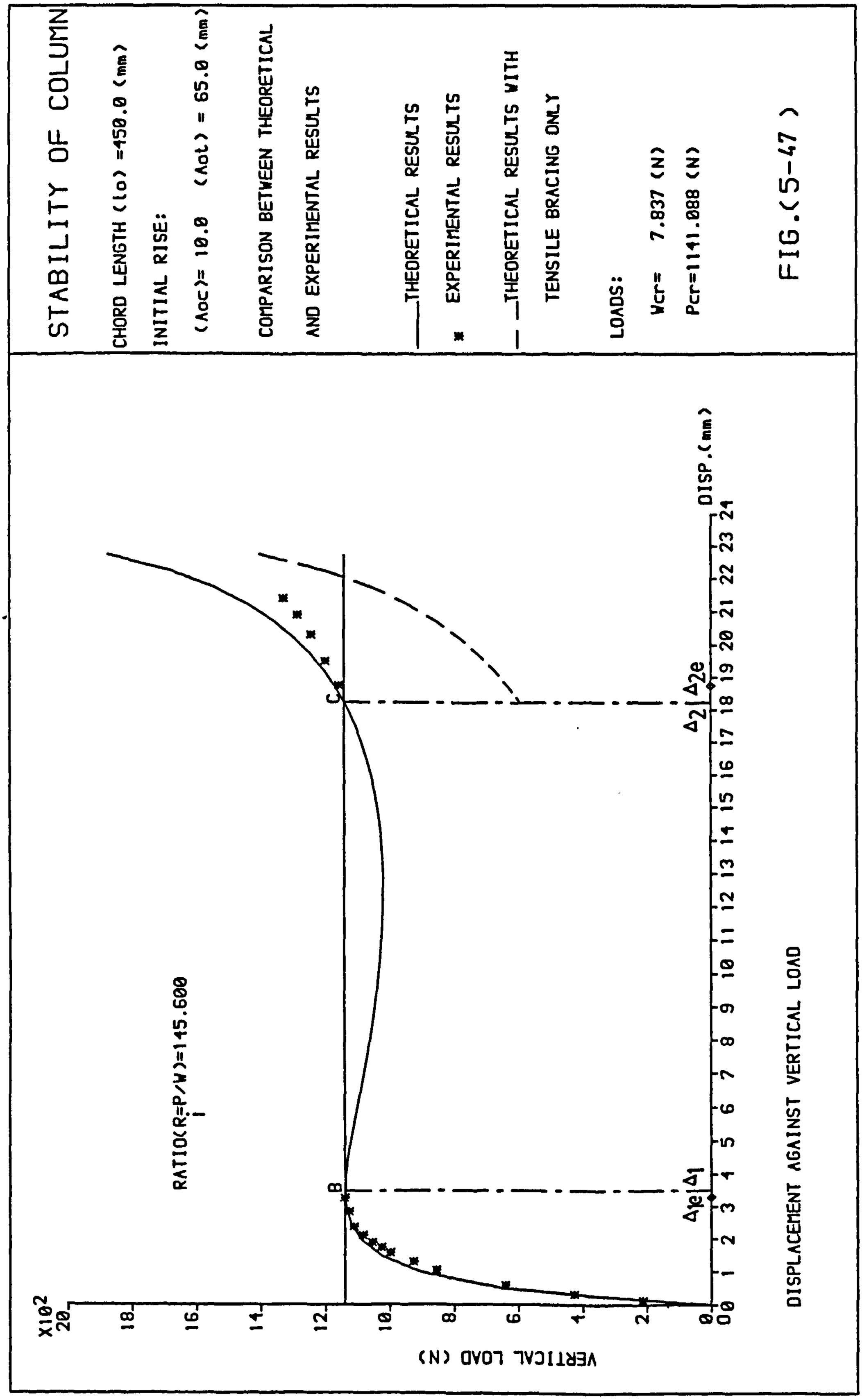
STABILITY OF COLUMN
CHORD LENGTH (lo) =450.0 (mm)
INITIAL RISE:
(Δoc)= 10.0 (Δot) = 65.0 (mm)
COMPARISON BETWEEN THEORETICAL
AND EXPERIMENTAL RESULTS
THEORETICAL RESULTS
EXPERIMENTAL RESULTS
THEORETICAL RESULTS WITH
TENSILE BRACING ONLY
LOADS:
Wcr= 7.837 (N)
Pcr=1141.088 (N)
FIG.(5-47)
DISP.(mm)
RATIO(R=P/W)=145.600
VERTICAL LOAD (N)
DISPLACEMENT AGAINST VERTICAL LOAD
C
B
A
Δ2e
Δ2
Δ1e
Δ1

STABILITY OF FRAME

TWO STORIES

CHORD LENGTH(lo)=520.0 (mm)

INITIAL RISE:

Aoc(1)=20.0 Aot(1)= 85.0 (mm)

Aoc(2)=20.0 Aot(2)= 85.0 (mm)

COMPARISON BETWEEN THEORETICAL

AND EXPERIMENTAL RESULTS

——THEORETICAL RESULTS

* EXPERIMENTAL RESULTS

— —THEORETICAL RESULTS WITH

TENSILE BRACINGS ONLY

LOADS:

Wcr= 4.077 (N)

Pcr= 163.080 (N)

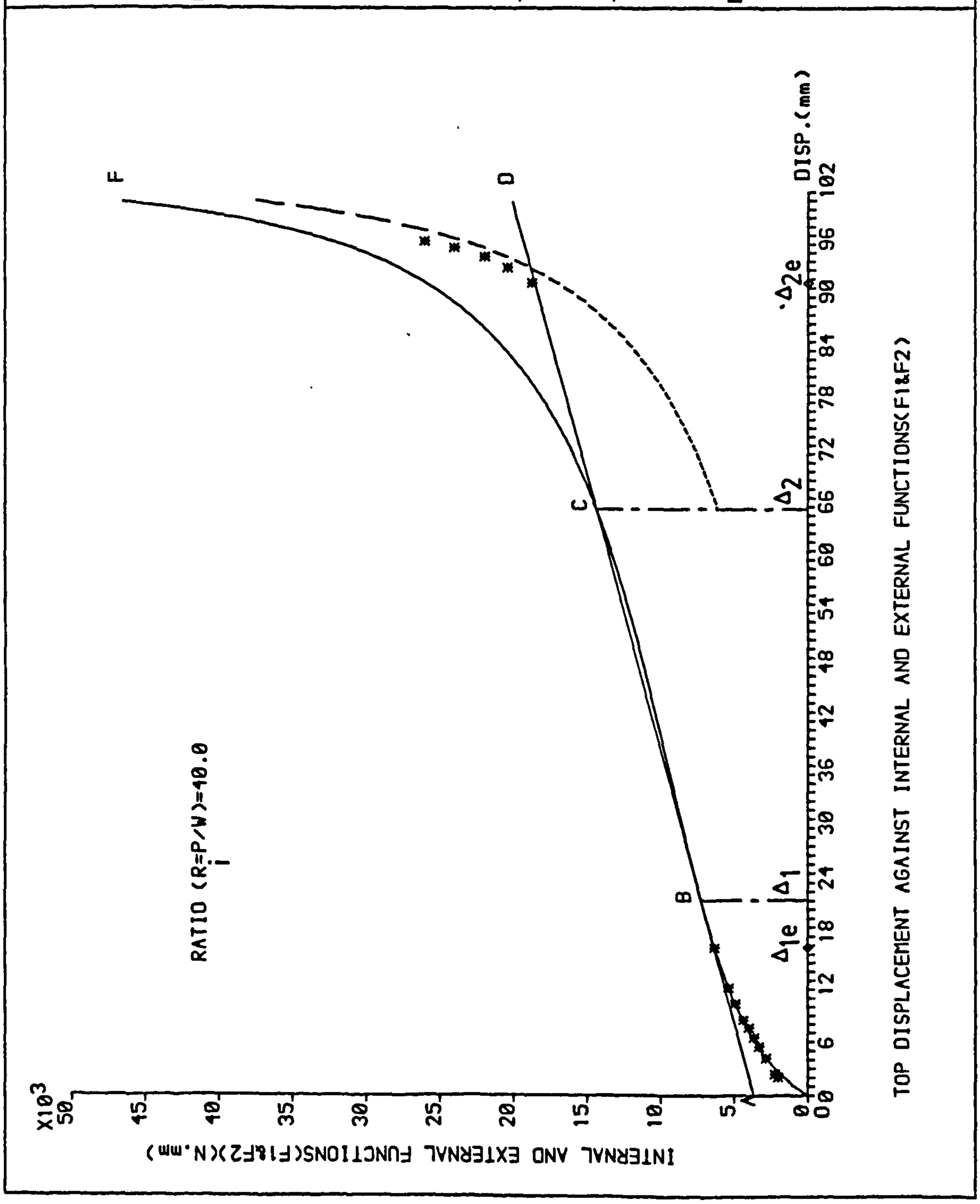

FIG.(5-48)

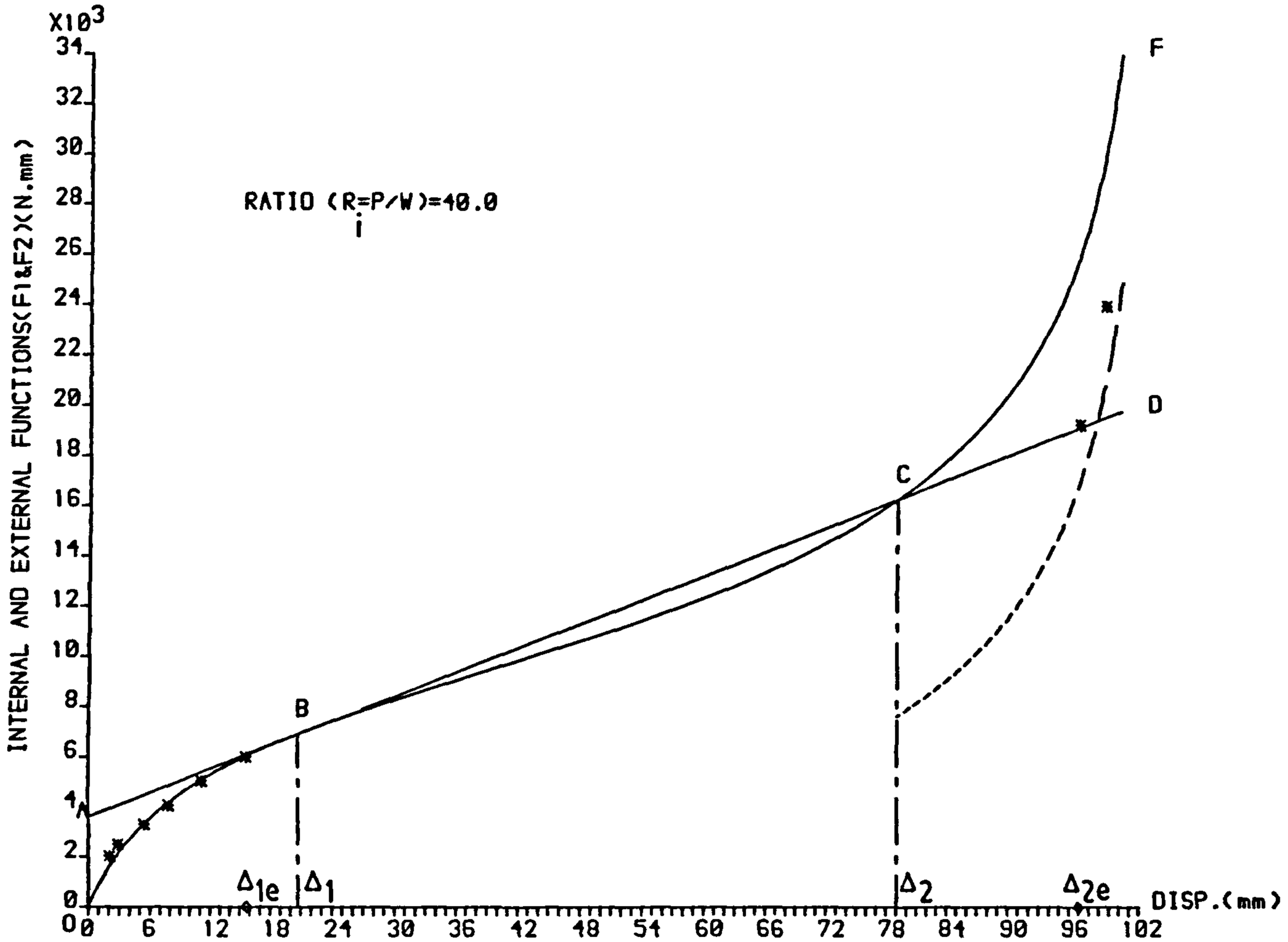

TOP DISPLACEMENT AGAINST INTERNAL AND EXTERNAL FUNCTIONS(F1&F2)

STABILITY OF FRAME

TWO STORIES

CHORD LENGTH(lo)=520.0 (mm)

INITIAL RISE:

Aoc(1)=20.0 Aot(1)= 95.0 (mm)

Aoc(2)=20.0 Aot(2)= 85.0 (mm)

COMPARISON BETWEEN THEORETICAL AND EXPERIMENTAL RESULTS

——THEORETICAL RESULTS

* EXPERIMENTAL RESULTS

— —THEORETICAL RESULTS WITH TENSILE BRACINGS ONLY

LOADS:

Wcr= 3.994 (N)

Pcr= 159.760 (N)

FIG.(5-49)

STABILITY OF FRAME

TWO STORIES

CHORD LENGTH(lo)=520.0 (mm)

INITIAL RISE:

Aoc(1)=20.0 Aot(1)= 95.0 (mm)

Aoc(2)=20.0 Aot(2)= 95.0 (mm)

COMPARISON BETWEEN THEORETICAL

AND EXPERIMENTAL RESULTS

____THEORETICAL RESULTS

* EXPERIMENTAL RESULTS

_ _THEORETICAL RESULTS WITH

TENSILE BRACINGS ONLY

LOADS:

Wcr= 3.915 (N)

Pcr= 156.599 (N)

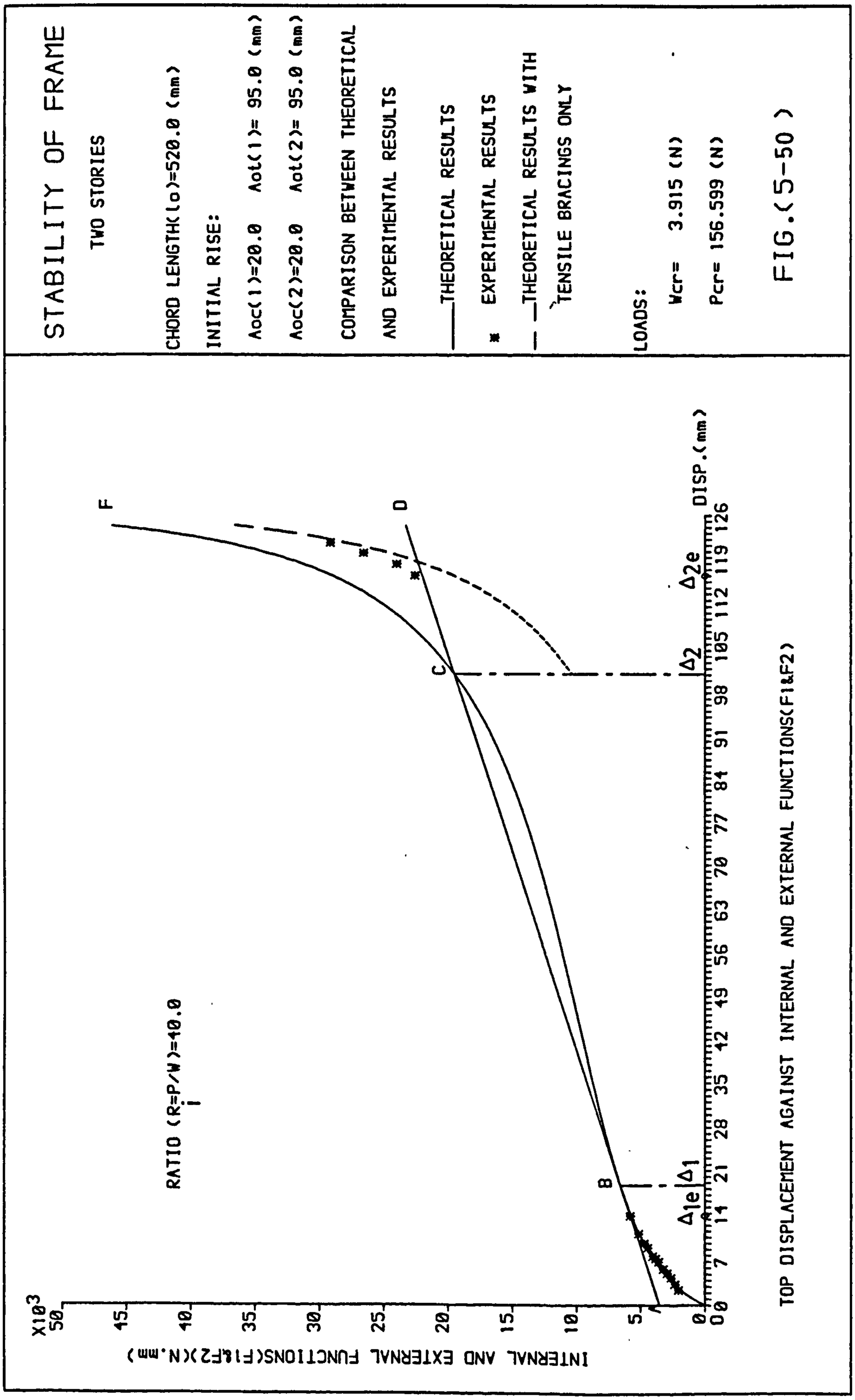

FIG.(5-50)

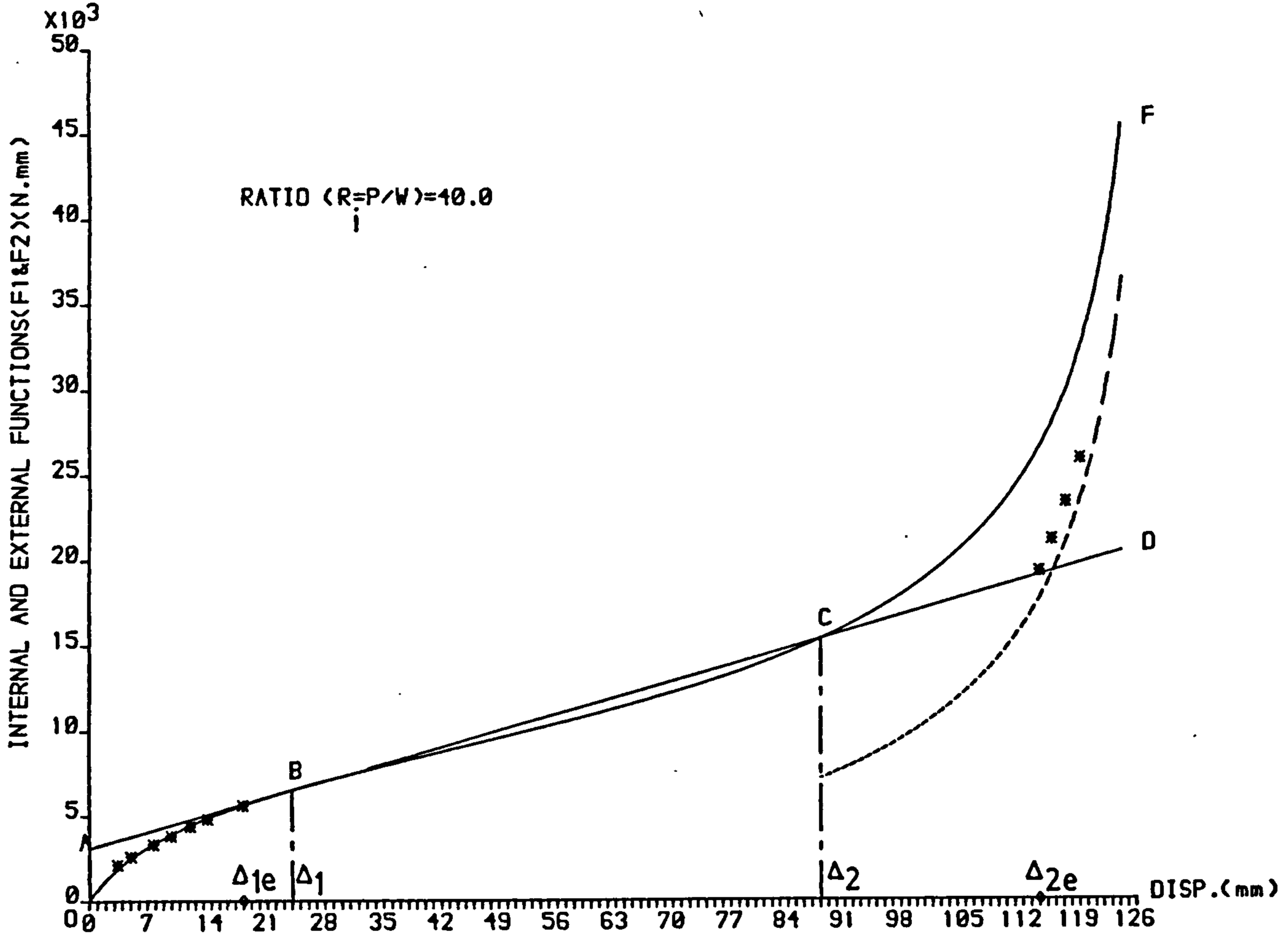

TOP DISPLACEMENT AGAINST INTERNAL AND EXTERNAL FUNCTIONS(F1&F2)

STABILITY OF FRAME

TWO STORIES

CHORD LENGTH(lo)=520.0 (mm)

INITIAL RISE:

Aoc(1)=20.0 Aot(1)= 95.0 (mm)

Aoc(2)=30.0 Aot(2)= 95.0 (mm)

COMPARISON BETWEEN THEORETICAL AND EXPERIMENTAL RESULTS

———THEORETICAL RESULTS

* EXPERIMENTAL RESULTS

— —THEORETICAL RESULTS WITH TENSILE BRACINGS ONLY

LOADS:

Wcr= 3.437 (N)

Pcr= 137.482 (N)

FIG.(5-51)

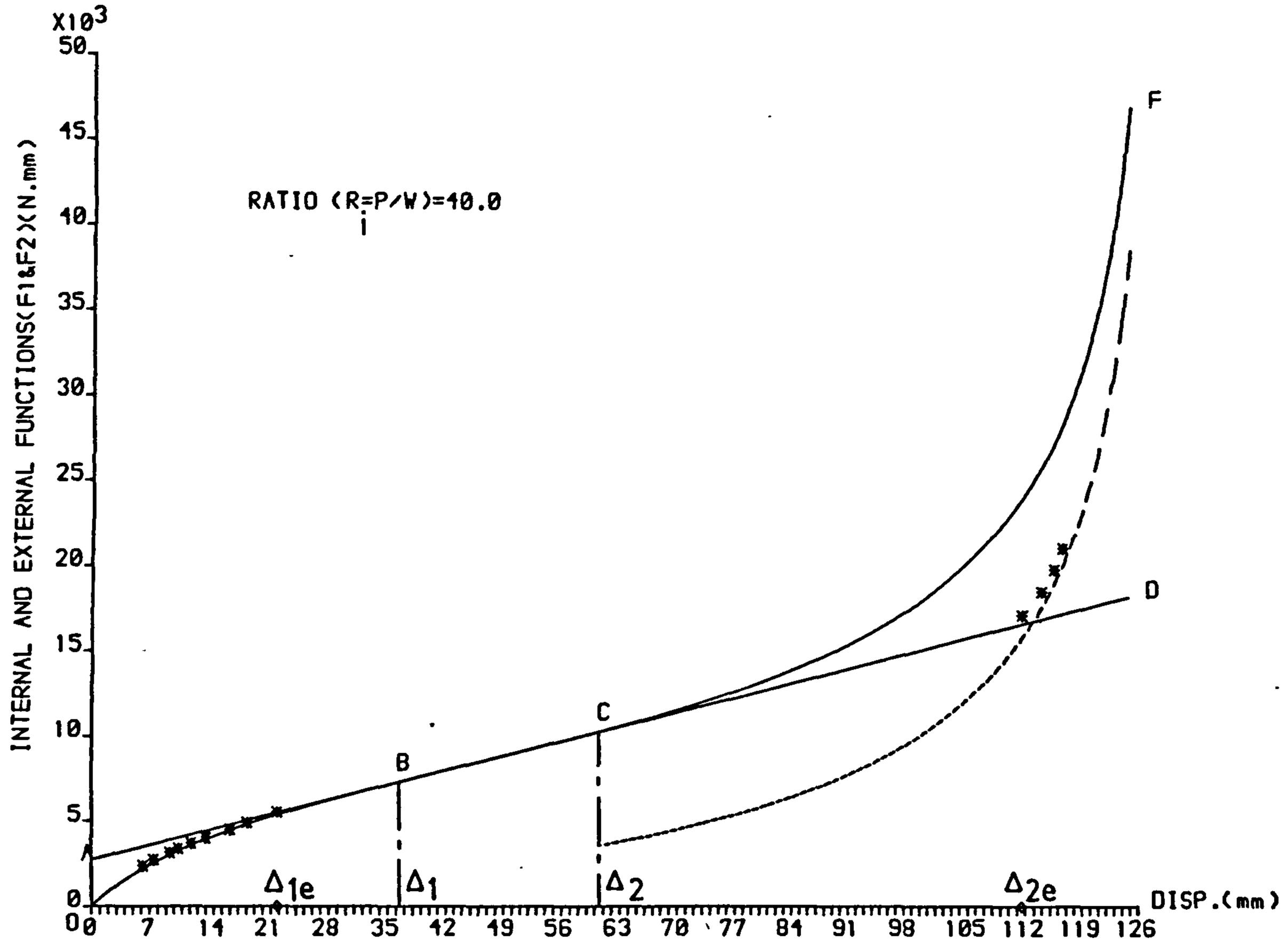

TOP DISPLACEMENT AGAINST INTERNAL AND EXTERNAL FUNCTIONS(F1&F2)

STABILITY OF FRAME

TWO STORIES

CHORD LENGTH(lo)=520.0 (mm)

INITIAL RISE:

Aoc(1)=30.0 Aot(1)= 95.0 (mm)

Aoc(2)=30.0 Aot(2)= 95.0 (mm)

COMPARISON BETWEEN THEORETICAL AND EXPERIMENTAL RESULTS

——THEORETICAL RESULTS

* EXPERIMENTAL RESULTS

— —THEORETICAL RESULTS WITH TENSILE BRACINGS ONLY

LOADS:

Wcr= 3.042 (N)

Pcr= 121.665 (N)

FIG.(5-52)

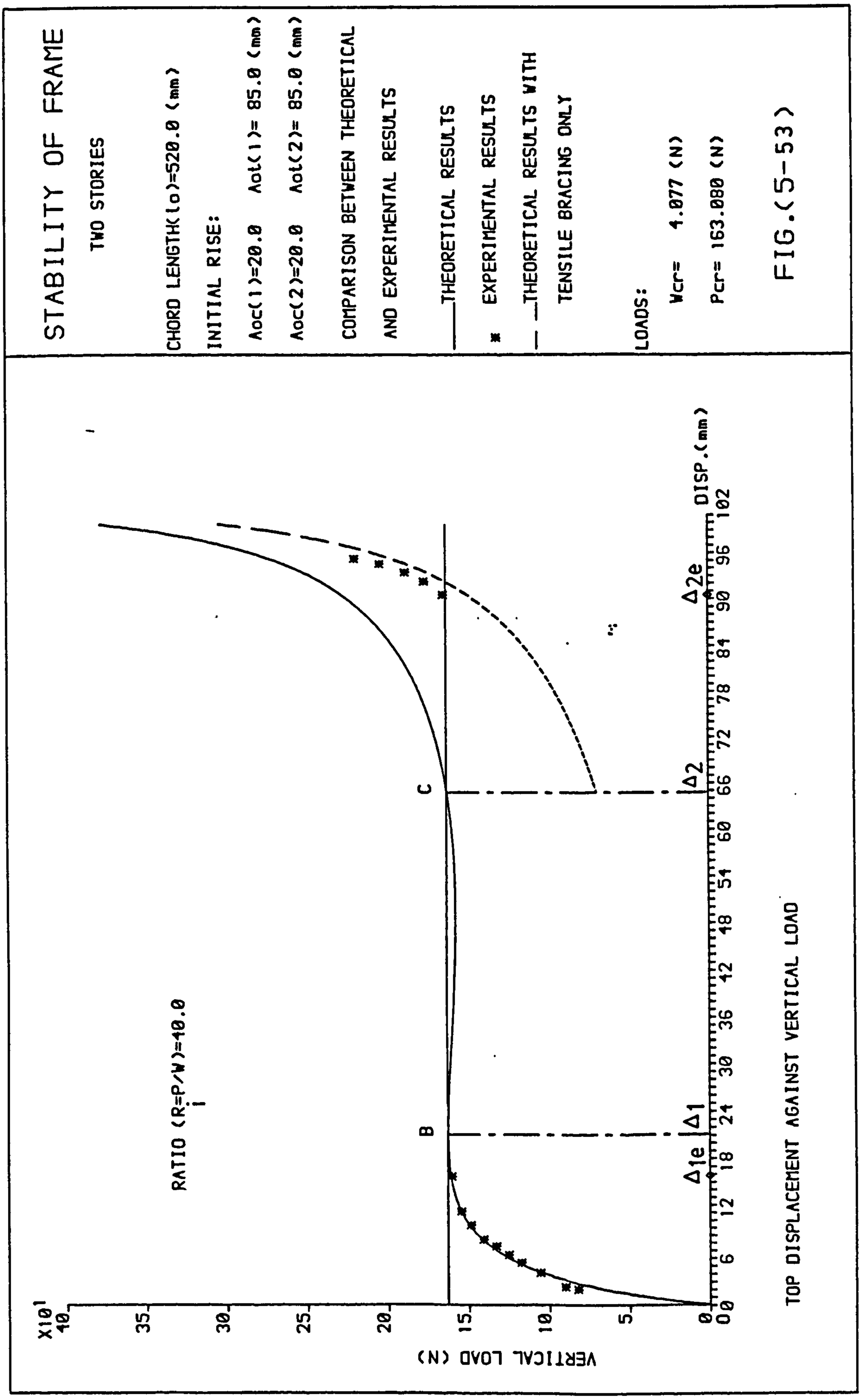
STABILITY OF FRAME
TWO STORIES
CHORD LENGTH(lo)=520.0 (mm)
INITIAL RISE:
Aoc(1)=20.0 Aol(1)= 85.0 (mm)
Aoc(2)=20.0 Aol(2)= 85.0 (mm)
COMPARISON BETWEEN THEORETICAL
AND EXPERIMENTAL RESULTS
THEORETICAL RESULTS
EXPERIMENTAL RESULTS
THEORETICAL RESULTS WITH
TENSILE BRACING ONLY
LOADS:
Wcr= 4.077 (N)
Pcr= 163.080 (N)
FIG.(5-53)
RATIO (R=P/W)=10.0
Δ2e DISP.(mm)
72 78 84 90 96 102
C
B
Δ2
Δ1
21 30 36 12 48 54 60 66
Δ1e
0 6 12 18
TOP DISPLACEMENT AGAINST VERTICAL LOAD
VERTICAL LOAD (N)
X10¹
40 35 30 25 20 15 10 5 0
00

STABILITY OF FRAME

TWO STORIES

CHORD LENGTH(lo)=520.0 (mm)

INITIAL RISE:

Aoc(1)=20.0 Aol(1)= 95.0 (mm)

Aoc(2)=20.0 Aol(2)= 85.0 (mm)

COMPARISON BETWEEN THEORETICAL AND EXPERIMENTAL RESULTS

——THEORETICAL RESULTS

* EXPERIMENTAL RESULTS

— —THEORETICAL RESULTS WITH TENSILE BRACING ONLY

LOADS:

Wcr= 3.994 (N)

Pcr= 159.760 (N)

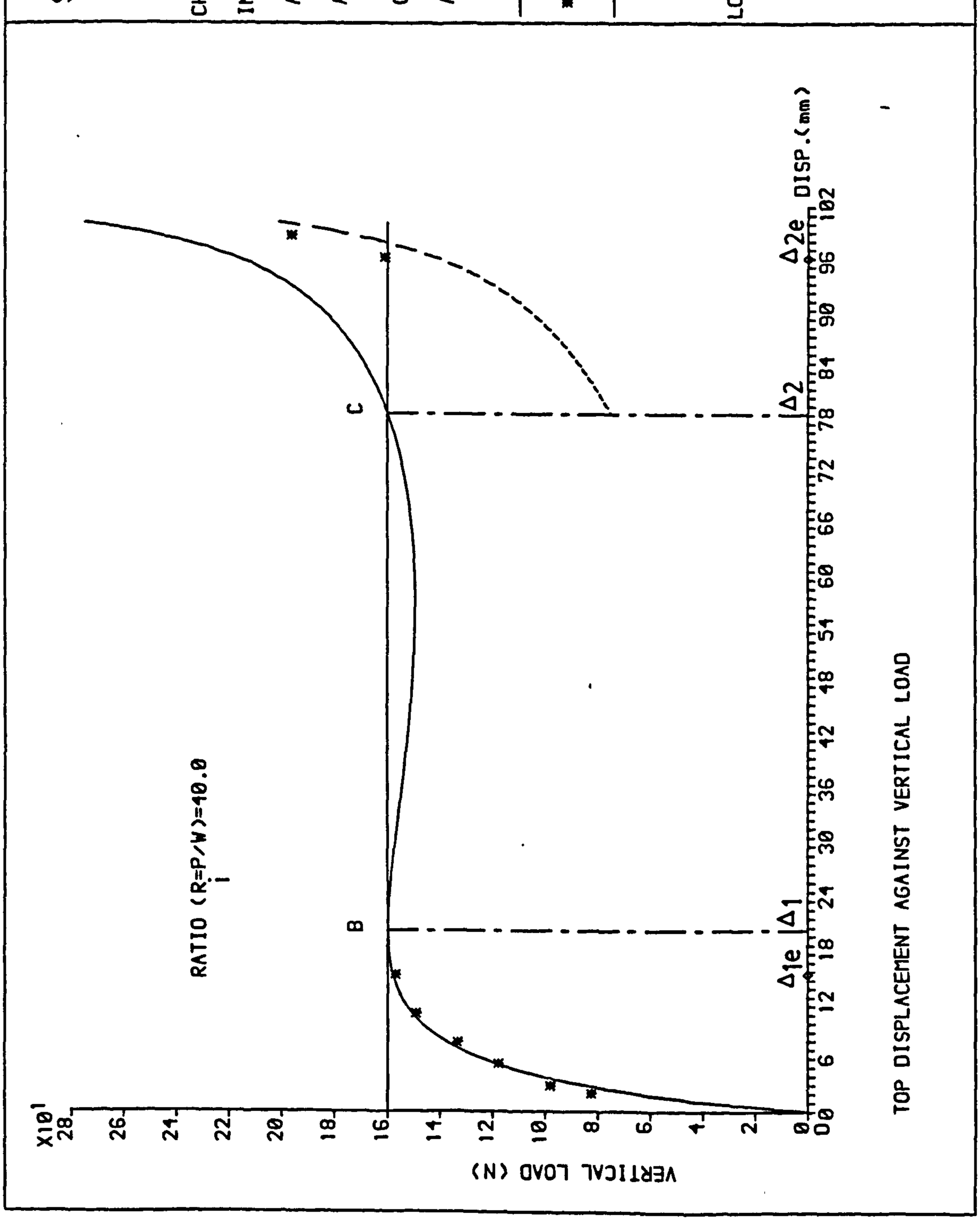

FIG.(5-54)

STABILITY OF FRAME

TWO STORIES

CHORD LENGTH(o)=520.0 (mm)

INITIAL RISE:

Aoc(1)=20.0 Aol(1)= 95.0 (mm)

Aoc(2)=20.0 Aol(2)= 95.0 (mm)

COMPARISON BETWEEN THEORETICAL AND EXPERIMENTAL RESULTS

____ THEORETICAL RESULTS

* EXPERIMENTAL RESULTS

_ _ THEORETICAL RESULTS WITH TENSILE BRACING ONLY

LOADS:

Wcr= 3.915 (N)

Pcr= 156.599 (N)

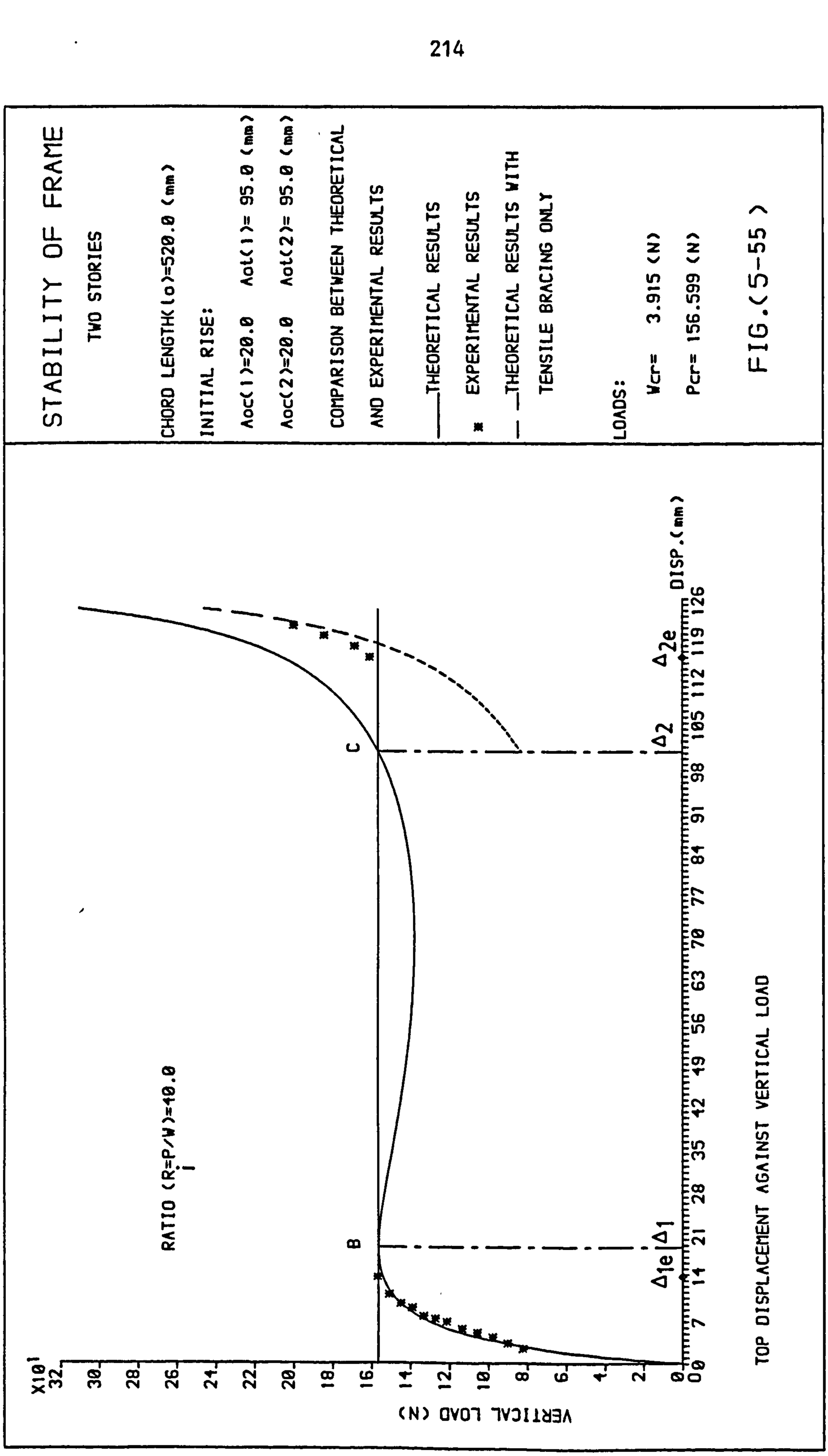

FIG.(5-55)

STABILITY OF FRAME

TWO STORIES

CHORD LENGTH(lo)=520.0 (mm)

INITIAL RISE:

Aoc(1)=20.0 Aot(1)= 95.0 (mm)

Aoc(2)=30.0 Aot(2)= 95.0 (mm)

COMPARISON BETWEEN THEORETICAL

AND EXPERIMENTAL RESULTS

——THEORETICAL RESULTS

* EXPERIMENTAL RESULTS

— —THEORETICAL RESULTS WITH

TENSILE BRACING ONLY

LOADS:

Wcr= 3.437 (N)

Pcr= 137.482 (N)

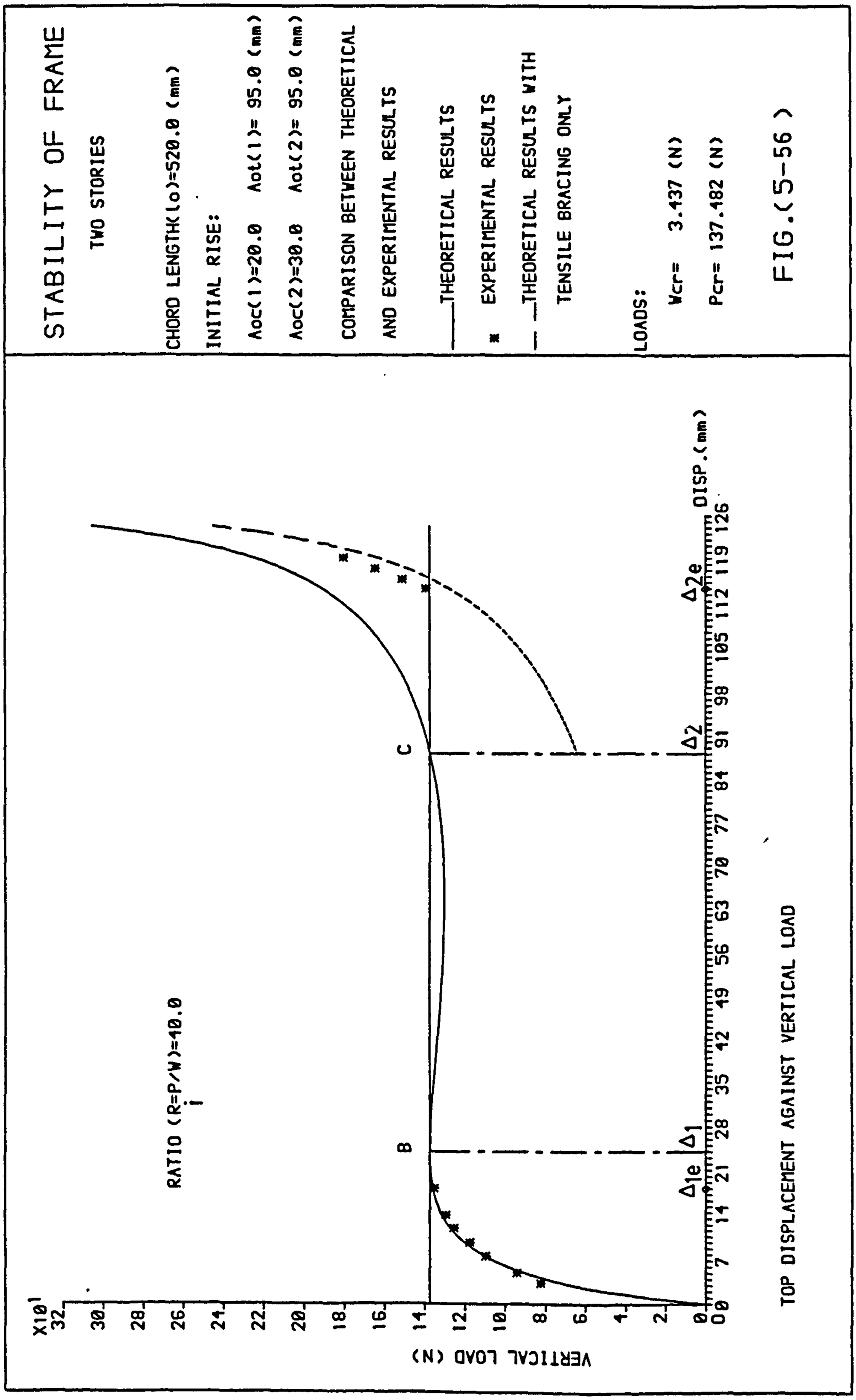

FIG.(5-56)

STABILITY OF FRAME

TWO STORIES

CHORD LENGTH(lo)=520.0 (mm)

INITIAL RISE:

Aoc(1)=30.0 Aol(1)= 95.0 (mm)

Aoc(2)=30.0 Aol(2)= 95.0 (mm)

COMPARISON BETWEEN THEORETICAL

AND EXPERIMENTAL RESULTS

——THEORETICAL RESULTS

* EXPERIMENTAL RESULTS

— —THEORETICAL RESULTS WITH

TENSILE BRACING ONLY

LOADS:

Wcr= 3.042 (N)

Pcr= 121.665 (N)

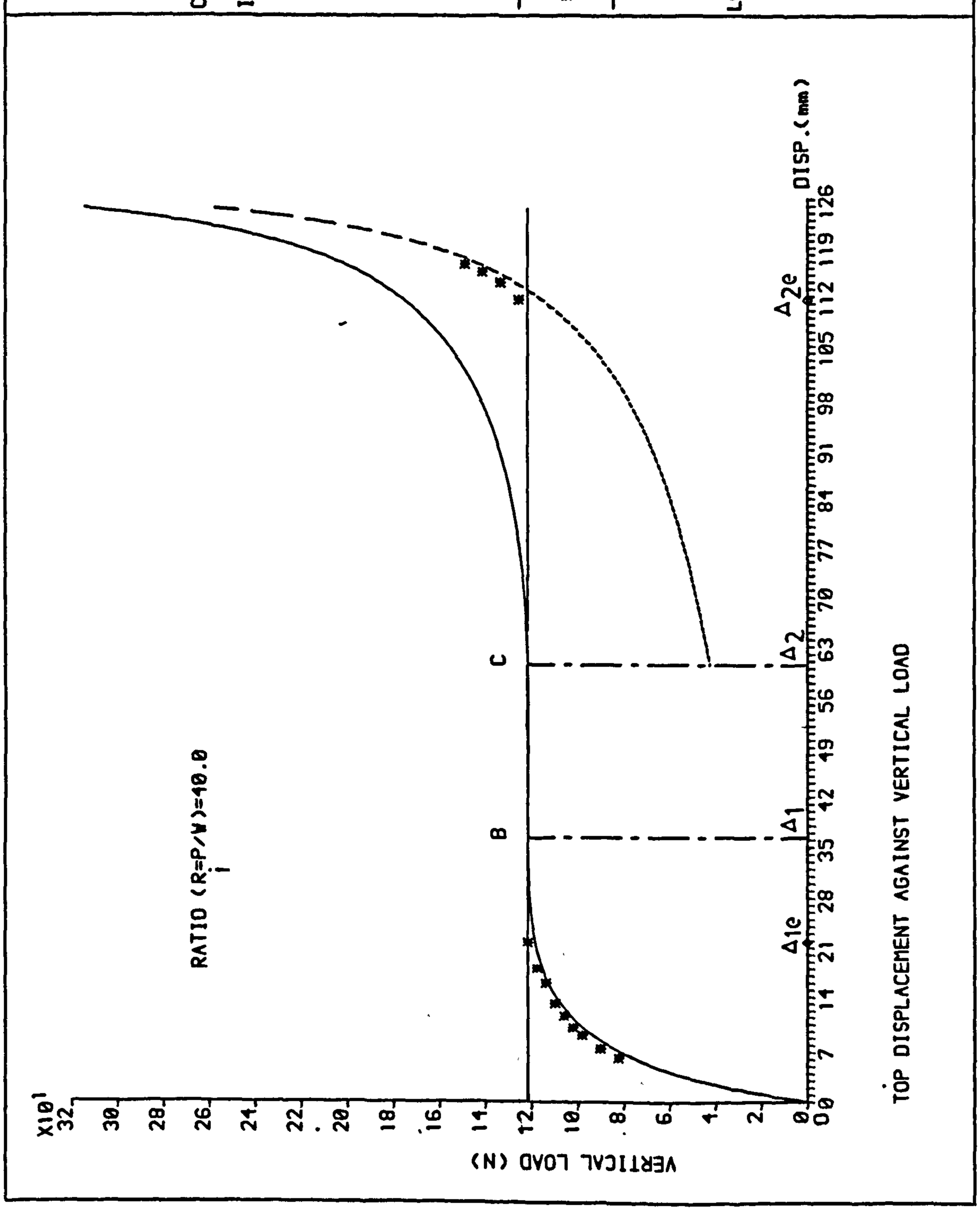

FIG.(5-57)

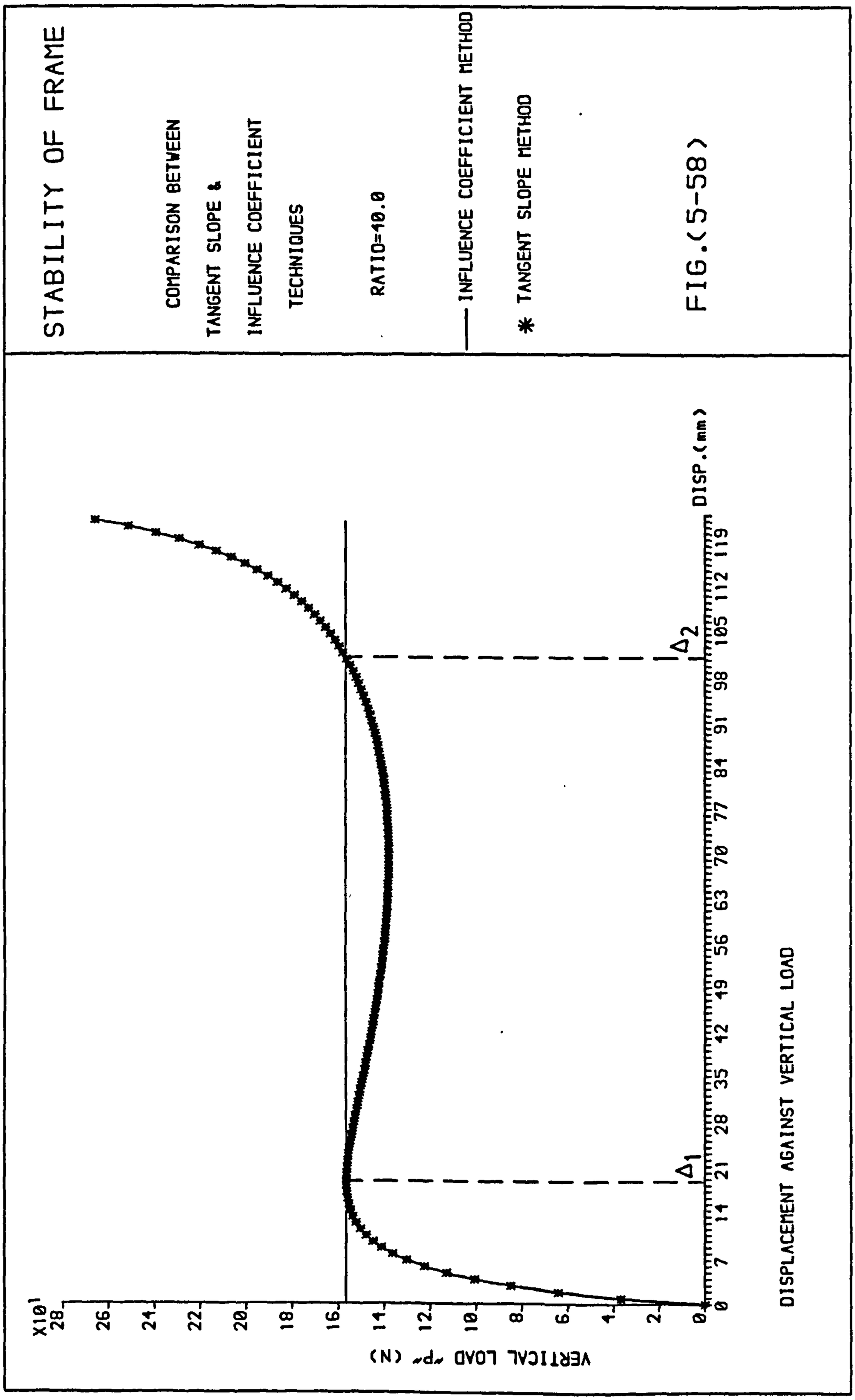
STABILITY OF FRAME
COMPARISON BETWEEN
TANGENT SLOPE &
INFLUENCE COEFFICIENT
TECHNIQUES
RATIO=10.0
— INFLUENCE COEFFICIENT METHOD
* TANGENT SLOPE METHOD
DISP.(mm)
Δ2
Δ1
DISPLACEMENT AGAINST VERTICAL LOAD
VERTICAL LOAD "P" (N)
X10¹

FIG.(5-58)

PART TWO

DYNAMIC INVESTIGATION

CHAPTER SIX

DYNAMIC BEHAVIOUR OF FRAME STRUCTURE RESTRAINED BY NON-LINEAR RESTRAINTS

6.1 Introduction

It is seen from the static investigation, explained in Chapters 3 and 4, that the applied loads, on the structures restrained by curved bracing systems, are functions not only of the lateral displacement "Δ" but also of the non-linear stiffnesses of the side bracings. Also the stability of the equilibrium position depends on the relationship between the combined applied loads "P & W" and also on the lateral displacement "Δ" .

If the structure is considered at any equilibrium state of the combined loads "P & W", where P is less than the critical load P_{cr1} (i.e. the vertical load at the onset of the transient instability region), and then a small disturbance is applied, such as deflecting the structure and then releasing it, the effect of this disturbance is to set up a very small oscillation about the equilibrium position. Alternatively if the vertical load "P" is very close to the critical load "P_{cr1}", then a small disturbance is sufficient to cause large deflections after the structure accelerates towards the end of the region of transient instability, which is the position of static stable equilibrium. The effect of this dynamic disturbance is investigated in this chapter.

In this chapter two numerical dynamic analyses are adopted to study the general dynamic buckling behaviour of this type of structure. The technique of analysis is based on the solution of differential equations of vibration for an idealized structure in which the inertial properties (mass, rotatory inertia etc.) of members are

assumed to be lumped at discrete points on the geometry of the structure. The lumped masses are assumed to be connected by massless members with the original elastic properties. The lumped-mass idealization is not a new concept. It has been widely used for the dynamic analysis of various structures [94,104,114]. In the case of framed structures it is convenient to assume the inertial properties of the members to be located at the joints.

The first method of numerical analysis consists of a step-by-step numerical integration of the equation of vibration. The method has been presented by Chaudhury [101] and the basic technique of this procedure is summarized in this chapter.

The second is a new method of numerical analysis consisting of a step-by-step numerical differentiation of the solution of the equation of motion, using a constant displacement interval.

6.2 Dynamic Equations for Idealized Frame Structures

The number of displacement components which must be considered in order to represent the effect of all significant inertial forces of a structure may be termed the number of dynamic degrees of freedom of the structure. In this section the structures to be considered are single degree of freedom (SDOF) systems.

6.2.1 Dynamic Equations for a Single Column Restrained by Curved Bracing System

The dynamic analysis of sway motion of the column shown in Fig. (6.1.a) can be simplified by considering the idealized structure of Fig. (6.1.b), in which half of the mass of the column is assumed

to be lumped at the top of the column. The forces acting at the top of the column are indicated in Fig. (6.1.c), and the general non-linear characteristic of the equivalent spring is shown in Fig. (6.4.a).

The response of the structure, at any instant of time "t" to the dynamic excitation can be obtained by taking moments about the hinged base "A" of the column, and will be represented by the following free (damped) vibration equation, where the applied load is constant and independent of time.

$$m \ddot{X}_d . H'' + C_d \dot{X}_d . H'' + (K\Delta . H'' - F_s) - PX_d = 0 \qquad (6.1)$$

Equation (6.1) can be written in the following form:

$$F_I . H'' + F_D . H'' + R_s - F_{2d} = 0 \qquad (6.2)$$

where,

$$F_I = m \ddot{X}_d \qquad (6.3)$$

F_I is the inertia force,

$$F_D = C_d \dot{X}_d \qquad (6.4)$$

in which C_d is the damping coefficient.

$\dot{X}_d$ is the velocity at the instant time.

The damping coefficient "C_d" can be written in the form such that:

$$C_d = \zeta_d . C_c \qquad (6.5)$$

where,

ζ_d is the damping ratio

and $C_c = 2\ m\omega$ (6.6)

C_c is the critical damping coefficient [94,101],

and ω is the natural frequency.

$$R_s = K.\Delta.H'' - F_s \quad (6.7)$$

F_s is the elastic force in the equivalent spring for the combined bracing system at the onset of the transient instability. The term K represents the non-linear stiffness properties corresponding to the lateral displacement "Δ" at the instant of time.

Also, $F_{2d} = P.X_d$ (6.8)

The term $P.X_d$ is dependent on time, where X_d is varying with time.

Equation (6.1) gives the relationships of the instantaneous values of acceleration, velocity, internal forces and external forces, at the top of the column. The internal forces are the elastic forces, in the elastic curved bracings. These forces can be calculated from the instantaneous values of the displacements by the static analysis explained in Chapters 2 and 3.

Since equation (6.1) is a non-linear second order differential equation, the principle of superposition does not hold. Thus, for example, the displacement "Δ" cannot be divided into two parts, i.e. the static displacement and dynamic displacement. The important class of non-linearity related to the displacement "Δ" is the geometric non-linearity. This has been, already explained in the previous chapters.

6.2.2 Dynamic Equations for a Multistorey Framework Restrained by Diagonal Curved Bracing System

In section (6.2.1) Newton's second law of motion is employed in deriving the equations of motion of the SDOF system shown in Fig. (6.1). This procedure may be used as the basis for developing a formula for evaluating the equation of motion of the general non-linear SDOF system shown in Fig. (6.2). In this system the lumped mass "m" is assumed at the top beam level of the frame. The constant horizontal force "W" is, also, applied at the top level of the frame.

The general non-linear characteristics of this system have been discussed in Chapters 3, 4 and 5.

Now the dynamic response of the idealized system shown in Fig. (6.2.b), at any instant of time "t", can be represented by the following non-linear differential equation.

$$F_I \cdot H'' + F_D \cdot H'' + R_s - F_{2d} = 0 \qquad (6.9)$$

where,

$$F_I = m \ddot{X}_d \qquad (6.10)$$

in which m is the equivalent mass acting at the top of the equivalent idealized structure, Fig. (6.2.b).

F_D represents the damping force,

and

$$R_s = F_1 - F_s \qquad (6.11)$$

The term R_s is a function of the characteristics of the bracing of each storey in the framework. The term F_1 in Eq. (6.11) can be

determined from equation (3.44) derived previously in chapter three, section (3.4.1). The term F_1 is dependant on the displacement "Δ_T" at the top of the frame which consequently depends on the time "t". The term F_s represents the elastic force in the equivalent spring for the combined bracing system at the onset of transient instability. Also,

$$F_{2d} = P.X_d \qquad (6.12)$$

in which the load P is the gravity force applied at the top of the structure. The displacement"X_d"is measured from the onset of transient instability (i.e $X_d = \Delta_T - \Delta_1$).

6.3 Numerical Methods for Dynamic Analysis

Two numerical procedures are employed to investigate the dynamic response of frameworks. The basic technique of analysis in the first procedure is a general step-by-step method of integration of the equation of motion, using a constant time interval. The basic technique of analysis in the second procedure is a general step-by-step method of differentiation of the equations of motion, using a constant displacement interval.

6.3.1 Constant Time Interval Method

Probably the most powerful technique for dynamic non-linear analysis is the step-by-step integration procedure [101,104,112,114,121], using a constant time interval. The technique consists of using the calculated values of acceleration, velocity and displacement at any instant of time "t" to calculate the magnitude of these variables at the instant $t+\delta t$ after a small interval of time "δt". This is

done in conjunction with the equation of vibration of the system, starting with the known initial values of velocity and displacement. The non-linear nature of the system is accounted for by calculating new properties appropriate to the current deformed state at the beginning of each time increment. The complete response is obtained by using the velocity and displacement computed at the end of one computational interval as the initial conditions for the next interval, thus,the process may be continued step-by-step from the initiation of loading to any desired time, approximating the non-linear behaviour as a sequence of successively changing linear systems.

The basic assumption of the process is that described by Newmark [114] in which the acceleration varies linearly during each time increment, while the properties of the system remain constant during this interval. The motion of the mass during the time interval is indicated graphically in Fig. (6.3) together with the equations (6.13), (6.14) and (6.15) for the assumed linear variation of the acceleration and the corresponding quadratic and cubic variations of the velocity and displacement respectively. The velocity can be evaluated by integrating Eq. (6.13) with respect to the variable"τ". Also, the displacement can be determined by integrating the resultant Eq. (6.14) with respect to the variable "τ".

It may be seen from Eq. (6.1) or (6.9) that in order to calculate the acceleration "$\ddot{X}_d$" at any instant of time "t" it is necessary to know the velocity "$\dot{X}_d$" and the displacement "X_d" at

$$\ddot{X}_{d(\tau)} = \ddot{X}_{d(t)} + \frac{\Delta \dddot{X}_d}{\delta t} \cdot \tau \qquad (6.13)$$

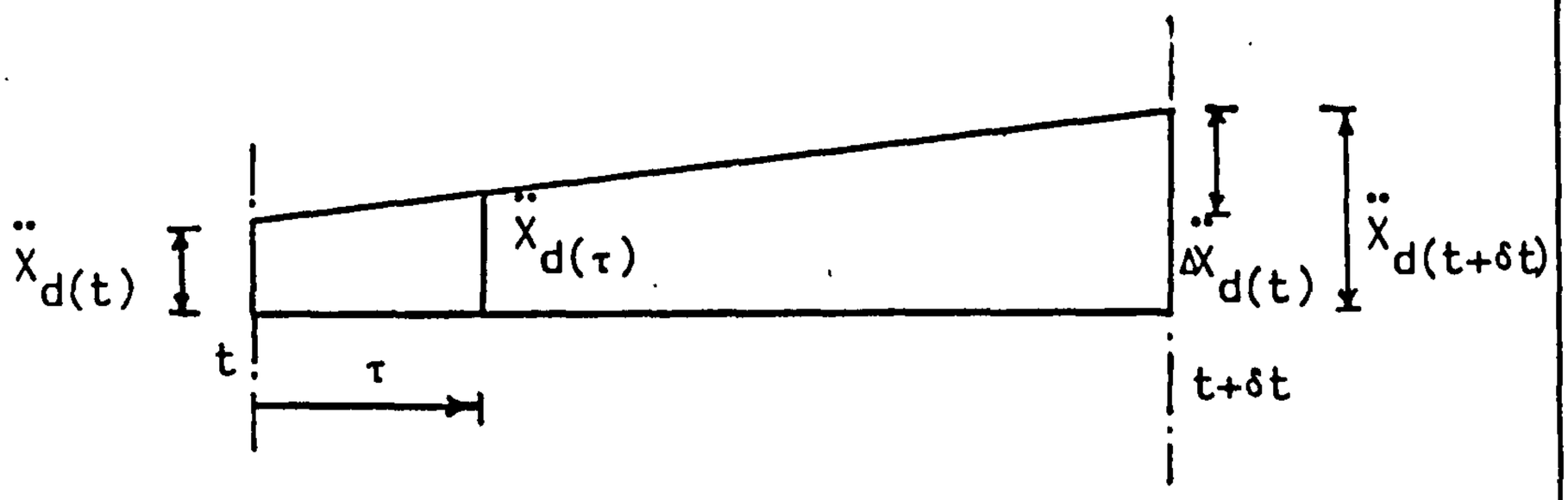

(a) Acceleration (linear)

$$\dot{X}_{d(\tau)} = \dot{X}_{d(t)} + \ddot{X}_{d(t)} \cdot \tau + \frac{\Delta \ddot{X}_d}{\delta t} \cdot \frac{\tau^2}{2} \qquad (6.14)$$

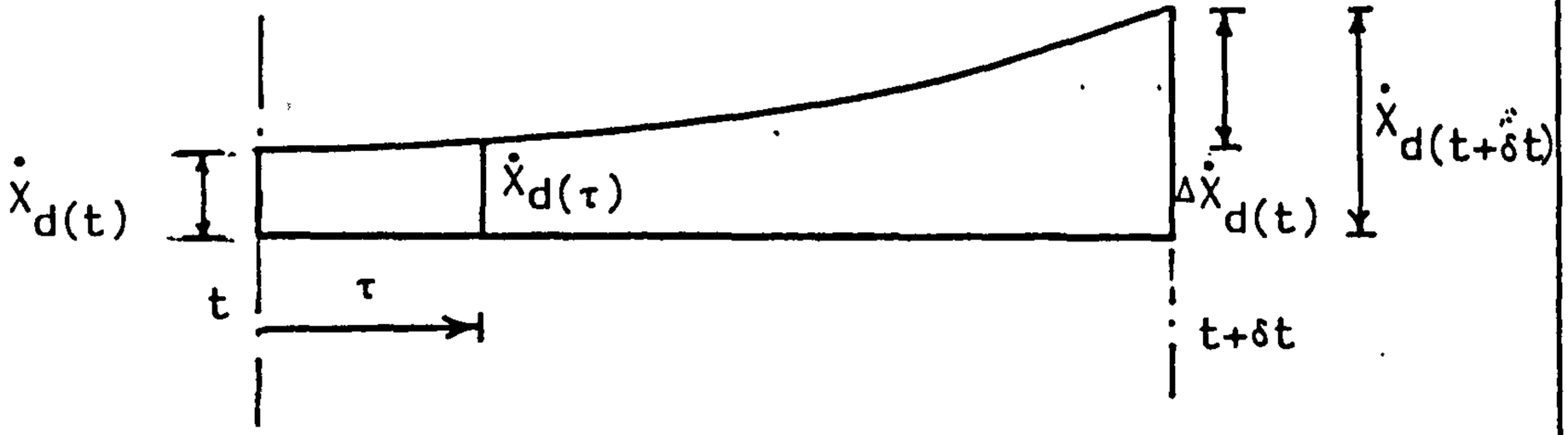

(b) Velocity (quadratic)

$$X_{d(\tau)} = X_{d(t)} + \dot{X}_{d(t)} \cdot \tau + \ddot{X}_{d(t)} \cdot \frac{\tau^2}{2} + \frac{\Delta \ddot{X}_d}{\delta t} \cdot \frac{\tau^3}{6} \qquad (6.15)$$

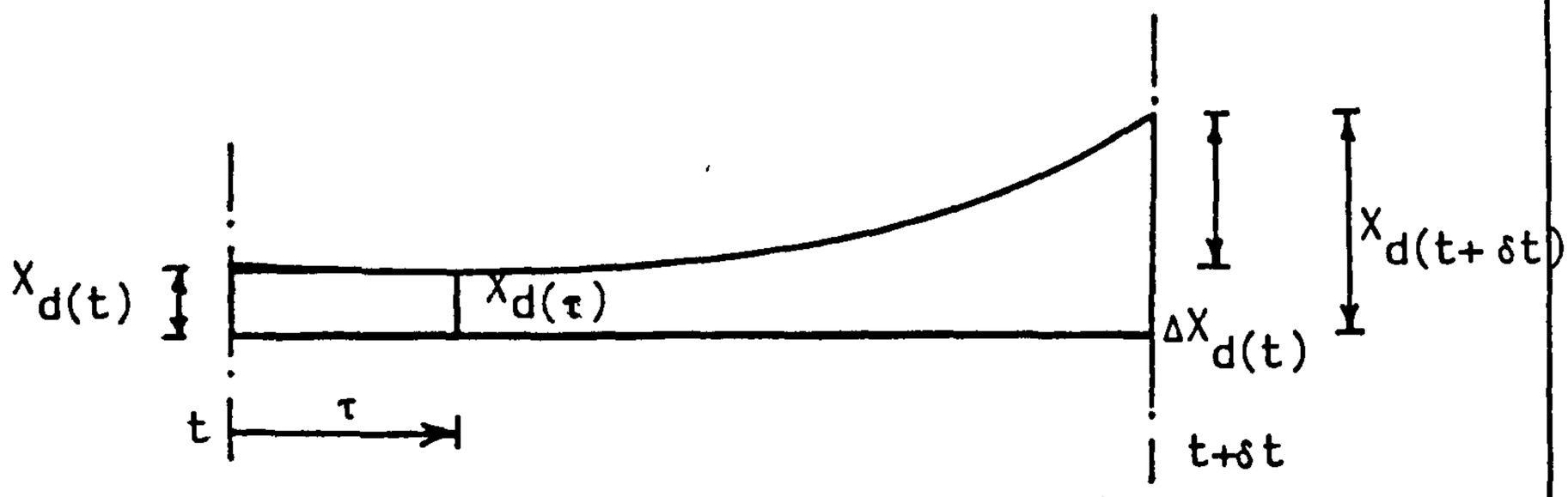

(c) Displacement (cubic)

Fig.(6-3): Assumption of Linear Acceleration

that instant. Newmark [114] suggested that the velocity and the displacement can be obtained from the assumption of linear variation of acceleration within the small time interval "δt", i.e. at the end of the interval ($\tau = \delta t$) or at time "$t+\delta t$" , the values of the velocity "$\dot{X}_{d\,(t+\delta t)}$" and the displacement "$X_{d\,(t+\delta t)}$" can be evaluated from Eq. (6.12) and (6.13) and this will lead to the following equations:

$$\dot{X}_{d(t+\delta t)} = \dot{X}_{d(t)} + \ddot{X}_{d(t)} \cdot \delta t + \frac{\Delta \dddot{X}_d}{2} \cdot \delta t$$

or

$$\dot{X}_{d(t+\delta t)} = \dot{X}_{d(t)} + \frac{\delta t}{2} \left(2\ddot{X}_{d(t)} + \Delta \ddot{X}_d\right)$$

Substituting the value $\ddot{X}_{d(t+\delta t)}$ instead of $\ddot{X}_{d(t)} + \Delta \ddot{X}_d$ (this can be seen from the linear variation of the acceleration in Fig. (6.3.a)) the following is obtained:

$$\dot{X}_{d(t+\delta t)} = \dot{X}_{d(t)} + \frac{\delta t}{2} \left[\ddot{X}_{d(t)} + \ddot{X}_{d(t+\delta t)}\right] \qquad (6.16)$$

and

$$X_{d(t+\delta t)} = X_{d(t)} + \delta t . \dot{X}_{d(t)} + \frac{1}{3} \delta t^2 \ddot{X}_{d(t)} + \frac{1}{6} \delta t^2 \ddot{X}_{d(t+\delta t)}$$

.... (6.17)

Newmark [114] presented the following general expression for displacement,

$$X_{d(t+\delta t)} = X_{d(t)} + \delta t . \dot{X}_{d(t)} + \left(\frac{1}{2} - \beta\right) \delta t^2 . \ddot{X}_{d(t)} + \beta \delta t^2 . \ddot{X}_{d(t+\delta t)}$$

.... (6.18)

where β is a parameter which takes into account the nature of variation of acceleration within the interval δt. A value of $\beta = \frac{1}{6}$ represents a linear variation in which case equation (6.18) becomes exactly the same as equation (6.17).

Newmark [114] proposed an iterative procedure in which an initial value for $\ddot{X}_{d(t+\delta t)}$ has to be assumed in order to calculate $\dot{X}_{d(t+\delta t)}$ and $X_{d(t+\delta t)}$ which are then used to obtain $X_{d(t+\delta t)}$ from the dynamic equilibrium equations (6.1) and (6.9). This cycle of calculation is repeated by using the value of $\ddot{X}_{d(t+\delta t)}$ calculated in the previous cycle until the values in subsequent cycles agree within the desired degree of accuracy. It was also suggested that the value of δt could be adjusted in order to make the calculation of linear variations converge within three cycles.

Chaudhury [101] proposed another procedure in which a small time interval $\frac{1}{2}\delta t$ is considered in Eqs. (6.16) and (6.17) in order to calculate $\dot{X}_{d(t+\delta t)}$ and $X_{d(t+\delta t)}$ which are then used to obtain $\ddot{X}_{d(t+\delta t)}$ from the dynamic equilibrium equations (6.1) and (6.9). It is convenient to use this procedure as the basis of the analysis to solve the non-linear differential equation (6.9). According to this assumption the following relationships are obtained from Eqs. (6.17) and (6.16)

$$X_{d(t+\delta t)} = X_{d(t+\frac{1}{2}\delta t)} + \frac{\delta t}{2} \cdot \dot{X}_{d(t+\frac{1}{2}\delta t)} + \frac{1}{12}\,\delta t^2 \cdot \ddot{X}_{d(t+\frac{1}{2}\delta t)}$$

$$+ \frac{1}{24}\,\delta t^2\,\ddot{X}_{d(t+\delta t)} \qquad (6.19)$$

$$X_{d(t+\frac{1}{2}\delta t)} = X_{d(t)} + \frac{\delta t}{2} \cdot \dot{X}_{d(t)} + \frac{1}{12}\,\delta t^2 \cdot \ddot{X}_{d(t)}$$

$$+ \frac{1}{24}\,\delta t^2 \cdot \ddot{X}_{d(t+\delta t/2)} \qquad (6.20)$$

$$\dot{X}_{d(t+\frac{1}{2}\delta t)} = \dot{X}_{d(t)} + \frac{1}{4}\,\delta t\,[\ddot{X}_{d(t)} + \ddot{X}_{d(t+\frac{1}{2}\delta t)}] \qquad (6.21)$$

$$\dot{X}_{d(t)} = \dot{X}_{d(t-\frac{1}{2}\delta t)} + \frac{1}{4}\,\delta t\,[\ddot{X}_{d(t-\frac{1}{2}\delta t)} + \ddot{X}_{d(t)}] \qquad (6.22)$$

Eliminating $X_{d(t+\frac{1}{2}\delta t)}$ and $\dot{X}_{d(t)}$ from Eqs (6.19), (6.20) and (6.21), the following is obtained,

$$X_{d(t+\delta t)} = X_{d(t)} + \delta t \cdot \dot{X}_{d(t+\frac{1}{2}\delta t)} - \frac{1}{24}\,[\ddot{X}_{d(t)} - \ddot{X}_{d(t+\frac{1}{2}\delta t)}]\,\delta t^2$$

.... (6.23)

Substituting Eq. (6.22)into Eq.(6.21), then,

$$\dot{X}_{d(t+\frac{1}{2}\delta t)} = \dot{X}_{d(t-\frac{1}{2}\delta t)} + \frac{1}{4}\,\delta t\,[\ddot{X}_{d(t-\frac{1}{2}\delta t)} + 2\ddot{X}_{d(t)} + \ddot{X}_{d(t+\frac{1}{2}\delta t)}]$$

.... (6.24)

Assuming the acceleration to vary linearly from the instant $(t-\frac{1}{2}\delta t)$ to the instant $(t+\frac{1}{2}\delta t)$, Eq. (6.24) can be written as:

$$\dot{X}_{d(t+\frac{1}{2}\delta t)} = \dot{X}_{d(t-\frac{1}{2}\delta t)} + \delta t \cdot \ddot{X}_{d(t)} \qquad (6.25)$$

Chaudhury [101] pointed out that the expression in Eq. (6.25) has the same accuracy as that for a time interval $\frac{1}{2}\delta t$, although it

actually uses the interval δt , and that expression (6.25) is as accurate as expression (6.16) for a linear variation of acceleration. He also pointed out that the pair of expressions (6.23) and (6.25) have a higher degree of accuracy than the pair (6.17) and (6.16).

Finally according to the assumption of linear acceleration within a small time interval "δt" and the pair of expressions (6.23) and (6.25) the velocity, displacement and the acceleration at any instant of time can be calculated.

The velocity $\dot{X}_{d(t+\frac{1}{2}\delta t)}$ can be calculated by Eq. (6.23) from the values of $\dot{X}_{d(t-\frac{1}{2}\delta t)}$ and $\ddot{X}_{d(t)}$ calculated in the previous step of time interval.

The restoring forces in each curved member can be calculated from the equations of static equilibrium mentioned in chapters 2 and 3, with the following approximations:

$$X_{d(t+\delta t)} = X_{d(t)} + \delta t \cdot \dot{X}_{d(t+\frac{1}{2}\delta t)} \tag{6.26}$$

The acceleration $\ddot{X}_{d(t+\delta t)}$ can be calculated by Eqs. (6.1) or (6.9), with the following approximation:

$$\dot{X}_{d(t+\delta t)} = \dot{X}_{d(t+\frac{1}{2}\delta t)} \tag{6.27}$$

The displacement $X_{d(t+\delta t)}$ can be calculated from equation (6.23).

For the initial cycle (t=0) of calculation equation (6.25) has to be slightly modified so that:

$$\dot{X}_{d(\frac{1}{2}\delta t)} = \dot{X}_{d(0)} + \frac{\delta t}{2} \cdot \ddot{X}_{d(0)} \qquad (6.28)$$

where, $\dot{X}_{d(0)}$ is the given initial value and $\ddot{X}_{d(0)}$ can be calculated from equations (6.1) or (6.9) with the given initial values of $X_{d(0)}$.

Chaudhury [101] pointed out that the error involved in the approximation (6.26) in conjunction with the original Eq. (6.23) is $\pm \frac{1}{24} \delta t^2 [\ddot{X}_{d(t)} - \ddot{X}_{d(t+\delta t)}]$ is expected to be of a very small order in the dynamic analysis. This error is not cumulative, as $X_{d(t+\delta t)}$ is calculated by equation (6.23) after $\ddot{X}_{d(t+\delta t)}$ has been obtained.

However the approximation (6.27) affects the damping force which is, in any case, dependent on the accuracy of assessment of the coefficient of damping in an actual structure.

6.3.2 Constant Displacement Interval Method

The technique employed in this section is simple in concept but has been found to yield excellent results with relatively little computational effort.

The procedure consists of using the calculated values of displacement, velocity and acceleration at any position $X_{d(i)}$ to calculate the magnitude of these variables at the position $X_{d(i+1)} = X_{d(i)} + \delta X_i$, after the small interval of displacement "δX_i". The procedure starts with the known initial values of velocity "$\dot{X}_{d(0)}$"

and displacement "$X_{d(0)}$". The non-linear nature of the system is accounted for by calculating new properties appropriate to the current deformed state at the beginning of each displacement increment. The complete response is obtained using the velocity and acceleration computed at the end of one computational interval as the initial conditions for the next interval, thus the process may continue step-by-step to any desired time.

The maximum displacement, can be defined as the limit where the velocity is zero. The procedure depends on approximating the non-linear behaviour of the structure as a sequence of successively changing linear systems as shown in Fig. (6.4.b).The basic assumption of the process is that the characteristics of the system remain constant during each displacement increment. The dynamic response of the system is evaluated for a series of small displacement increments "δX", generally taken of equal length for computational convenience.

The condition of dynamic equilibrium is established at the beginning and the end of each interval, and the motion of the system during the displacement increment is evaluated approximately on the basis of an assumed response mechanism.

6.3.2.1 Incremental Equation of Equilibrium

Figure (6.4) illustrates a typical non-linear force-displacement curve for F_1 expressed as a function of displacement "Δ" . (The symbol F_1 will be used when referring to a function of time or to function of displacement). The equation of motion of the system may be

written at displacements $X_{d(i)}$ and $X_{d(i+1)} = X_{d(i)} + \delta X_i$ as follows:

$$m \ddot{X}_{d(i)} \cdot H'' + C_d \dot{X}_{d(i)} \cdot H'' + R_{s(i)} - P \cdot X_{d(i)} = 0 \qquad (6.29)$$

and

$$m \ddot{X}_{d(i+1)} \cdot H'' + C_d \dot{X}_{d(i+1)} \cdot H'' + R_{s(i)} + K^* \cdot \delta X_i$$

$$- P X_{d(i)} - P \cdot \delta X_i = 0 \qquad (6.30)$$

Since Eq. (6.30) is satisfied at both $X_{d(i)}$ and $X_{d(i+1)}$ i.e. in the range of the small interval δX_i only, therefore it can be considered that the value of $X_{d(i)}$ is constant while δX_i is the variable. According to this, the values $\dot{X}_{d(i+1)}$ and $\ddot{X}_{d(i+1)}$ can be written in the following forms:

$$\dot{X}_{d(i+1)} = \frac{d}{dt} [X_{d(i)} + \delta X_i] = \delta \dot{X}_{d(i)}$$

and

$$\ddot{X}_{d(i+1)} = \frac{d^2}{dt^2} [X_{d(i)} + \delta X_i] = \delta \ddot{X}_{d(i)}$$

where $X_{d(i)}$ is independent of the time "t" during the displacement interval δX_i. Therefore Eq. (6.30) can be rearranged, such that:

$$m \cdot \delta \ddot{X}_{d(i)} \cdot H'' + C_d \cdot \delta \dot{X}_{d(i)} \cdot H'' + (K^* - P) \cdot \delta X_i = P \cdot X_{d(i)} - R_{s(i)}$$

or

$$\delta \ddot{X}_{d(i)} + \frac{C_d}{m} \delta \dot{X}_{d(i)} + \left(\frac{K^* - P}{m \cdot H''} \right) \delta X_i = \frac{P \cdot X_{d(i)} - R_{s(i)}}{m \cdot H''} \quad \ldots\ldots(6.31)$$

then $$\delta\ddot{X}_{d(i)} + \frac{C_d}{m} \cdot \delta\dot{X}_{d(i)} + \omega^2 \cdot \delta X_i = C_{11} \qquad (6.32)$$

where, $$\omega^2 = \frac{K^* - P}{m.H''} \qquad (6.33)$$

ω is the circular frequency or the angular velocity of the motion during the small displacement interval δX_i, measured in radians per unit of time ;.

and $$K^* = \frac{F_{1(i+1)} - F_{1(i)}}{\delta X_i} \qquad (6.34)$$

in which K^* is the secant slope indicated in Fig. (6.4.b) .

This slope can be determined after the evaluation of $F_{1(i)}$ and $F_{1(i+1)}$ at the beginning and the end of the small displacement interval δX_i. The values $F_{1(i)}$ and $F_{1(i+1)}$ can be easily determined as explained in the static investigations, chapter 3,

Also $$C_{11} = \frac{P.X_{d(i)} - R_{s(i)}}{m.H''} \qquad (6.35)$$

in which the constant value "C_{11}" is independent on the time during the small displacement interval.

Equation (6.32) represents the incremental form of the equilibrium equation of the motion during the small displacement interval "δX_i".

6.3.2.2 Solution of the Incremental Equation of Motion

The general solution of Eq. (6.32) [9] consists of two functions. The first is called the complementary function (u). The second is called the particular function (v).

The general solution δX_i is given by the sum of the complementary function "u" and the particular integral "v", i.e.

$$\delta X_i = u + v \tag{6.36}$$

Let u+v be substituted for δX_i in Eq. (6.32), then the equation becomes:

$$\frac{d^2}{dt^2}(u+v) + \frac{C_d}{m} \cdot \frac{d}{dt}(u+v) + \omega_i^2(u+v) = C_{11}$$

i.e. $$\frac{d^2u}{dt^2} + \frac{d^2v}{dt^2} + \frac{C_d}{m} \cdot \frac{du}{dt} + \frac{C_d}{m} \cdot \frac{dv}{dt} + \omega^2 u + \omega^2 v = C_{11}$$

i.e. $$\left(\frac{d^2u}{dt^2} + \frac{C_d}{m} \cdot \frac{du}{dt} + \omega^2 u\right) + \left(\frac{d^2v}{dt^2} + \frac{C_d}{m} \cdot \frac{dv}{dt} + \omega^2 v\right) = C_{11}$$

Let v be any solution of the equation (6.32) such that:

$$\frac{d^2v}{dt^2} + \frac{C_d}{m} \cdot \frac{dv}{dt} + \omega^2 v = C_{11} \tag{6.37}$$

This would mean that:

$$\frac{d^2u}{dt^2} + \frac{C_d}{m} \cdot \frac{du}{dt} + \omega^2 u = 0 \tag{6.38}$$

The solution of Eq. (6.38) is dependent on the sign of the value ω^2, therefore there are two possibilities:

<u>The first</u> : If ω^2 is positive, the solution of Eq. (6.38)[104] is in the following form:

$$u = e^{-\xi_d \omega t} [A_1 \sin(\omega_D t) + B_1 \cos(\omega_D t)] \tag{6.39}$$

or

$$u = e^{-\zeta_d \omega t} \cdot A. \cos(\omega_D t - \theta) \tag{6.40}$$

where,

$$\zeta_d = \frac{C_d}{C_c}$$

in which, $\zeta_d < 1$ (6.41)

and $$\omega_D = \omega \sqrt{1 - \zeta_d^2} \tag{6.42}$$

ω_D is the damping vibration frequency.

The second : if ω^2 is negative, then Eq. (6.38) will be in the following form:

$$\frac{du^2}{dt^2} + \frac{C_d}{m} \cdot \frac{du}{dt} - \omega^2 u = 0 \tag{6.43}$$

The solution of Eq. (6.43) [104] can be written such that:

$$u = e^{-\zeta_d \omega t} [\, D \cosh(\omega_D t) + G \sinh(\omega_D t)] \tag{6.44}$$

where, $$\omega_D = \omega \sqrt{\zeta_d^2 - 1} \tag{6.45}$$

in which, $\zeta_d > 1$ (6.46)

The unknown constants A and θ in Eq. (6.40) or D and G in Eq. (6.44) can be obtained from the given boundary conditions at the beginning of each interval.

The particular integral "v" in the general solution of the differential equation of motion, depends usually on the type of the

function on the right side of the equation. The right side of Eq. (6.32) is a constant and therefore the solution can be obtained by trying $v=v_o$, where v_o is a constant. Substitution of $v=v_o$ in Eq. (6.37) gives:

$$\frac{d^2}{dt^2}(v_o) + \frac{C_d}{m}\cdot\frac{d}{dt}(v_o) + \omega^2 v_o = C_{11} \qquad (6.47)$$

since, $\frac{d}{dt}(v_o) = \frac{d^2}{dt^2}(v_o) = 0$

Then, $\omega^2 v_o = C_{11}$

i.e. $v=v_o = \frac{C_{11}}{\omega^2}$ (ω^2 is positive) (6.48)

or $v=v_o = \frac{-C_{11}}{\omega^2}$ (ω^2 is negative) (6.49)

Finally the general solution of the equation (6.32) is given by the sum of the equations (6.40) and (6.48) or equations (6.44) and (6.49).

i.e. if ω^2 is positive, then:

$$\delta X_i = e^{-\zeta_d \omega t} \cdot A. \cos(\omega_D t - \theta) + \frac{C_{11}}{\omega^2} \qquad (6.50)$$

and if ω^2 is negative, then:

$$\delta X_i = e^{-\zeta_d \omega t} [D \cosh(\omega_D t) + G \sinh(\omega_D t)] - \frac{C_{11}}{\omega^2} \qquad (6.51)$$

Since Eq. (6.50) or (6.51) represents the displacement δX_i , therefore the velocity $\delta \dot{X}_{d(i)}$ at any instant within the range of the displacement interval, can be determined by differentiating Eq. (6.50) or (6.51), as follows:

$$\delta\dot{X}_{d(i)} = -A.\ e^{-\zeta_d \omega t}[\omega_D \sin(\omega_D t-\theta) + \zeta_d\ \omega\cos(\omega_D t-\theta)] \qquad (6.52)$$

in which $\omega^2 > 0$

and

$$\delta\dot{X}_{d(i)} = e^{-\zeta_d \omega t}[(D\omega_D - \zeta_d \omega G)\ \sinh(\omega_D t) + (G\omega_D - \zeta_d D\omega)\ \cosh(\omega_D t)]$$

.... (6.53)

in which $\omega^2 < 0$

Also the acceleration $\delta\ddot{X}_{d(i)}$ may be determined by differentiating Eq. (6.52) or (6.53), such that:

If $\omega^2 > 0$, then:

$$\delta\ddot{X}_{d(i)} = A\ e^{-\zeta_d \omega t}[(\zeta_d{}^2\omega^2-\omega_D{}^2)\ \cos(\omega_D t-\theta) + 2\zeta_d \omega\omega_D \sin(\omega_D t-\theta)]$$

....(6.54)

and if $\omega^2 < 0$, then:

$$\delta\ddot{X}_{d(i)} = e^{-\zeta_d \omega t}\{[D\omega_D{}^2-\zeta_d \omega\dot{\omega}_D(D+G)+\zeta_d{}^2 D\omega^2]\ \cosh(\omega_D t)$$

$$+[G\omega_D{}^2-\zeta_d \omega\omega_D(D+G) + \zeta_d{}^2\omega^2 G]\ \sinh(\omega_D t)\} \qquad (6.55)$$

The unknown constants A and θ in the Eqs. (6.50), (6.52) and (6.54) or D and G in the Eqs. (6.51), (6.53) and (6.55) depend on the initial conditions of the system at the beginning of each increment of the displacement.

The initial conditions at the onset of each increment are:

$$t=0\ ,\ \delta X_i = 0,\quad \delta\dot{X}_{d(i)} = \dot{X}_{d(i)} \text{ and } \delta\ddot{X}_{d(i)} = \ddot{X}_{d(i)} \tag{6.56}$$

where $\dot{X}_{d(i)}$ and $\ddot{X}_{d(i)}$ are the velocity and the acceleration at the onset of the interval δX_i . The value "t" represents the variation of time during the displacement interval. This time varies between zero, at the onset of the interval, and t at the end of this interval.t will not be constant during each interval.

The unknown constants A and θ in Eqs. (6.50), (6.52) and (6.54) can be determined by substituting the conditions of Eq. (6.56) into Eqs. (6.50) and (6.52).

i.e. at, t=0

$$\delta X_i = 0 = A\cos(\theta) + \frac{C_{11}}{\omega^2} \tag{6.57}$$

$$\text{and} \qquad \delta\dot{X}_{d(i)} = \dot{X}_{d(i)} = A.\dot{\omega}_D.\sin(\theta) - A.\zeta_d.\omega.\cos(\theta) \tag{6.58}$$

$$\text{hence,} \qquad \frac{-\dot{X}_{d(i)}.\omega^2}{C_{11}} = \omega_D\tan(\theta) - \zeta_d.\omega$$

$$\text{therefore,} \quad \theta = \tan^{-1}\left[\frac{-\dot{X}_{d(i)}.\omega^2}{C_{11}.\omega_D} + \zeta_d\,.\,\frac{\omega}{\omega_D}\right] \tag{6.59}$$

Substituting this expression of θ into Eq. (6.57) leads to the expression for the constant A.

$$A = \frac{-C_{11}}{\omega^2\cos(\theta)} \tag{6.60}$$

The increments of the time "t" at the end of the displacement interval can be determined by using the following equation:

$$f(t) = A\, e^{-\zeta_d \omega t} \cdot \cos(\omega_D t - \theta) \div \frac{C_{11}}{\omega^2} - \delta X_i = 0 \qquad (6.61)$$

where θ and A are defined in Eqs. (6.59) and (6.60) respectively.

The value of t can be obtained from Eq. (6.61) by using iterative methods [9]. One of these methods is explained in chapter 2, section (2.2.1.3).

In the case of negative ω^2, the unknown constants D and G in Eqs. (6.51), (6.53) and (6.55) can be determined as follows:

$$\text{At} \quad t=0 \; ; \qquad \delta X_i = 0 = D - \frac{C_{11}}{\omega^2}$$

$$\text{then,} \qquad D = \frac{C_{11}}{\omega^2} \qquad (6.62)$$

$$\text{Also,} \qquad \dot{\delta X}_{d(i)} = \dot{X}_{d(i)} = G.\omega_D - \zeta_d.D.\omega$$

$$\text{then,} \qquad G = \frac{\dot{X}_{d(i)} + \zeta_d.D.\omega}{\omega_D} \qquad (6.63)$$

Substituting Eq. (6.62) into Eq. (6.63), therefore,

$$G = \frac{\omega \dot{X}_{d(i)} + \zeta_d C_{11}}{\omega.\omega_D} \qquad (6.64)$$

The increment of the time "t" at the end of the displacement inverval, can be determined by using the following equation:

$$f(t) = e^{-\zeta_d \omega t}[D.\cosh(\omega_D.t) + G.\sinh(\omega_D.t)] - \frac{C_{11}}{\omega^2} - \delta X_i = 0$$

.... (6.65)

where D and G are defined in Eqs. (6.62) and (6.64) respectively.

The value of t can be obtained from Eq. (6.65), again, by the iterative method explained in Chapter 2,section (2.2.1.3).

Finally, in the case of ω^2 being positive, the velocity and the acceleration at the end of the interval "δX_i" can be obtained by substituting Eqs. (6.59), (6.60) and the result from Eq. (6.61) into Eqs. (6.52) and (6.54) respectively. While, in the case of ω^2 being negative, substitution of Eqs. (6.62), (6.64) and the result from Eq. (6.65) into Eqs. (6.53) and (6.55) give the velocity and the acceleration at the end of this interval.

The values of the velocity and the acceleration at the end of any interval "δX_i" are then used as initial conditions for the next interval.

6.3.2.3 Summary of The Constant Displacement Interval Method

For any given displacement increment "δX_i" and the damping ratio "ζ_d" , the analysis procedure consists of the following operations:

1) Initial velocity and displacement values "$\dot{X}_{d(i)}$ and $X_{d(i)}$" are known, either from values at the end of the preceding increment or as initial conditions of the problem.

2) With these values and the specified non-linear properties of the structure, the stiffness K^* for the interval,as well as the elastic functions$F_{1(i)}$ and $F_{1(i+1)}$ are found.

3) The circular frequency of the motion "ω", and the constant C_{11} are calculated from the Eqs. (6.33) and (6.35) respectively. Also the sign of the value ω^2 can be determined, therefore, the damped frequency "ω_D" can also be determined from Eq. (6.42) or (6.45).

4) The unknown values of θ and A or D and G are computed from the Eqs. (6.59) and (6.60) or (6.62) and (6.64) respectively.

5) The initial acceleration can be obtained from Eq. (6.54) or (6.55) by substituting the value of t=0.

6) The time increment "t" during the given displacement interval can be calculated from Eq. (6.61) in the case of ω^2 being positive or from Eq. (6.65) in the case of ω^2 being negative.

7) Finally the velocity and the acceleration at the end of the increment are obtained from the Eqs. (6.52) and (6.54), if ω^2 is positive or the Eqs. (6.53) and (6.55) if ω^2 is negative, respectively.

Also the displacement and the time at the end of the interval are given by $X_{d(i+1)} = X_{d(i)} + \delta X_i$ and $t_{i+1} = t_i + t$.

When step (7) has been completed, the analysis for the displacement increment is finished and the entire processes can be carried on consecutively for any desired time and the complete response history of the structure can be evaluated.

The accuracy of this step-by-step method will depend on the length of the displacement increment "δX_i".

The displacement increment must be short enough to permit a reliable representation of the behaviour of the sturcture.

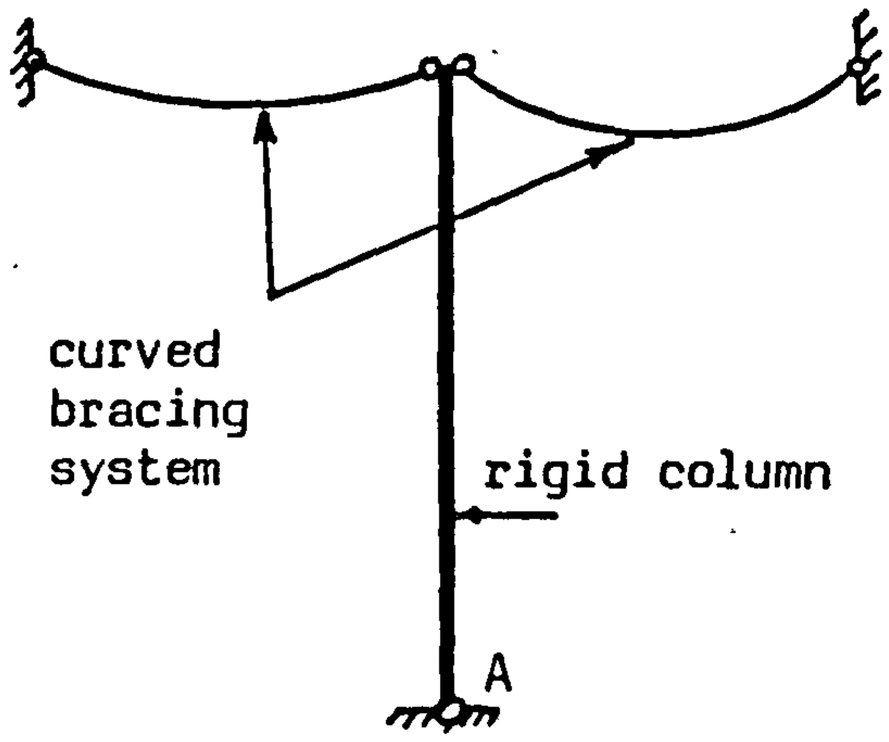

(a) Actual structure

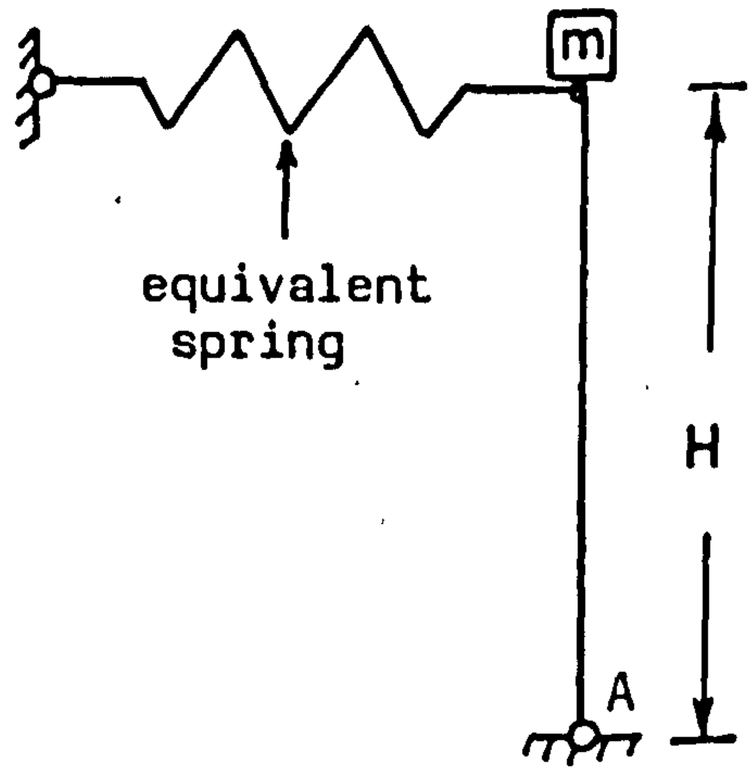

(b) Idealized structure

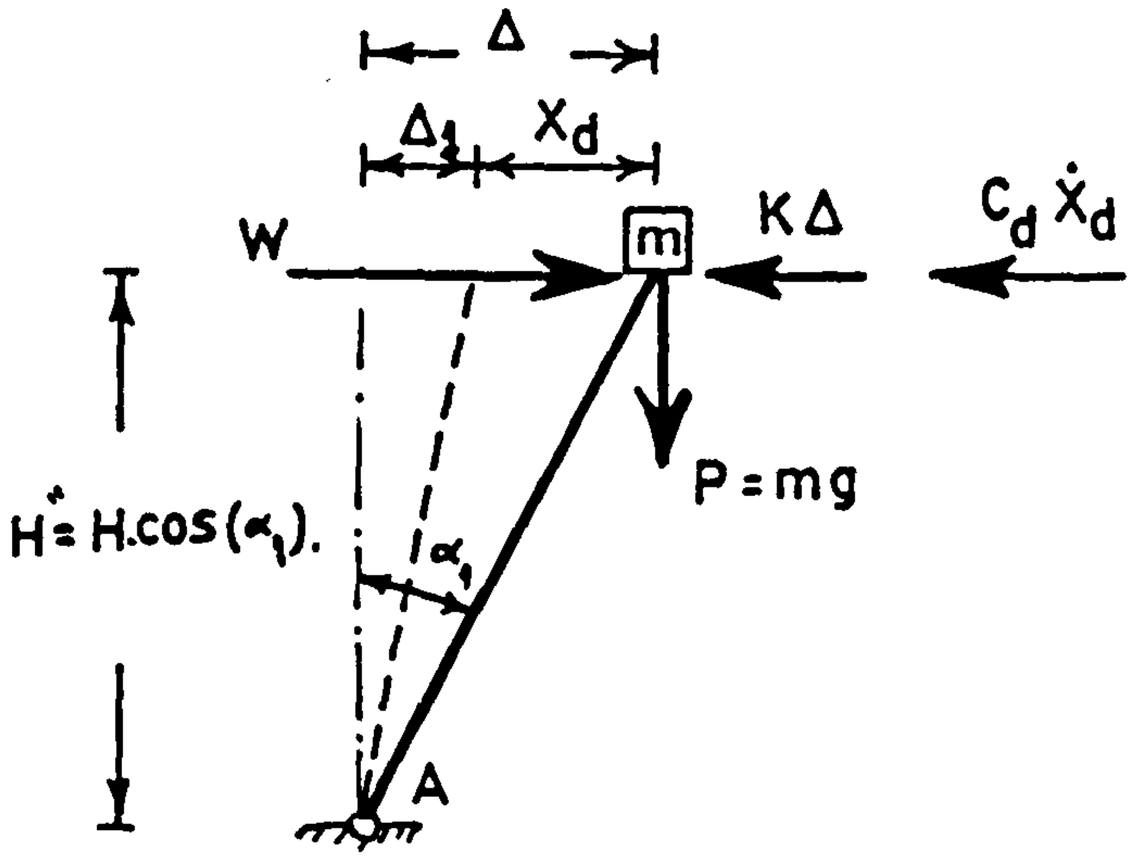

(c) External and internal forces

Fig.(6-1): A System of Single Degree of Freedom

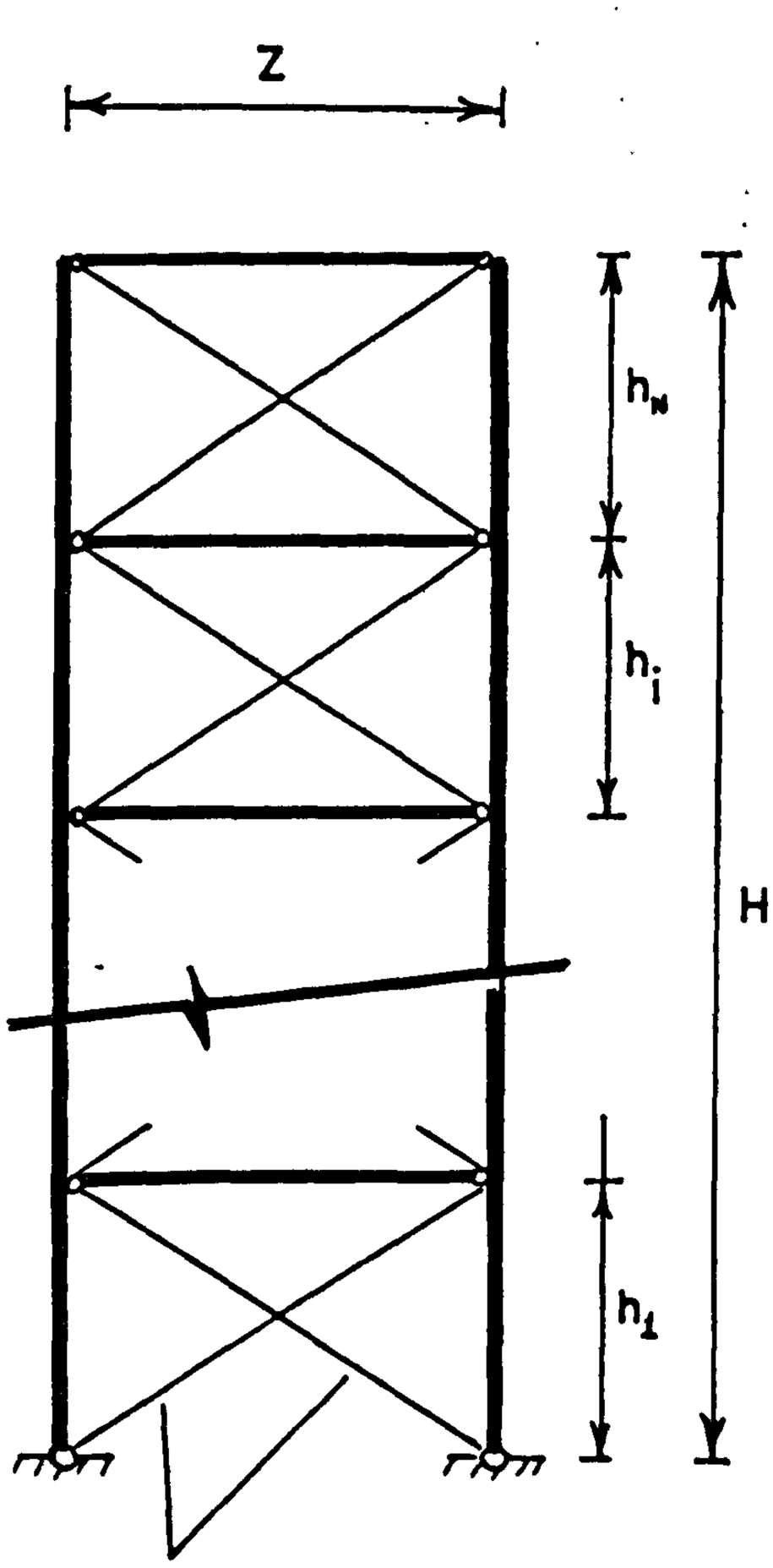

(a) Actual structure

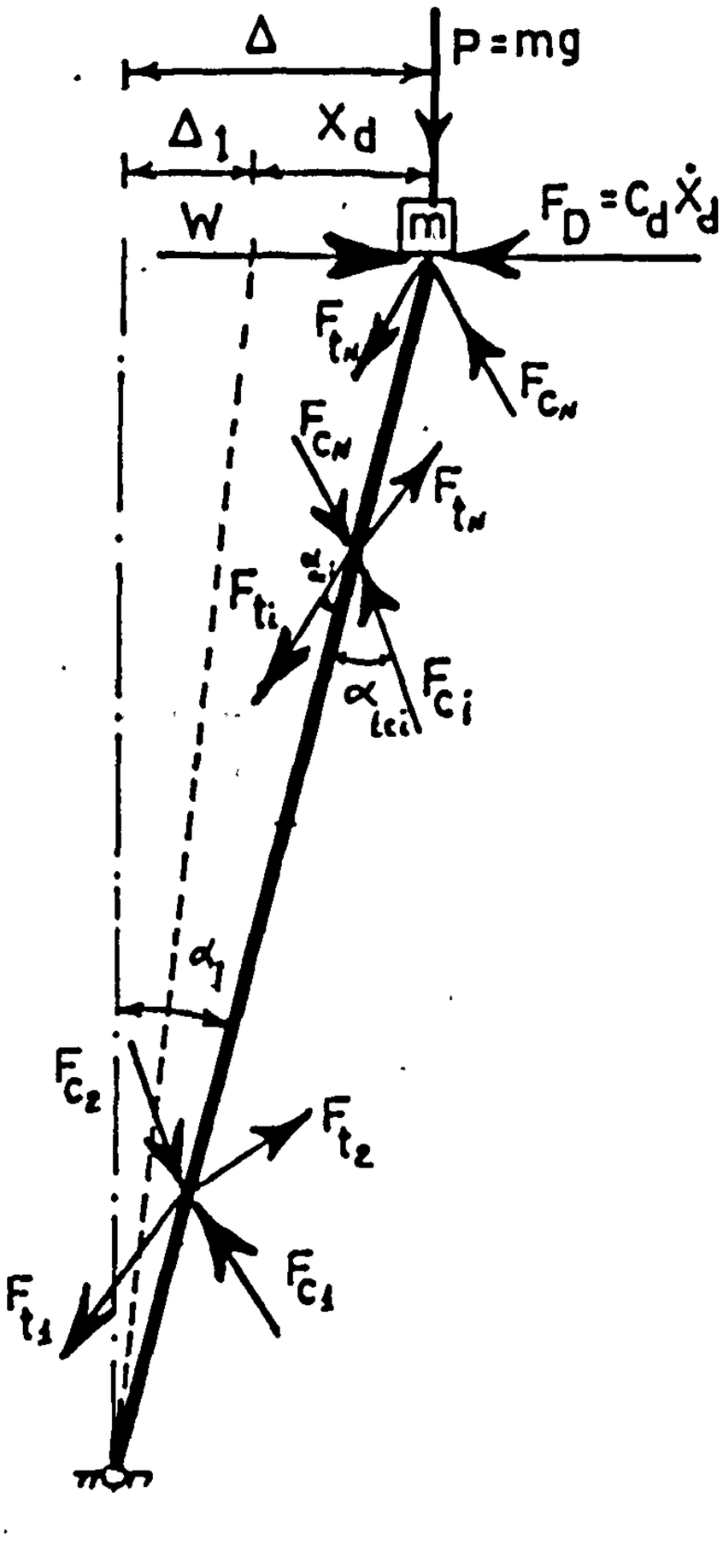

(b) Internal and External forces applied on the equivalent idealized structure

Fig.(6-2): General Non-linear SDOF System

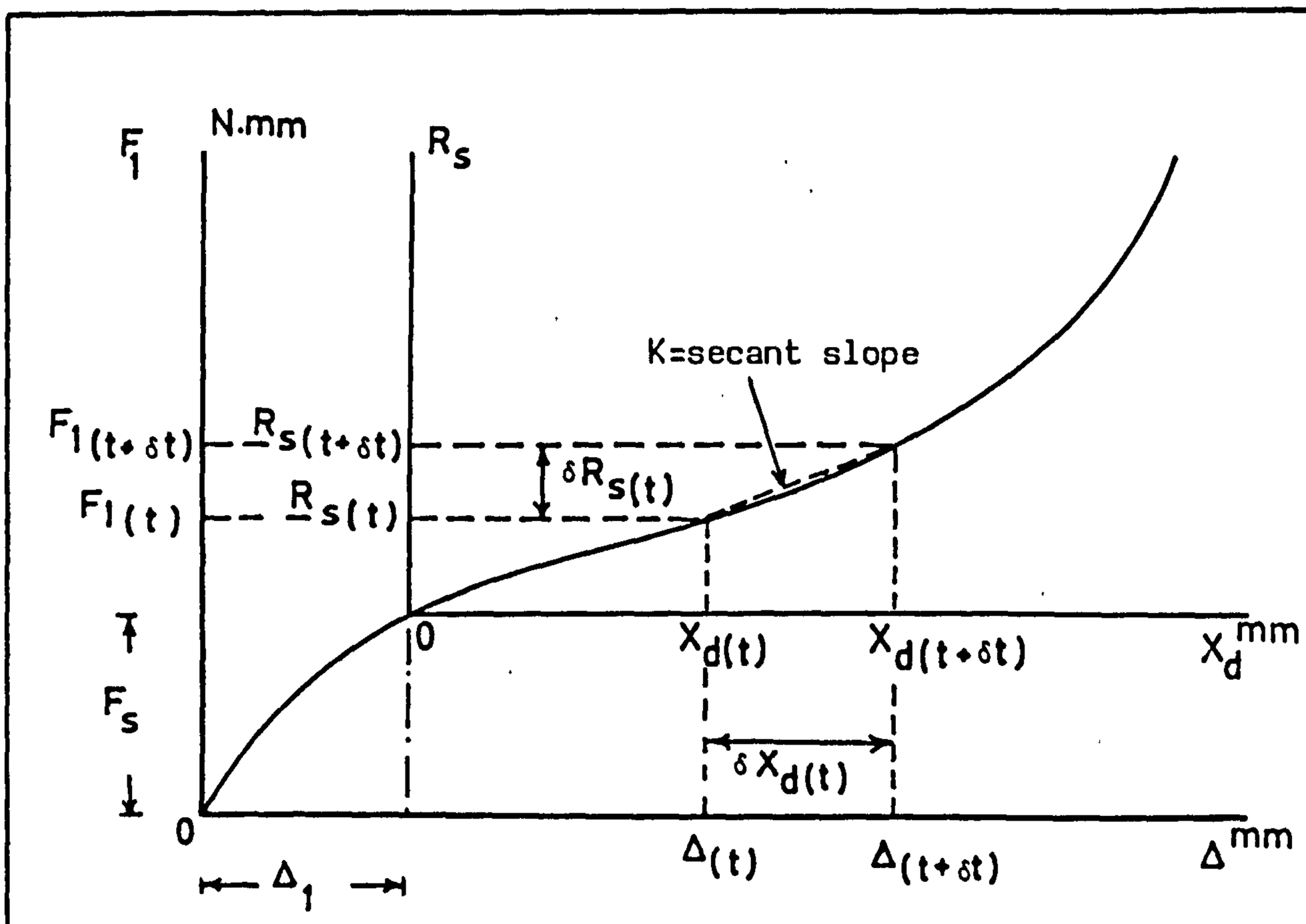

(a) Non-linear restoring moment "F_1" as a function of time "t"

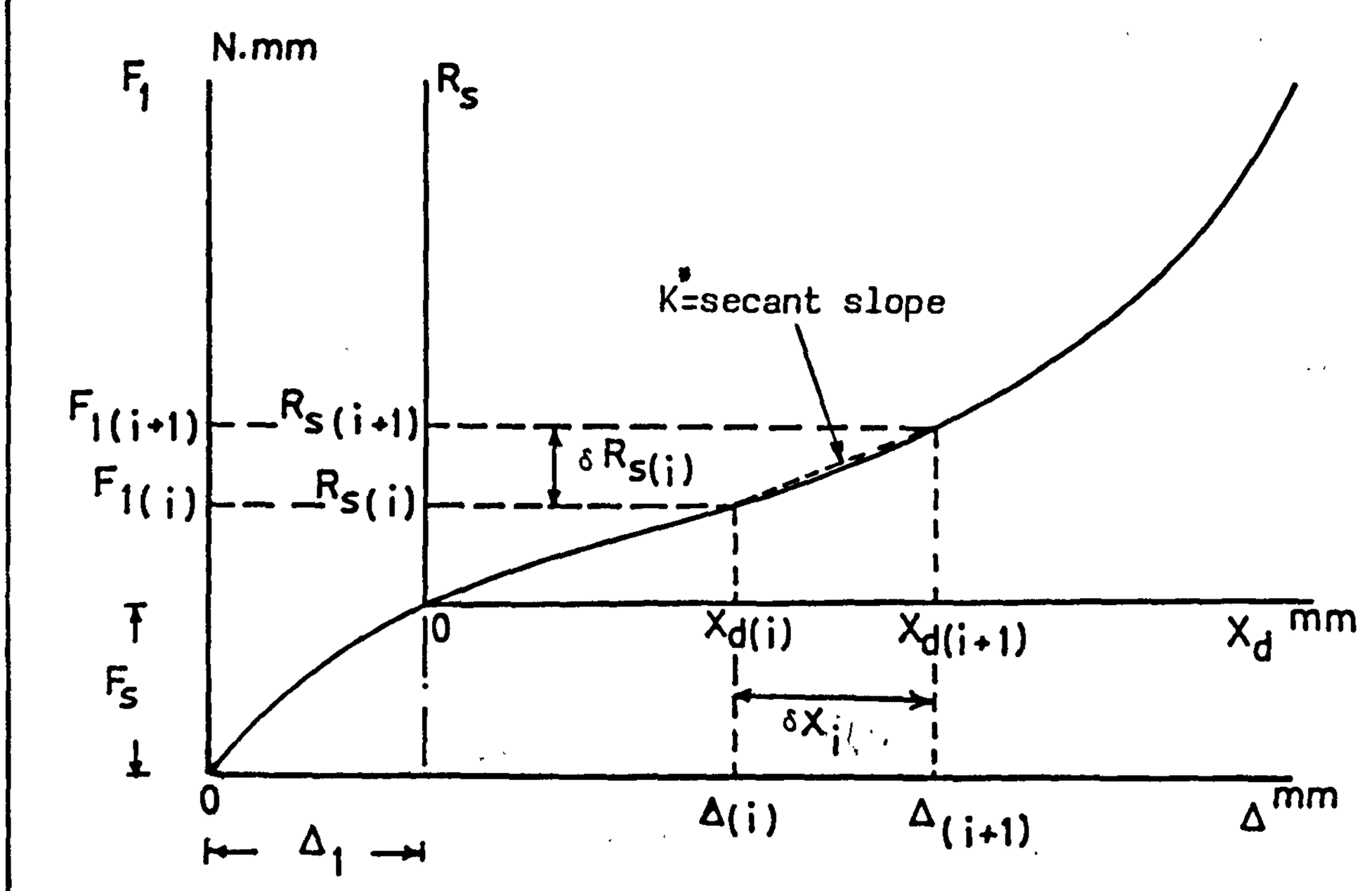

(b) Non-linear restoring moment "F_1" as a function of displacement "Δ"

Fig.(6-4): Non-linear Characteristics of SDOF systems

CHAPTER SEVEN
EXPERIMENTAL DYNAMIC BEHAVIOUR

7.1 Introduction

In this chapter the experimental dynamic behaviour of the frame structure considered in the static analysis is investigated.

The dynamic excitation occurs at the onset of the transient instability region under a constant static applied load. This means that the model which has been used for dynamic investigation is an extension of the static frame model. Reference will be made, therefore, to the frame model used in the static tests. The model was used for determination of the various dynamic parameters,such as acceleration and displacement, involved in the dynamic motion of the frame structure. The ultimate objective of these forms of experiment is the development of a well validated calculation technique to describe the effects of instability of the structure in the transient instability region.

7.2 Design and Construction of Model

The experimental model consisted of two identical single bay, two storey steel frames. The description and the overall dimensions of each frame are illustrated in section 4.5, and Fig. (4.4). The distance between the two frames was taken as twice the span of a frame. To ensure lateral stability, cross bracing consisting of 25x25x3 mm angle was installed between the two frames. Horizontal cross bracing of 12.5 x 6.25 mm bars, was used at the top of the frames to ensure that both frames acted together. A wooden plate of 6 mm thickness was used at the top panel level of the frames to

allow the application of the vertical loads. The general arrangement is shown in Plate (7.1). The wooden plate was marked to locate the applied vertical load positions. A symmetric application of the vertical load with respect to the centre line of the two frames was adopted. A number of dried sand bags were prepared to be ready for applying as vertical loads during the test procedure.

The sand bags were prepared with accurate different weights such as 0.8, 0.6 and 0.4 kgs.

Horizontal loading was applied through a system of pulleys and thin strong string, the latter being attached to a small piece of wood fixed at the edge of the wooden plate centred between the two frames. The string was hooked at the top joint level of the frames. The system of pulleys was fixed to a rigid vertical stanchion as shown in Plates (7.1) and (7.2).

Each frame had two hinged bases which were situated on a guide rail fixed to rigid I beam supports. The model was constructed placing each frame in the test position and then clamping the guide rail base to the I beam supports. The beam supports were levelled before the frame was fixed. Each frame was adjusted to a vertical position (i.e. in x-y plane and y-z plane) so that it was as near as possible to being in a true vertical planes, this was checked using a plumb bob which hung from the centre of the top joint of the frame. The dimensions of each storey were adjusted to as closely as possible, adjustment being made by using the pitch setting gauges and the variable screwed joints. The side cross bracings were then welded to the columns of the frames. The horizontal cross bracing was also welded at the top beams level of the two frames, as

shown in Plate (7.2). The wooden plate was screwed over the top panel level of the frames.

After construction, the verticality of the columns, of each frame, within their own plane was checked, again, by meąsuring the diagonals and pitches between joints of each storey, then the model was held in its vertical position to be ready for test.

7.3 Test Programme

Five tests were carried out. The only variable in this type of test was the initial rise of the bracing members. Different combinations were arranged between bracings in compression and in tension for each test, as in the case of the static tests, Table (4.4).

7.4 Instrumentation

7.4.1 Systematic Development of Experimental Work

The parameters of interest in this work are the displacement and the acceleration in the overall dynamic behaviour of the framework for various combinations of bracing system. The measurement of these parameters were required. This section describes the type of instrumentation used to record the quantities required and convert the signals to a convenient form for digital computer analysis.

7.4.2 Measurement of the Dynamic Response of the Structure

The response of the structure was measured at the top panel of the framework in the form of acceleration and lateral displacement.

The instrumentation used is shown in block diagram form in Fig. (7.1).

The acceleration response of the structure was measured using an accelerometer and amplifier. The accelerometer was attached magnetically at the top panel level of the frame. The signals from the accelerometer were fed into the charge preamplifier and then into the recording instruments.

The displacement response of the structure was measured by a rotary potentiometer which is an indirect method of measuring displacement.

7.4.2.1 Measurement of the Displacement by the Use of Potentiometer

To measure the lateral displacement at the top panel point of the framework a conductive plastic servo potentiometer (120) was used. The potentiometer was screwed into the bearing shaft of the hinged base of the left column of the right framework as shown in Plate (7.3). The potentiometer is a device that measures the rotation of the frame column. The rotation generates an electrical signal. The magnitude of the signal represents the degree of rotation. The wiper of the potentiometer is mechanically linked to the object whose rotation is being monitored. Generally if the object being monitored is rotated a fraction of a degree, the rotation will change the position of the wiper on the potentiometer. Changing the position of the wiper will, in turn, cause the circuit resistance of the potentiometer to be linearly altered. This will cause more or less current to flow through the milliammeter. If a milliammeter were calibrated relative to rotation in degrees, then this very simple circuit of the potentiometer could be used to measure the rotation of the frame column from its vertical position.

Hence the lateral displacement at the top panel level of the framework can be determined from the following formula:

$$\Delta = H.\ \sin(\alpha_a) \qquad (7.1)$$

where α_a is the actual measured rotation of the frame column and

H is the total height of the two storey framework.

The potentiometer operates from a laboratory DC power supply. A laboratory DC power supply type 430 and a digital multimeter type 7145 were used for the calibration of the potentiometer. The latter was connected to the multimeter to read off directly the output electrical signals. The calibration graphs are shown in Fig. (7.2). It is seen from these graphs that the output signals from the potentiometer have not been altered linearly in a range of rotations less than 35 degrees. For this reason the potentiometer was set up to read angles greater than 35 degrees, where the calibration graphs shows that the output signals have been altered linearly after this limit of degrees. According to this, the true rotation of the column of the frame was calculated by the following equation:

$$\alpha_a = \alpha - \alpha_o \qquad (7.2)$$

where

α_a is the actual rotation of the column,

α_o is the initial reading angle by the potentiometer at the vertical position of the frame,

α is the measured angle by the potentiometer after deformation.

It is seen also from Fig. (7.2) that the sensitivity of the potentiometer, in the linear range, is equal to the slope of each straight line divided by the supply volts and is equal to 2.601 mv/degree/volt, approximately.

7.4.3 Recording Instruments

The signals from the instruments described in section 7.4.2 were recorded using a tape recorder. After a test these were then transferred through a digitiser to an Apple II_e micro computer for further processing.

7.4.3.1 Recording and Conversion of Data for Computer Analysis

The instrumentation used is shown in block diagram form in Fig. (7.3).

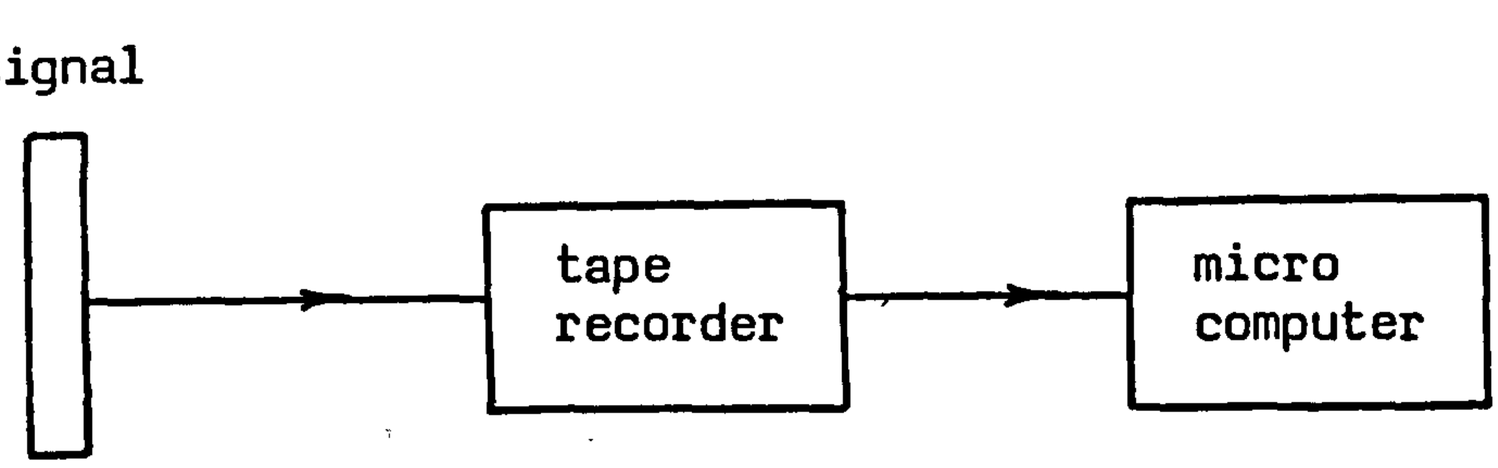

Fig. (7.3) : Instrumentation used to prepare data for digital computer analysis

The tape recorder used was a "Store 4" manufactured by RACAL RECORDERS LTD. The basic tape recorder has four channels. Channel No 4 may be used to record voice ammouncements using the attached microphone. The tape speeds can be varied from 15/16 to 60 inches/second (2.38 to 152.4 cm/sec). The tape speed 7½ inches per seconds

was used for recording and replaying during the tests. The instrument was set up according to the procedures recommended by the manufacturer. The purpose of the tape recorder was to record the analogue signals prior to digitisation. This was necessary because the experimental model and the digitising computer were situated in different locations.

An Apple II_e micro-computer was used to digitise the records. The computer comprises a central core of 64K words, two disc drive units, and AI13 analogue input system. The AI13 analogue input system is a high performance 12-bit acquisition system for the Apple II micro-computer.

7.5 Experimental Procedure

Details of the experimental technique employed and the actual test procedure will be discussed in this section.

The series of tests, which were classified in Table (4.4) were carried out. Before each test the model was adjusted to a vertical position and held in this position. The curvature and the initial rise for each bent bracing member was adjusted exactly and then the bracings were connected to the model as shown in Plate (7.1). The ends of each bracing member were checked for a tight fit at the hinged joints. The Accelerometers and potentiometer were attached to the model as shown in Plate (7.2). Next, the electrical circuits were connected.

The first step in loading was to apply a horizontal load only which was proportional to the equivalent mass of the structure. This

means that at any step of loading the vertical load including the self weight of the structure was in the same ratio to the horizontal load. The structure was allowed to sway before applying the first increment of vertical load, i.e. under the self weight of the model and the corresponding horizontal load. Since the self weight of the structure is less than the critical load "P_{cr1}" (i.e the load at the onset of the transient instability region) and the structure was released from the rest in the state $\Delta=0$ which of course is not a static equilibrium state of the loaded system, then the structure experienced a small vibration about its stable equilibrium position. However the structure did not "pass" into its unstable state. Now, for a specified value of ratio "R=40" a small increment of horizontal load "$\Delta W=0.04$ kg" was applied and then the corresponding vertical load, pre-weighted sand bags ($\Delta P=1.6$ kg) , were also applied carefully by hand to avoid any disturbances and to minimise the adverse effects. The increments in vertical load were applied symmetrically with respect to the centre line of the two frame model. After each load increment the structure experienced a small vibration and took up a new static position.

Depending on the degree of deflection the load increments were decreased as the transient instability condition was approached.

The last load increment was when the structure was observed to sway dynamically. At this stage the applied vertical load was very close to the static buckling load "P_{cr1}" , and the system moved "past" its unstable region and experienced very large vibrations. It could then be said that the system had buckled dynamically.

Finally, the series of tests were then repeated for all combinations of bracing systems shown in Table (4.4).

7.6 Evaluation of Test Results

The following procedure was developed for digitising the analogue records.

A basic apple programme was written for digitisation. This programme interacts with the AI13 analogue input system which necessitates the use of the machine language programme.

The digitisation is carried out by the computer when a signal is received by the AI13 analogue system. Four input channels are sampled. This operation is repeated until the required amount of data has been recorded onto a disc for temporary storage. The data, thereafter, has to be retrieved from the temporary storage disc and converted to the correct values.

The choice of sampling interval Δt is important in any digital analysis. If the interval chosen is too small, the sampled data will be highly correlated and will cover only a small portion of the record. Alternatively if the sampling interval is too large, important events may be missed. The time increment Δt was chosen as 7.54 milliseconds, 384 numbers were sampled from each channel record and were used as the data for time series. The time interval with which one set of reading was digitised was calculated by the following formula :

$$\Delta t = 210.0 + 30.0 \times DP \quad \text{clockcycle} \qquad (7.2)$$

where DP is the delay parameter,

1 clockcycle = 0.9779 microseconds [123].

Use of 1 for the delay parameter was justified meaning that Δt = 0.235 milliseconds which was very short for one set of readings to be recorded. A delay parameter of 250 means a time increment of about 7.54 milliseconds would be needed to record one set of readings. This means that a time of about 1 second would be required to record simultaneously 132 digitised reading approximately, from the response of the four channels. Actually a total time of about 3 seconds was needed to represent the actual behaviour of the structure.

The results obtained are shown in Figs. (7.4) - (7.13). It can be seen that the variation of displacement, at the beginning of each test, is small corresponding to the time variation. This means that, the structure was oscillating about its stable equilibrium position due to the increments in the loading system. The value of displacement in this range is less than the displacement at the onset of the transient instability region (i.e. the onset of the dynamic behaviour).

Also, it can be seen that the peak of the acceleration occurs at a displacement greater than the end of the transient instability region. This means that the structure moved "past" its stable equilibrium at the end of the region of transient instability.

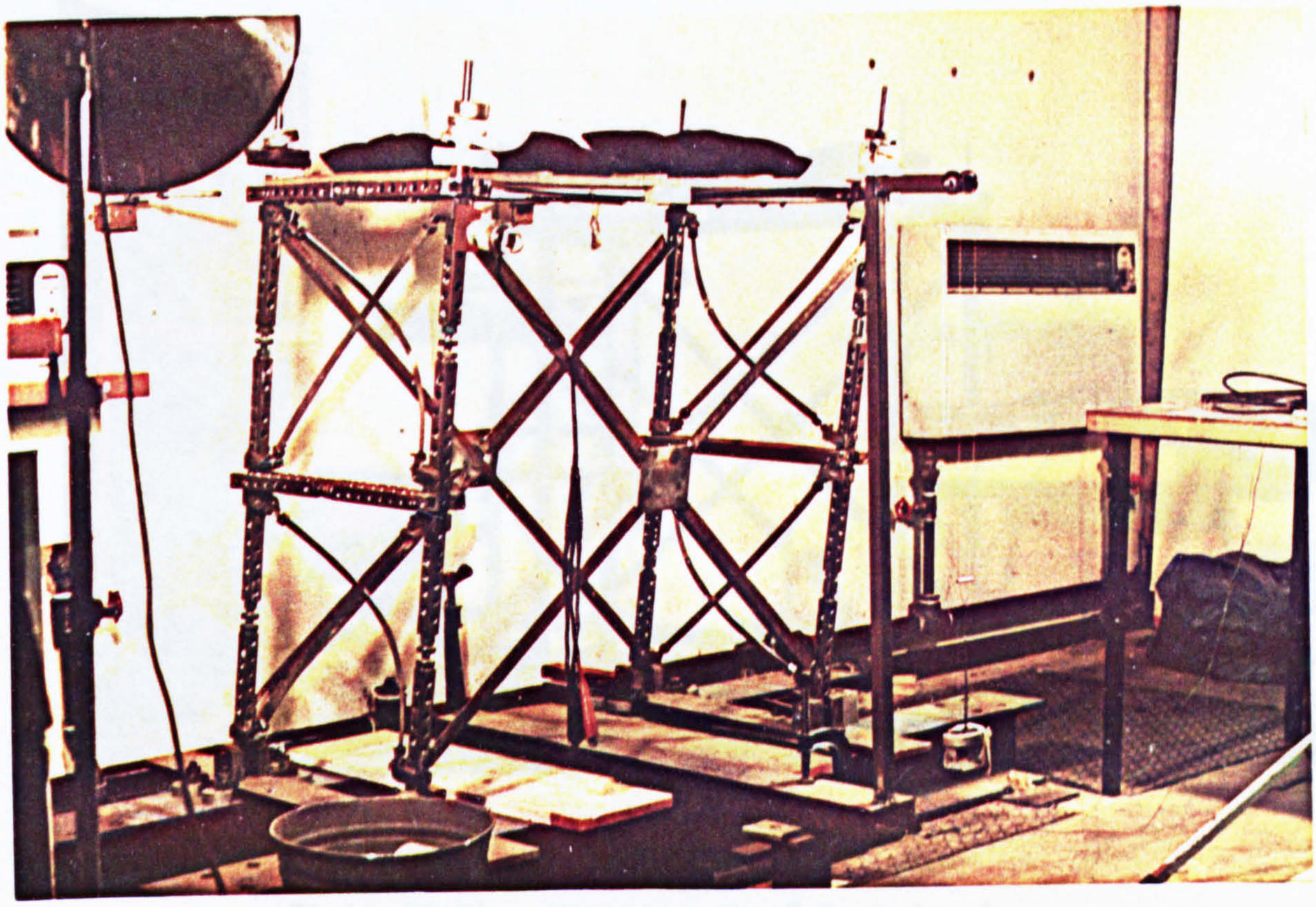

Plate (7.1) : Experimental Model for Dynamic Experiment

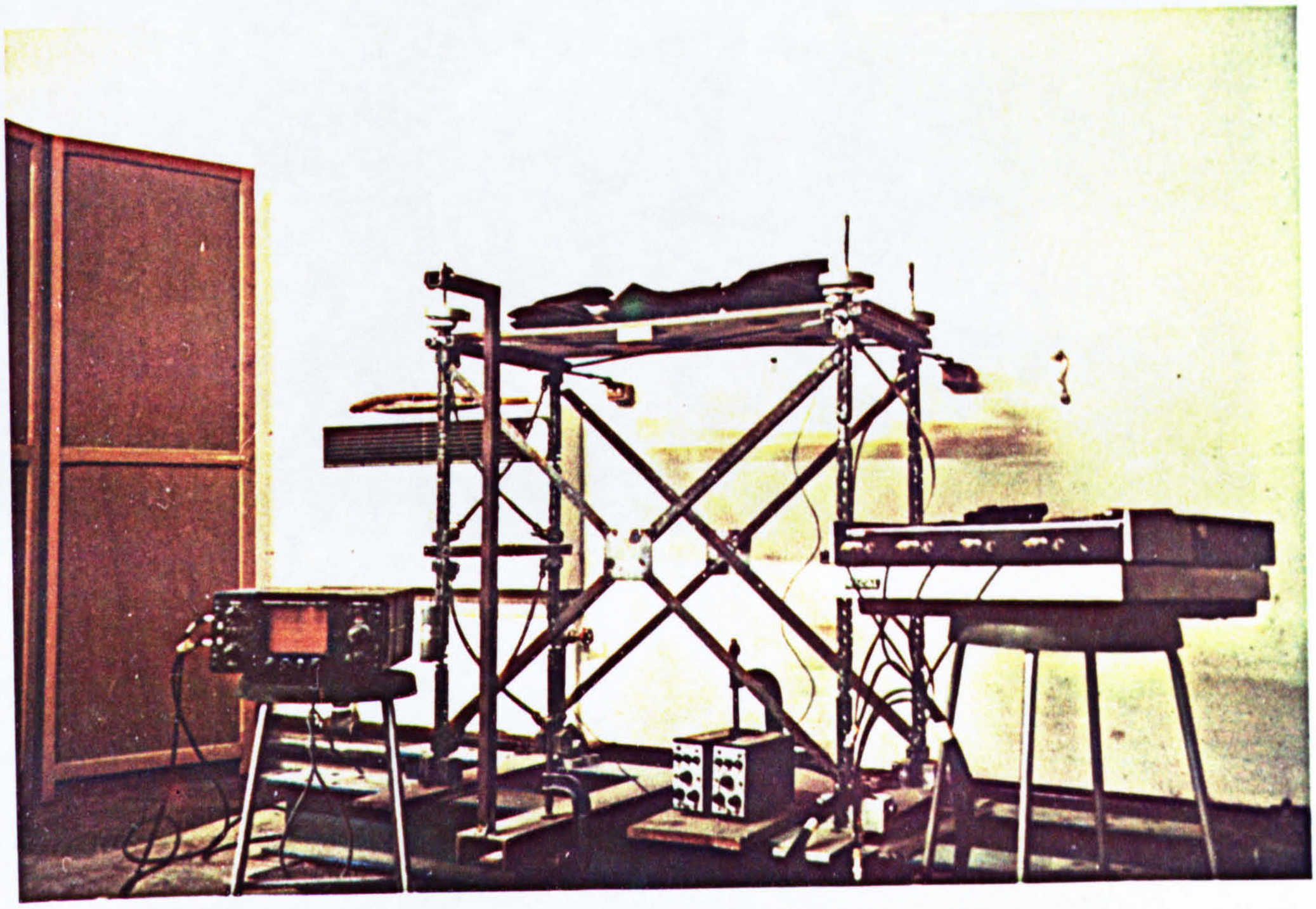

Plate (7.2) : Arrangement of Experiment

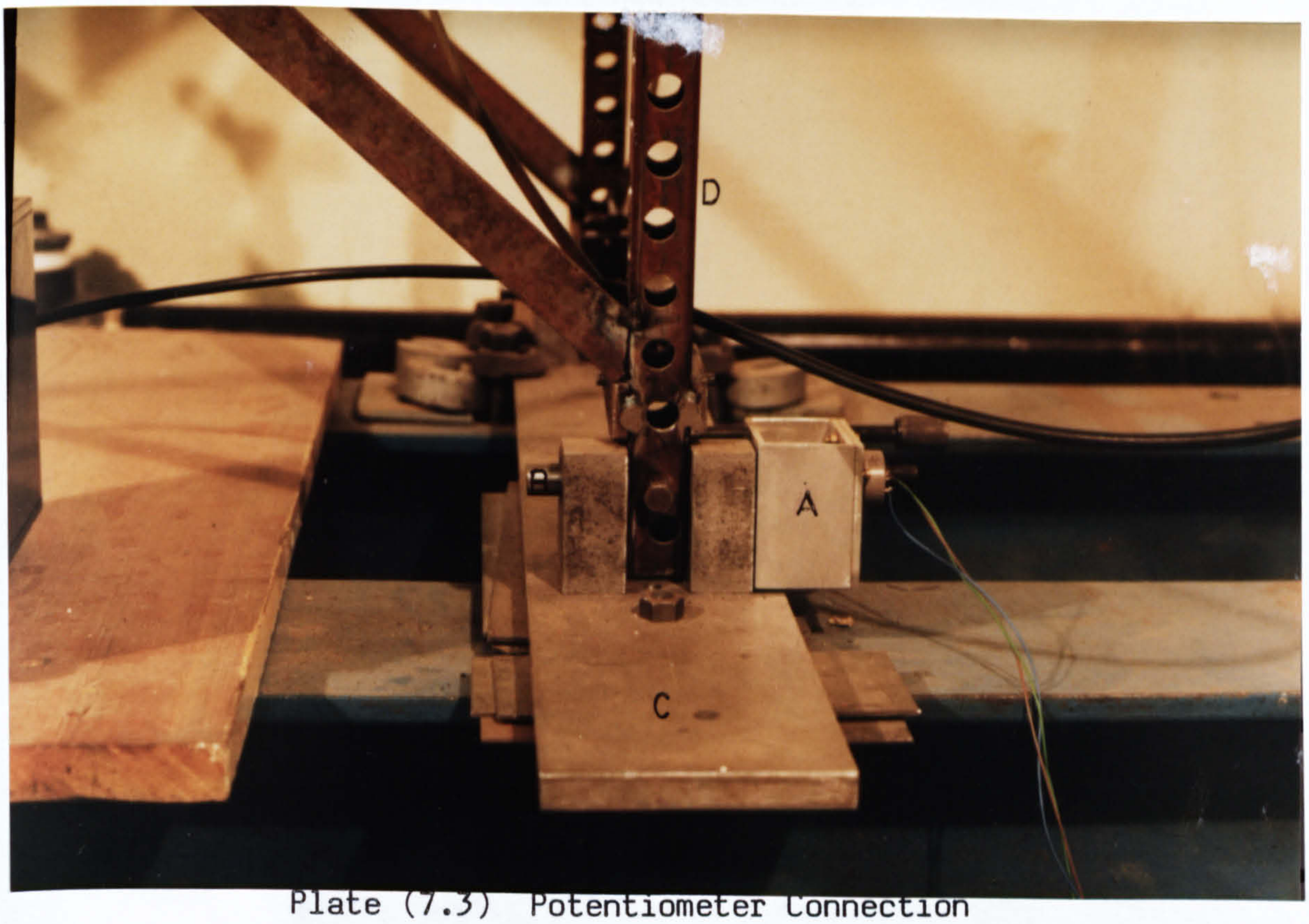

Plate (7.3) Potentiometer Connection

Key to Plate (7.3)

A - potentiometer

B - bearing shaft of the hinged base

C - bearing plate

D - frame column

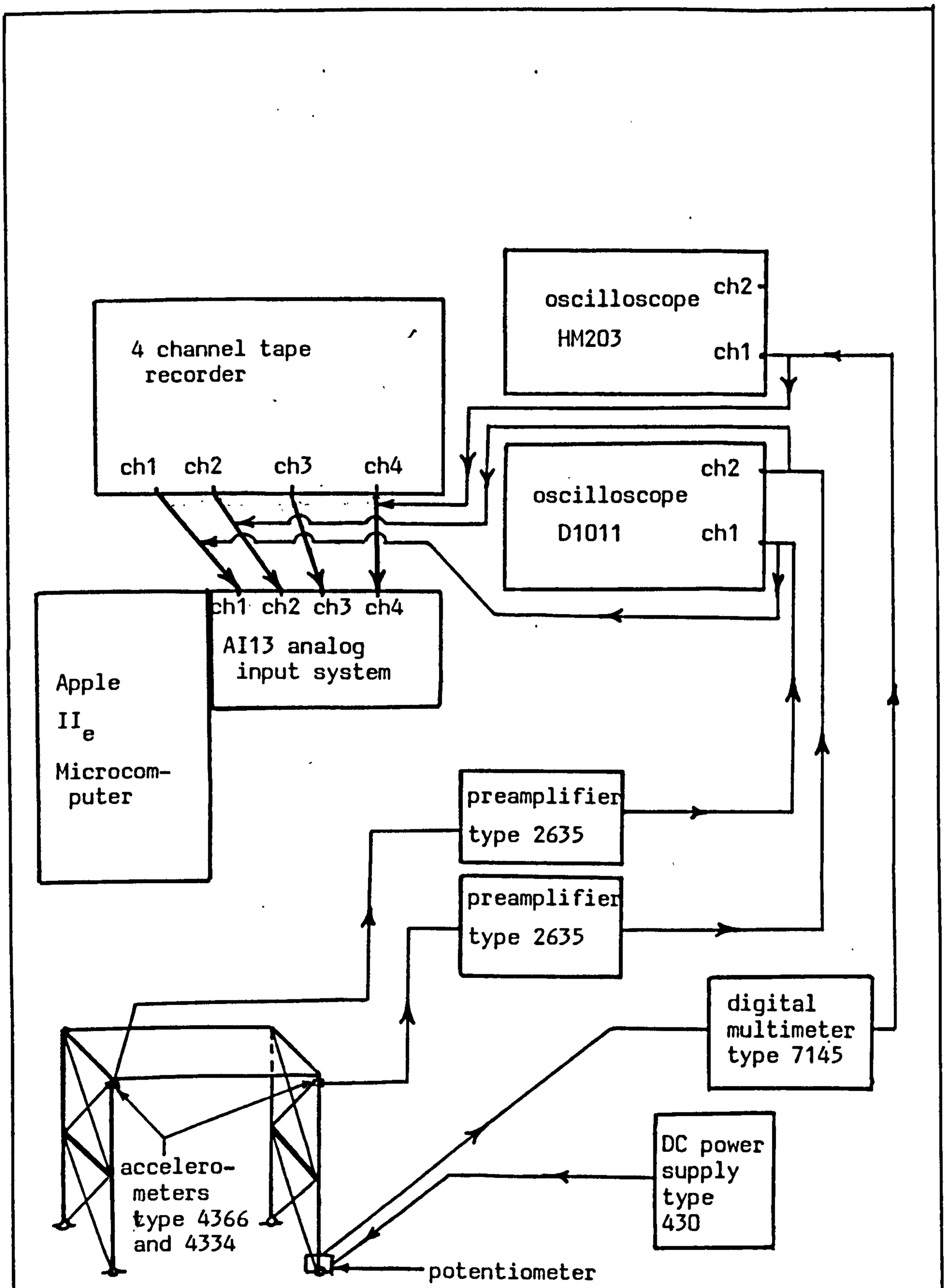

Fig.(7-1): Schematic Diagram of Experiment

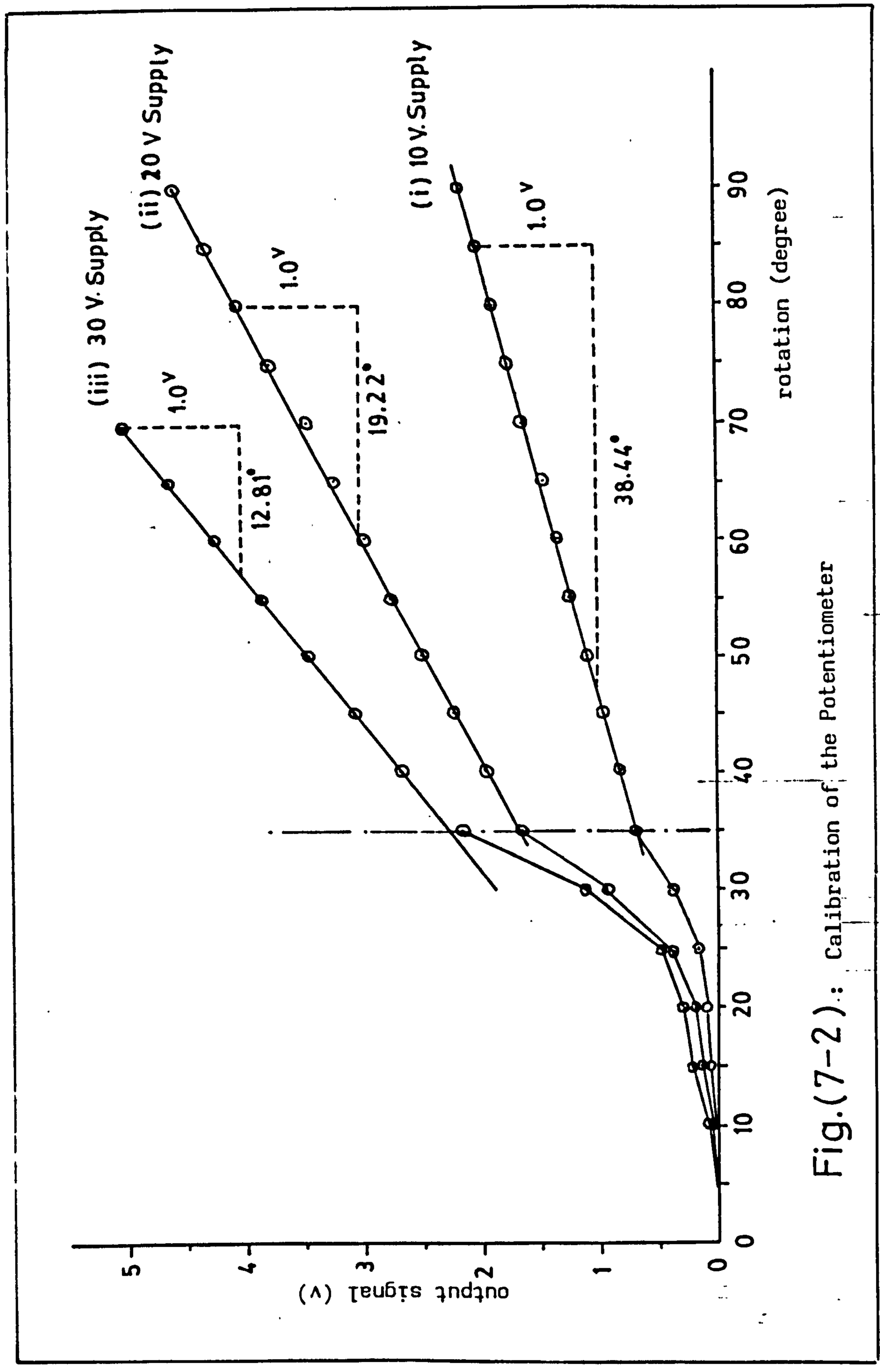

Fig.(7-2).: Calibration of the P

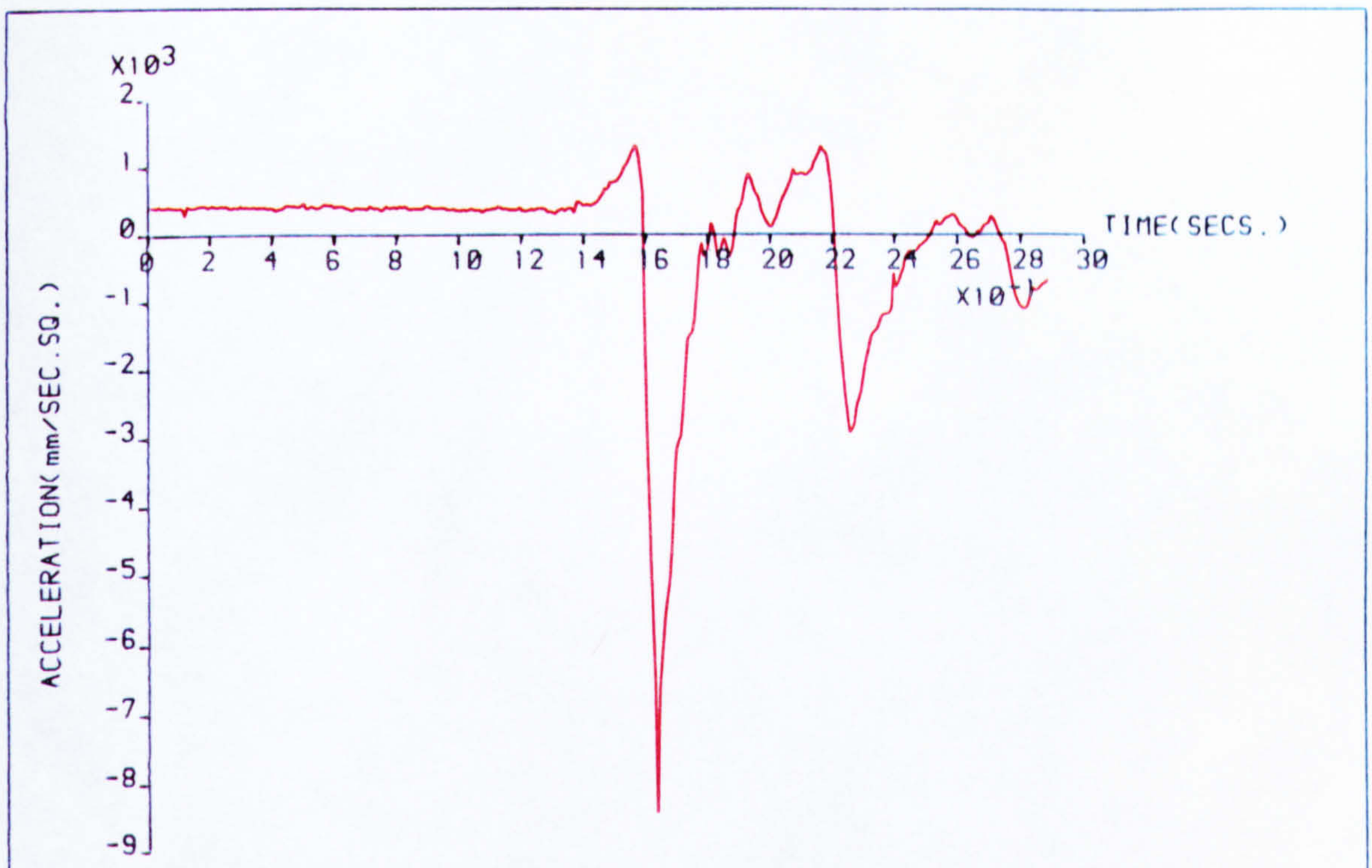

FIG.(7-4) VARIATION OF ACCELERATION

DYNAMIC BEHAVIOUR OF TWO STOREY FRAME

DIGITISED EXPERIMENTAL RESULTS

AC(1)=20.0 AT(1)=85.0 (mm)

AC(2)=20.0 AT(2)=85.0 (mm)

TEST LOADS: W=4.119 P=164.741 (N.)

TEST RESULTS FOR LEFT FRAME

TEST RESULTS FOR RIGHT FRAME

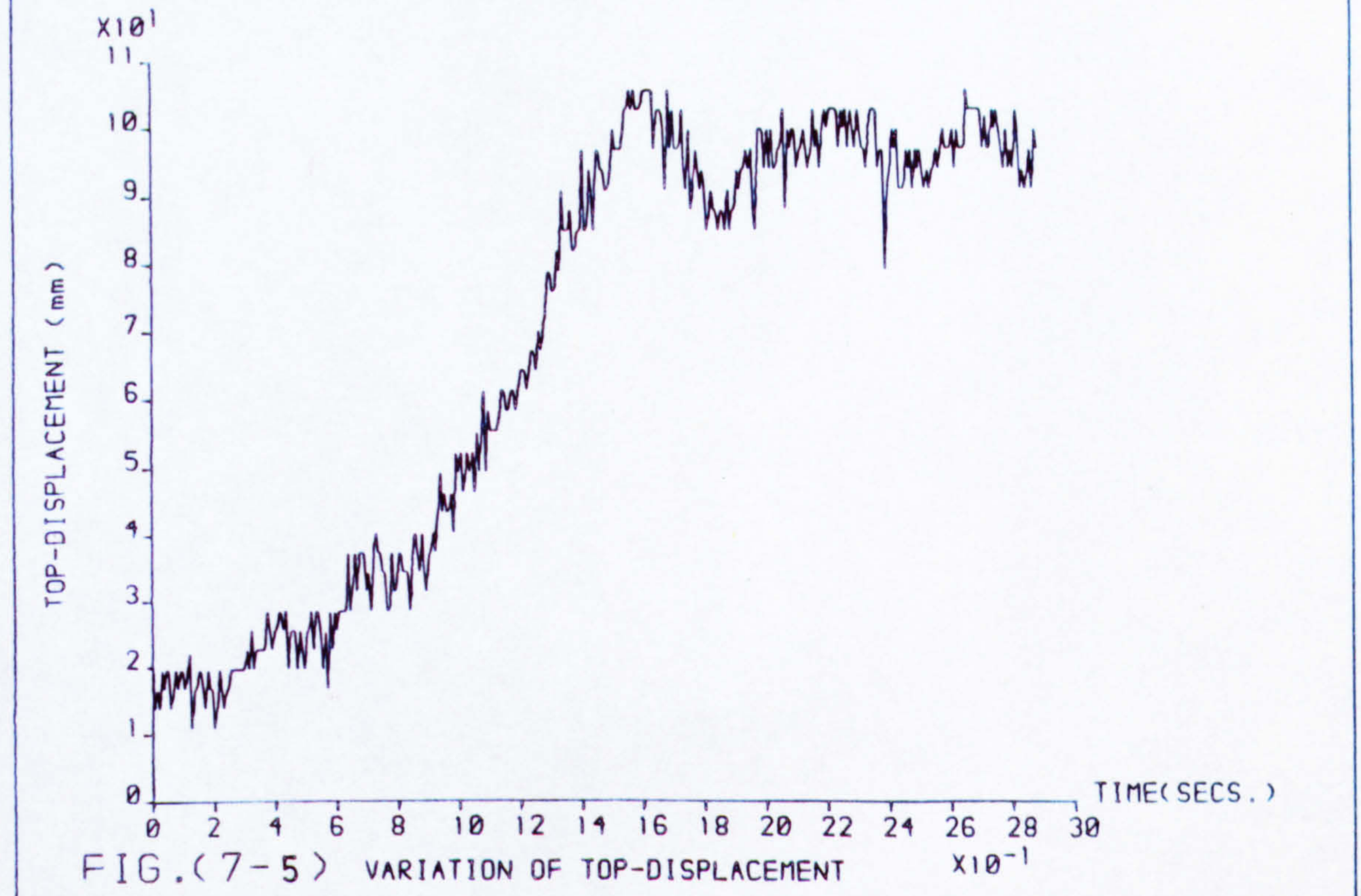

FIG.(7-5) VARIATION OF TOP-DISPLACEMENT

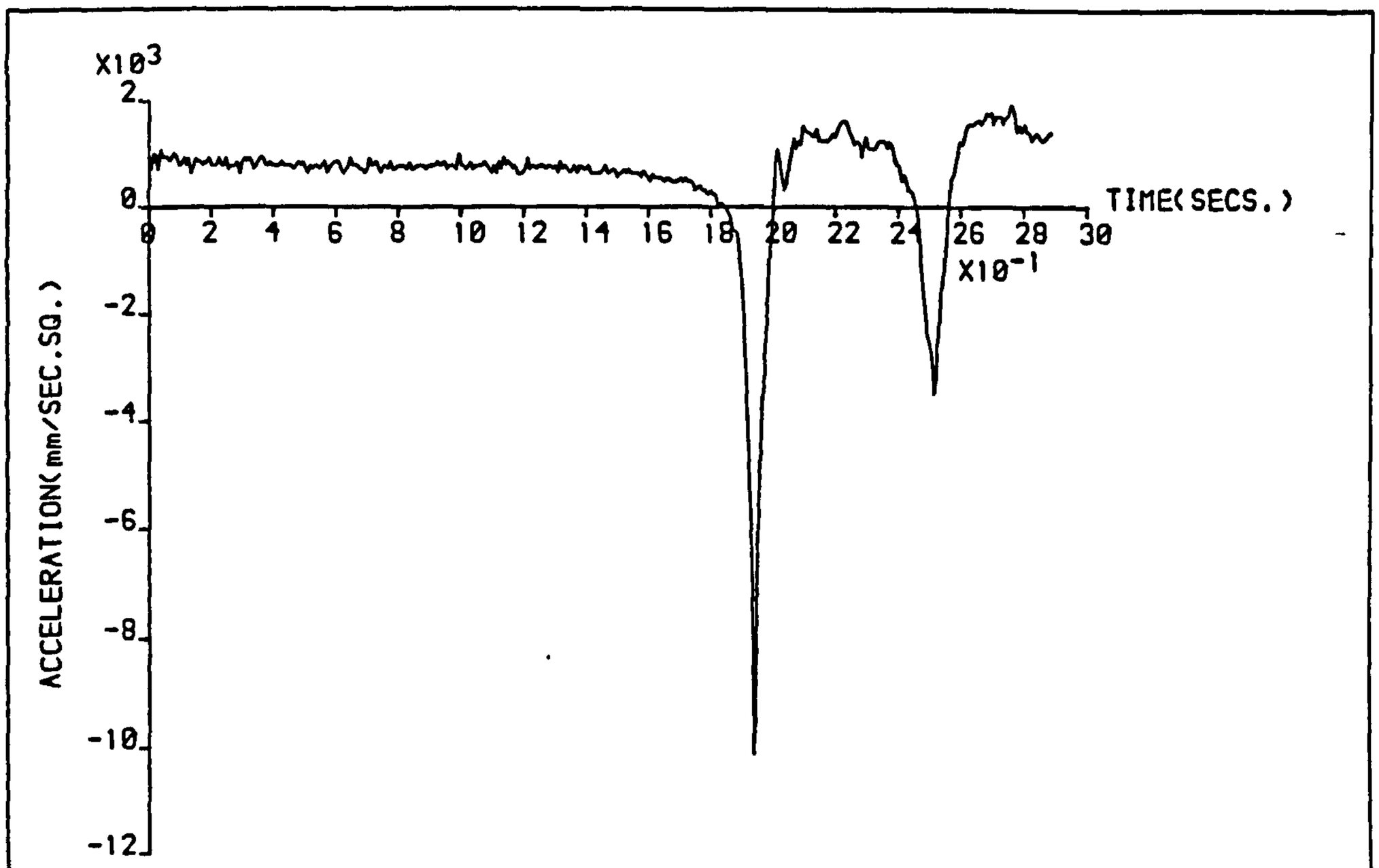

FIG.(7-6) VARIATION OF ACCELERATION

DYNAMIC BEHAVIOUR OF TWO STOREY FRAME TEST LOADS: W=4.040 P=161.799 (N.)

DIGITISED EXPERIMENTAL RESULTS

AC(1)=20.0 AT(1)=95.0 (mm) TEST RESULTS FOR RIGHT FRAME

AC(2)=20.0 AT(2)=85.0 (mm)

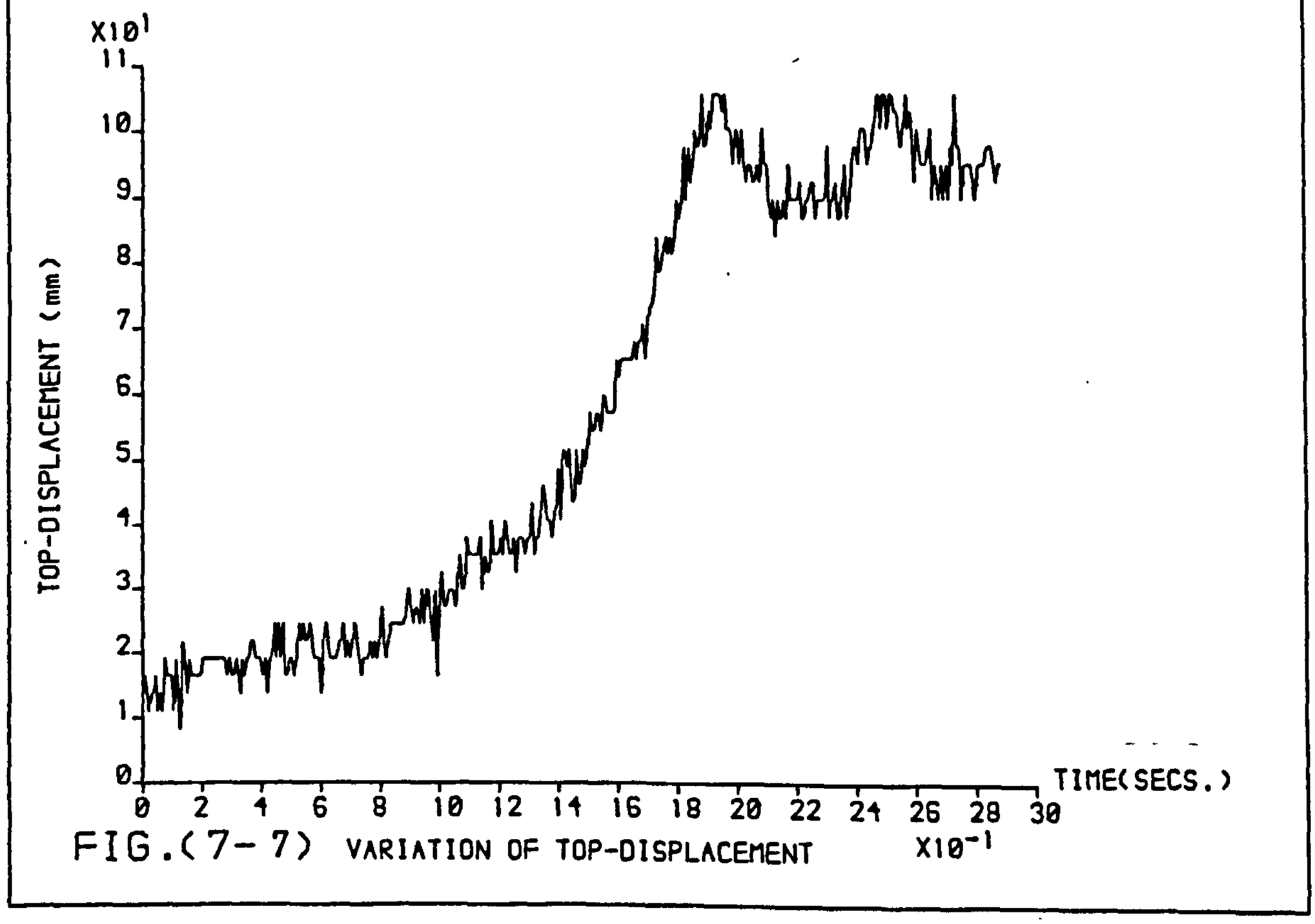

FIG.(7- 7) VARIATION OF TOP-DISPLACEMENT

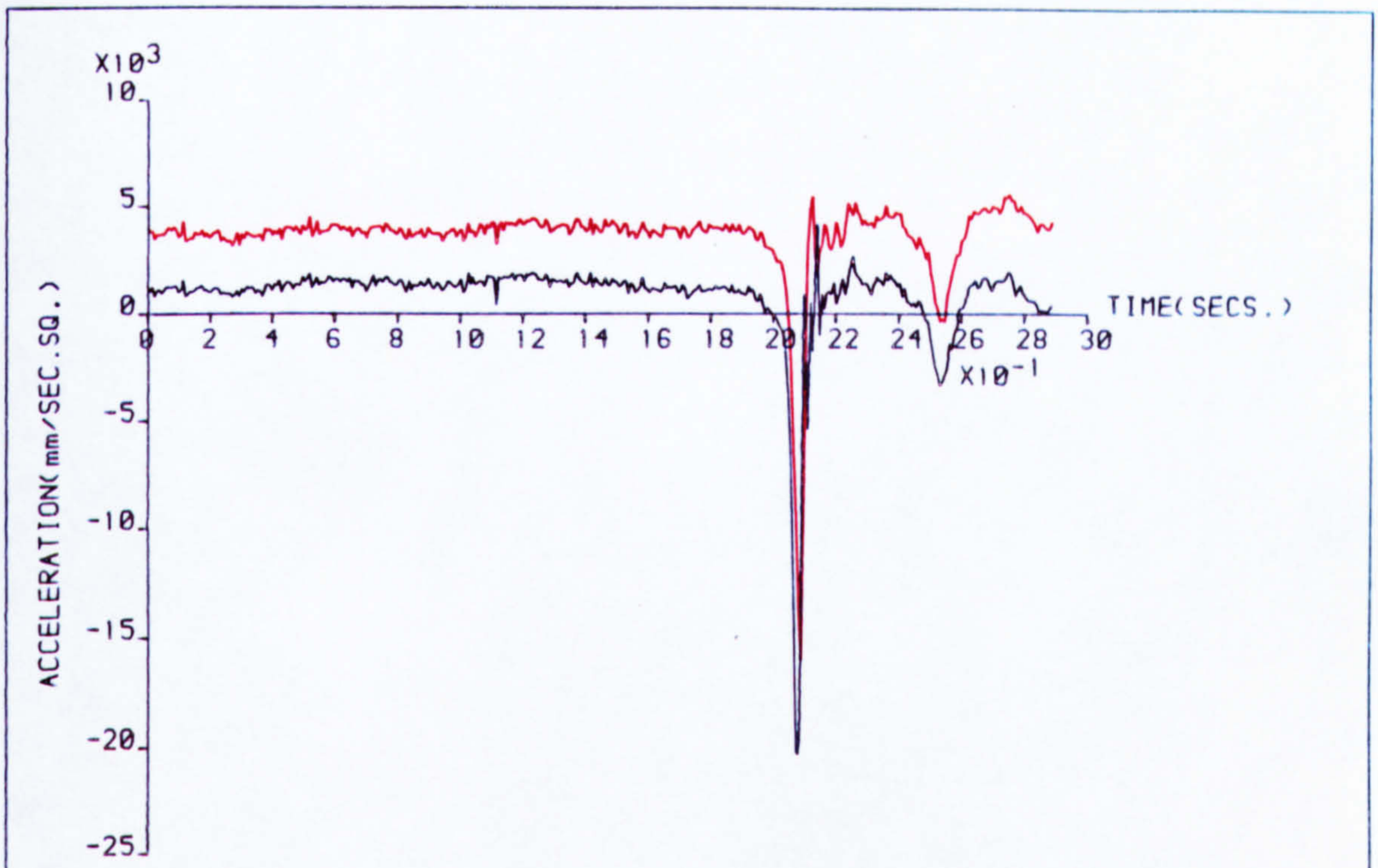

FIG.(7-8) VARIATION OF ACCELERATION

DYNAMIC BEHAVIOUR OF TWO STOREY FRAME

DIGITISED EXPERIMENTAL RESULTS

AC(1)=20.0 AT(1)=95.0 (mm)

AC(2)=20.0 AT(2)=95.0 (mm)

TEST LOADS: W=4.020 P=160.818 (N.)

TEST RESULTS FOR LEFT FRAME

TEST RESULTS FOR RIGHT FRAME

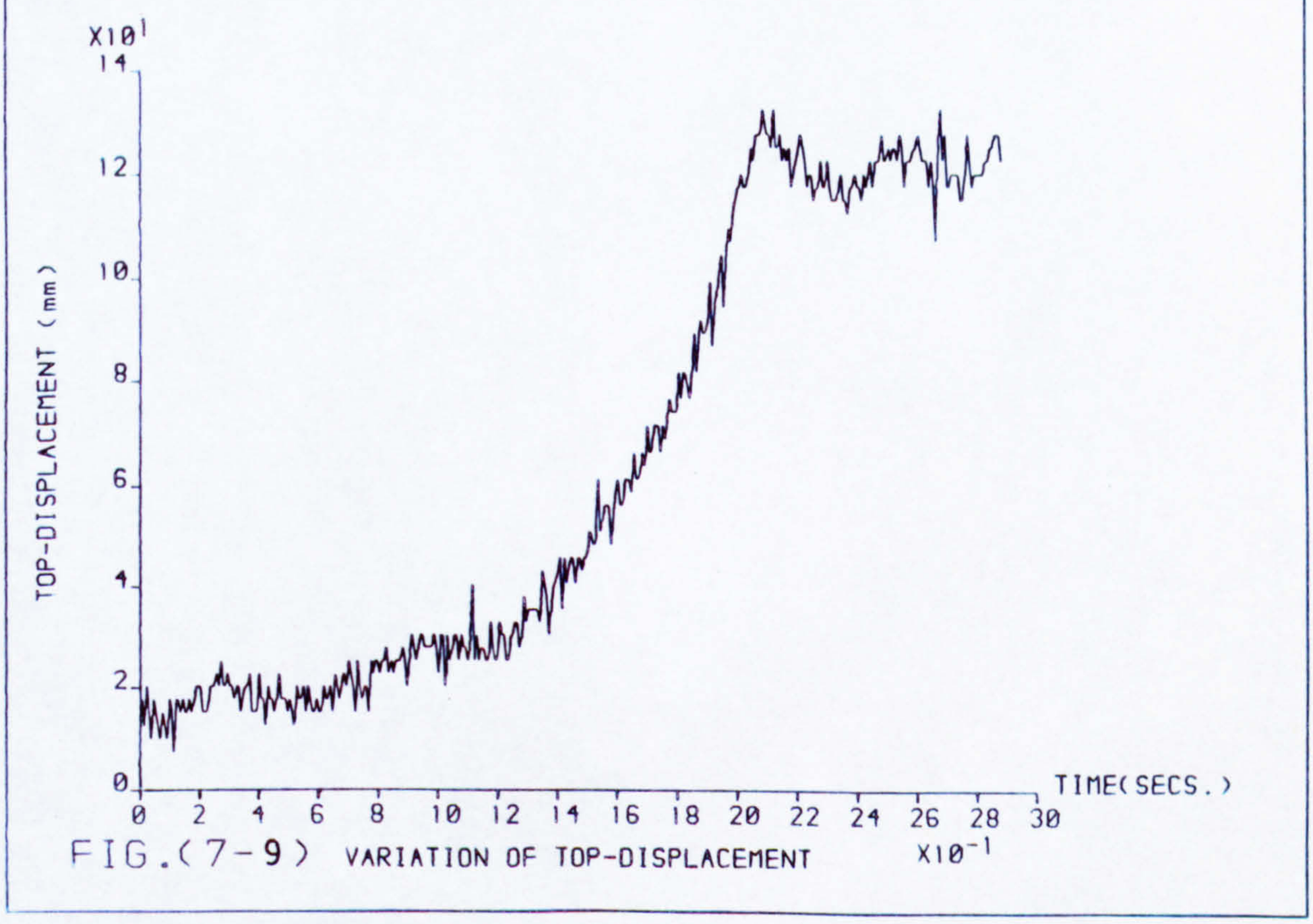

FIG.(7-9) VARIATION OF TOP-DISPLACEMENT

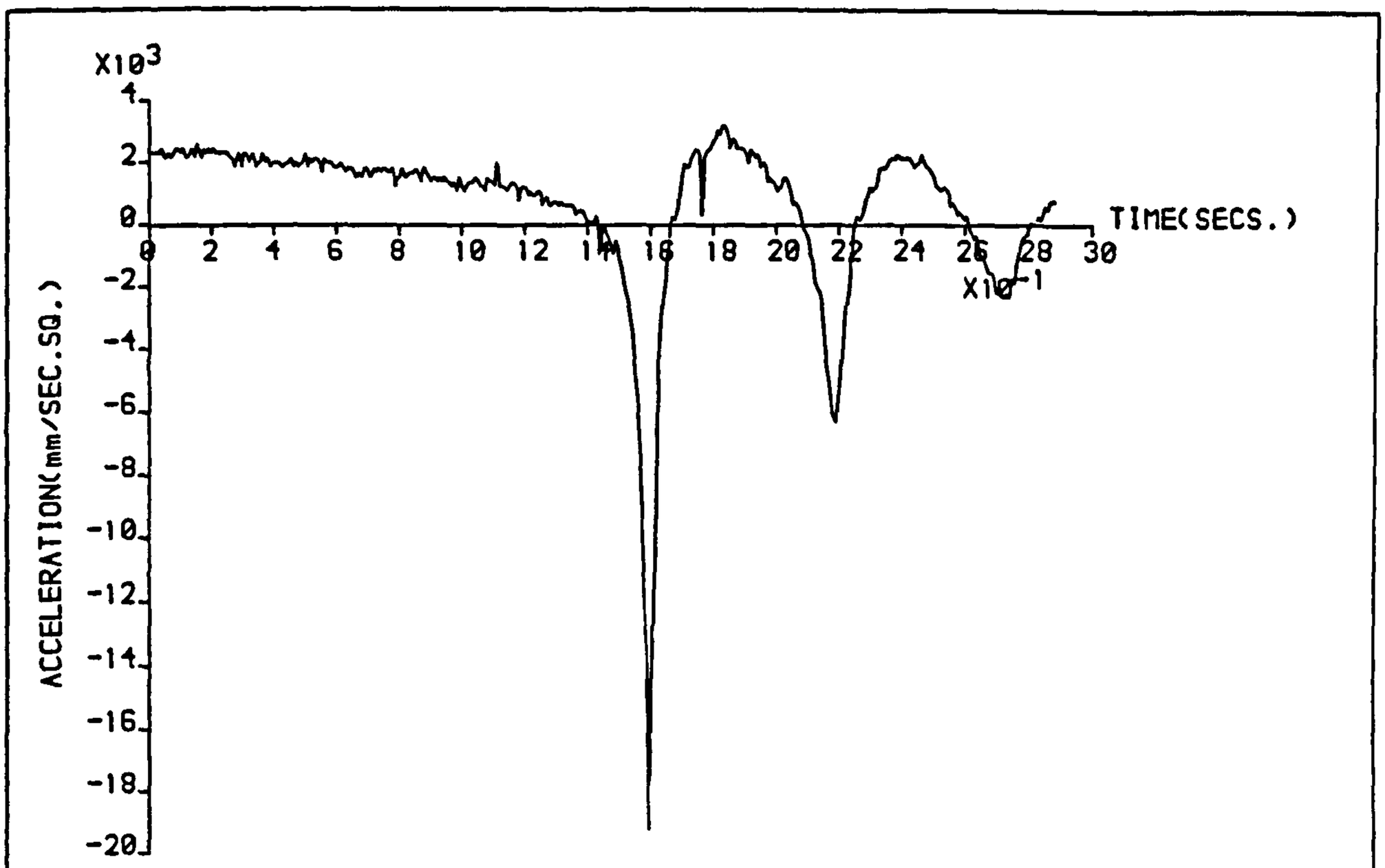

FIG.(7-10) VARIATION OF ACCELERATION

DYNAMIC BEHAVIOUR OF TWO STOREYFRAME TEST LOADS: W=3.432 P=137.284 (N.)

DIGITISED EXPERIMENTAL RESULTS

AC(1)=20.0 AT(1)=95.0 (mm) TEST RESULTS FOR RIGHT FRAME

AC(2)=30.0 AT(2)=95.0 (mm)

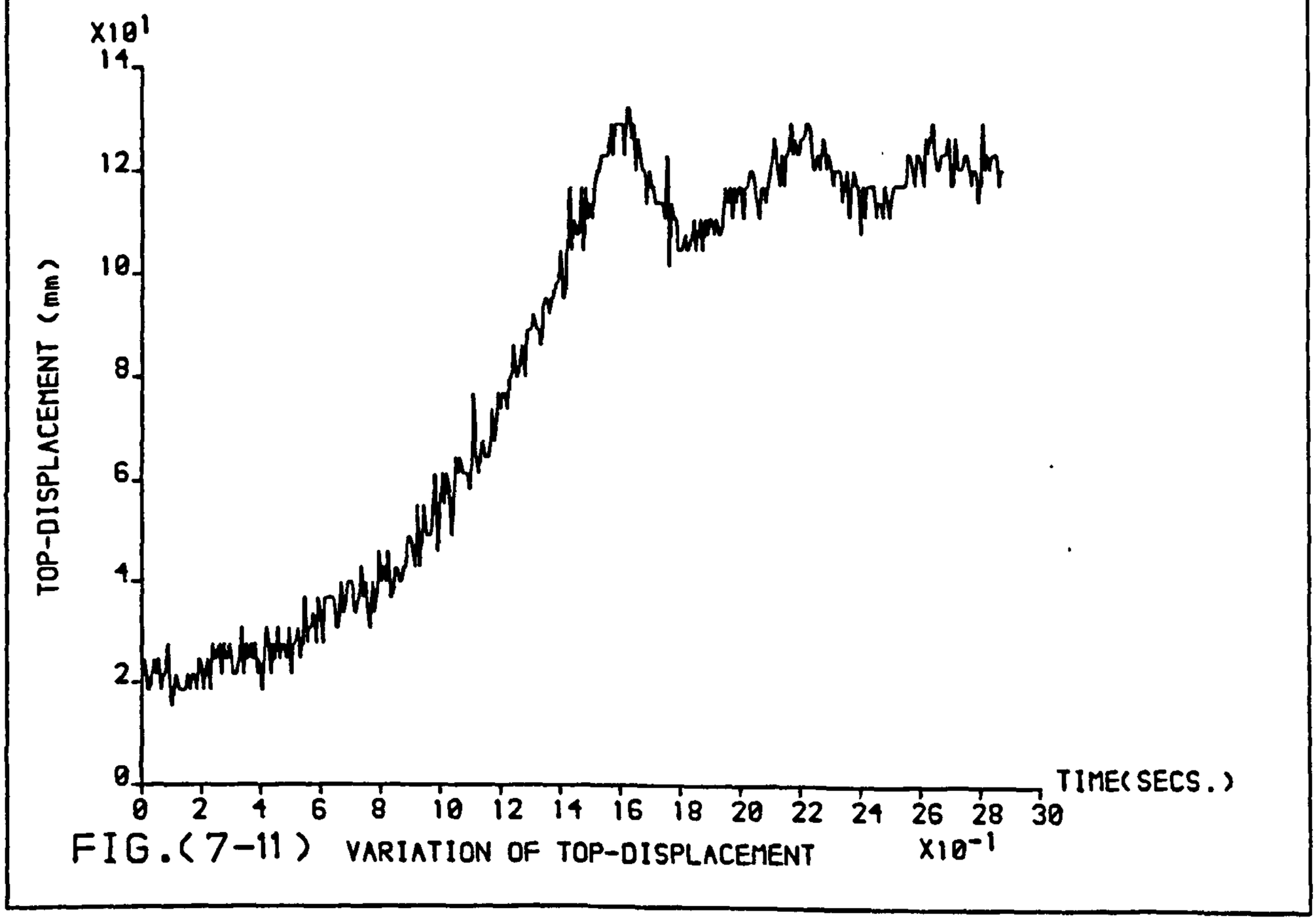

FIG.(7-11) VARIATION OF TOP-DISPLACEMENT

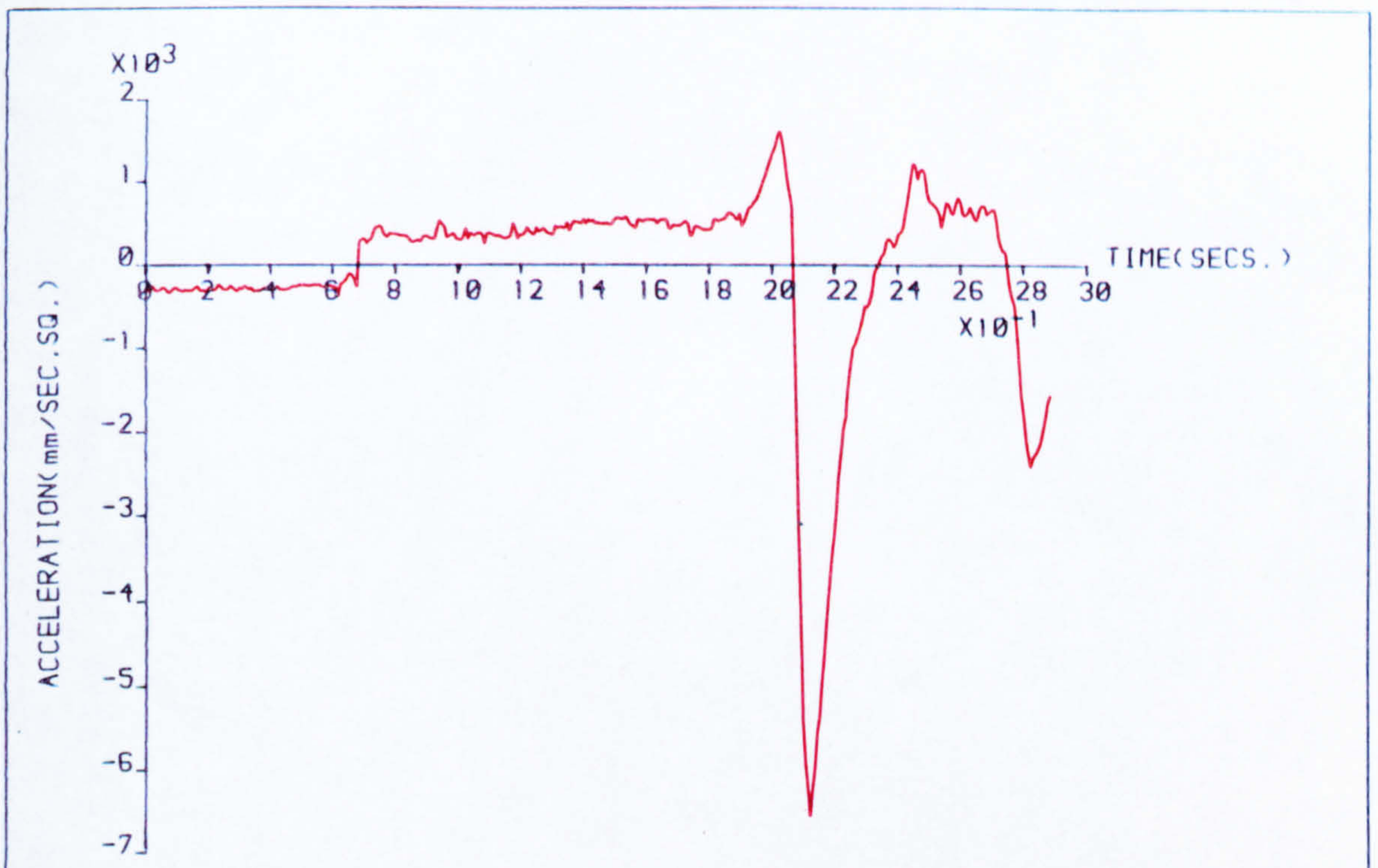

FIG.(7-12) VARIATION OF ACCELERATION

DYNAMIC BEHAVIOUR OF TWO STOREY FRAME

DIGITISED EXPERIMENTAL RESULTS

AC(1)=30.0 AT(1)=95.0 (mm)

AC(2)=30.0 AT(2)=95.0 (mm)

TEST LOADS: W=3.187 P=127.478 (N.)

TEST RESULTS FOR LEFT FRAME

TEST RESULTS FOR RIGHT FRAME

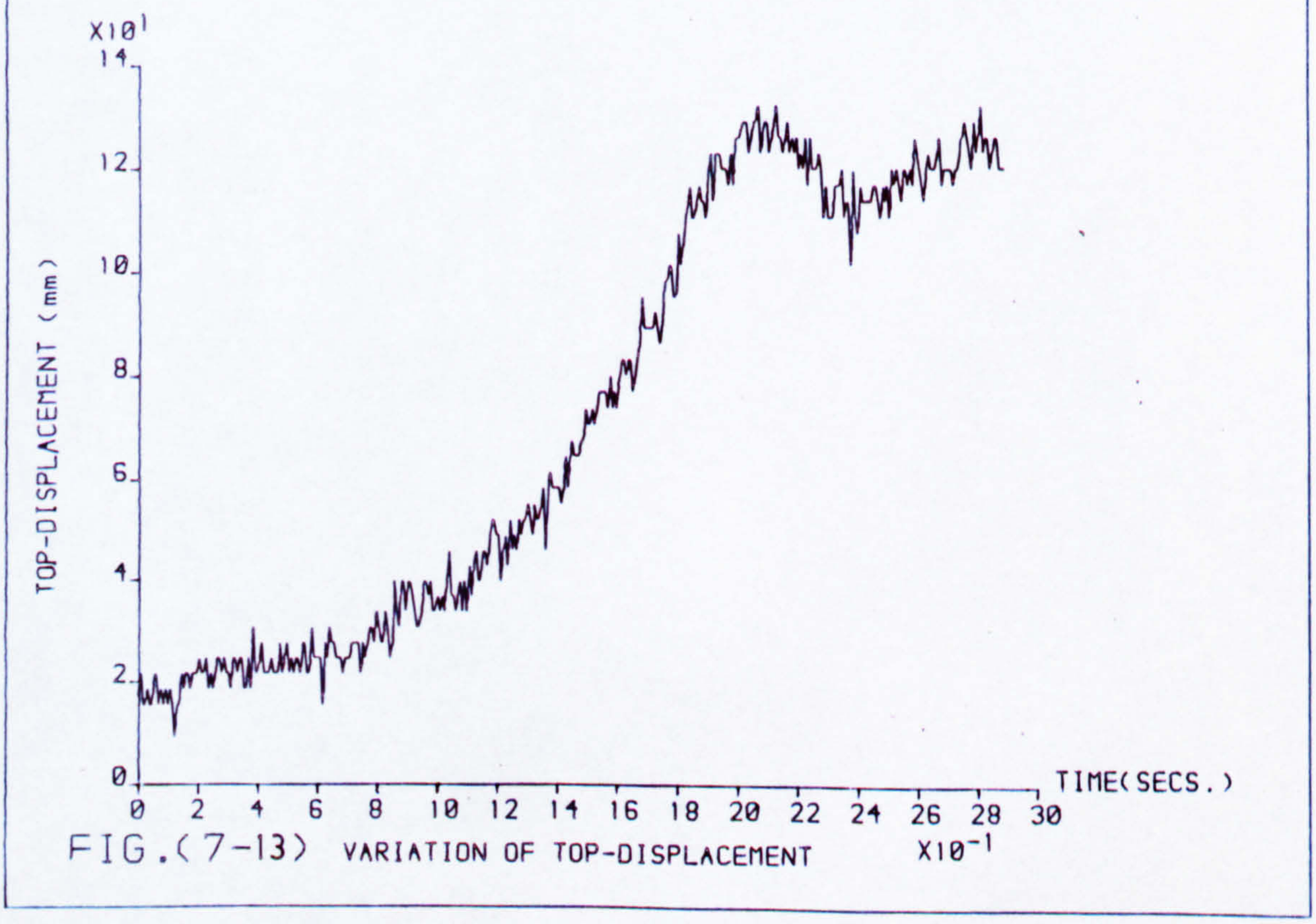

FIG.(7-13) VARIATION OF TOP-DISPLACEMENT

CHAPTER EIGHT

COMPARISON OF THEORETICAL AND EXPERIMENTAL DYNAMIC RESULTS

8.1 Introduction

In order to provide a comparison between theoretical and experimental dynamic results, the single bay two storey frame model was analysed by the methods of theoretical dynamic analyses, previously described in Chpater six, section 6.3 . The theoretical dynamic responses of the frame structure were computed by assuming that the structure was initially at rest at the start of the instability and that dynamic behaviour was initiated by the application of a small constant horizontal force of 20 grams.

8.2 Comparison of Theoretical Results Obtained by Constant Time Interval and Constant Displacement Interval Methods

The free undamped dynamic response obtained by the constant displacement interval method is compared with that from the constant time interval method in the Figs. (8.1) and (8.2). The combinations of the bracing system used for the comparison are given in the figures. The characteristic of the compression bracing is assumed ineffective after the plastic limit of the member.

Figures (8.1) and (8.2) show more convincingly the remarkable accuracy of the constant displacement interval method by comparing the acceleration and displacement computed at different times. The agreement between the two sets of results is so close that the minute discrepandies are indiscernible on the curves plotted. The results by the constant displacement interval are lower than the

results by the constant time interval as shown in Table (8.1). The discrepancies appear to reflect the effect of the value of the interval used in each method. The results of the constant time interval method were obtained with a constant time interval representation equal to 0.0025 second, while the results of the constant displacement interval method were obtained from a constant displacement interval representation of 0.25 mm.

If required, more and more accurate results may be obtained by using smaller intervals of refinement in the solutions, at the expense of greater computational effort. However, the computational time effort of each method varies according to the value of the corresponding interval.

Table (8.1) : Comparison between Constant Time Interval and Constant Displacement Interval Methods

Comparison of:	Constant time interval method	Constant displacement interval method
Time (sec)	1.81321	1.81260
Peak value of disp. (mm)	132.13382	132.1038
Peak value of Acceleration (mm/sec^2)	-17743.74820	-17500.3373

8.3 Comparison of Experimental and Theoretical Results

The dynamic tests were carried out with the five combinations of bracings shown in Table (4.4).

The free undamped theoretical results, for each combination of bracing, were calculated and compared with the corresponding experimental results. A set of results are shown in the Figs. (8.3) and (8.4). The combination of the bracings used for the comparison is given in the figures. The theoretical results were calculated twice. In the first, the two storey framework was assumed to be restrained by fully elastic curved bracings (the response according to this case is represented by the blue curves), while in the second the characteristics of compression bracings were assumed ineffective in the regions after the plastic limits of these bracings (the response according to this assumption is represented by the black curves). The experimental dynamic response, for the combination shown in the figures, is represented by the red curves. It is seen from Fig. (8.3) that the peak value of the theoretical acceleration of the framework restrained by fully elastic bracings (blue curves) is much lower than the corresponding experimental acceleration, also the time base at the peak values is different. While the theoretical results, taking account of plasticity in the compression bracings, are in good agreement with the experimental results.

In Fig. (8.4), the free undamped theoretical results show that the displacement of the structure returns to the initial position, i.e. to the onset of transient instability, while the experimental response shows that the structure is obviously oscillating about the static equilibrium point at the end of the transient instability. This discrepancy between the theoretical and experimental responses could be due to the effect of damping. Therefore the free damped vibration results were recalculated, to take account of damping.

The damping ratio "ζ_d" used in the calculation was calculated from the experimental dynamic results. The following approximation was used to calculate the damping ratio "ζ_d"

$$\zeta_d = \text{Ln} \left(\frac{Q_1}{Q_2}\right) / (2\pi)$$

in which Q_1 is the amplitude of motion at the beginning of a cycle, and Q_2 is the amplitude at the end of the cycle.

The damping ratio "ζ_d" varied from 8% to 17% for the different combinations of bracings. A value of 10% was used for calculating the theoretical free damped vibration for all combinations of bracings.

In the theoretical dynamic analysis, the characteristics of the compression bracings were assumed ineffective after the region of plastic limit of each member, where the compression bracings have already failed by buckling in the region of transient instability, as explained previously in Chapter five.

The theoretical free damped vibration results were compared with the experimental dynamic results as shown in the Figs. (8.5) to (8.14)..

It can be seen from the Figs. (8.5) - (8.14) that reasonable good agreement is generally obtained between the theoretical and experimental results for all combinations of bracings. It is seen also from the figures that the theoretical time response of the structure up to the first peak values, for acceleration and displacement, are generally in good agreement with the experimental time response.

The experimental dynamic response was assumed to start when the lateral displacement was equal to the experimental static displacement at the beginning of the transient instability region.

8.3.1 Comparison of Dynamic Displacements

The experimental displacement at the beginning of each test, i.e. at zero time, is lower than the theoretical displacement. This means that the actual stiffnesses of the bracing system are less than the theoretical stiffnesses, and this reflects, again, the effect of the partial plasticity of the compression members.

The theoretical lateral displacement at the maximum peak, for all combinations of bracing sets, (i.e. when the frame starts to reverse the direction of the first travel) are in very good agreement with the corresponding experimental peaks, as shown in the displacement diagrams.

The experimental displacements in the region between the beginning and the first peak of each combination of bracing are slightly higher than the theoretical results. This indicates the possible stiffening effect of the compression bracing in the partially plastic region, which has been considered as fully elastic stiffening in the theoretical analysis.

It is seen also, from the displacement of experimental and theoretical curves that, the structure is obviously oscillating about the static equilibrium point at the end of the transient instability region. However, the experimental amplitude of displacement decays more rapidly than the theoretical result. The value of the damping factor "ζ_d" could be more significant in this case.

Generally the experimental displacement values agree reasonable well with the theoretical results.

8.3.2 Comparison of Accelerations

The experimental results for the absolute maximum values of acceleration, for all combinations of bracing sets, generally agree well with the theoretical results, with discrepancies, in the maximum accelerations varying from -11% to +11%. The positive discrepancies are associated with the results measured for the right frame in the model, for which, the experimental acceleration at the top of this frame is higher than the theoretical results as shown in the Figs. (8.7), (8.9) and (8.11). The experimental maximum peak of accelerations, in tests 1 and 5, Figs. (8.5) and (8.13) are 11% lower than the maximum theoretical peaks, and this discrepancy is associated with the accelerations measured at the top of the left frame in the model.

In order to find an explanation for the apparent discrepancy, the accelerations, at the top of the left and right frames in the experimental model, were measured for the third combination of bracing sets. A comparison between the obtained results and the theoretical results is shown in Fig. (8.9). It is observed that the curve representing the measured acceleration at the top of the left frame (the green curve) is a constant shift up the curve representing the measured values at the top of the right frame (the red curve). It can also be observed, from the figure, that the maximum theoretical peak of acceleration is approximately 11% lower than the experimental peak for the right frame (the red curve) and

11% higher than the experimental peak of the acceleration at the top of the left frame (the green curve). To discuss the reason for this discrepancy in the results it is important to point out that it is not particularly easy to make a good estimation of a dead load of a model structure. This is because setting out and construction are often not precise, and occupancy loads are uncertain. For this reason a small difference between the estimation of the actual masses of the two frames in the model is likely to be a source of error between the two measured accelerations of the model. Also the effects of various experimental errors may be a second source of discrepancy in the test results, as shown in the discussion of the results, section 8.5 .

A summary of the theoretical and experimental results is given in Table (8.2).

8.4 Effect of Initial Rise "A_o" of the Bracings on the Dynamic Behaviour of the Framework

The numerical results presented in Table (8.2) indicate that, with constant values of the initial rises of the tension bracings, an increase in the initial rise of the compression bracing has the effect of decreasing the maximum lateral displacement and therefore decreasing the absolute maximum acceleration. Also, the results in the table indicate that, with constant values of the initial rises of compression bracings, an increase in the initial rise of the tension bracing has the effect of increasing the maximum displacement and hence increasing the absolute maximum acceleration. This trend of results is consistant with that obtained from the static results, chapter five, section 5.7..

8.5 Discussion of The Results

In comparing the results obtained by theoretical analysis and model tests it must be appreciated that the degree of correspondence obtained is influenced by errors which are present in both sets of results. Good correspondence between theoretical and experimental results does not necessarily mean that the theory is accurate and the experimental technique is sound, unless both sets of results are accurate, since good correspondence can also be obtained between two erroneous sets of results when errors are of similar sense and order. Poor correspondence on the other hand, may be due to deficiencies in the experiments and not due to any inaccuracy of the theory. It is important to be able to identify all possible sources of errors which may be present in both theoretical and experimental investigations and be able to assess their sense and relative importance if the results are to be correctly interpreted.

8.5.1 Experimental Error Discussion

Errors arise in any experimental investigation due to unavoidable deficiencies in the test equipment. Some of these errors may be minimised with a rigorous test procedure when their cause and effects are understood, but some others remain undetermined.

The electrical instruments such as the accelerometer and potentiometer are precision scientific equipment, and provided they are in good working order, errors in acceleration and displacement will be very small. However through regular use and occasional manhandling, defects can develop in the potentiometer equipment, which

may affect its precision. One possible defect which is seldom recognized is due to the mechanical link of the potentiometer wiper drifting out of correct adjustment for the calibration control. This defect which was detected in the potentiometer indicator in regular use resulted in errors in the displacement readings. But since the potentiometer indicator used in the tests had been specifically checked to ensure that the calibration control was correctly set, this source of error can be discounted.

The model was of simple construction with very accurate parts and joints, and could be fabricated to a high standard of finish. Nevertheless, dimensional inaccuracy due to the inherent cross sectional variation of the main elements of the frame in addition to the manhandling variation of the circular shape of the curved bracing members and the inherent thickness variation of the bracing members could still be a source of error which could influence the degree of correspondence between theoretical and experimental results.

Unsymmetric application of the load with respect to the centre line, of the two frame model, will affect the accuracy of the test results due to unsymmetrical bending. However, in all the tests, fairly symmetric horizontal loading and vertical load located over the top wooden plate were achieved, as indicated in Plates (7.1) and (7.2). The vertical load, due to the self weight of the two frame model, may be subjected to slight lack of symmetry in distribution. Therefore errors due to small unsymmetric loading may affect the accuracy of test results. Errors from this source should be small because all precautions were taken into account during the application of the vertical loads.

8.5.2 Theoretical Error Discussion

Inaccuracies associated with the theoretical analysis arise in the modelling and discretisation processes. In idealising the frame model as restrained by non-linear restraints, the characteristic of the compression bracing in the partial plastic region is assumed to be as in a full elastic region. This would result in calculated frame deflections and accelerations being underestimated to a certain extent, but this would depend on the initial rise of the compression bracing, therefore the theoretical dynamic response at points close to the onset of the transient instability region will, to a certain extent, be underestimated.

The discretisation of the continuum into a finite number of elements, in the theoretical analyses, introduces errors of convergence into the numerical results. The nature of these errors depends not only on the interval division but also on the type of problem being solved and on the element characteristics. These errors should be quite small at most points of the analyses except at points close to the end of the first travel, i.e. at the first peak values, where the characteristic curve of the system is very sensitive to a small change in the interval, and the errors in the theoretical accelerations, at these points, are dependent on the difference between the true and the calculated characteristics of the system.

Table 8.2 : Summary of The Theoretical and Experimental Dynamic Results

Initial rise"A_o" mm				Absolute maximum acceleration (m/sec^2)		Maximum displacement		Notes
1st storey		2nd storey						
Comp.	Tens.	Comp.	Tens.	Theor.	Exp.*	Theor.	Exp.	
20	85	20	85	9.395	8.438 L	104.995	105.366	* L : the value was measured for the left frame R : the value was measured for the right frame in the model
20	95	20	85	9.726	10.149 R	105.223	105.652	
20	95	20	95	18.146	16.015 L 20.410 R	132.368	132.323	
20	95	30	95	17.408	19.272 R	131.667	131.865	
30	95	30	95	7.425	6.567 L	130.693	130.938	

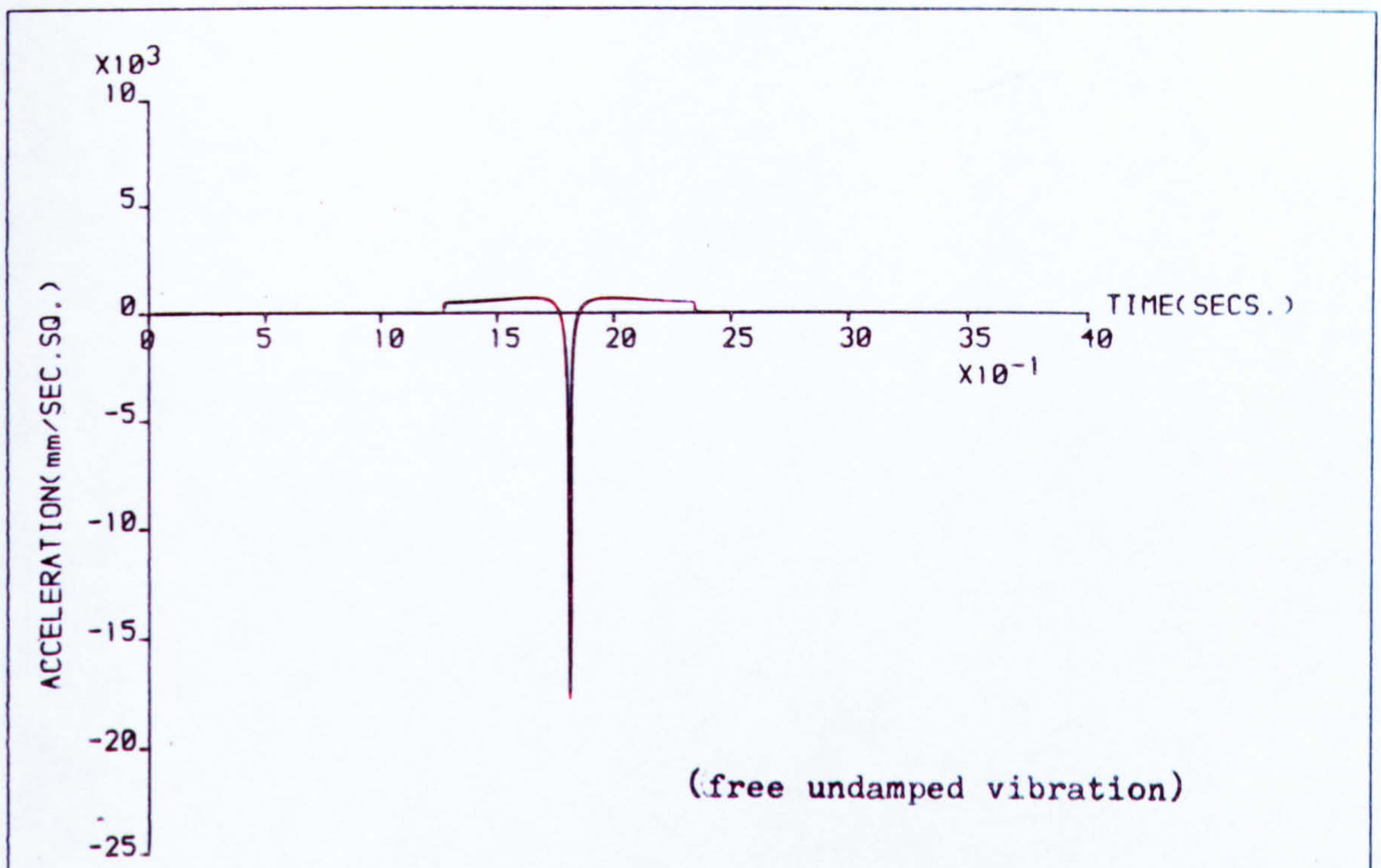

(free undamped vibration)

FIG.(8-1) VARIATION OF ACCELERATION

DYNAMIC BEHAVIOUR OF TWO STOREY FRAME
COMPARISON BETWEEN CONSTANT
DISP. INTERVAL & CONSTANT
TIME INTERVAL METHODS

LOADS: WW=0.1960 (N.)
W= 3.915 P=156.599 (N.)
____ CONSTANT DISP.INTERVAL RESULTS

CONSTANT TIME INTERVAL RESULTS

AC(1)=20.0 AT(1)=95.0 (mm)
AC(2)=20.0 AT(2)=95.0 (mm)

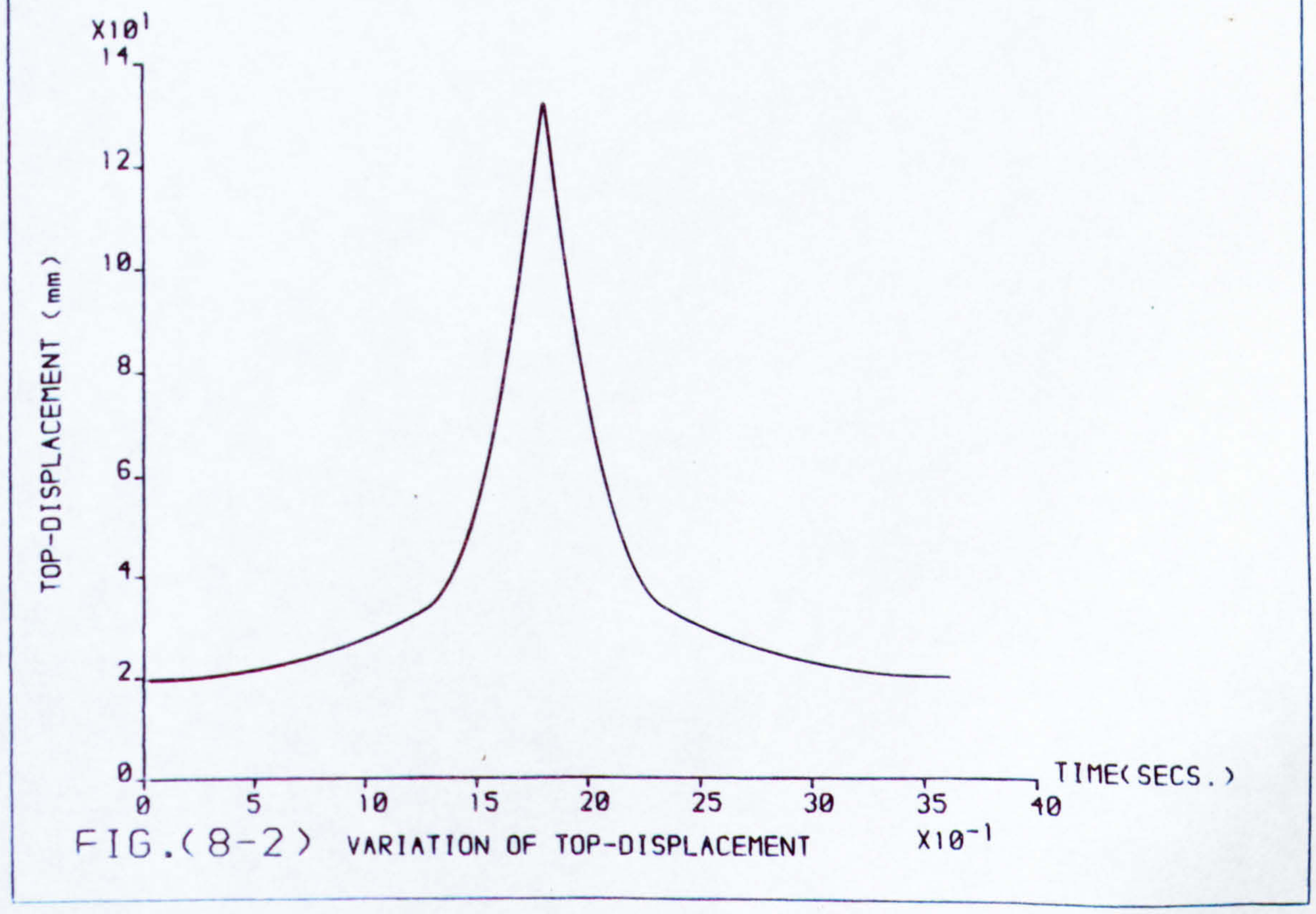

FIG.(8-2) VARIATION OF TOP-DISPLACEMENT

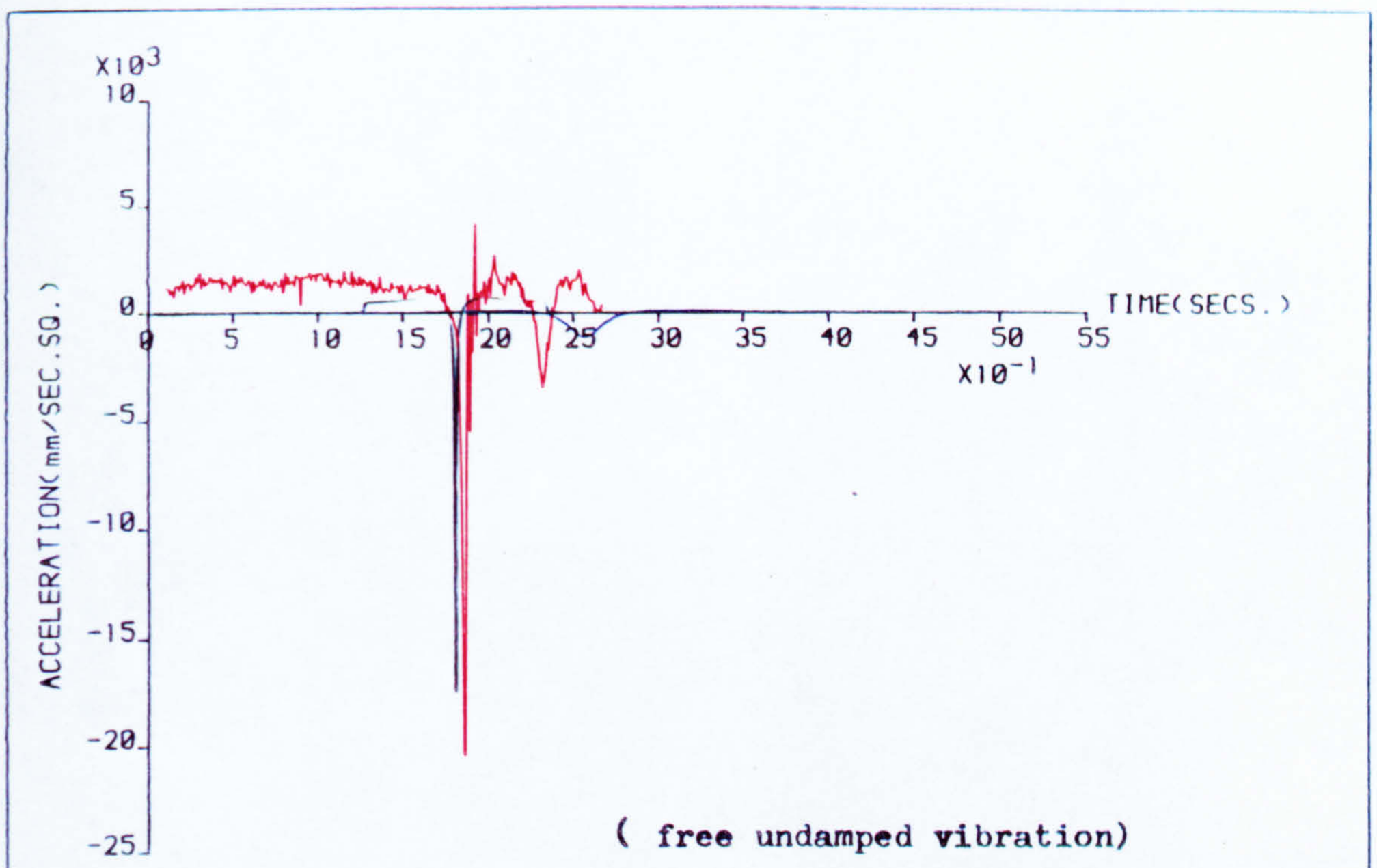

FIG.(8-3) VARIATION OF ACCELERATION

DYNAMIC BEHAVIOUR OF TWO STOREY FRAME
COMPARISON BETWEEN THEORETICAL
& EXPERIMENTAL RESULTS

AC(1)=20.0 AT(1)=95.0 (mm)
AC(2)=20.0 AT(2)=95.0 (mm)

LOADS:	WW	W	P
THEORETICAL:	0.196	3.915	156.599 (N)
TEST :	0.196	4.020	160.818 (N)

THEORETICAL(TOTALLY ELASTIC BRACING)
TEST RESULTS FOR RIGHT FRAME
THEORETICAL WITH EFFECT OF PLSTICITY

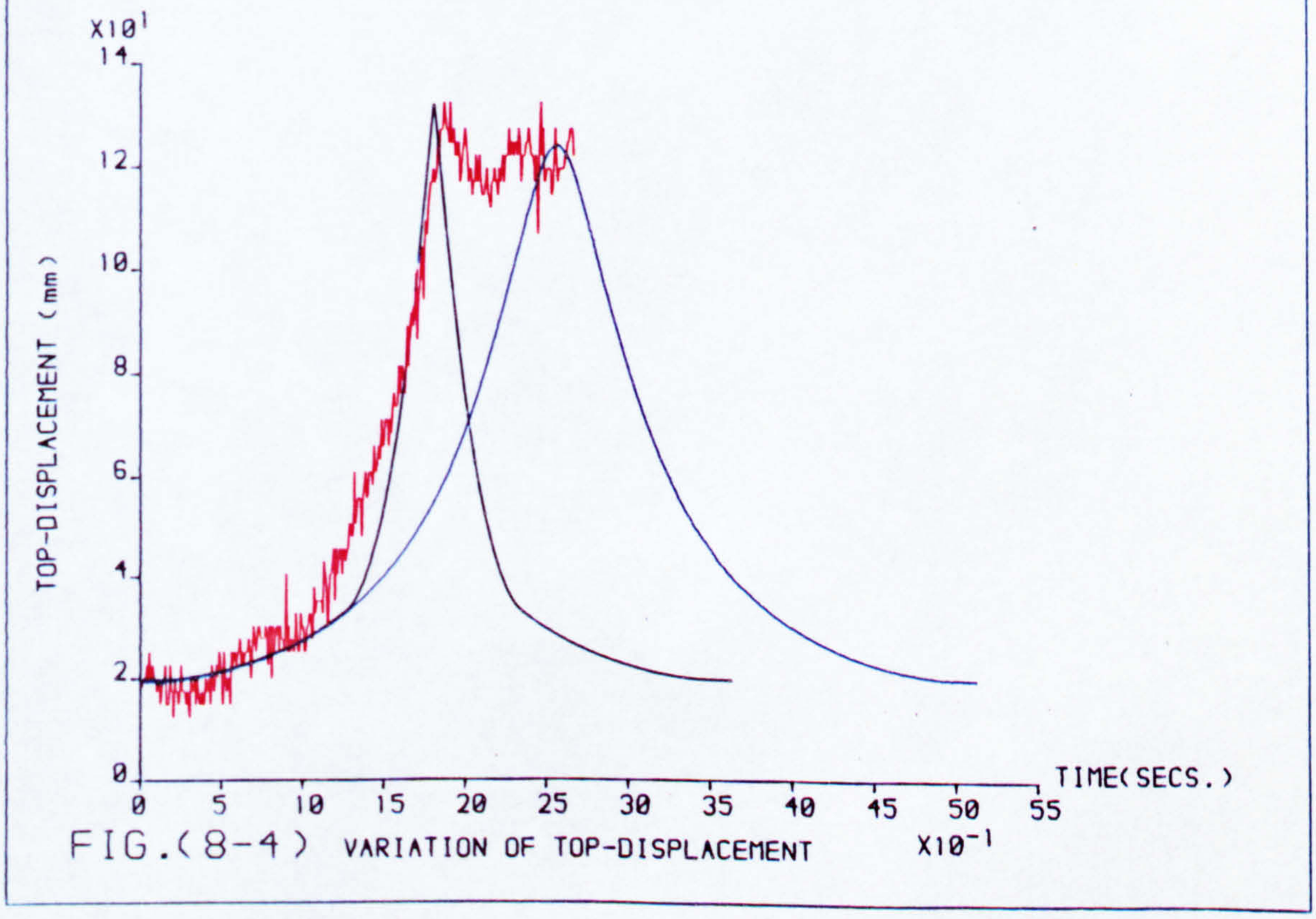

FIG.(8-4) VARIATION OF TOP-DISPLACEMENT

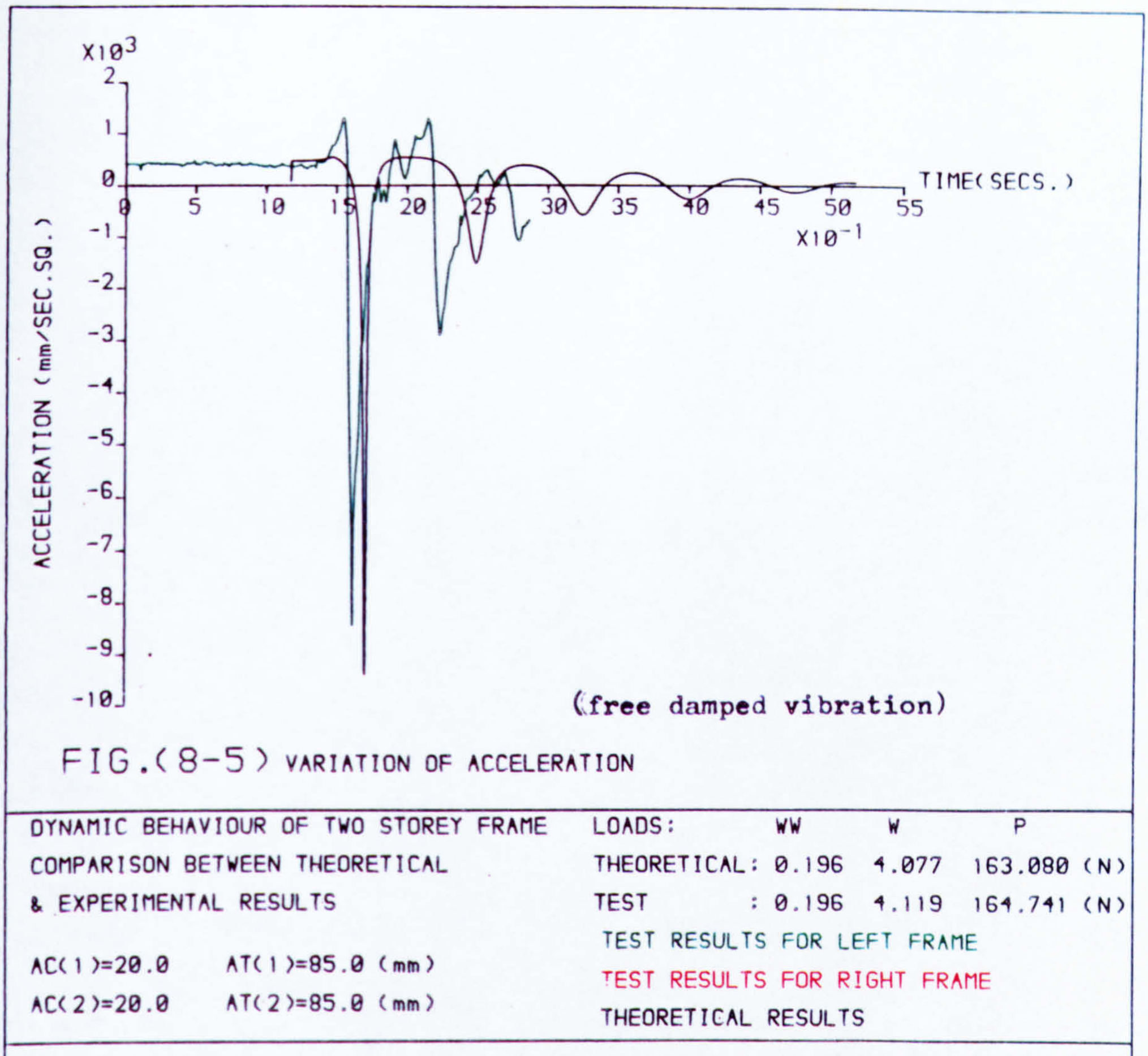

FIG.(8-5) VARIATION OF ACCELERATION

DYNAMIC BEHAVIOUR OF TWO STOREY FRAME
COMPARISON BETWEEN THEORETICAL
& EXPERIMENTAL RESULTS

AC(1)=20.0 AT(1)=85.0 (mm)
AC(2)=20.0 AT(2)=85.0 (mm)

LOADS:	WW	W	P
THEORETICAL:	0.196	4.077	163.080 (N)
TEST :	0.196	4.119	164.741 (N)

TEST RESULTS FOR LEFT FRAME
TEST RESULTS FOR RIGHT FRAME
THEORETICAL RESULTS

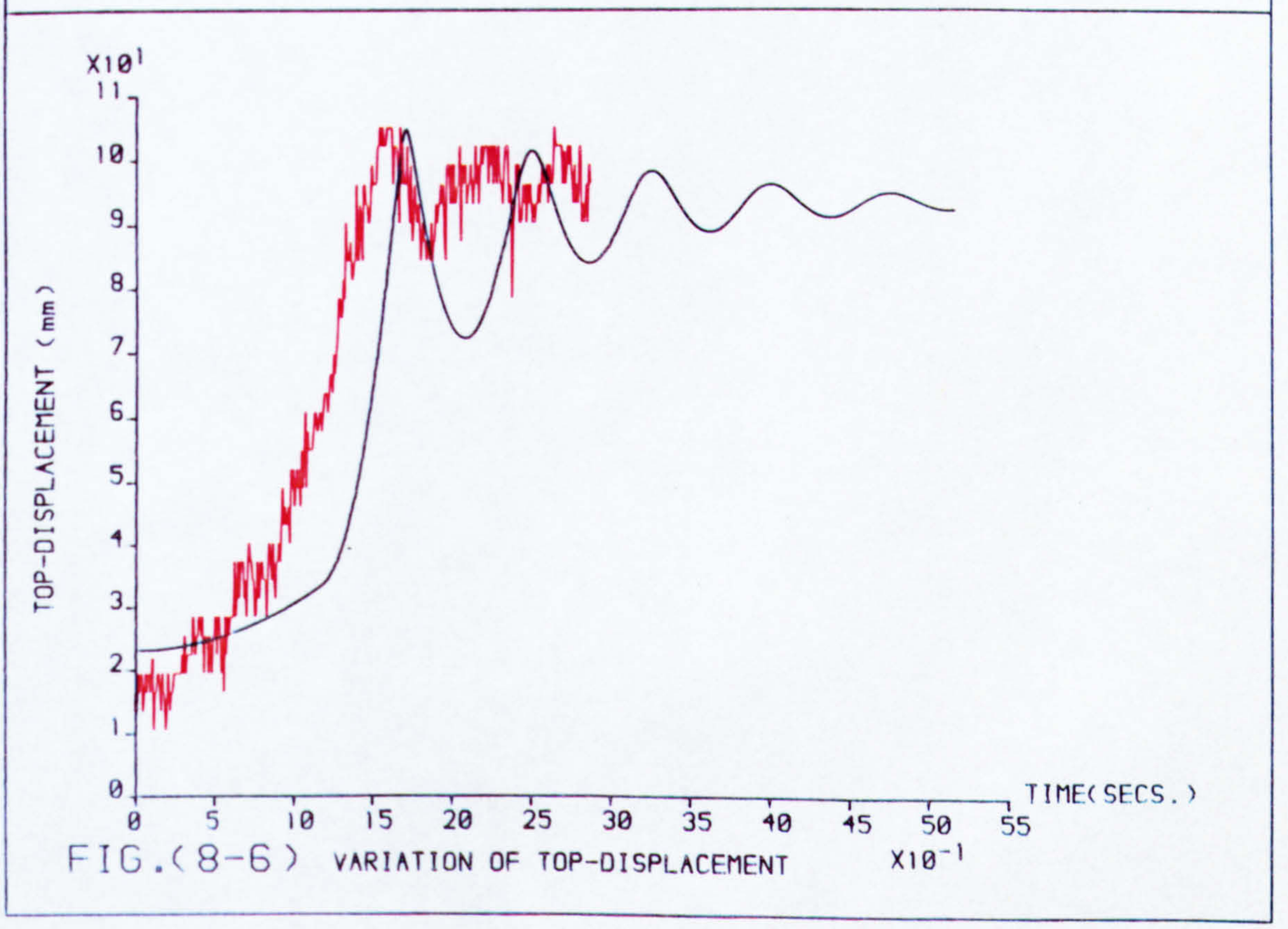

FIG.(8-6) VARIATION OF TOP-DISPLACEMENT

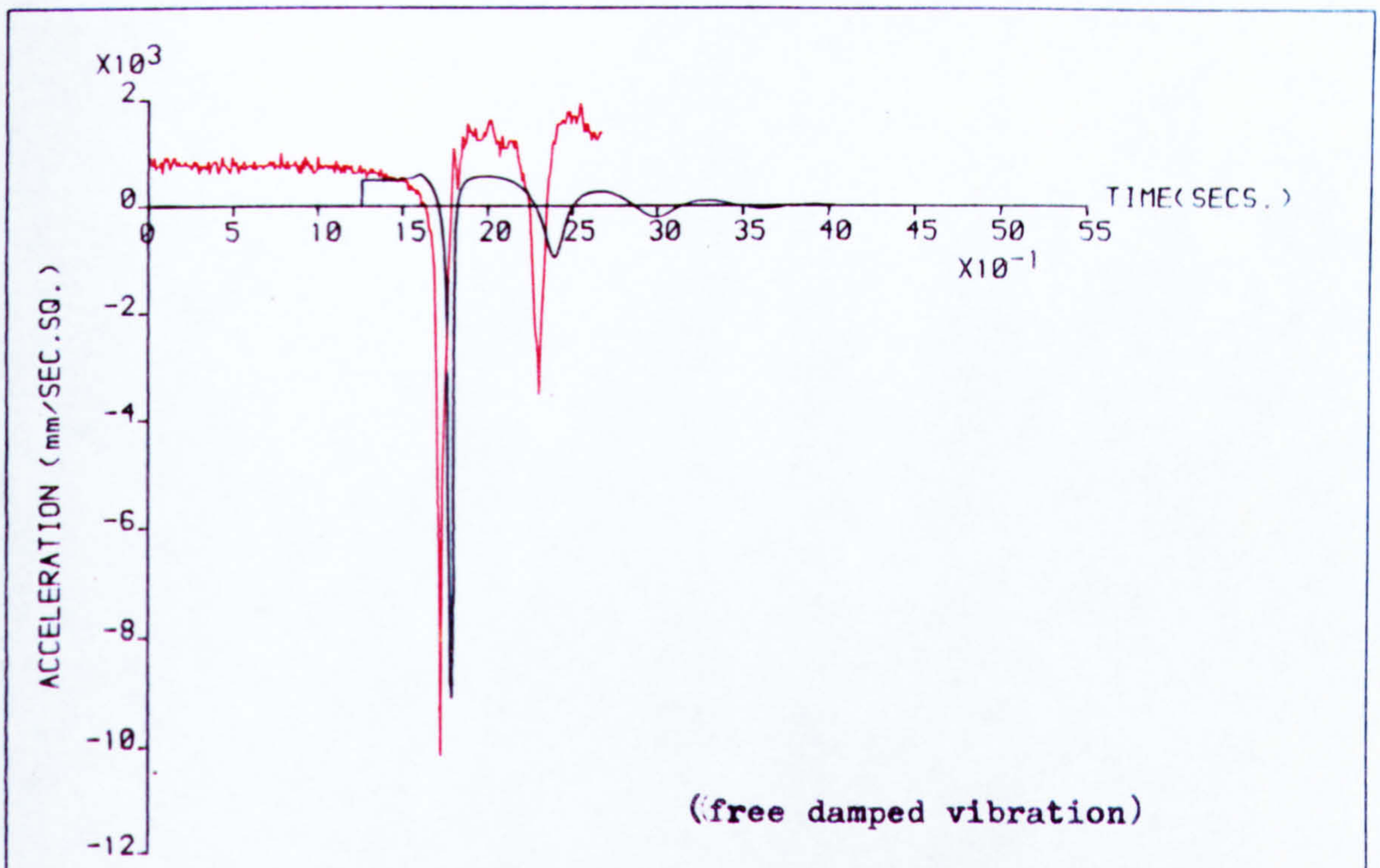

(free damped vibration)

FIG.(8-7) VARIATION OF ACCELERATION

DYNAMIC BEHAVIOUR OF TWO STOREY FRAME
COMPARISON BETWEEN THEORETICAL
& EXPERIMENTAL RESULTS

LOADS:	WW	W	P
THEORETICAL:	0.196	3.994	159.759 (N)
TEST :	0.196	4.040	161.799 (N)

AC(1)=20.0 AT(1)=95.0 (mm)
AC(2)=20.0 AT(2)=85.0 (mm)

TEST RESULTS FOR RIGHT FRAME
THEORETICAL RESULTS

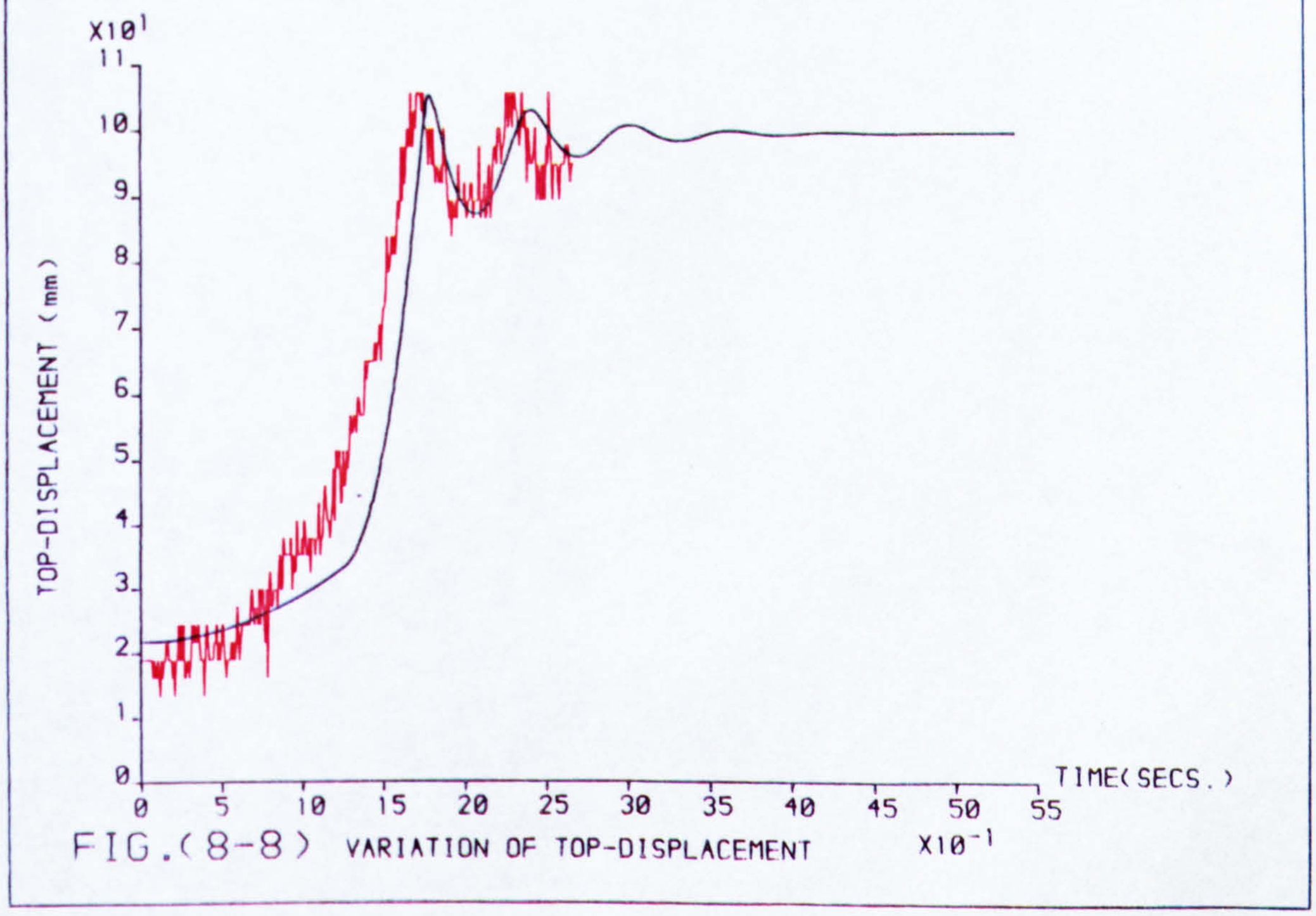

FIG.(8-8) VARIATION OF TOP-DISPLACEMENT

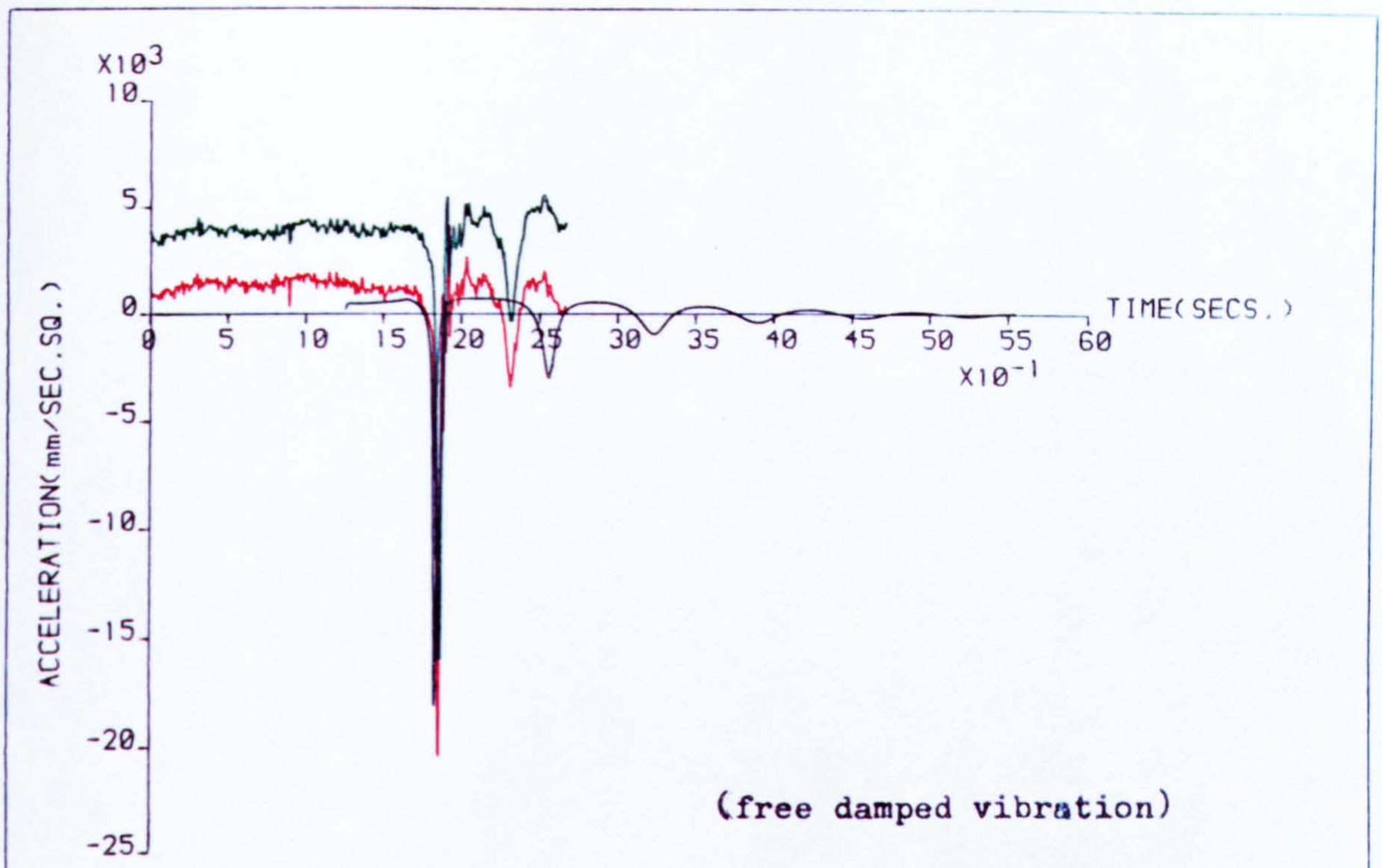

(free damped vibration)

FIG.(8-9) VARIATION OF ACCELERATION

DYNAMIC BEHAVIOUR OF TWO STOREY FRAME
COMPARISON BETWEEN THEORETICAL
& EXPERIMENTAL RESULTS

AC(1)=20.0 AT(1)=95.0 (mm)
AC(2)=20.0 AT(2)=95.0 (mm)

LOADS:	WW	W	P
THEORETICAL:	0.196	3.915	156.599 (N)
TEST :	0.196	4.020	160.818 (N)

TEST RESULTS FOR LEFT FRAME
TEST RESULTS FOR RIGHT FRAME
THEORETICAL RESULTS

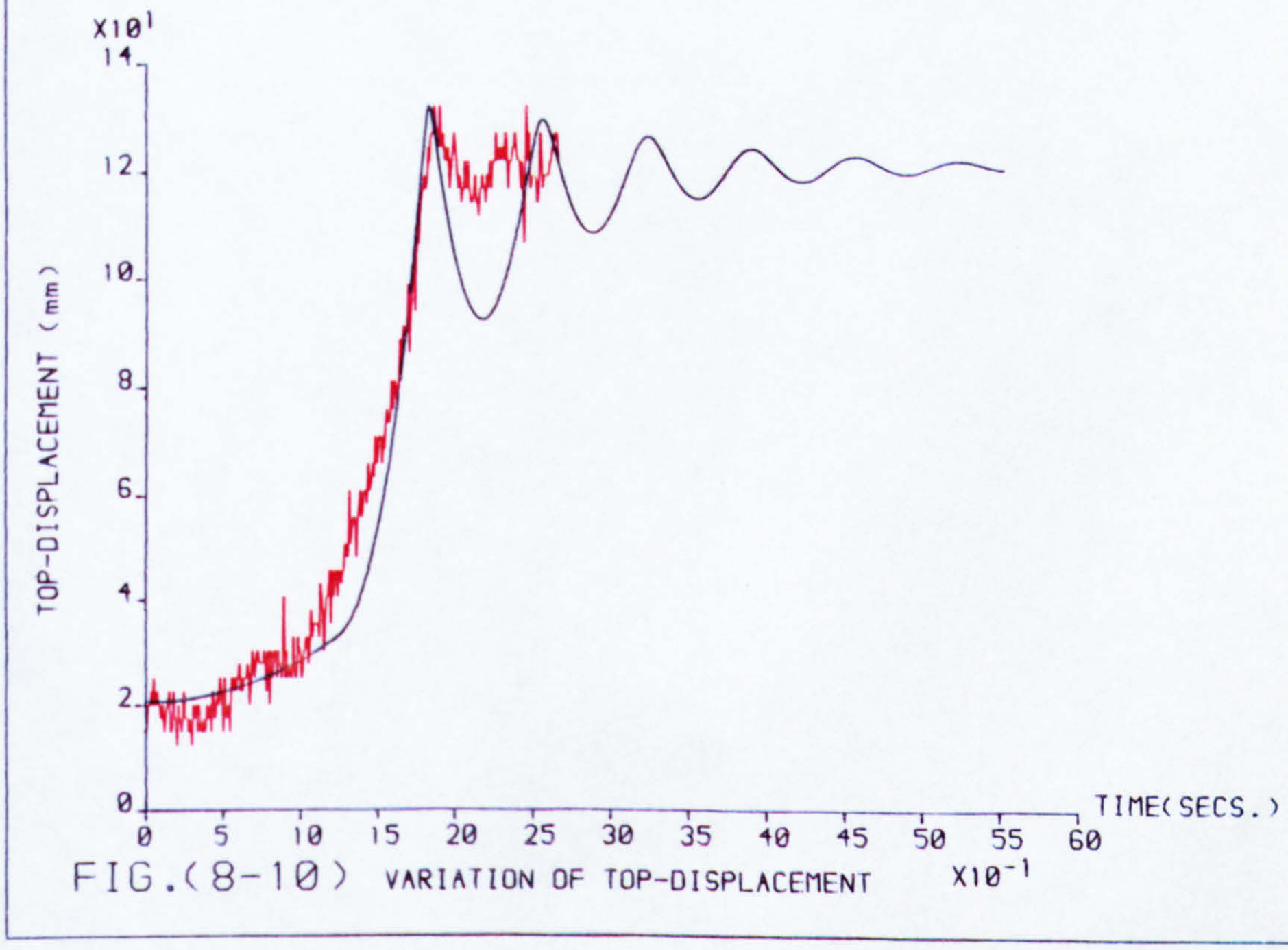

FIG.(8-10) VARIATION OF TOP-DISPLACEMENT

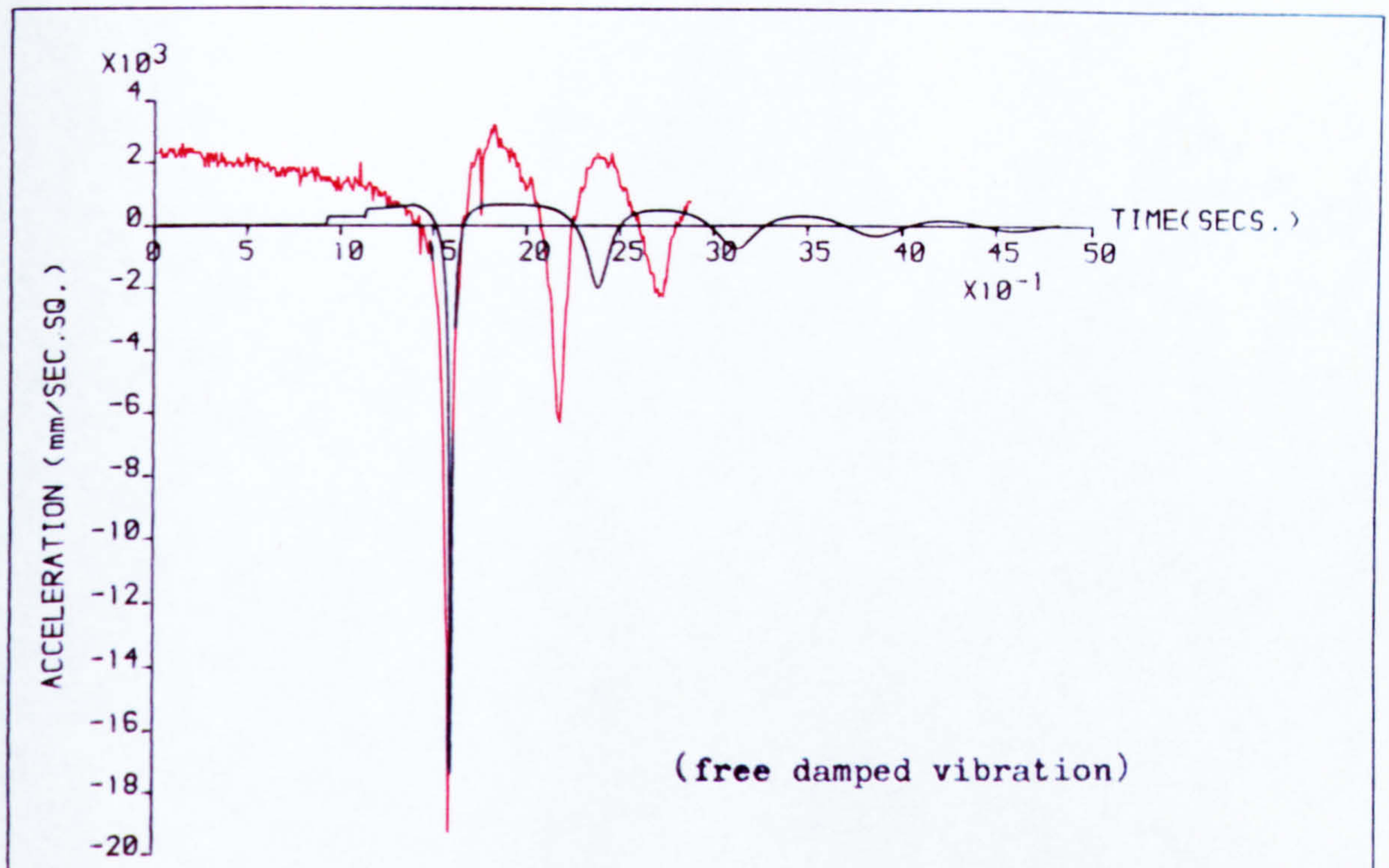

FIG.(8-11) VARIATION OF ACCELERATION

DYNAMIC BEHAVIOUR OF TWO STOREY FRAME
COMPARISON BETWEEN THEORETICAL
& EXPERIMENTAL RESULTS

LOADS:	WW	W	P
THEORETICAL:	0.196	3.437	137.481 (N)
TEST :	0.196	3.432	137.284 (N)

AC(1)=20.0 AT(1)=95.0 (mm)
AC(2)=30.0 AT(2)=95.0 (mm)

TEST RESULTS FOR RIGHT FRAME
THEORETICAL RESULTS

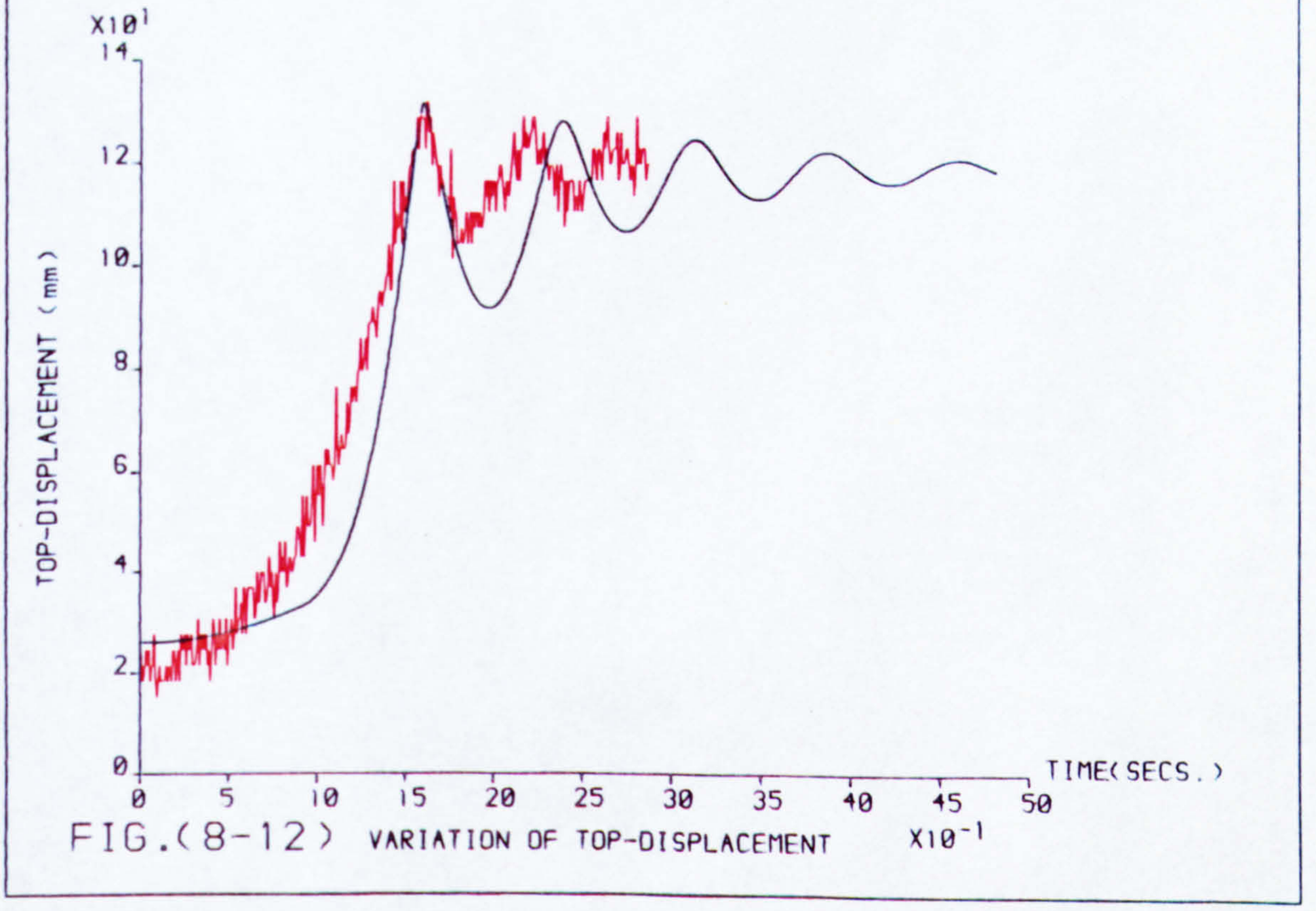

FIG.(8-12) VARIATION OF TOP-DISPLACEMENT

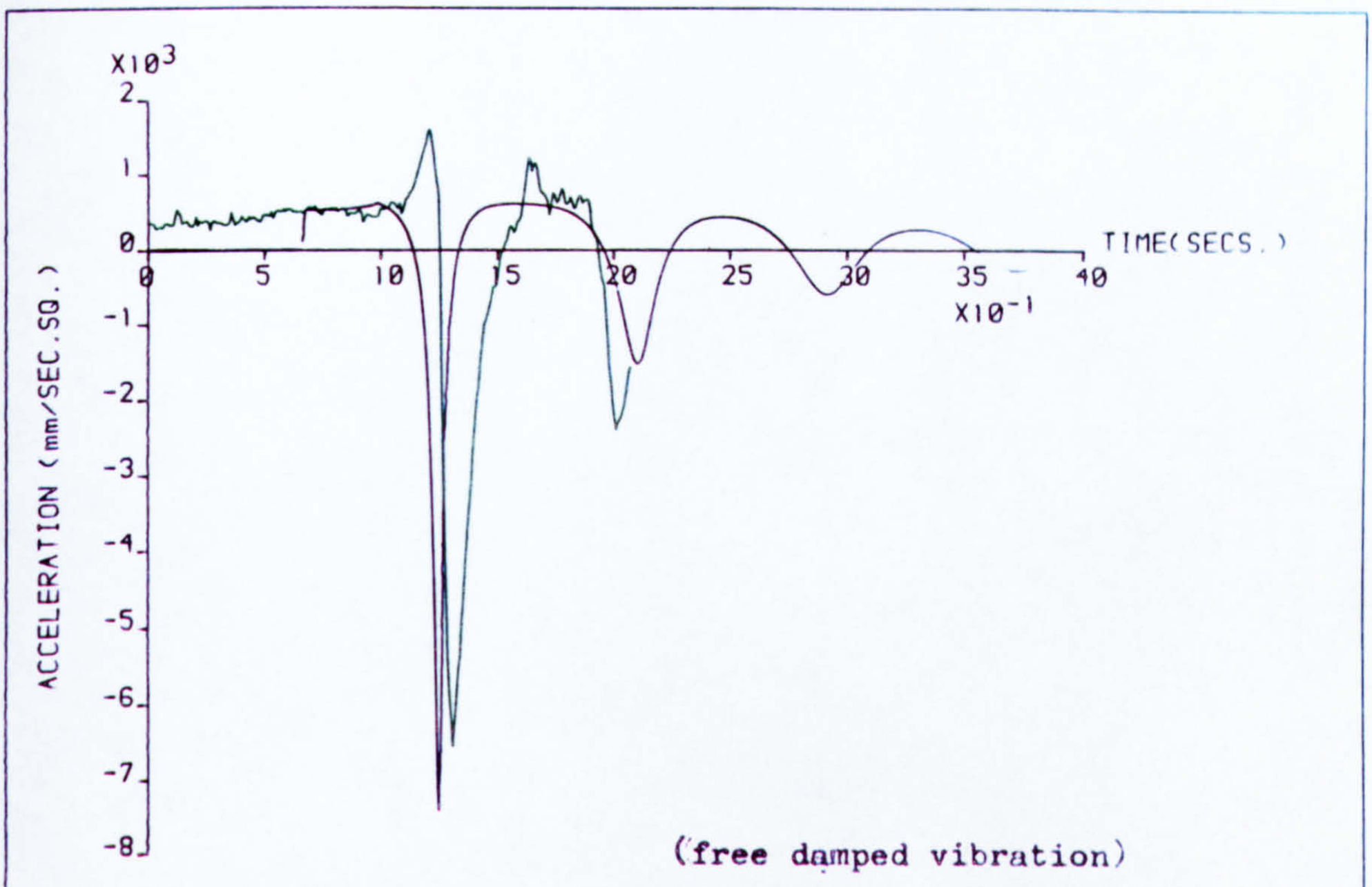

(free damped vibration)

FIG.(8-13) VARIATION OF ACCELERATION

DYNAMIC BEHAVIOUR OF TWO STOREY FRAME
COMPARISON BETWEEN THEORETICAL
& EXPERIMENTAL RESULTS

AC(1)=30.0 AT(1)=95.0 (mm)
AC(2)=30.0 AT(2)=95.0 (mm)

LOADS:	WW	W	P
THEORETICAL:	0.196	3.042	121.665 (N)
TEST :	0.196	3.187	127.478 (N)

TEST RESULTS FOR LEFT FRAME
TEST RESULTS FOR RIGHT FRAME
THEORETICAL RESULTS

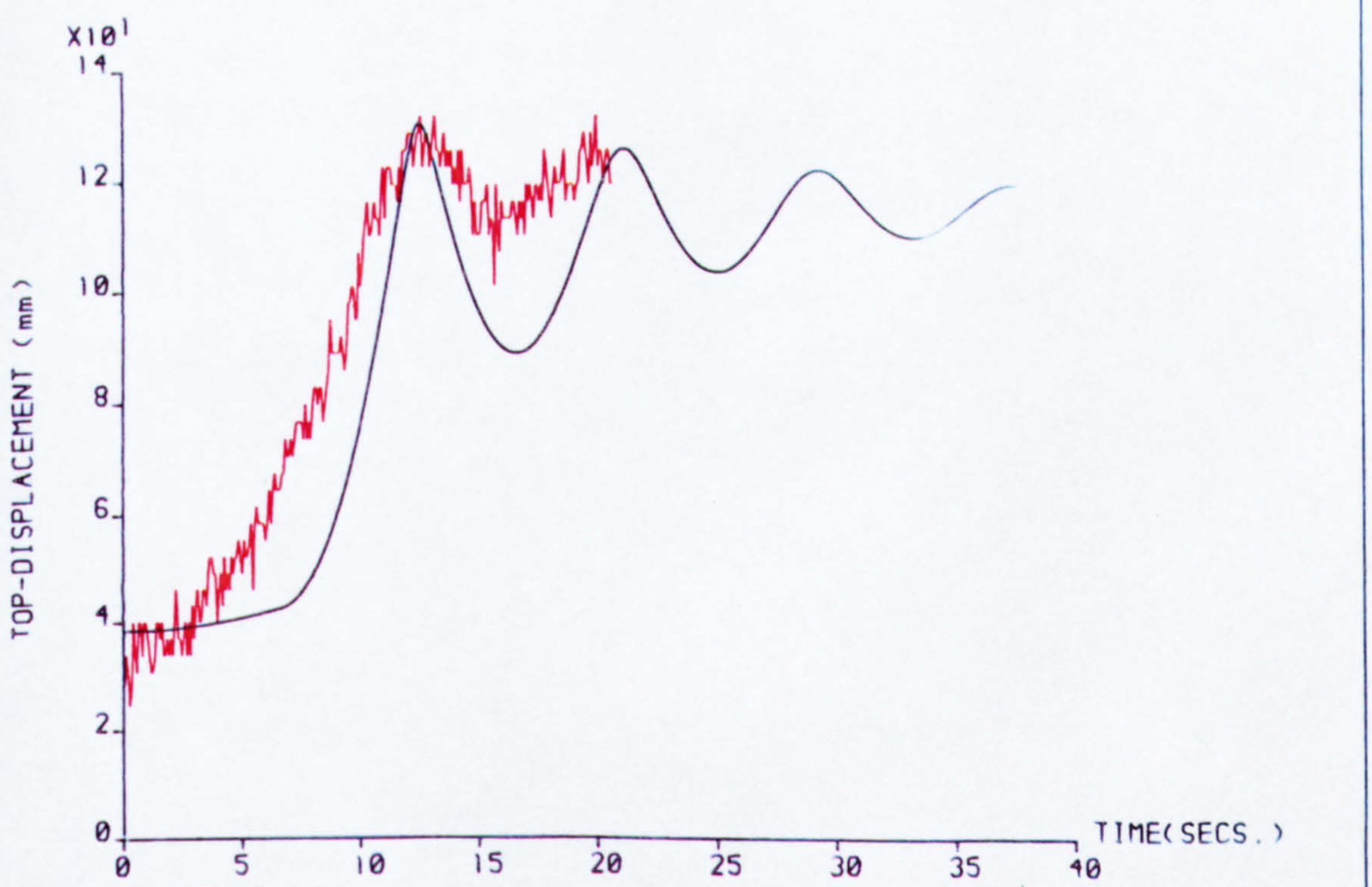

FIG.(8-14) VARIATION OF TOP-DISPLACEMENT

CHAPTER NINE
CONCLUSIONS AND SUGGESTIONS FOR FUTURE WORK

9.1 Description of The Research

The influence of imperfections in the initial geometry of bracing systems of frame structures in a variety of tall building systems is frequently disregarded, or at best approximated by rule of thumb methods, in the lateral load analysis due to lack of understanding of the behaviour of these types of structures. The work described in this thesis not only helps the designer achieve a better understanding of the behaviour of these types of frameworks, restrained by curved bracing systems, but also allows him to use the relatively simple existing techniques to analyse the complicated non-linear frame structural elements.

The buckling and dynamic behaviour of structural systems that have imperfections in the initial geometry of bracing elements, under static loading have been studied. The characteristics of individual curved members have been determined using the theory of large deformations. The theory of elastic buckling stability, of frame system, has been illustrated using the tangent slope and influence coefficient techniques. Stable equilibrium, of this type of structural system, is possible for loads both above and below the critical load "P_{cr1}", those above the critical load being stable after the structure "snaps through" to a new stable equilibrium.

The dynamic behaviour of the structure in the "snap through" region or in the "transient instability" region has been investigated using constant time and constant displacement interval techniques.

The general accuracy of all these techniques has been substantiated by experimental tests on a small scale single column, restrained by curved member or members, and two storey frame work models, and by comparison of the results of the individual curved members, with other investigations as described in Chapter five.

9.2 Characteristics of Individual Curved Bracings

The relationships between members stiffnesses and axial deformations were established for axial or eccentric forces, various lengths, and initial bowing. From the obtained results, for the individual curved members, the following are concluded:

1) The stiffness of the curved struts decreases as the axial displacement increases.

2) The stiffness of the curved ties increases as the axial displacement increases.

3) Swannell's solution is a very good representation of stiffness-displacement behaviour when the ratio A_o/L_o is less than 5%, but at greater ratios the error increases rapidly.

4) The experimental behaviour of the individually curved struts indicates that the partially plastic behaviour is reached particularly early when the strut is relatively short. Conversely this behaviour is delayed when the strut is exceptionally long. Therefore, the actual behaviour of the strut, when the material reaches this condition, is less stiff than it would have been had it remained elastic, consequently displacements are greater than would be expected from the theoretical results.

5) The experimental results concerning the characteristics of individual members agree very well with the theoretical results using the theory of large deformations.

9.3 General Behaviour of Braced Framework Stiffened by Curved Bracing System

The general behaviour of the structural framework restrained by a curved bracing system under a combined load system "P & W", has been discussed and can be summarized as follows:

1) If the combined load "P&W" is applied to the structure gradually from zero, the structure will be stable under the action of the given loads at a point where the lateral displacement "Δ" is less than the critical displacement "Δ_1".

2) If the system of applied load "P&W" is then increased the displacement "Δ" will increase until a limit defined by $\frac{dP}{d\Delta} = 0$ or $\frac{dW}{d\Delta} = 0$ and $\Delta=\Delta_1$ is reached. The value of the vertical load corresponding to this limit condition provides the first instability critical load "P_{cr1}" , with corresponding critical displacement equal to Δ_1 .

3) A small increase in the load system at this limit will lead to a sudden change in the deflection "Δ" until a new equilibrium position is reached, at a point where $\Delta=\Delta_2$. The dynamic effects are very important in this case. The stage between Δ_1 and Δ_2 represents the region of unstable equilibrium or the "transient instability" region.

4) Further increase in the applied load system "P&W" increases the lateral displacement "Δ" and the structure will be

in stable equilibrium.

5) Transient instability is particularly dependent on the ratio R = P/W. If this ratio is high then transient instability is more likely to occur.

9.3.1 Estimating the Efficiency of the Tangent Slope Method

The tangent slope and the influence coefficient techniques have been employed to define the limiting conditions of the transient instability region, to calculate the critical load "$P_{cr\bar{1}}$" and the corresponding critical displacement "Δ_1" at the onset of this region , and also to determine the lateral displacement "Δ" corresponding to any applied load system "P&W".

The tangent slope technique yields results of comparable accuracy to those given by the influence coefficient technique, and has distinct computational advantages. The influence coefficient technique, on the other hand, is extremely versatile.

The experimental results concerning the general behaviour of this type of structures agree very well with the expected theoretical results calculated by the tangent slope technique.

9.3.2 Influence of Initial Rise "A_o" of the Combined Bracing System

It has been shown that some imperfections such as the initial curvature of bracing members and the out-of-plumb erection of tall building frames stiffened by vertical trusses cannot be neglected. A critical state has been defined by considering the combination of those imperfections. The critical load causing this critical state

has been determined. The effect of the initial rise of the tension bracings magnifies the range of the transient instability region which causes a reduction in the critical load. The effect of the initial rise of the compression bracings,also, magnifies the range of the transient instability region and reduces the value of the critical load. Experiments verified this transient instability region and the influence of the imperfections. The presence of major imperfections in the tension bracings and minor imperfections in the compression bracings of the system have an appreciable effect on the critical load.

9.4 Dynamic Behaviour of Braced Framework Stiffened By Curved Bracing System

The dynamic analysis of the structural framework stiffened by a curved bracing system has been discussed. The dynamic behaviour started where a critical state (transient instability region) had been defined by considering the combination of the initial imperfections. The dynamic behaviour of this structural system has been illustrated using constant time interval and constant displacement interval techniques.

The numerical constant displacement procedure is simpler than some existing procedures and is found to be more accurate. This numerical method of dynamic analysis is applicable to any undamped, damped, free and forced vibration of structural frameworks. The dynamic response of non-linear frameworks can also be obtained. The constant displacement interval technique has been shown to be an efficient method for evaluation of the dynamic response of a frame structure restrained by a non-linear bracing system.Sufficiently accurate results

can be obtained by the method using a small interval of displacement. The accuracy of the results have been confirmed by comparing them with accurate constant time interval results and with available experimental results.

The effect of the inelastic material of the compression members on the dynamic behaviour magnifies the range of the transient instability region which causes a further magnification of the dynamic response.

9.4.1 Influence of Initial Rise "A_o" of the Bracing on the Dynamic Response

The dynamic behaviour of the framework restrained by curved bracing system allows the structure to sway freely through the transient instability region. The response of the structure started at the onset of this region and continued to pass the end of this instability region. The structure was obviously oscillating about the static equilibrium point at the end of instability region. The dynamic response of the structure in this critical state has been determined, for different combinations of bracing system. The effect of decreasing the initial rise of the compression bracings magnifies the range of the dynamic response, as does an increase in the initial rise of the tension bracing. Accordingly the dynamic response, of minor imperfections in the compression bracings and major imperfections in the tension bracings, has a relatively important influence on the overall buckling behaviour of the system.

9.5 Suggestions for Future Work

In connection with the problems examined, a number of related topics of practical interest deserve examination in future studies.

In system construction of braced frame structures, the columns and the beams are usually connected by rigid joints which have to serve the primary function of transmitting shear forces between the components. The detailing of the joints is often such that the moment connection between the beams and the columns can be achieved. The effects of joints rigidity on the braced frame behaviour need to be examined.

The study on the restrained frame structures by curved bracings has considered only the deformation in the curved bracings. Bending and tortional deformations of the structure due to non-uniform lateral loading or structural asymmetry produce deflection and warping in the columns and beams of the framework. Since the bending and the warping stiffnesses of the columns and the beams provide certain amounts of restraint against the bending and torsional deformations of the framework it is desirable to examine the bending and the warping action of the columns and the beams of the framework, and assess its contribution to the overall behaviour of the structure.

The present work has been concerned purly with non-linear elastic analysis for curved bracings for multistorey frameworks. Effects of plastic yielding of the main elements of the framework and bracings are known to produce a non linear structural response

and redistribution of the action in the bracings. The need for extending the present study to the investigation of non-linear elasto-plastic behaviour, of steel structures with non-linear restraints, is apparent.

REFERENCES

1 AJMANI, J.L. "Stability of Columns Restrained by Side-rails". Journal of the Structural Engns. No. 8., Volume 49. August, 1971.

2 ALLEN, H.G. AND BULSON, P.S. "Background to Buckling" McGraw-Hill Book Company, U.K., Ltd. 1980.

3 BOLTON, A. "A Simple Understanding of Elastic Critical Loads" Journal of the Structural Engineering, Vol. 54, No. 6, pp. 213-218, June, 1976.

4 BOLTON, A. "The Critical Load of Portal Frames When Sidesway is Permitted" J. of the Structural Engineers, August, 1965.

5 BRUSH, D. AND ALMROTH, B. "Buckling of Bars, Plates and Shells" McGraw-Hill Book Co. Inc., New York, 1975.

6 BLEICH, F. "Buckling Strength of Metal Structures" McGraw-Hill Book Co. Inc., New York, 1952.

7 BOWMAN, F. "Introduction to Elliptic Functions" English Universities Press. Ltd. 1953.

8 BYRD, P.F. AND FRIEDMAN, M.D. "Handbook of Elliptic Integrals for Engineers and Scientists" 2nd Ed. Springer, Berlin. 1971.

9 BIRD, J.O. AND MAY, A.J.C. "Technician Mathematics" Level 4 and 5, Longman Group Ltd. 1981.

10 BURTON RODIN "Calculus With Analytic Geometry" Prentice-Hall Inc., 1970.

11 BALFOUR, A. AND MARWICK, D.H. "Programming in Standard Fortran 77" The Chancer Press Ltd., Bungay, 1982.

12 BOYCE, W.E. "Buckling of a Column With Random Initial Displacement" Journal of the Aerospace Sciences, Vol. 28, pp 308-312, 320, 1961.

13 BREBBIA, C. AND CONNOR, J. "Geometrically Non-linear Finite Element Analysis" Journal of the Eng. Mechanics Division, ASCE, Vol. 95, No. EM2, Paper 6516, April 1969, pp 463-483.

14 CHEN, W.F. AND ATSUTA, T. "Theory of Beam-Column" Volume 1
McGraw-Hill Book Co. Inc., New York, 1976.

15 COULL, A. AND DYKES, A.R. "Fundamentals of Structural Theory"
McGraw-Hill Publs, 1972.

16 CRISFIELD, M.A. "Incremental Iterative Solution Procedures for Non-linear Structural Analysis"
"Numerical Methods for Non-linear Problems"
Vol. 1, C. Taylor, E. Hinton and D.R.J. Owen, eds,
Pineridge, Swansea, England, 1980, pp 261-290.

17 COX, M.G. AND HAYES, J.G. "Curve Fitting" : A Guide and Suite of Algorithms for the Non-specialists User : Report NAC26, National Physical Laboratory, Teddington, Middx, 1973.

18 CONWAY, H.D. "The Non-linear Bending of Thin Circular Rods"
Journal of App. Mech. 23, Trans. ASME, 78, SerE, 1956, 7.

19 CHARLES, BIRNSTIEL AND JORAME S.B.I. "Factors Influencing Frame Stability"
Proc. ASCE, Structural Div., Vol. 106, ST2, Feb 1980.

20 COX, H.L. "Stress Analysis of the Metal Construction"
J. of the Royal Aeronautical Society, Vol.44, pp 231-282, 1940.

21 ELLYIN, F. "Non-linear Response and Stability of Structures"
Canadian Journal Civ. Eng. 10, 27-35, 1983.

22 FUNG, YUAN-CHEN "Buckling of Low Arches or Curved Beams of Small Curvature"
Polytechnic Institute of Brooklyn, 1952.

23 FRASER, W.B. AND BUDIANSKY, B. "The Buckling of a Column With Random Initial Deflections"
Journal of Applied Mechanics, Vol. 36, 1969, p 233.

24 FOX, L. AND I.B. PARKER, "Chebyshev Polynomials in Numerical Analysis"
Oxford University Press, 1968.

25 FRASER, D.J. "Evaluation of Effective Length Factors in Braced Frames"
Canadian Journal Civ. Eng. 10, 18-26, 1983.

26 GREGORY, M.S. "Elastic Instability : Analysis of Buckling Modes and Loads of Framed Structures"
London, Spon's Civil Eng. Series, 1967.

27 GAUDHAN, J. "The Stability of Steel Compression Members" J. of ISE. The Structural Engineer, Vol. 55, No. 8, August, 1977.

28 GOLDBERG, J.E. "Approximate Methods in Stress and Stability" Analysis of Tall Building Frames" Regional Conference on Tall Building, Bankok, Jan. 1974.

29 GOLDBERG , J.E. "On the Lateral Buckling of Multi-storey Building Frames With Shear Bracing" Final Report of the Sixth Congress International Association for Bridge and Structural Eng. Stockholm, 1960.

30 GILBERT, R.B. AND CALLADINE, C.R. "Interaction Between the Effects of Local and Overall Imperfections on the Buckling of Elastic Columns" J. Mech. and Phys. of Solids 22, 1974, p 519.

31 GALOUSSIS, E.G. "On a Critical State of Braced Structures Caused by Imperfections" The Sino-American Symposium, Sept, 1982.

32 GALOUSSIS, E.G. "The Stability of Imperfect Structural Systems Reinforced by Vertical Trusses" Instability and Plastic Collapse of Steel Structures, Proc. of the Michael R Horne Conference. Manchester, Granada, 1983.

33 GERARD, G. AND BAKER. "Handbook of Structural Stability" Vol. I, II, III NAGA TN 3783, 1957.

34 HORNE, M.R. AND MERCHANT, W. "The Stability of Frames" Pergamon Press Ltd., Oxford, England, 1965.

35 HORNE, M.R. "An Approximate Method for Calculating the Elastic Critical Load of Multi-Storey Plane Frames" Journal of the Structural Eng., Vol. 53, No. 6, June 1973, pp 242-248.

36 HARRISON, H.B. "Large Deflection Analysis of Elastic Columns and Frames" International Colloquim on Stability of Structures Under Static and Dynamic Loads, Washington D.C. Mar-17-19, 1977.

37 HANCOCK, H. "Elliptic Integrals" Wiley, New York, 1917.

38 HAYES, J.D. "Numerical Methods for Curve and Surface Fitting" Bull, Inst. Maths Applies. 10, pp 144-152, 1974.

39 HAYES, J.D. "Numerical Approximation to Functions and Data"
Chapter 5, Athlone Press, London, 1970.

40 HORNE, M.R. "The Elastic-Plastic Theory of Compression Members"
J. Mech. Phys. Solids, 4, 104-120, 1956.

41 HYELMSTAD, K.D. AND POPOV, E.P. "Characteristics of Eccentrically Braced Frames"
J of Struct. Eng. ASCE, ST2, Vol. 110,Feb. 1984.

42 JOHNSTON, B.G. "Guide to Stability Design Criteria for Metal Structures"
J. Wiley. Int. Publs., New York, 1976, 3rd Ed.

43 JENKINS, J.A., T.B. SEITZ, AND J.S. PREEMIĖNIECKI
"Large Deflections of Diamond-Shaped Frames"
International of Solids and Structures, Vol. 2, 1966, pp. 591-603.

44 KIRBY, P.A. AND NETHERCOT, D.A. "Design for Structural Stability"
McGraw-Hill Publs., 1979.

45 KORN, A. "The Approximation of Stability Effects on Frames"
Pub. Int. Ass. Bridge Struct., 28, 101-112, 1968.

46 KORN, A. "Effect of Bowing on Rectangular Plane Frames"
Journal of the Struct. Division, ST3, March, 1981, Vol. 107, pp 569-574.

47 LIND, N.C. "Simple Illustration of Frame Instability"
Journal of the Structural Division, ASCE, 103, ST1, pp1-8, 1977.

48 LAWRENCE, H.N.L. "Stability of Non-linear Systems"
Journal of the Eng. Mechanics Division, Vol. 88, EM2, pp 81-93, 1962.

49 LIVESLEY, R.K., AND CHANDLER, D.B. "Stability Functions for Structural Framework"
Manchester University, University Press, England, 1956.

50 LIVESLEY, R.K. "Matrix Method of Structural Analysis"
Pergamon, 1975.

51 LOW, M.W. "Some Model Tests on Multistorey Rigid Frames"
Proc. ICE, Vol. 13, 1959.

52 LAY, M.G. AND GALAMBOS, T.V. "The Experimental Behaviour of Restrained Columns"
Welding Res. Council Bull. No. 110, 17-38, 1965.

53 LU, L.W. "A Survey of Literature on The Stability of Frames"
Welding Res. Council Bull, Engng. Foundation, No. 81, 1-11, 1962.

54 MAJID, K.I. "Non-linear Structures"
Butterworth, London 1972.

55 MAJID, K.I. "Theory of Structures with Matrix Notation"
London, Newns-Butterworth. Publs, 1978.

56 MACLEOD, I.A. AND MARSHALL, J. "Elastic Stability of Building Structures"
Instability of Plastic Collapse of Steel Structures, Proc. of the Micheal R. Horne Conference, Manchester, Granada, 1983.

57 MACLEOD, I.A. "Simplified Equations for Deflection of Multi-Storey Frames"
Buil. Sci. Vol. 6, 25-31, 1971.

58 MILNER, H.R. "Accurate Finite Element Analysis of Large Displacements in Skeletal Frames"
Computer & Structures Vol. 14 No 3-4, pp 205-210, 1981.

59 MERCHANT, W. "The Failure Load of Rigidly Jointed Frameworks as illustrated by Stability"
J. of Struct. Eng. ASCE, Vol. 32 , p 165, 1954.

60 MERCHANT, W. "The Buckling of Pin-ended Struts Under Axial Load"
J. of Struct. Eng. Vol. 27, pp 363, Sept, 1949.

61 MITCHELL, T.P. "The Non-linear Bending of Thin Rods"
J. Appl. Mech. 26, Trans, ASME, 81, Ser. E, 1959.

62 MEROVICH, A.T., NICOLETTI, J.P. AND HARTLE, E. "Eccentric Bracing in Tall Buildings"
J. of Structural Division, ASCE, ST9, September 1982.

63 MASSONET, C.E. "European Approaches to P-Δ Method of Design"
J. of Struct. Division ASCE, Vol.104, No. ST1, Jan 1978, pp 193-198.

64 MARTIN, H.C. "Finite Element and the Analysis of Geometrically Non-linear Problems"
Proc.Japan-US Seminar on Matrix Methods in Structural Analysis and Design, Tokyo, Japan, 1969.

65 MARCAL, P.V. "Effect of Initial Displacement on Problems of Large Deflection and Stability"
Brown University Engineering Report ARPA E54, No. 1967.

66 MATHESON, J.A.L. "Hyperstatic Structure" Vol. 1,
Butterworth & Co Ltd., 1971.

67 NAG. FORTRAN LIBRARY MANUAL, MARK II
"Strathclyde University - Computer Centre"
Volume 2, D02K - E02
Volume 6-S "Approximation of Special Functions"

68 ORAN, C. "Tangent Stiffness in Plane Frames"
Journal of Struct. Div., ASCE, Vol. 99, No ST6, June, 1973.

69 POWELL, G.H. "Theory of Non-linear Elastic Structures"
J. of the Struct. Div., ASCE, Dec. 1969.

70 POSKITT, T.J. "Numerical Solution of Non-linear Structures"
J. of the Struct. Div., ASCE, Vol. 93, No. ST4, August, 1967.

71 PEIRCE, B.O. "A Short Table of Integrals"
GINN Company, 4th Edition, 1956.

72 POPOV, E.P. "An Update on Eccentric Seismic Bracing"
Eng. Journal, AISC, 3rd Quarter, 1980.

73 ROORDA, J. "The Buckling Behaviour of Imperfect Structural Systems"
J. of Mech. and Phys. of Solids, Vol. 13, pp 267-280, 1965.

74 ROEDER, C.W. AND POPOV, E.P. "Design of Eccentrically Braced Steel Frame"
Engineering Journal, AISC, 4th Quarter, 1981.

75 ROOSOW, E.C., BARNEY, G.B. AND LEE, S.L. "Eccentrically Loaded Steel Column with Initial Curvature"
J. of Struct. Div., ASCE, Vol. 93, ST2, 1967.

76 SABMINS, G.M., HARRIS, H.G., WHITE, R.N. AND MIRZA, M.S.
"Structural Modelling and Experimental Techniques"
Prentice-Hall, Inc. Englewood Cliffs, 1983.

77 SWANNELL, P. "The Elastic Buckling of Columns Constrained by An Initially Curved Rail"
Transaction Institution of Engineers, Australia,
Vol. CE15, No. 1, 1973.

78 SOUTHWELL, R.V. "Theory of Elasticity"
Oxford University Press, 1941.

79 SAAFAN, S.A. "Non-linear Behaviour of Structural Plane Frames"
J. of the Struct. Div., ASCE, Vol. 89, No. ST4,Aug. 1973,
pp 557-579.

80 SALEM, A.H. "Structural Frameworks"
Ph.D. Thesis, Manchester University, 1958.

81 SALVADORI, M.G. AND SCHWARZ, R.J. "Differential Equations in Engineering Problems"
New York, Prentice - Hall Inc. 1954.

82 SUPPLE, W.J. "Structural Instability"
(Chaps. 2, 3 and 8), I.P.C.Guildford, 1973.

83 STEVENS, L.K. "Elastic Stability of Practical Multistorey Frames"
Proc. ICE, 36, 99-117, 1967.

84 TIMOSHENKO, S.P. "Buckling of Curved Bars with Small Curvature"
J. App. Mech., 2, p17, 1935.

85 TIMOSHENKO, S.P. AND GERE, J.M. "Theory of Elastic Stability"
2nd ed - McGraw-Hill Book Co. Inc., New York, NY, 1961.

86 TSAI, W.T. "Non-linear Behaviour of Compression Members"
Proc. ASCE. Structural Div., Vol 103, No ST7, July 1977.

87 WOOD, R.H. "Effective Lengths of Columns in Multistorey Buildings"
J. Inst. Struct. Eng., 1974.

88 WOOD, R.H. "A Graphical Method of Predicting Sidesway in the Design of Multistorey Buildings"
Proc. Inst. Civ. Engrs., Part 2, volume 59, June 1975.

89 WOOD, R.D. AND O.C. ZIENKIEWICZ "Geometrically Non-linear Finite Element Analysis of Beams, Frames, Arches and Axisymmetric Shells"
Computer and Structures, Vol. 7, pp 275-735, 1977.

90 ZIEGLER, H. "Principles of Structural Stability"
Blaisdell, New York, 1966.

REFERENCES IN DYNAMICS

91 ARCHER, J.S. "Conssistent Mass Matrix for Distributed Mass System"
Proc. Am. Soc. Civ. Engrs. Struct. Div. Vol. 89, ST4, pp 161, 1963.

92 BATHE, K.J. AND CRACEWSKI, S. "On Non-linear Dynamic Analysis Using Substructing and Mode Superposition"
J. Computer and Struct., Vol. 13, No 5-6, Oct-Dec. 1981.

93 BERGEN, P.N. AND CLOUGH, R.W. "Convergence Criteria for Iterative Process"
AIAA, Vol. 10, p 1107, 1972.

94 BERG, G.V. Proc. Am. Soc. Civ. Engrs. 87, EM2, 1, 1960.

95 BIGGS, J.M. "Introduction to Structural Dynamics"
McGraw-Hill, 1964.

96 BISHOP, R.E.D. AND JOHNSON "The Mechanics of Vibration" Cambridge University Press, London, 1960.

97 BUDIANSKY, B. "Dynamic Buckling of Elastic Structures Criteria and Estimates" Dynamic Stability of Structures. G. Hermann, ed., Pergamon Press, New York, NY, 1967, pp 83-106.

98 BUDIANSKY, B. AND HUTCHINSON, J.W. "Dynamic Buckling of Imperfection Sensitive Structures" Proceedings, 11th International Congress of Applied Mech. Munchen, 1964, Sprin 1966, pp 636-651.

99 BAZZI, B. AND ANDERHEGGEN, E. "The ρ-Family of Algorithms for Time-Step Integration with Improved Numerical Dissipation" Earthquake Eng. and Structural Dynamics, Vol. 10, 537-550, 1982.

100 CHAJES, A. AND JOHNSON, B. "Multiple Frequencies in Dynamic Systems" Journal of the Struct. Div., ST1, January 1978, pp 200-204.

101 CHAUDHURY, N.K., BROTTON, D.M. AND MERCHANT, W. "A Numerical Method for Dynamic Analysis of Structural Frameworks" Int. J. Mech. Sci., Vol. 8, pp 149-162. 1966.

102 CORNWELL, R.E., CRAIG, R.R. AND JOHNSON, C.P. "On the Application of the Mode Acceleration Method to Structural Engineering Problems" J. Earthquake Eng. and Structural Dynamics, Vol 11, No. 5, pp 679-688, 1983.

103 CAUGHEY, T.K. "Classical Normal Modes in Damped Linear Dynamic Systems" Journal of Applied Mechanics "June 1960, pp 269-271.

104 CLOUGH, R.W. AND PENZIEN, J. "Dynamics of Structures" McGraw-Hill, Inc., 1975.

105 DAY, A.S. "An Introduction to Dynamic Relaxation" The Engineer, London, Vol. 219, pp 218-221, 1965.

106 DOVE, R.C. AND ADAMS, P.H. "Experimental Stress Analysis and Motion Measurement" Charles E. Merril Books. Inc., Columbus, Ohio, 1964.

107 DAVIES, G. AND NEAL, B.G. "The Dynamical Behaviour of a Strut in a Truss Framework" Proc. Roy. Soc., A253, 542, 1959.

108 DAVIES, G. AND NEAL, B.G. "An Experimental Examination of the Dynamical Behaviour of a Strut in a Rigidly Jointed Truss Framework" Proc. Roy. Soc., A274, 225, 1963.

109 HOFF, N.S. AND VICTOR, G. BUCE "Dynamic Analysis of the Buckling of Laterally Loaded Flat Arches" Polytechnic Institute of Brooklyn Aeronautical Laboratory, (PIBAL), Report No 191, October 1951.

110 HOFMEISTER, L.D. "Dynamic Analysis of Structures Containing Non-linear Springs" Computers and Structures, Vol. 8, pp 609-614, 1978.

111 LAZAN, B.J. "Damping of Material and Members in Structural Mechanics" Pergamon Press, New York, 1968.

112 MEIROVITCH, L. "Analytical Methods in Vibrations" Macmillan Company, New York, 1967.

113 MORRIS, N.F. "The Use of Model Superposition in Non-linear - Dynamic" J. Computer and Structure, Vol. 7, No. 1, pp 65-72, 1977.

114 NEWMARK, N.M. "A Method of Computation for Structural Dynamics" J. Eng. Mech. Div. ASCE, Col. 85, No. EM3, pp 67-94, 1959.

115 ORAN, C. AND KASSIMALI, A. "Large Deformations of Framed Structures Under Static and Dynamic Loads" Computer and Structures, Vol. 6, pp 539-547, 1976.

116 OTTER, J.R.H. "Computations for Prestressed Concrete Reactor Pressure Vessels Using Dynamic Relaxation" Nuclear Structural Engineering, Vol. 1, 1965, pp 61-75.

117 PADOVAN, J. "Non-linear Vibrations of General Structures" Journal of Sound and Vibration, Vol. 72, pp 427-441, 1980.

118 PASLAY, P.R. AND GURTIN, M.E. "The Vibration Response of a Linear Undamped System Resting on a Non-linear Spring" Journal of Applied Mechanics, ASME, 27, 272-274, June, 1960.

119 PREUMONT, A. "Frequency Domain Analysis of Time Integration Operators" Earthquake Engineering and Struct. Dynamics, Vol. 10, 691-697, 1982.

120 PREWITT, R.W. AND FARDO, S.W. "Instrumentation : Transducers Experimentation and Applications" Howard W Sams & Co. Inc., 1979.

121 ROY, R. AND CRAIG, J.R. "Structural Dynamics" John Wiley & Sons Inc., 1981.

122 ROGERS, G.L. "Dynamic of Framed Structures"
John Wiley & Son, 1959.

123 STEPHENSON, A.P. "6502 Machine Code for Beginners"
(c) Butterworth & Co. Ltd., 1983.

124 SRINIVASAN, A.V. "Steady-State Response of Beams Supported on Non-linear Springs"
AIAA Journal, Vol. 4, No. 10, October 1966.

125 TIMOSHENKO, S. "Vibration Problems in Engineering"
P 126, D. Van Norsted, 1953.

126 TSE, F.S.,MORSE, I.E . AND HINKIE, R.T.
"Mechanical Vibrations : Theory and Applications"
2nd Ed. Allyn and Bacon, Inc., 1978.

127 TONG, K.N. "Mechanical Vibration"
John Wiley & Son, Inc. New York, 1960.

128 VITO, P.R. "On The Stability of Vibrations of a Particle in a Plane Constructed by Identical Non-linear Springs"
Int. J. Non-linear Mechanics, Vol. 9, pp 325-330, 1974.

129 WARBURTON, G.B. "The Dynamical Behaviour of Structures"
2nd Ed. Pergamon Press, 1976.